

Small Organic Molecules: Building Blocks of Functional Materials

Inauguraldissertation

zur

Erlangung der Würde eines Doktors der Philosophie

vorgelegt der

Philosophisch-Naturwissenschaftlichen Fakultät

der Universität Basel



von

Markus Gantenbein

aus Grabs (SG), Schweiz

Basel, 2015

Genehmigt von der Philosophisch-Naturwissenschaftlichen Fakultät der Universität Basel auf
Antrag von

Prof. Dr. Marcel Mayor und Prof. Dr. Edwin C. Constable

Basel, den 21. April 2015

Prof. Dr. Jörg Schibler

für Janine und meine Familie

„Science is like a love affair with nature; an elusive, tantalising mistress. It has all the turbulence, twists and turns of romantic love, but that's part of the game.“

Vilayanur S. Ramachandran

Acknowledgments

I am deeply grateful to my supervisor Professor Dr. Marcel Mayor for confidence in my work and for giving me the opportunity to complete my dissertation in his research group. I am indebted to him for his mentorship, his intellectual support and for giving me the freedom to explore on my own, and at the same time the guidance to recover when my steps faltered. His patience and support helped me to overcome many difficult situations and to finish this dissertation.

I would like to thank Professor Dr. Edwin Constable and Dr. Thomas Schäfer for the co-examination of this thesis.

Moreover, I thank Professor Dr. Dennis Gillingham for chairing the exam.

I am greatly appreciative to the successful collaborations in the course of this thesis. I want to give a special thanks to Dr. Daniel Häussinger and Dr. Heiko Gsellinger for the discussions concerning the NMR spectroscopy and the highly diligent analysis of the racemization dynamics of biphenyls. Furthermore, I thank Professor Dr. Thomas Wandlowski and Dr. Veerabhadrarao Kaliginedi for performing single molecule conductance measurements. I thank Dr. Michel Calame, Professor Dr. Christian Schönenberger, Dr. Jan Brunner and Anton Vladyka for investigating the isocyano anchor group in break junction measurements, which unfortunately did not find place in this thesis.

I also would like to thank Dr. David Vonlanthen and Dr. Jürgen Rotzler for their help and teaching me in practical skills.

I am very thankful to Manuel Hellstern and Lorenzo Delarue Bizzini for their devotion during their master thesis.

I owe my deepest gratitude to Manuel Hellstern for being my lab mate. It was an honor for me to work with you for the last 4 years.

I was lucky to meet and interact with Michel Rickhaus. I am beholden for your friendship and the enjoyable time we spent in the lab and everywhere else.

I would like to thank the entire Mayor group for the stimulating discussions and the nice environment that they provided.

I am happy to thank Dr. Loïc Le Pleux for teaching me electrochemistry and for all the fruitful scientific discussions.

Dr. Michal Juríček, Dr. Loïc Le Pleux, Michel Rickhaus, Lukas Felix, and Kevin Weiland I am deeply grateful for proofreading the manuscript.

I also would like to acknowledge all students (Jan Hanusch, Felix Brunner, Florian Fenniger, Vidya Mannancherril, Alex Gaspers, Adrian Hodel, Martina Garni, Frederik Malzner) who provided numerous compounds during my thesis.

I would like to thank the “Werkstatt” team for their continuous support for maintaining our lab. In addition, I am thankful to Beatrice Erismann, Marina Mambelli, and Brigitte Howald without whom none of this work presented here would have been possible. I also thank Markus Hauri and Roy Lips from the “Materialausgabe” for their support.

I am very appreciative of Dr. Heinz Nadig for the measurement of HRMS-spectra, Werner Kirsch and Sylvie Mittelheiser for elemental analyses, and Dr. Markus Neuburger for measuring solid state structures.

Foremost, I thank my parents Helene, Steve, Markus, and Hedi for their limitless love and always believing in me. I am also grateful to my sister Fabienne, my little brother Sandro, and my godchild André.

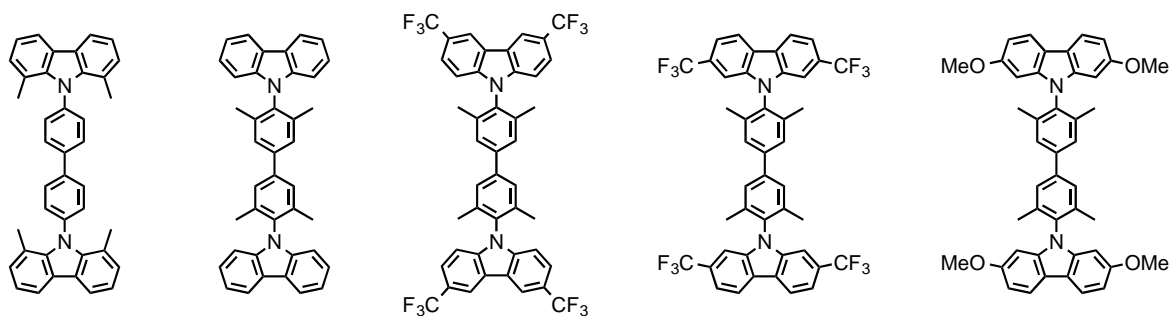
Many friends outside the lab helped me overcome setbacks. I thank all my close friends Büsch, Bonens, Stöff, Res, Luk, and Pinky, my roommates Bünz, Flo, and Mätü, and all the members of SC Binningen II, I greatly value their friendship.

Thank you Janine for always loving me.

Summary

Chapter 1

The potential of phosphorescent organic light emitting diodes (phOLEDs) in full-color flat-panel display solid state lighting devices is fueling the interest in high triplet energy materials. 4,4'-Bis(9-carbazolyl)-biphenyl (CBP) is one of the most widely used host material in phOLEDs. Because of its triplet energy (E_T) of 2.56 eV, it is a suitable hole transporting material for green phosphorescent emitters, such as tris(2-phenylpyridine)iridium(III) [Ir(ppy)₃]. However, the commonly used dye bis[(4,6-difluorophenyl)-pyridinato-N,C2]-picolinateiridium(III) (Flrpic) in blue phOLEDs exhibits a E_T of 2.65 eV. Therefore, new high- E_T host materials are required to allow for efficient OLED-devices.

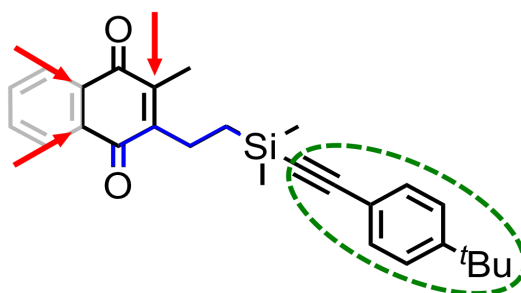


The design of blue pixel host materials is based on the idea of reducing the level of conjugation between the carbazole subunit and the biphenyl backbone. Therefore, a series of CBP derivatives was synthesized and studied with spatially restricted degrees of freedom in their biphenyl-*N*-carbazole junctions by introducing spatial demanding methyl moieties either in positions 1 and 8 of the carbazole unit or in positions 3,5,3',5' of the biphenyl backbone. Moreover, the electronic features of the carbazole synthons were investigated by attaching electron-withdrawing or electron-donating groups in the positions 3 and 6 or positions 2 and 7 of the carbazole subunits.

Chapter 2

Acetylenes are highly intriguing building blocks in molecular electronics. Besides their modularity, synthetic accessibility and efficient post-functionalization by click-chemistry, acetylenes allow a broad scope of protecting groups that makes them ideally suited for targeted assembly of multifunctional self-assembled monolayers (SAMs). The idea of an

electrochemically-triggered deprotection of acetylene enables the specific addressability of the desired reaction site. When this deprotection of the immobilized acetylene takes place on a conductive surface, post-functionalization leads to the formation of a multifunctional SAM.



The design of a reductively cleavable acetylene protecting group is based on the idea of spatial separation of the actual connection to the acetylene from the redox active moiety. In order to enable the efficient attack of the silyl moiety by the formed anion, it was important to separate the two mentioned reactive centers in an appropriate distance from each other. Its length has been chosen such that the resulting attack leads to the spontaneous formation of an energetically favored six membered ring. The investigated system is completed by 4-*tert*-butylphenylacetylene, since the optical properties are readily distinguishable from the π - π^* transitions of the redox center. The liberated acetylene can, due to its molecular weight also be detected by gas chromatography–mass spectrometry giving a second indicator for the success of the reaction.

Chapter 3

In this chapter, the progress towards the synthesis of a ball-shaped, highly symmetric thiospherophane ($C_{48}S_{12}$) is discussed. This ball-shaped molecule consists of eight identical benzene subunits, which are interconnected via a sulfur atom. The insertion of these sulfur heteroatoms would transform the fullerene closed-shell structure into a hollow molecular cage.

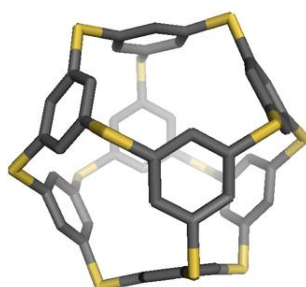


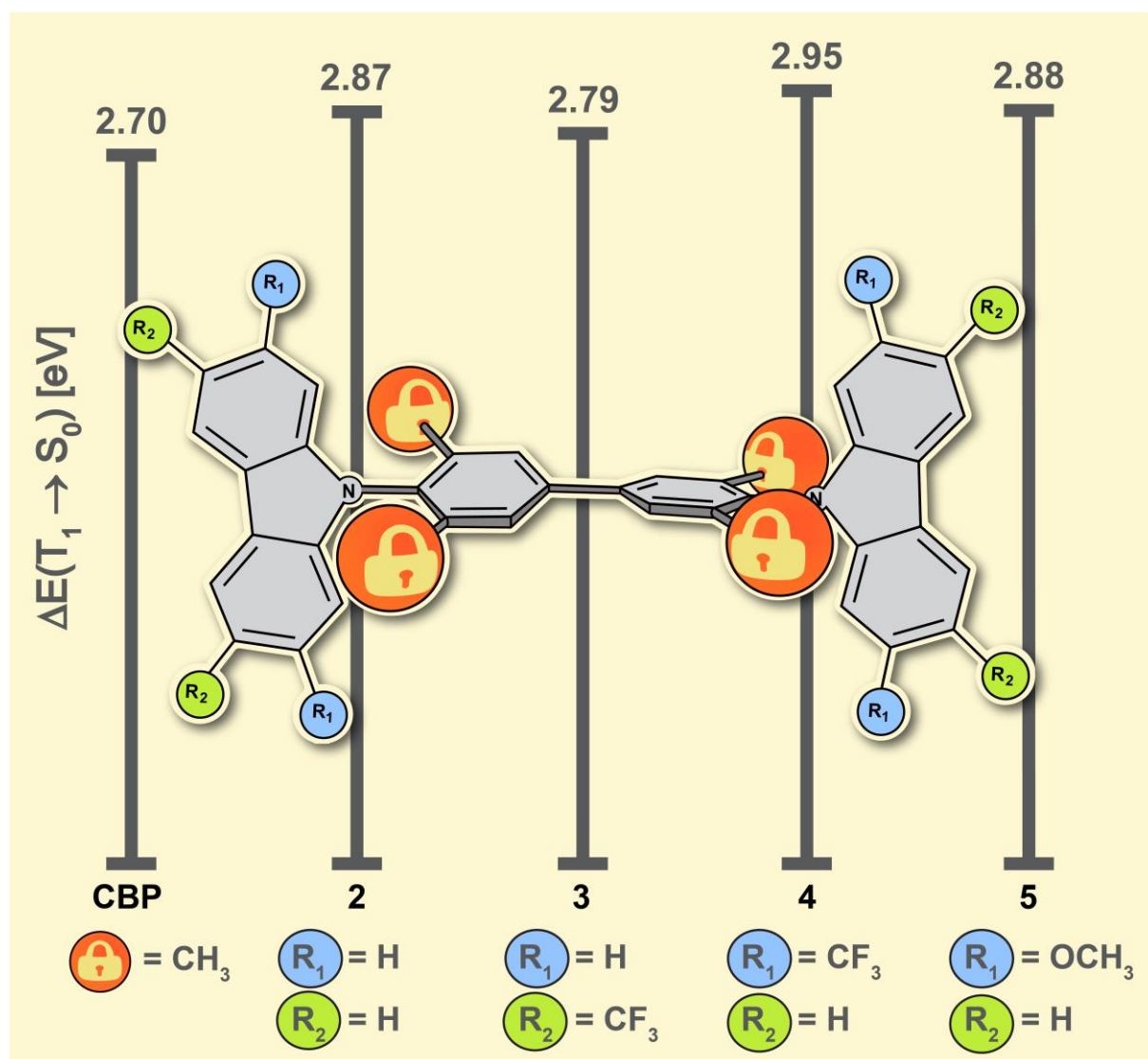
Table of Contents

Chapter 1: High-Triplet State Energy Materials for OLED devices	1
Introduction	2
Improving the Light	2
OLED Architecture	4
Working Principle of OLEDs	6
OLED Families	7
Dyes in Phosphorescent Emitting OLEDs	8
Host Material	9
Aim of the Work	15
Molecular Design	17
Results and Discussion	18
Synthesis	18
Structural Properties	24
Thermal Properties	27
Photophysical Properties	30
Electrochemical Properties	35
Conclusion and Future Perspectives	40
Experimental Section	43
General Remarks	43
Synthetic Procedures	44
Chapter 2: Development of Novel Ethynyl Protecting Group for SAM Formation	61
Introduction	62
Self-Assembled Monolayer	62
Thiolate SAMs on Gold Surface	63
SAMs on Carbon-Based Surfaces	65
Electrografting of Aryl Diazonium Salts	66
Mechanism of Grafting	67
Characterization of the Grafted Organic Layer	69
Stability of Organic Layer	73
Sensing Based on Diazonium Grafting	73
Electrochemically Sensitive Protecting Groups	76
Aim of the Work	78
Molecular Design	81
Synthetic Strategy	83
Results and Discussion	84
Synthesis	84
Chemical Reduction	85
Electrochemical Reduction	87
Conclusion and Future Perspectives	93

Experimental Section.....	96
General Remarks	96
Synthetic Procedures.....	97
Chapter 3: Progress Towards the Synthesis of Thiospherophane C₄₈S₁₂.....	103
Introduction.....	104
Fullerene.....	104
Heterofullerenes	105
Aim of the Work	107
Synthetic Strategies.....	108
Wrap Approach I	109
Wrap Approach II	111
Bowl Approach	112
Results and Discussion	113
Bowl Approach	113
Wrap Approach I	118
Wrap Approach II	119
Conclusion and Future Perspectives	125
Experimental Section.....	128
General Remarks	128
Synthetic Procedures.....	129
Bibliography.....	141
Appendix	157
Abbreviations	157
Curriculum Vitae.....	161
List of Publications.....	163

Chapter 1

High-Triplet State Energy Materials for OLED devices^[1]



Introduction

Improving the Light

There is no doubt that the invention of the incandescent light bulbs in 1879 by Thomas Alva Edison was a great discovery. The idea of making the night to day was fascinating world wide, leading to the tremendous amount of artificial light, which is used nowadays. About 20% of our energy goes into lighting applications, ranging from simple signals to general illumination.^[2] In the USA an even more impressive number of 38% of all consumed energy is used for residential or commercial buildings. The fear of not knowing what is out there due to the absence of light has certainly set the triumphal procession for the distribution of the artificial light in this dimension. The invention of artificial light was not only fueling the economy due to elongation of working time, but also society benefits by offering more time for recreational activities. Nevertheless, the non-efficient and upward-directed lighting systems of residential and commercial places show the tremendous growth of light pollution (Figure 1).

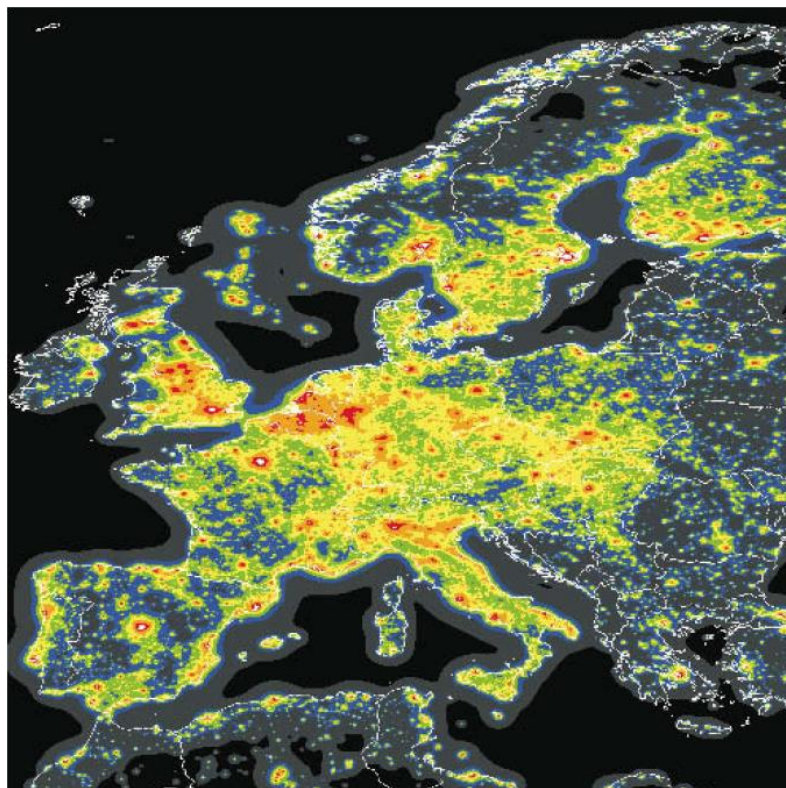


Figure 1: Artificial night sky brightness at sea level for Europe. In the red area is the Milky Way no longer visible. Reprinted from Elvidge and co-workers.^[3]

Sustainability or going green as one of the greatest topic arising the last few years, the incandescent light bulbs were pushed in the spotlight of environmental developments. Although, optimizing shielding advices,^[4] intelligent light controlling systems, or daylight harvesting architectures,^[5] is commendable, the problem relies more profound. As more than 55% of the whole generated electricity is used for electrical devices, the 20% which are used for lighting systems are not negligible.^[6] Besides the relative short lifetime (1000 – 2000 hours) of the incandescent bulb lamps, only 15% of the energy is used as light, and 85% is released as heat.^[7] By using new lighting technologies like organic light emitting diodes (OLEDs) this lost of energy could be reduced by more than 25%, which would not only reduce the light pollution but also save a tremendous amount energy waste.^[6]

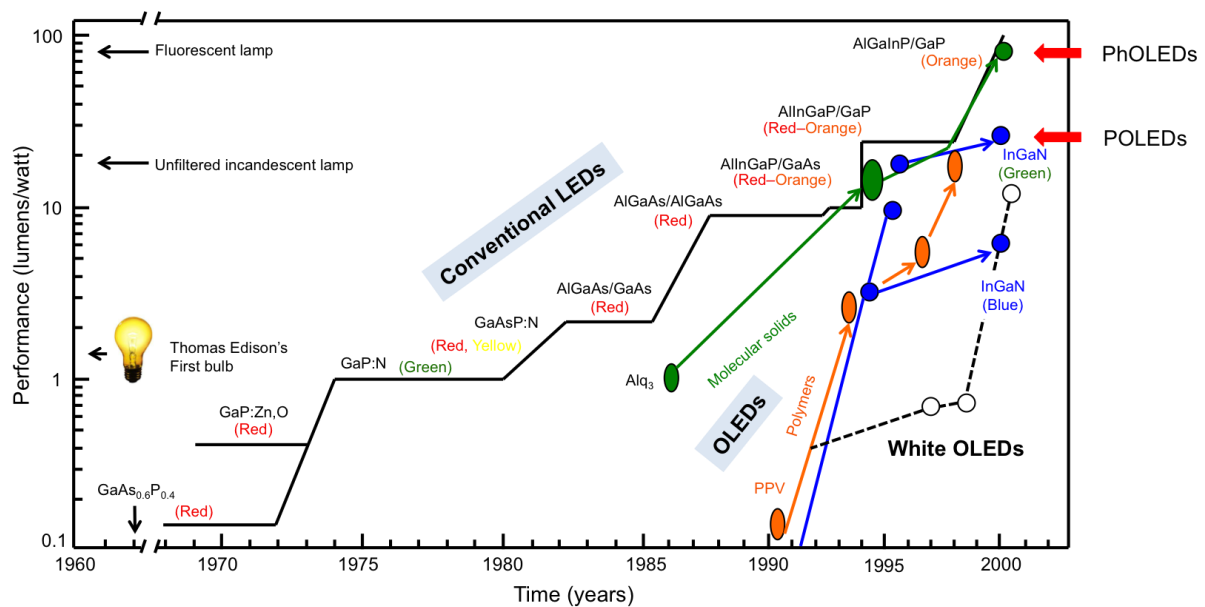


Figure 2: Progress for display source efficiency in various lighting. PhOLEDs and PLEDs refer to devices based on phosphorescent emitting dyes and fluorescence phosphorescent polymers, respectively. Adapted from Forrest.^[8]

OLEDs represent a strong candidate in next generation solid-state lighting devices alternative to conventional incandescent bulbs or fluorescent lamps. OLEDs produce light similar as light-emitting diodes (LEDs) do, except that in OLEDs the positive and negative charges originate in organic compounds, and LEDs in crystalline semi conductors. Using these revolutionary lamp properties, including tuning of color, flexible lighting source, and

transparency, the light can be switched on and off in high frequencies without any problems. Furthermore, the slimness (10 – 1 mm) of this lighting device and ability to perform on large areas may allows lighting of commercial buildings without the usage of lighting fixtures.^[2,7,9,10] Nevertheless, there are still some issues to overcome. For example encapsulation due to the OLED’s high sensitivity towards air and moisture inducing degradation of the device. Many feasible solutions for the encapsulation of rigid substrates are present (e.g., atomic layer deposition (ALD), or glass-cap), but are more challenging for flexible devices. The storage lifetime is directly linked with encapsulation technologies, whereas operational lifetime is mainly limited by material degradation during operating conditions.^[6] Performance and efficiency are the most important criteria in this competitive market (\$90 billions) of existing and upcoming lighting technologies.^[10] Rapid progress in the optimization of OLED device performance in the past and present century will decrease costs of production. Therefore OLEDs represent a competitive player in the near future of lighting technologies (Figure 2).^[11]

OLED Architecture

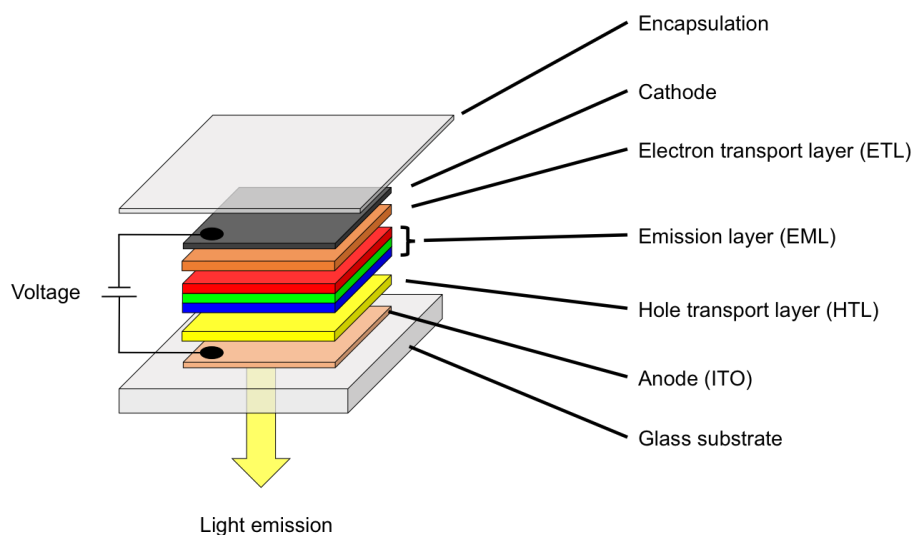


Figure 3: A typical stack layout of a multilayered OLED consisting of a hole transporting layer (HTL), electron transporting layer (ETL) and an emission layer (EML), which represents the heart of an OLED. Reprinted from Brütting and co-workers.^[12]

In 1978 Ching W. Tang and Steven VanSlyke demonstrated the first doubly layered thin film OLED using vacuum deposition techniques.^[13] Shortly after, a group at Cambridge University

reported a large-area OLED based on the conjugated polymer poly(p-phenylene vinylene).^[14] In order to enhance current efficiency and lumen output, nowadays vertical stacking of multilayer OLEDs is more complex.^[15] However, an organic layer sandwiched between an anode and a cathode still represents the principal of a thin-film OLED device. This multilayered architecture is essential regarding efficiency and lifetime, since the properties of each layer can be addressed and tuned individually through the proper choice of material (Figure 3). A multilayered OLED requires a hole transport layer (HTL) that transports the holes from the positively charged anode towards the emission layer (EML). Notably, the electrons are injected from the cathode into the electron transport layer (ETL). The holes and electrons recombine ideally in the EML, comprising one or more emitting dyes, providing electroluminescence. Choosing an appropriate dye, emission in different regions of the visible spectrum is possible. To optimize transport properties separate blocking and injection layers are required. Properties of commonly used materials in HTL and ETL for OLED devices are listed in table 1.

Table 1: Glass transition temperature (T_g), HOMO/LUMO, triplet energy level and hole/electron mobility for selected hole and electron transport materials. Data obtained from Tao and co-workers.^[16]

compound	T_g (°C)	HOMO (eV)	LUMO (eV)	E_T (eV)	μ^a ($\text{cm}^{-2} \cdot \text{V}^{-1} \cdot \text{s}^{-1}$)	electric field ($\text{V} \cdot \text{cm}^{-1}$)
TPD ^[17–20]	65	5.4	2.4	2.34	$1.0 \cdot 10^{-3}$	$1.5 \cdot 10^5$
NPB ^[17,19,20]	95	5.4	2.3	2.29	$8.8 \cdot 10^{-4}$	–
TCTA ^[17,20–22]	151	5.7	2.4	2.76	$2.0 \cdot 10^{-5}$	–
TAPC ^[23,23–25]	78	5.5	2.0	2.87	$1 - 10 \cdot 10^{-3}$	$1.0 - 4.4 \cdot 10^5$
Alq ₃ ^[26–30]	172	5.8	3.0	2.00	$7.2 \cdot 10^{-6}$	$6.4 \cdot 10^5$
BCP ^[18,29,30]	83	6.7	3.2	2.50	$5.6 \cdot 10^{-6}$	$6.4 \cdot 10^5$
TPBI ^[31,32]	124	6.2	2.7	2.74	$3.3 - 8.0 \cdot 10^{-6}$	$4.7 - 7.0 \cdot 10^5$
^t Bu-TAZ ^[33,34]	70	6.3	2.7	2.75	–	–
PO15 ^[16,35]	106	6.6	2.9	3.07	–	–

^aHole mobility for TPD, NPB, TAPC, and TCTA, electron mobility for the others.

Working Principle of OLEDs

The most important parts of the working principle can be separated into four fundamental steps as denominated in figure 4. By applying an external voltage two types of charge carriers are injected from the opposite electrodes. At the anode, the hole transport layer gets oxidized generating a hole, whereas the cathode reduces the electron transport layer by injecting electrons into the device (1). Both, the electron and the hole, start to drift towards the emission layer (EML) by hopping processes (2). At the EML the initially free electrons and holes form strongly bound electron–hole pairs (excitons) (3), which induce light emission (4). The color can be tuned by the dopant of the host material. This organic material based electroluminescence devices allow low driving voltage and at the same time bright emission.^[36]

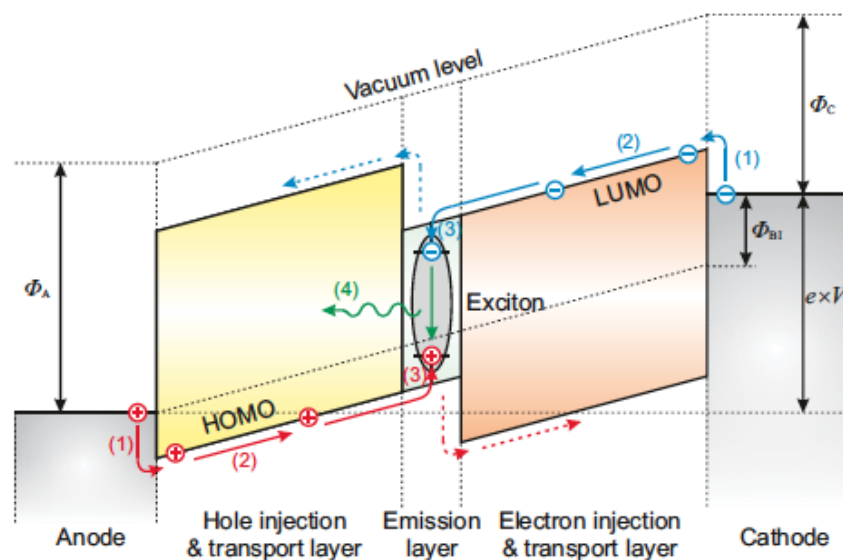


Figure 4: Schematic energy diagram of a three layer OLED illustrating the four fundamental steps of the working principle.^[12] (1) Electrons are injected from the anode into the lowest unoccupied molecular orbital (LUMO) by reduction of the ETL. Similarly, holes are injected into the HTL by removing electrons from the highest occupied molecular orbital (HOMO). To establish a current flow through the device, a built-in voltage Φ_{Bi} has to be overcome by applying an external voltage (V); Φ_A and Φ_C are the work functions for the anode and the cathode, respectively. (2) By proper alignment of the HOMO and LUMO levels the holes and the electrons are transported towards the EML. Due to high LUMO levels of the HTL (yellow), electrons will be blocked at the EML, and holes will be blocked due to the low HOMO level at the ETL (orange), respectively. (3) Recombination of the hole and electron in the EML are forming excitons. (4) Emission of light occurs due to radiative exciton decay by either fluorescence or phosphorescence. Reprinted from Brütting and co-workers.^[12]

OLED Families

OLED devices can be separated in roughly three different families (Figure 5). This division is based on the optical and physical properties of the materials, which are used in such a device. The most common used family is the fluorescent family. They profit from a long lifetime and therefore, most flat-panel displays available on market are using this technique. However, they suffer from low efficiency according to spin statistics.^[37] Another interesting family of OLEDs is based on polymer materials. If polymers are used in such a multilayer device, the production costs of OLEDs will be reduced due to facile multilayer device fabrication.^[7] The most interesting family represents the phosphorescent family. Due to spin statistics, the ratio of singlet and triplet states formed under electrical excitation is 1 : 3, owing to their multiplicity.^[38] Unlike fluorescent, phosphorescent emitters can harvest both singlet and triplet excitons, and thus, their maximum internal efficiency can approach theoretically an internal quantum efficiency of 100% by harvesting both—singlet and triplet excitons—simultaneously through intersystem crossing.

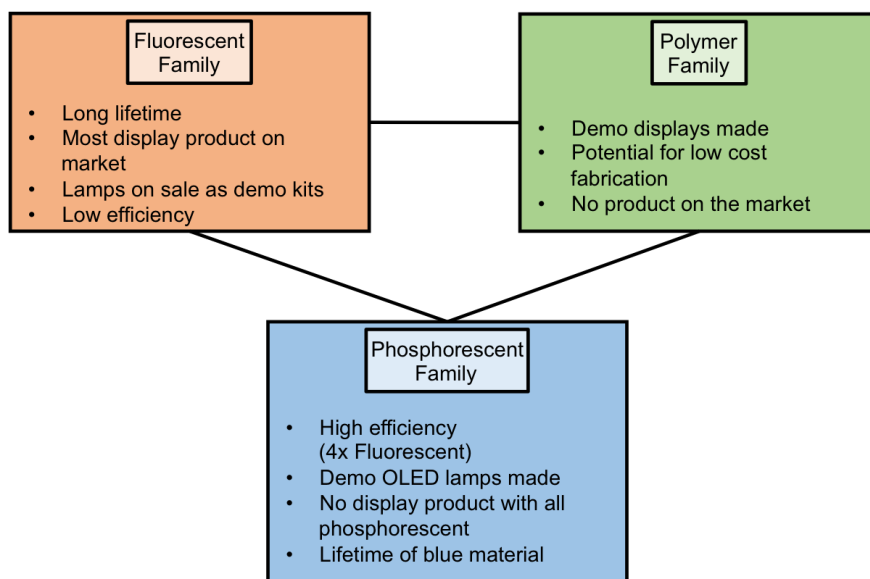


Figure 5: The free families of OLEDs.

If the pathway of electroluminescence via fluorescence is followed the maximum of efficiency will be 25%, since only one fourth of the recombined excitons remain in the singlet state on initial charge recombination (Figure 6). Therefore, it has been a major breakthrough

in improving electroluminescence efficiency by moving the point of interest in research from fluorescent^[39,40] to phosphorescent triplet emitters in OLEDs.^[37,41–45] However, lifetime of lighting devices often suffer from the relatively low efficiency of the blue light emission.

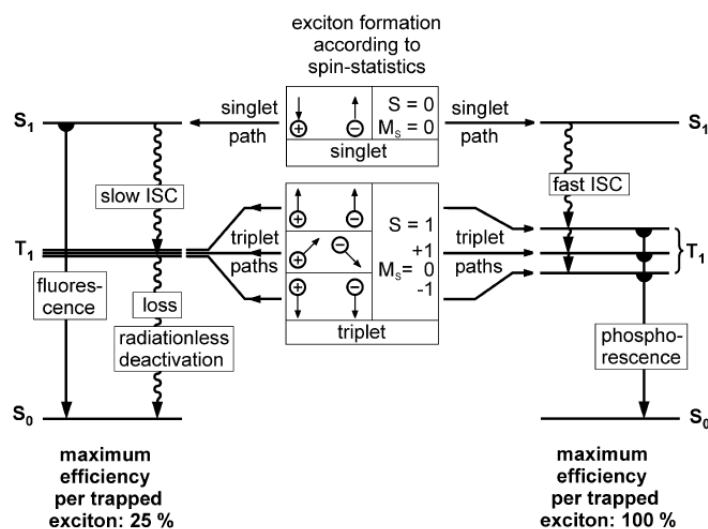
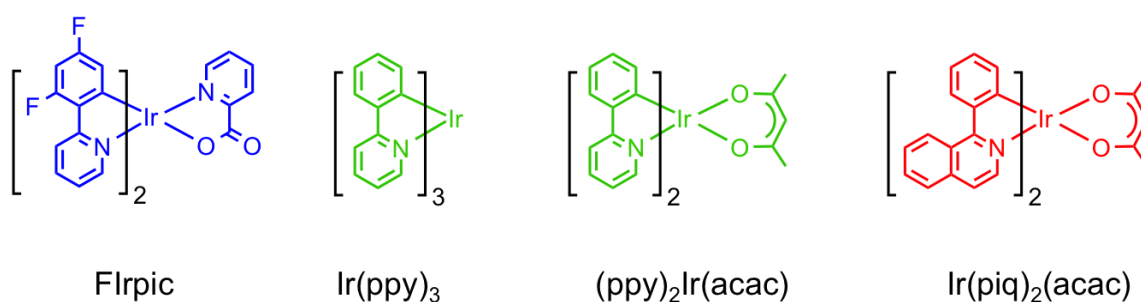


Figure 6: Possible pathways of an excitation recombination according to spin-statistics. Theoretical maximum internal efficiency per trapped exciton is 25% and 100% for fluorescence and phosphorescence, respectively. Reprinted from Yersin.^[46]

Dyes in Phosphorescent Emitting OLEDs



Scheme 1: Structures for most common used blue, green and red phosphorescent dyes.

The most widely used dopants in phosphorescent organic light-emitting diodes (phOLEDs) are triplet-emitting Ir^{III}-complexes. The best well-known triplet emitters are bis[2-(4,6-difluorophenyl)pyridinato-C²,N](picolinato)iridium(III) (Flrpic)^[47,48] for blue; tris[2-phenyl-

pyridinato-C²,N]iridium(III) [Ir(ppy)₃]^[41,42] and bis[2-(2-pyridinyl-N)phenyl-C](acetylacetonato)iridium(III) [(ppy)₂Ir(acac)]^[43] for green; and bis(1-phenylisoquinoline)(acetylacetonate)iridium(III) [Ir(piq)₂(acac)]^[49] for red dyes. Their triplet energies are 2.65 eV,^[50] 2.42 eV,^[51] and 2.00 eV,^[52] estimated from the highest energy peak in phosphorescence spectra for blue (FIrpic), green (Ir(ppy)₃) and red emissive (Ir(piq)₂(acac)), respectively. These dyes are usually doped in a concentration ranging from 1 – 20% to reduce quenching,^[53,54] triplet–triplet annihilation, which originates from the long lifetime of phosphorescent heavy metal complexes (up to microseconds), and long range diffusion of excitons (>100 nm) that could get quenched in the adjacent HTL or ETL.^[47,48]

Host Material

To achieve efficient electro-phosphorescence, host materials have to fulfill several requirements. (i) It is essential that the triplet excited state of the host material is higher than that of the triplet emitter to prevent reverse energy transfer from the guest back to the host and to effectively confine triplet excitons on the guest molecules.^[50,55] (ii) The HOMOs and LUMOs of the host material should match with those of neighboring active layers to reduce the hole and electron injection barrier, and thus lowering the driving voltage of the device.^[36] (iii) The host material should provide thermal and morphological stability, which can reduce the possibility of phase separation upon heating and thus, prolonging the device operational lifetime.^[16] Generally, bulky and spatial demanding moieties are introduced into the molecular configuration to enhance the glass transition temperature (T_g), and form morphologically stable and uniform amorphous films.^[18] (iv) The hosts are expected to have good and balanced charge carrier transport properties for the hole–electron recombination process. The host materials can be summarized in three separated categories: hole-transport type, electron-transport type, and bipolar-transport type material. The choice of appropriate host materials in red^[56,57] and green^[58,59] OLEDs is well developed compared to blue emitting OLEDs, due to their low triplet energy levels. For the blue emitting pOLEDs it becomes considerably challenging to meet these requirements for host materials arising from the high E_T (≥ 2.65) of the blue guest (dopant). As high- E_T materials generally require decreased π -conjugation, this may adversely affect the charge transport properties^[60] as well as thermal and morphological stabilities.^[61] Since formation of excitons is energetically unfavorable on

wide gap materials, a compromise between the HOMO and the LUMO level is required. These large band gaps would lead ultimately to higher driving voltages and lower power efficiencies of the devices.^[62,63]

Energy Transfer Between Host and Dopant

The host–guest energy transfer occurs via two different mechanisms,^[26] the Förster resonance energy transfer (FRET)^[64] and the Dexter electron transfer.^[65] The Förster energy transfer relies on radiationless dipole–dipole interactions (Coulomb interactions) where the excited singlet state is transferred to the dopant. This is a fast (ca. 10^{-12} s) and long range process (up to 10 nm).^[66,67] Notably, the emission spectrum of the host matrix needs to overlap significantly with the absorption spectra of the guest molecule (Figure 7, left). This overlap between the emission and absorption spectra can be easily examined by UV-vis measurements.

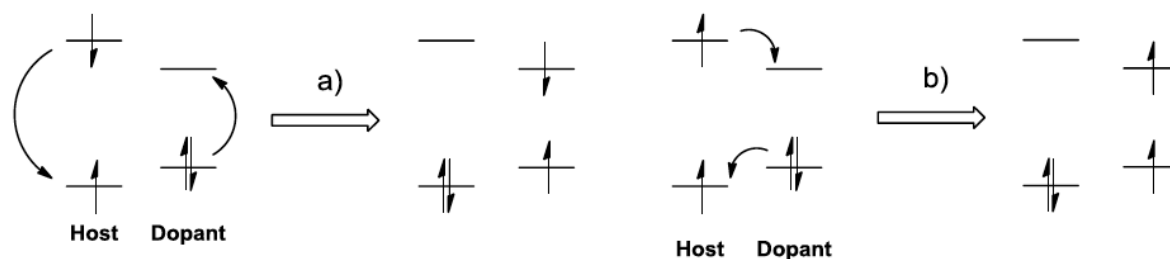
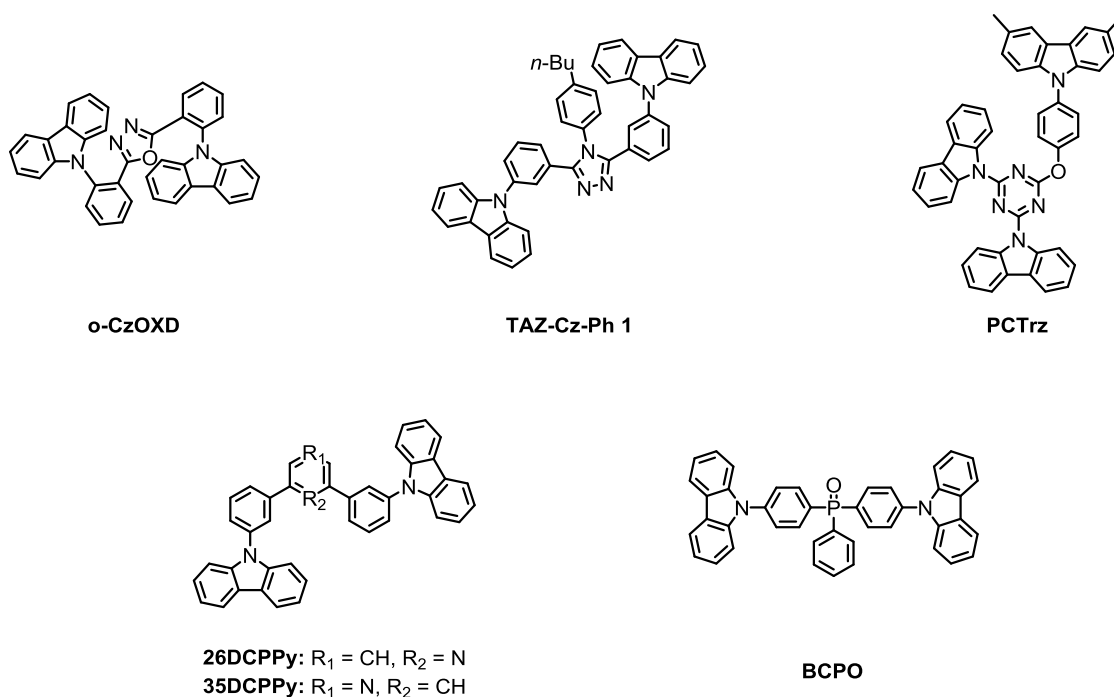


Figure 7: Host–guest energy transfer; a) Förster resonance energy transfer (FRET), showing an excited singlet state, transferred from the host to the dopant. b) Transfer of the excited triplet state from the host to the guest molecule, known as Dexter energy transfer. Reprinted from Tao and co-workers.^[16]

In contrast, the Dexter energy transfer is an electron-exchange interaction between the host exciton and the dopant, due to mechanical tunneling electrons, which is a short distance process ranging from a few Å up to 1 nm.^[66] Efficient Dexter transfer requires the match of energies of the singlet and triplet excitons on the host with the exciton energies on the guest (Figure 7, right).

Bipolar Host Materials

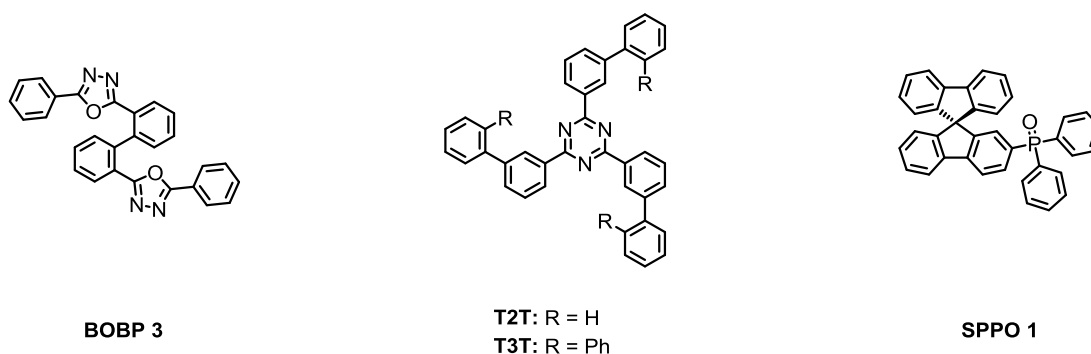


Scheme 2: Molecular structures of selected bipolar host material for pOLEDs.

Due to its unique structural motives, bipolar host systems gained more interests, because they may will simplify the device structure.^[17,68] Very intuitively, the recombination zone is close to the EML–ETL interface when using a hole-transport type host and shifts towards the EML–HTL interface when conducting a electron-transport type host material.^[69] A very challenging issue to overcome is the fact that the electron-donating and electron-withdrawing moieties unavoidably lower the band gap of the material by intramolecular charge transfer. This low triplet energy of the host may cause energy transfer from the guest back to the host, which consequently decreases the efficiency of pOLEDs.^[70] This issue was addressed by incorporation spatial demanding groups^[71,71,72] or non-*para* linkage between the two subunits,^[37,56,57–61] both leading to a interruption of the π -conjugation and rising the triplet energy (Scheme 2). Since 4,4'-bis(9-carbazolyl)-biphenyl (CBP) derivatives are the most widely used hole-transport and oxadiazole derivatives represent commonly electron-transport type materials, the carbazole–oxadiazole hybrid is a very interesting bipolar structural motive. *o*-CzOXD displays enhanced T_g values of 97 °C, attributed to the oxadiazole moiety, and an E_T of 2.68 eV. These superior properties of *o*-CzOXD increas the performance of both green (Ir(ppy)₃; 77.9 cd · A⁻¹) and red ((piq)₂Ir(acac); 13.6 cd · A⁻¹) pixel in pOLEDs.

Similarly hybrid structures of 1,2,4-triazol (electron-transport type) and 9-phenylcarbazole (hole-transport type) display promising properties, suitable for blue electrophosphorescence devices. Tunable triplet energies by varying the substitution pattern of the phenyl-carbazole unit leads to high E_T ranging from 2.8 to 3.0 eV.^[73] The best maximum current efficiency of $14.2 \text{ cd} \cdot \text{A}^{-1}$ was observed for 3,5-(bis(3-(9-carbazoyl)phenyl)-4-(4-butylphenyl)-4*H*-[1,2,4]-triazole (TAZ-Cz-Ph 1).^[73] A novel bipolar host material is combining the electron donating carbazole with an electron accepting pyridine unit affording a unique molecular design of 26DCzPPy and 35DCzPPy. Both are displaying E_T values of 2.71 eV, therefore they are performing well in blue FIrpic-based pOLEDs.^[74] The combination of the hole conducting phenoxy-carbazole and the electron deficient 1,3,5 triazine (PCTrz) leads to a monodisperse molecular mixed host that combines good transport properties for both types of charges. The E_T of 2.91 eV makes it suitable for FIrpic fabricated pOLEDs exhibiting a current efficiency of $13.5 \text{ cd} \cdot \text{A}^{-1}$, whereas the T_g of $148 \text{ }^\circ\text{C}$ ensures morphological stability during the operational lifetime of the device.^[75] An universal bipolar host with remarkable properties ($T_g = 137 \text{ }^\circ\text{C}$, $E_T = 3.01 \text{ eV}$) was observed for carbazole–phosphine oxide hybrid structure BCPO. Its low turn on voltage as well as good current efficiency for blue (2.8 V; $45.1 \text{ cd} \cdot \text{A}^{-1}$), green (2.1 V; $83.4 \text{ cd} \cdot \text{A}^{-1}$), and red (2.7 V; $20.4 \text{ cd} \cdot \text{A}^{-1}$) dopants emphasize BCPO as potential host for white organic light emitting dyes (WOLEDs).^[76]

Electron Transport Type Host Material

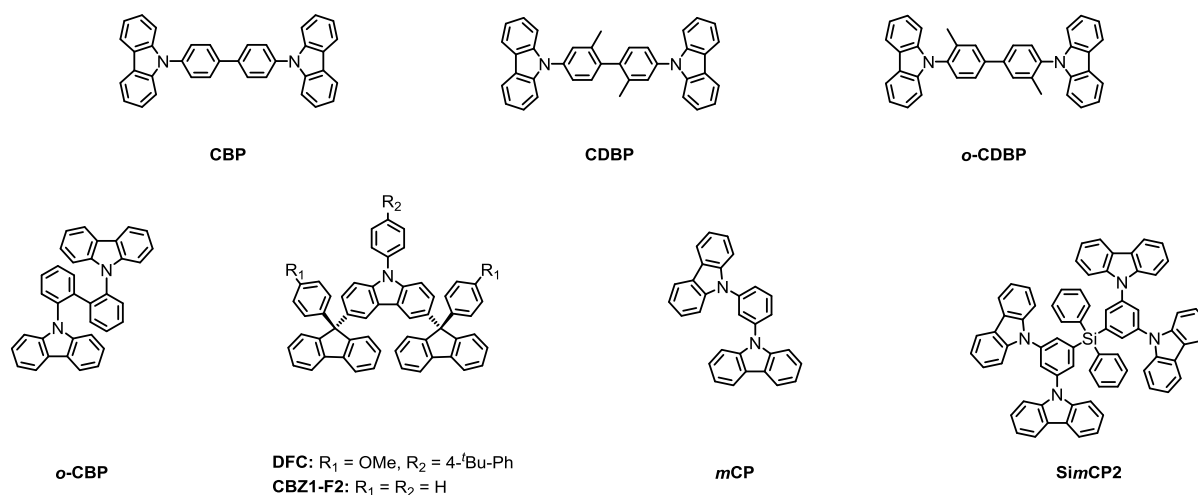


Scheme 3: Molecular structure of selected electron-type host material for pOLEDs.

To meet the requirements of high electron mobility, high triplet energy, low electron injection barrier, and thermal stability, an electron withdrawing oxadiazol moiety was

attached at the *ortho*-position of the biphenyl backbone (BOBP 3), similar to *o*-CBP. Attributed to the well matched spectral properties with the green dopant Ir(ppy)₃ and BOBP 3, a maximum current efficiency of 26 cd · A⁻¹ was observed.^[77] Higher triplet energies were observed for star-shaped structures based on 1,3,5-triazine derivatives, namely 2.80 eV and 2.69 eV for T2T and T3T, respectively. The excellent performance (54 cd · A⁻¹) of T2T in green emitting pOLED, is attributed to its superior balanced electron–hole recombination within the EML.^[78] By implementation of a phosphine oxide moiety that acts as point of saturation between the phenyl groups and the spiro-fluorene group (SPPO 1), the triplet energy is enhanced to 2.9 eV. SPPO 1 was successfully investigated for a blue electrophosphorescent device, exhibiting a current efficiency of 37.2 cd · A⁻¹, which is attributed to its multi-functionality of being an exciton blocking and electron transporting material.

Hole Transport Type Host Materials



Scheme 4: Molecular structure of selected hole-transport host material for pOLEDs.

Carbazole based structural motives have been widely used as hole-transport type material. The most prominent host for triplet emitters is CBP. pOLEDs using CBP as host material showed good peak efficiencies for green (57.2 cd · A⁻¹) and red (58.2 cd · A⁻¹) dopants.^[79] Besides its rather simple synthesis, the relative low T_g of 62 °C^[80] leads to crystallization in

the device and an E_T of 2.56 eV, which is lower than those of commonly used blue triplet emitters (> 2.65 eV),^[81] results in an inefficient energy transfer from host to dopant and poor device efficiency. Researchers try to overcome these issues by introduction of bulky methyl (CDBP) or trifluoromethyl groups mounting at the 2,2'-position of the biphenyl backbone, arising a high E_T of 2.95 – 3.0 eV and a higher T_g (ca. 100 °C) compared to CBP.^[55,82] These properties doubled the maximum external quantum efficiency of a Flrpic-based pOLED. A similar idea was followed, when the methyl units were attached at the 3,3'-position of biphenyl subunit (*o*-CDBP) or the carbazole moiety was interlinked in *ortho*-position with the biphenyl (*o*-CBP). Both investigated methods lead to a decreased π -conjugation throughout the molecular rod, conducting triplet energies ranged from 2.73 – 3.01 eV. The improved T_g ranging from 78 – 115 °C can be attributed to the spatial arrangement of the interlinked subunits.^[83] The non-conjugated hybrid structure of carbazole ($E_T = 2.95$ eV) and fluorene (DFC, $E_T = 3.05$ eV)^[84] leads to rather high T_g of 180 °C. Nevertheless, its triplet energy of 2.53 eV makes them only suitable for green and red dopant based pOLEDs.^[85] A similar work presented fluorene–carbazole linked molecules (CBZ1-F2) as effective host material with higher triplet energies (2.88 eV) suitable for blue dyes.^[86] Another initial example is 1,3-bis(carbazole-9-yl)benzene (*m*CP), interlinking two carbazole with one phenyl unit in *meta*-position, decreasing π -conjugation and therefore increasing E_T (2.9 eV).^[87] This relatively high E_T makes *m*CP a widely used host in blue emitting pOLEDs. To improve its low T_g (60 °C) and formation of hill-like pattern in thin films,^[88] structurally related motives were investigated, such as SimCP2. Connecting two *m*CP units by a diphenyl-silane moiety exhibits a structure with enhanced properties, such as increased T_g (148 °C) and better performance. This is attributed to the bulky substituents, separating the dopant molecules and therefore reducing T_1 – T_1 annihilation. Furthermore, the tetraphenyl silane subunit provides a more balanced hole and electron recombination property. Additionally, a lower ISC-rate compared to *m*CP was found, arising a higher energy transfer rate from guest to host.^[89]

Aim of the Work

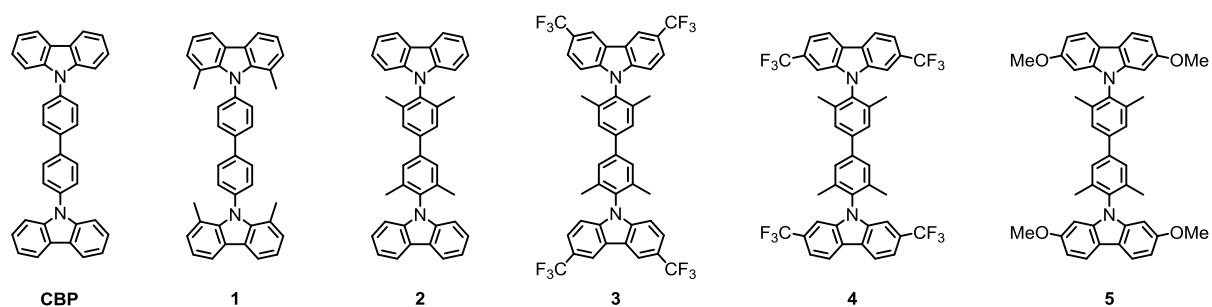
Nowadays the production of full-color flat-panel displays is strongly linked with the commercialization of highly efficient material that can generate all blue, red, and green colors. The promising implementation of OLEDs in flat-panel displays and solid state lighting devices gained attention after the first OLED material.^[39] Whereas, the efficiency of electroluminescence in OLEDs, based on green and red dyes is already reaching satisfying values, the efficiency based on the blue FIrpic pixel still needs further improvements. To improve the efficiency of the host material, its requirements can be summarized as followed:

- i) To prevent back energy transfer from the guest to the host and to efficiently promote the exothermic energy transfer from host to guest, the E_T of the matrix material must be higher than the E_T of the phosphorescent emitter. This fact is making the use of high- E_T materials imperative to confine the triplet excitons in the emitter. Relying on the fact that CBP ($E_T = 2.56$ eV) is a suitable matrix for green phosphorescent emitters like Ir(ppy)₃, the scaffold of the CBP backbone provides the structural base. According to the triplet energy of the commonly used blue phosphorescent emitter used FIrpic, E_T values higher than 2.75 eV are required.
- ii) Good charge carrier transport properties are required for enabling facile charge injection from the adjacent layers. Balanced charges in the emitting layer and prevention of charge accumulation, determine the efficiency of the OLED.
- iii) It is crucial to reduce the driving voltage for charge injection due to appropriate aligning of the frontier orbitals of the host molecules with the hole transport layer (HTL) and electron transport layer (ELT). This can be achieved by functionalization of the carbazole subunit with electron donating (+I effect) or electron withdrawing (-I effect) substituents shifting the HOMO and LUMO energy levels.
- iv) The glass transition temperature is responsible for a phase separation within a pOLED device and therefore also effecting the operational lifetime considerably. CBP shows a relatively low T_g value that originates from the intermolecular π - π interactions of the biphenyl-carbazole junction resulting in relative low thermal and morphological stability of the device. These interactions are reduced by the combination of all these features mentioned above. The spatial demanding substituents mounting on the carbazole and the

almost perpendicular orientation of the carbazole and biphenyl subunit will decrease intermolecular π - π interaction and therefore increase the glass transition temperature.

The aim of this work was to design, synthesize, and study a series of CBP derivatives as potential candidates of host material in blue emitting phOLEDs (Scheme 5).

CBP derivatives **1** and **2** are investigated to freeze the conjugation between the biphenyl backbone and the carbazole subunits. Target structures **3** and **4** have been envisaged to compare the difference in properties if the electron-withdrawing substituent is introduced either at the positions 3 and 6 (**3**) or positions 2 and 7 (**4**) of the carbazole subunits. To complete the series compound **5**, bearing electron-donating moieties will be synthesized.



Scheme 5: Series of CBP derivatives as potential candidates of host material in blue emitting OLEDs.

Molecular Design

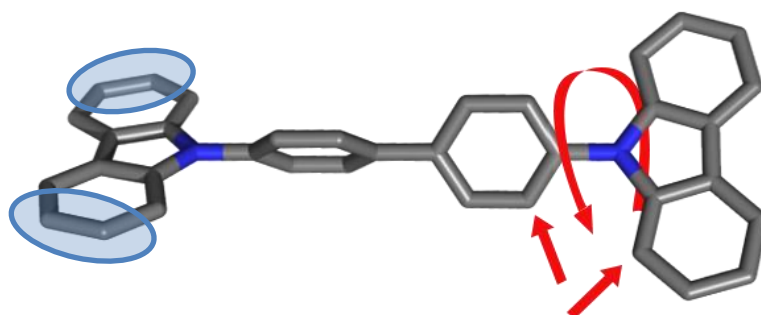


Figure 8: Molecular design of the compound bearing features required for high triplet energy matrix material in blue emitting OLEDs. Introducing spatial demanding methyl groups in the positions 3, 5, 3', and 5' leads to an inter-planar twist between the carbazole subunit and the biphenyl backbone. Functionalization of the carbazole synthon with electron-withdrawing or electron-donating groups in the positions 2 and 7 or positions 3 and 6 induces a shift of the HOMO and LUMO levels.

The requirements mentioned before are provided by different structural features of the molecule of interest (Figure 8). The specific parts of the structural motives addresses the requirements as followed:

Introducing spatial demanding methyl groups in the 3,3',5,5'-positions of the biphenyl backbone or at the positions 1 and 8 of the carbazole subunit will introduce an inter-plane twisting angle between these subunits leading to an almost perpendicular orientation between the two subunits. This interrupted charge conjugation throughout the whole rod will promote a higher triplet energy of the matrix material (Figure 8, red arrows).

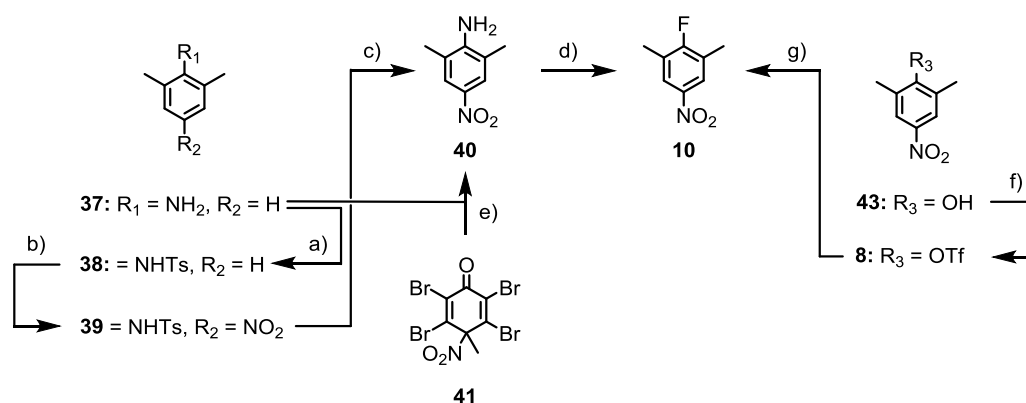
Relying on the good hole transport mobility of CBP and *m*CP the facile and balanced charge injection from the neighboring layers will be provided by the structural backbone. The alignment of the HOMO and LUMO level with the adjacent HTL and ETL will be achieved by functionalization of the carbazole subunit with electron donating (+I effect) or electron withdrawing (-I effect) shifting the HOMO and LUMO energy levels (Figure 8, blue cycles).

To increase thermal and morphological stability intermolecular interactions have to be reduced. The spatial demanding substituents mounting on the carbazole and the almost perpendicular orientation of the carbazole and biphenyl subunit will decrease intermolecular π - π interaction and therefore increase the glass transition temperature.

Results and Discussion

Synthesis

Synthesis of Fluoro-2,6-dimethyl-4-nitrobenzene (10)

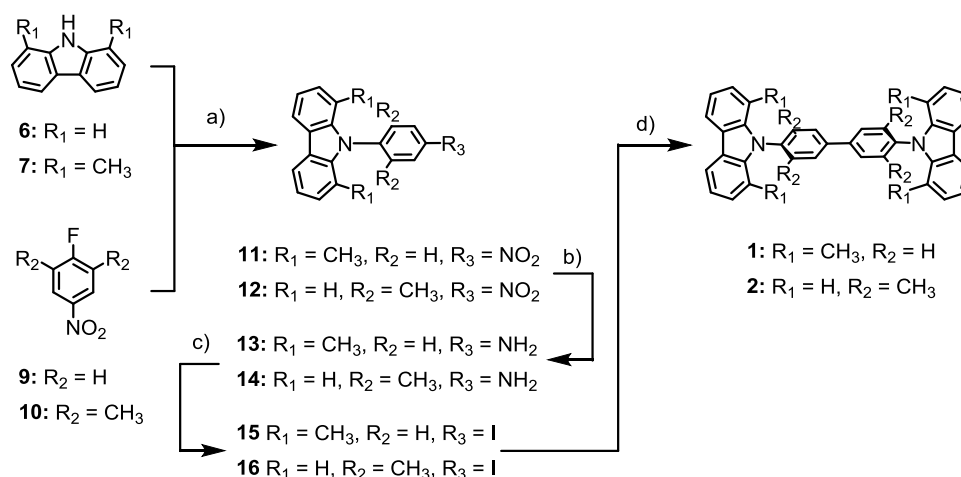


Scheme 6: Synthesis of building block **10**. Reaction conditions: a) *p*-TsCl, pyridine, 115 °C, 2 h, 93%; b) NaNO₂, nitric acid, acidic acid, water, 90 °C, 4 h, 59%; c) H₂SO₄, 50 °C, 2 h, 36%; d) HF-pyridine, NaNO₂, -15 °C, 3 h, 88%; e) EtOH, 0 °C – rt, 4 h, 12%, f) TfO₂, pyridine, DCM, 0 °C, 1 h, 98%; g) [(cinnamyl)₂Pd]₂ (2.5 mol%), *tert*-BuBrettPhos (7 mol%), CsF, MePh, 110 °C, 24 h, 93%.

Since large amounts of fluoro-nitro **10** were required within this project, a fast and high yielding synthesis of **10** was investigated in various strategies. Firstly, a literature known procedure was followed, starting from the commercially available 2,6-dimethyl aniline (**37**).^[90] The nitro-aniline **39** was successfully transformed into the desired fluoro-nitro compound **10** using a Balz-Schiemann reaction with HF-pyridine as fluorine source.^[91] Nevertheless, this pathway includes several issues, such as low yielding steps as well as difficulties when these reactions were performed in a larger scale. The tosylation of 2,6-dimethyl aniline provided protected amine **38** in excellent yield (93%). Notably, the nitration step remains challenging since performing this reaction on a large scale dropped the yield tremendously and was therefore investigated for improvements. As the undesired oxidation of the protected amine was observed in the nitration-step, the use of different protecting groups (e.g., acetyl, benzyl) and different nitration reagent (e.g., pure HNO₃, AgNO₃) were investigated. However, no significant improvement has been achieved so far. A very promising approach was carried out by Arnatt and co-workers using tetra bromo **41** as nitration reagent.^[92] This is in particular interesting since a direct nitration of dialkyl-

substituted anilines in *para*-position via radical nitration pathway is enabled. Unfortunately, also this approach was not satisfying, providing the nitro-aniline **40** in low yield. Successful synthesis fluoro-nitro compound **10** was achieved in a high yielding three-step synthesis. Starting from the commercially available 2,6-dimethyl-4-nitro phenol **43**. The phenolic alcohol was transformed into the triflate **8** using triflic anhydride and pyridine. According to a procedure reported by Buchwald and co-workers, a Pd-catalyzed fluorine insertion was successful replacing the triflate moiety by a fluorine, providing the fluoro-nitro compound **10** in excellent yield and multigram scale.^[93]

Synthesis of CBP Derivatives **1** and **2**

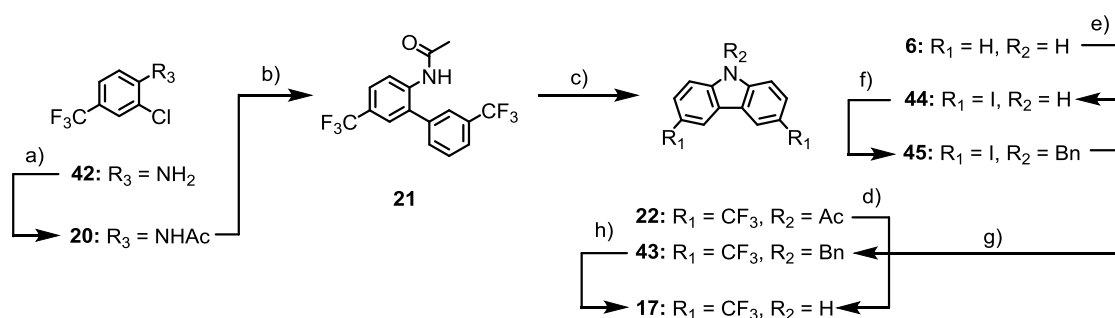


Scheme 7: Synthesis of target structures **1** and **2**. Reaction conditions: a) Cs₂CO₃, DMF, 12 h, 150 °C, **11** (86%), **12** (87%), b) SnCl₂ · 2H₂O, EtOH, reflux, 4 h, **13** (91%), **14** (94%); c) BF₃ · Et₂O, *tert*-butylONO, THF, KI, I₂, MeCN, -10 °C to rt, 12 h, **15** (75%), **16** (79%); d) Turbo Grignard, TEMPO, THF, -10 °C to rt, 2 h, **1** (96%), **2** (97%).

After screening of various nucleophilic aromatic substitution (S_NAr) reaction conditions, C–N bond formation between fluoro-nitro compound (**9** or **10**) and carbazole (**6** or **7**^[94]) was achieved in good yield of 86% (**11**) and 87% (**12**), respectively. Reduction of the nitro moiety with tin chloride provided amines **13** and **14**,^[95] which were further transformed into the corresponding iodides **15** and **16** using modified Sandmeyer reaction conditions.^[96] The homo-coupling of the aryl-iodides **15** and **16** afforded screening experiments, since classical Ullmann reaction conditions,^[97] alternative Cu(I)-sources,^[98] as well as immobilized Cu(II)-sources,^[99] did not provide the desired homo-coupled products in reasonable yields. To our delight, the insertion of the Grignard moiety via Knochel's Turbo Grignard reaction,^[100]

followed by the oxidative homocoupling using (2,2,6,6-tetramethylpiperidin-1-yl)oxyl (TEMPO) as co-oxidant,^[101] provided the desired CBP derivatives **1** and **2** in excellent yield of 96% and 97%, respectively. Optical and electronic properties have been analyzed and will be discussed below. An importing finding of these studies has to be already mentioned here, as it steered the molecular design and also the synthetic pathway of additional CBP derivatives, which were investigated within this project. Due to the fact, that the origin of the high triplet state energy arises from the rotational restricted biphenyl backbone only small differences in optical properties were observed by comparing **1** and **2**. These findings lead to the conclusion, that the spatial arrangement of the phenyl-carbazole junction is equally efficient whether the methyl groups are mounted at the carbazole (**1**) or at the biphenyl subunit (**2**). As mentioned before, also the HOMO or LUMO level of the matrix material has to be encountered, the methyl groups are maintained at the biphenyl backbone to profit from the not yet functionalized carbazole subunits in order to tune the optical properties of the CBP derivatives. If the methyl groups are attached at the biphenyl subunit, handling issues like solubility will be solved. This is strongly connected to the findings within the synthesis of the poorly soluble **1** compared to **2**.

Synthesis of 3,6-Substituted Carbazole

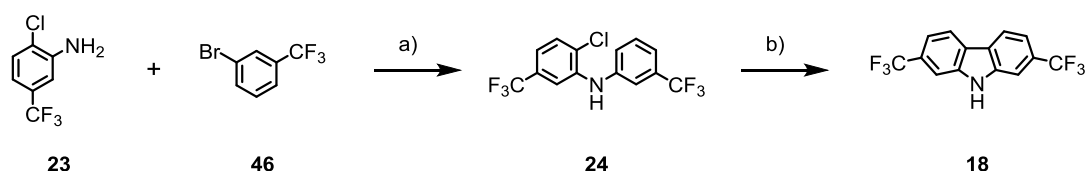


Scheme 8: Synthesis of carbazole **17**. Reaction conditions: a) AcCl, TEA, DCM, rt, 2 h, 91%; b) SPhos Pd G2 (2 mol%), 3-(trifluoromethyl)phenylboronic acid, K₃PO₄, THF : H₂O (20 : 1), 80 °C, 12 h, 93%; c) Pd(OAc)₂ (2mol%), Cu(OAc)₂ (20 mol%), MePh, 120 °C, 24 h, 98%; d) H₂SO₄ : MeOH (1:5), 80 °C, 0.5 h, quant; e) NIS, DCM : DMF (10 : 1), 40 °C, 20 h, 55%; f) NaH, benzyl bromide, DMF, rt, 12 h, 82%; g) CuI, CF₃COONa, NMP, 24 h, 170 °C, 21%; or AgF, TMSCF₃, CuCF₃, DMF, 4 h, rt, 26%; h) *tert*-ButyIOK, oxygen, DMSO, THF, 4 h, rt, 76%.

The functionalization of a carbazole at the positions 3 and 6 seems at first sight very straightforward. Nevertheless, some problems have to be solved for the CF₃-functionalization. Firstly, the iodine was introduced at the 3,6-position by treating carbazole

with *N*-iodosuccinimide in *N,N'*-dimethylformamide providing the carbazole **44** in moderate yield. Subsequent amine protection with benzyl bromide in *N,N'*-dimethylformamide yielded protected carbazole **45** in 82%. The transformation of the iodine into a CF₃ moiety was quite challenging although it is well known in literature.^[102,103] In analogy to a literature known procedure sodium CF₃-carboxylate was used as source as a CF₃-source combined with high boiling solvents and a Cu(I)-source.^[102] These trifluoromethylation reaction conditions are not very satisfyingly, due to no reproducibility of the conversion into the desired compound **43**. Using a combination of AgF, trimethylsilyl-CF₃ and CuCF₃ as trifluoromethylation reaction conditions appeared very promising.^[103] One has to mention that these reaction conditions have one big drawback. Firstly the undesired perfluoroalkylation is very hard to detect by common analyzing methods like ¹H NMR. Secondly the separation of the perfluoroalkylated from trifluoromethylated carbazoles was exclusively possible by using size exclusion chromatography techniques (e.g., gel permeation chromatography [GPC]). Since large quantities of the CF₃-crabazole **17** are required, this synthetic strategy was not considered. By following another strategy towards the 3,6-carbazole **17**, the CF₃-moieties were introduced at the very beginning starting from the commercial available 2-chloro-4-(trifluoromethyl)-aniline (**42**). In analogy to a literature known reaction sequence, acetyl protection of the amine afforded **20** in excellent yield.^[104] The diaryl **21** was obtained in 93%, applying a Suzuki–Miyaura cross-coupling protocol. The key step of this reaction sequence was a tandem C–H functionalization and C–N bond formation yielding acetyl-protected carbazole **22**. The deprotection of the acetyl moiety in a solvent mixture of sulfuric acid and methanol provided desired carbazole **17** not only in high yield but also in large quantities.

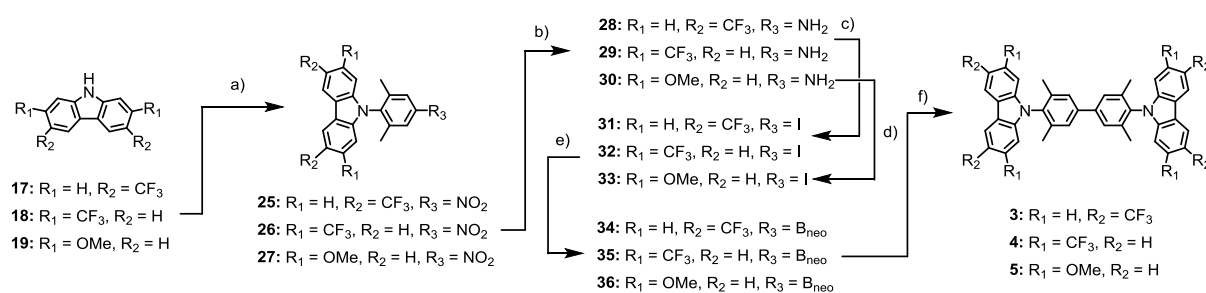
Synthesis of 2,7-Substituted Carbazole



Scheme 9: Synthesis of carbazole **18**. Reaction conditions: a) Pd₂(dba)₃, BINAP, NaOtBu, MePh, 90 °C, 12 h, 93%; b) NaOtBu, [HPtBu₃][BF₄], Pd(OAc)₂, MePh, 160 °C (MW), 3 h, 81%.

Initial attempts to synthesize carbazole **18** based on a one-pot tandem Buchwald–Hartwig reaction, C–H functionalization, C–C bond-formation reaction sequence were not satisfying.^[94] Even after extensive screening of various reaction conditions, isolation of the desired carbazole **18** was not successful. However a stepwise reaction protocol by coupling the commercially available aniline **23** and 1-bromo-3-(trifluoromethyl)benzene (**46**) provided diaryl **24** in good yield. It has to be mentioned that this Buchwald–Hartwig reaction turned out to be very sensitive due to competitive amination of the chloro aryl at temperatures above 90 °C. For the stepwise reaction approach, the diaryl product **24** was filtered through Celite® plug and was used without further purification. Subsequently, the desired 2,7-CF₃ carbazole **18** was formed via C–H functionalization and C–C bond formation in excellent yield of 81% as well as large quantities.

Synthesis of CBP Derivatives 3 – 5



Scheme 10: Reaction conditions; a) Cs₂CO₃, **10**, DMF, 12 h, 150 °C, **25** (82%), **26** (78%), **27** (86%); b) SnCl₂ · 2H₂O, EtOH, reflux, 4 h, **28** (92%), **29** (93%), **30** (97%); c) BF₃ · Et₂O, *tert*-BuONO, DCM, KI, I₂, -10 °C to rt, 12 h, **31** (82%), **32** (90%); d) PTSA, NaNO₂, KI, MeCN, H₂O, 10 °C, 2 h, **33** (83%); e) Turbo Grignard, B(O^{*i*}Pr)₃, neopentyl glycol, THF, -10 °C to rt, 12 h; f) SPhos Pd G2 (2 mol%), K₃PO₄, THF : H₂O (20:1), 60 °C, 12 h, **3** (95%), **4** (93%), **5** (97%) over 2 steps.

The remaining carbazole **19** was synthesized in analogy to a literature known procedure.^[105] Having all the required carbazoles in hand, assembly strategy of **2** was followed as close as possible. Therefore, fluoroaryl **10** was coupled via S_NAr reaction with the carbazoles **17** – **19**, yielding nitrophenylcarbazoles **25** – **27** in good yields around 80%. The nitro groups were subsequently reduced to the amines **28** – **30**,^[95] which were directly subjected to modified Sandmeyer reaction conditions.^[96] While the conditions were successfully applied for the CF₃-derivatives **28** and **29** providing iodoaryls **31** and **32** in good yield, they failed in the case of the methoxy-derivative **30**. This observation is attributed to the methoxy group that most likely will be attacked by the BF₃-etherate resulting in the liberation of the phenolic

substituents. However, applying Sandmeyer conditions developed by Knochel and co-workers, iodoaryl **33** was isolated in 83%.^[106] Unfortunately, the homo-coupling reaction conditions developed for **2**, provided **3** and **4** in poor yield and failed completely for **5**. A more successful approach was the transformation of the iodophenyl carbazoles **31** – **33** into the corresponding boronic esters **34** – **36**^[107] that were exposed without purification to a Suzuki–Miyaura cross-coupling reaction conditions together with equimolar amounts of their iodoaryl precursors **31** – **33**. The desired CBP derivatives **3** – **5** were isolated in excellent yields above 90% over two steps. All target CBP derivatives **1** – **5** and their precursors were fully characterized by ¹H and ¹³C NMR spectroscopy, mass spectrometry (MS), and elemental analysis (EA). The identity of the CBP derivatives **2** – **4** was further corroborated by their solid-state structures obtained by X-ray diffraction of suitable single crystals. Optical and electronic properties of the target compounds will be discussed in the course of this thesis.

Structural Properties

Solid-state structures of **2** – **4** that were obtained by X-ray analysis are shown in figure 9.

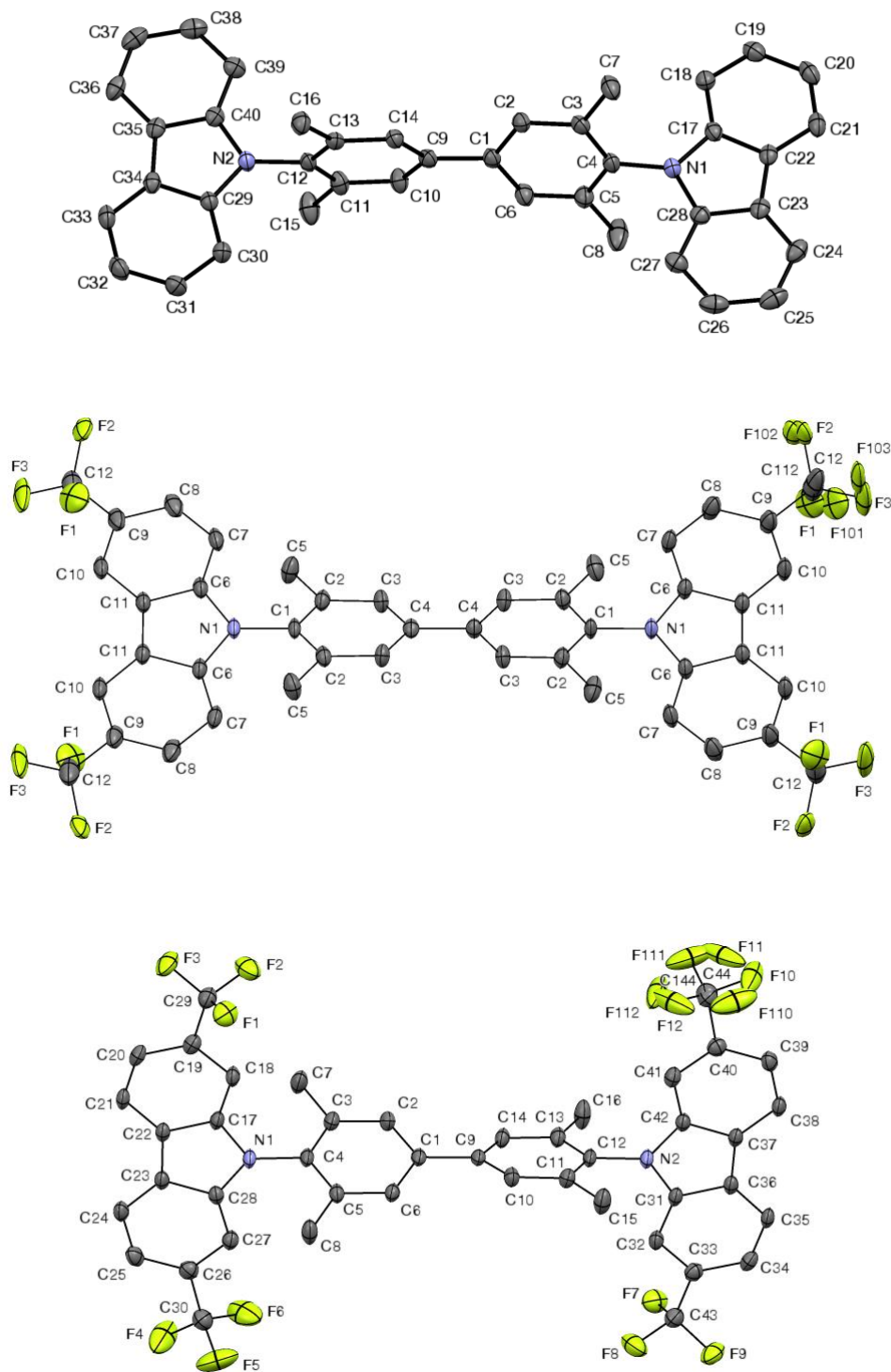


Figure 9: Solid-state structure of the CBP derivatives **2** – **4**.

Suitable crystals for X-ray diffraction analysis were obtained by dissolving CBP derivatives **2**, **3**, and **4** in a solvent mixture of methylene chloride and hexane (1 : 1) followed by slow evaporation in the dark. Of particular interest in these interlocked CBP derivatives were the two inter-planar twist angles between the biphenyl and carbazole subunit (α between green and orange plane, β between blue and grey plane, see Figure 10). For completeness the inter-planar twist angle was calculated by density functional theory (DFT) for the compounds **1**, **2**, and **5** using B3LYP hybrid functional theory using a 6-31G* basis set in Spartan 10. Being aware of the comparability for the obtained twist angles, due to the fact that in the obtained X-ray structures, effects of intermolecular packing are considered as well, the calculated molecular structures provide good ideas about the spatial arrangement of their subunits. The inter-planar twist angles of the CBP derivatives **1** – **5** are summarized in table 2.

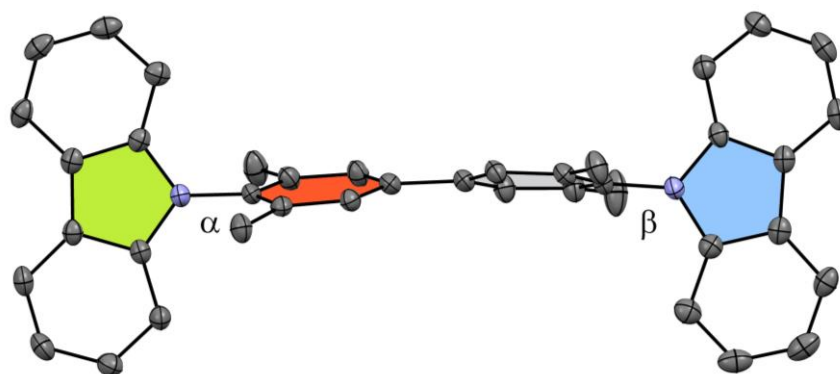


Figure 10: Solid-state structure of **2**. The inter-plane angle between the central carbazole ring (green) and the connected biphenyl ring (orange) is α and the one between the biphenyl (grey) and the carbazole ring (blue) is β .

As expected all CBP derivatives show an inter-plane torsion angle larger than the parent compound CBP. This was attributed to the methyl groups attached to the carbazole subunit or biphenyl backbone. For all derivatives inter-plane angles larger than 75° are found, indicating a very limited interaction between the electron clouds of neighboring aromatic subunits. In other words, the large angles break the π -electron conjugation along the molecule's axis. Compound **2**, mounting the four methyl groups at the biphenyl subunit, crystallizes in a non-standard monoclinic $P2_1/n$ space group and thus, the inter-plane angles of 85.05° (α) and 75.81° (β) differ from each other. Comparing the calculated values of 82.84° (α) and 80.12° (β) an inhomogeneity was observed but still in well agreement with

the values obtained from the solid-state structure. Analyzing the calculated values of compound **1**, almost perpendicular inter-plane angles were obtained for both angles 89.96° (α) and 89.93° (β), respectively. This may originate from the methyl groups attached at the positions 1 and 8 of the carbazole subunits notably, having a stronger influence on the twisting angle. A centro-symmetric orthorhombic space group *Fddd* was obtained for compound **3** and thus the inter-plane angles α and β are the same, both being 88.96°. CBP derivative **4** crystallizes in the triclinic space group $P\bar{1}$, and its inter-plane twist angles of 79.67° (α) and 76.66° (β) are decreased compared to **3**.

Table 2: Data obtained from X-ray diffraction analysis or using B3LYP hybrid functional theory using a 6-31G* basis set in Spartan 10.

compound	crystal system	space group	inter-plane twist angle (α/β)°	lattice parameter		
				a (Å)	b (Å)	c (Å)
CBP ^[108]	monoclinic	<i>P2₁/c</i>	49.5/49.5 ^b	8.0120(4)	16.0080(7)	10.2428(5)
1	–	–	90.0/89.9 ^a	–	–	–
2	monoclinic	<i>P2₁/n</i>	85.1/75.8 ^b 82.8/80.1 ^a	12.2971(7)	7.6414(5)	31.6860(19)
3	orthorhombic	<i>Fddd</i>	89.0/89.0 ^b	6.9076(3)	25.8233(11)	41.998(2)
4	triclinic	$P\bar{1}$	79.7/76.7 ^b	8.6414(5)	9.2900(6)	23.1385(15)
5	–	–	90.0/89.5 ^a	–	–	–

^aData obtained from geometry optimizations at the B3LYP/6-31G* level of theory. ^bData obtained from X-ray crystal structure.

This effect was attributed to the attached CF₃-groups, which are further away from the CBP axis in the positions 3 and 6 compared to the positions 2 and 7. Intuitively one might thus argue that they have a bigger lever to flatten the molecule during packing in the solid state. The calculated inter-plane angles for **5** are almost perpendicular for both angles with 89.95° (α) and 89.44° (β).

Thermal Properties

To implement these structures in an OLED device, thermal stability, and in particular, glass transition temperatures (T_g) are investigated in this section. CBP has a major drawback exhibiting a T_g value of only 62 °C.^[109,110] This low glass transition temperature leads to a phase separation in the matrix layer and therefore decreasing the lifetime of such an OLED device tremendously. Measurements were recorded on a Perkin Elmer DSC Advanced Double-Furnace 8000 using scanning rates of 10 °C · min⁻¹, and the glass transition temperature (T_g), crystallization temperature (T_c) and melting point (T_m) were obtained from the second scanning cycle (Figure 11).

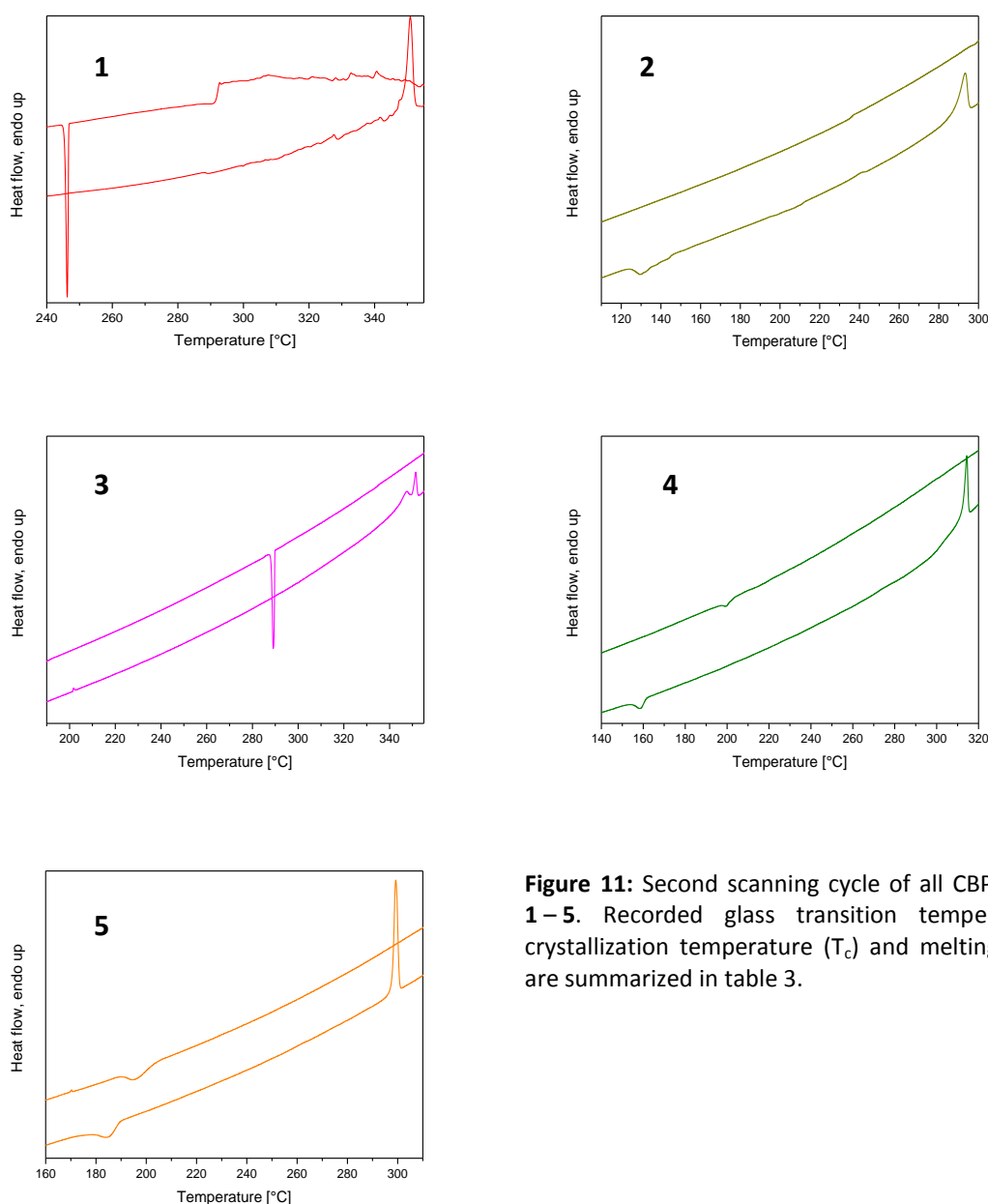


Figure 11: Second scanning cycle of all CBP derivatives 1–5. Recorded glass transition temperature (T_g), crystallization temperature (T_c) and melting point (T_m) are summarized in table 3.

The properties of the parent CBP were also recorded to calibrate the experimental set-up and its recorded T_m , T_c , and T_g values are in very good agreement with the literature.^[109,110] All recorded temperatures for compounds **1** – **5** are summarized in table 3. Since the glass transition temperatures were of particular interest in this series, these values will be discussed first. For the investigated series, the highest T_g value of 202 °C was observed for compound **3**. To the best of our knowledge, this is one of the highest literature reported T_g value for a CBP based compound.^[55,82,109,111,112]

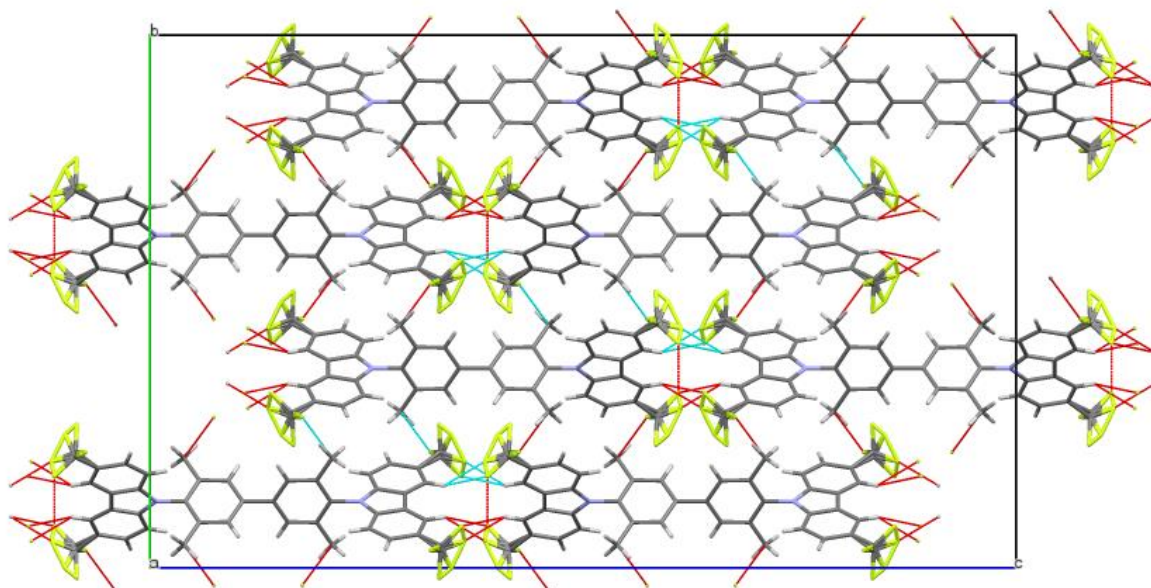


Figure 12: Crystal structure of **3** viewed along the a axis showing short intermolecular C-H...F-C contacts indicated by cyan lines and C...C contacts indicated in red.

This high T_g value is attributed to the spatial arrangement within the solid-state crystal structure (Figure 12). The methyl groups at the biphenyl backbone induce an almost perpendicular angle between the carbazole and the biphenyl unit. Furthermore, the phenyl units themselves are not aligned in a uniform plane. Additionally, the electron withdrawing CF_3 -substituents prevent a successful π - π stacking, by reducing the intermolecular interaction of both subunits. The scanning cycle of compound **2** revealed a T_g value of 129 °C already twice as high as for parent compound CBP. Unfortunately, no clear T_g value could be determined for compound **1**, even after several attempts of different scanning cycles. By

attaching the CF₃-moiety at the positions 3 and 6 the obtained T_g value dropped for compound **4** compared to **3** still being satisfying 158 °C. Notably, the methoxy CBP derivative **5** provides also a high T_g value of 184 °C. This increase of all T_g values is attributed to the methyl groups inducing an inter-plane twist and furthermore increase the capability of remaining in the amorphous state at higher temperatures. No trend could be observed for the functionalization of the carbazole subunit by attaching either electron-donating or withdrawing groups. Nevertheless, all compounds **3–5** performing higher T_g values compared to compound **2**, a marginal influence can be concluded as well due to the spatial demanding groups.

Table 3: Results of DSC measurements.

compound	melting point ^b , T _m (°C)	crystallization temperature ^b , T _c (°C)	glass transition temperature ^b , T _g (°C)
CBP	288 ^a	196 ^a	66 ^a
1	351	246	–
2	293	236	129
3	348	289	202
4	314	199	158
5	299	196	184

^aCBP values are in good agreement with the literature.^[109,110] ^bMelting point, crystallization temperature and glass transition temperature were obtained from the second heating/cooling scan using a scan rate of 10 °C min⁻¹.

By analyzing the T_m values of the target compound **1–5** similar values 351 °C and 348 °C were observed for **1** and **3**, respectively. Compound **4** also revealed a T_m higher than 300 °C, whereas compound **2** and **5** provided slightly decreased values of 293 °C and 299 °C, respectively. The stability at high temperatures was confirmed by repetitive heating scans, starting at 20 °C and ending at 400 °C. Due to no significant shift of the T_m value for the whole series, a high thermal stability can be attributed to all compounds **1–5**. This improved thermal stability is important for their potential application in OLED devices.

Photophysical Properties

Investigations of optical properties by UV-vis absorption and fluorescence spectroscopy of the CBP series **1** – **5** are summarized in table 4. UV-vis absorption spectra were measured in aerated methylene chloride solution at concentration of 10^{-5} M. Recorded UV-vis and emission spectra are shown in figure 13. To get a better understanding of the different absorption bands and to which subunit they can be assigned to, the literature known CBP is analyzed first. The longest wavelengths absorption bands at $\lambda_{\text{max}} = 293$ nm and $\lambda_{\text{max}} = 340$ nm for CBP were assigned to the π - π^* transition carbazole subunit.^[113,114]

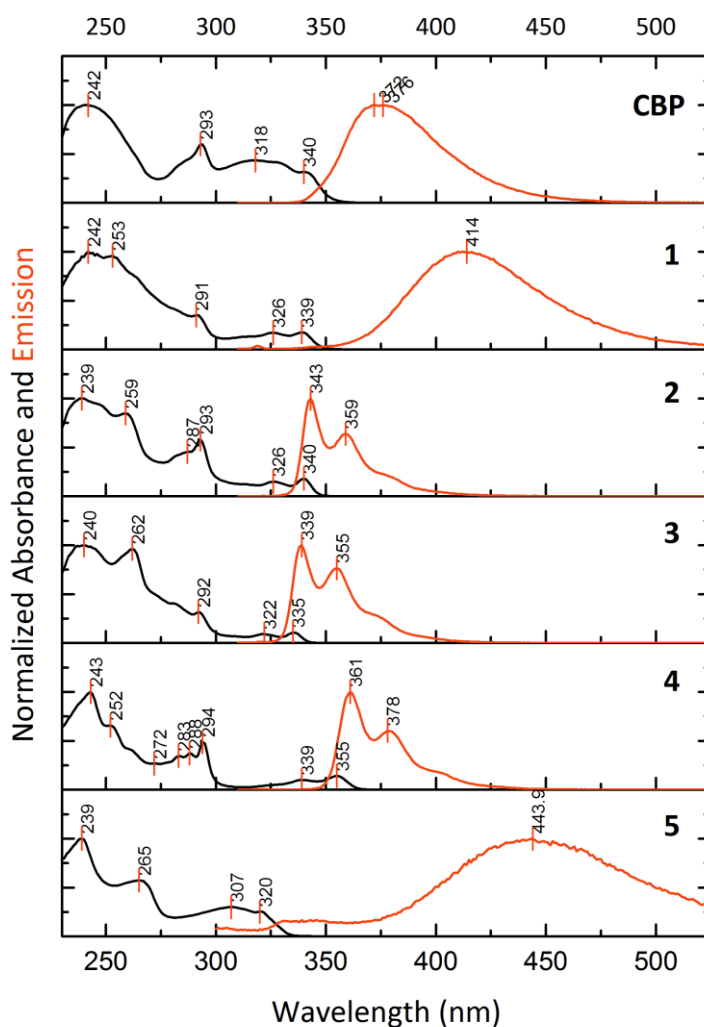


Figure 13: UV-visible (black line) and emission spectra (orange lines) of CBP and CBP derivatives **1** – **5** in methylene chloride solution (10^{-5} M).

The broad absorption range between $\lambda_{\text{max}} = 318$ and 340 nm can be attributed to the charge transfer between the biphenyl backbone and the carbazole subunit. In order to understand how the methyl groups attached at the carbazole subunit or mounting at the biphenyl backbone influences the inter-plane angle, and therefore the UV-vis absorption spectra compounds **1** and **2** are explained first. For both compounds **1** and **2** absorption maxima at $\lambda_{\text{max}} = 293$ nm and $\lambda_{\text{max}} = 340$ nm was observed, according to the orbitals centered at the carbazole subunit. As expected the methyl groups decrease π -conjugation throughout the rod and therefore the intensity of the broad absorption band at $\lambda_{\text{max}} = 318$ nm is decreased as well compared to parent compound CBP. Thus, this signal can be considered as a measurement of the conjugation between the orbitals centered at the biphenyl backbone and the carbazole subunit.^[82,111,115] The influence of the different substitution pattern was investigated by attaching the electron withdrawing CF_3 -groups at the positions 3 and 6 (**3**) or at the positions 2 and 7 (**4**). Compound **3** shows a similar absorption maxima localized at $\lambda_{\text{max}} = 292$ nm and $\lambda_{\text{max}} = 335$ nm compared to **2**. For compound **4** the absorption band at $\lambda_{\text{max}} = 295$ nm is comparable, however the second carbazole centered absorption band is bathochromically shifted by 20 nm compared to **3**. This difference in absorption might be rationalized with the effect of an increased conjugation over both two CF_3 -groups in **4**. A similar effect has been shown by a pioneering work of Leclerc and co-workers, where they compared an extended conjugation in poly-2,7-carbazole comprising a rigid poly-*para*-phenylene backbone compared to the poly-3,6-carbazole.^[116] Furthermore, the transition ($\lambda_{\text{max}} = 300 - 320$ nm) between the biphenyl- and carbazole subunit is weak for both compounds **3** and **4**, supporting the hypothesis of a frozen flexibility and a perpendicular arrangement of both subunits at the carbazole-biphenyl junction. Exchanging the electron withdrawing CF_3 -groups of **4** with electron donating methoxy groups **5** resulted as expected in a blue shift of the absorption maxima of the carbazole centered orbitals ($\lambda_{\text{max}} = 265$ nm and 320 nm).

In the fluorescence spectra, compound **1** revealed similar structureless emission with a maximum at $\lambda_{\text{max}} = 374$ nm and 414 nm for CBP and **1**, respectively. The red shift of the emission maxima for **1** can be assigned to the methyl groups mounting at the carbazole subunit. In contrast to the broad emission spectra of **1**, a well resolved emission was observed for compound **2**. One can argue that the insertion of the methyl groups at the

biphenyl backbone induces the large blue shift of the fluorescence ($\lambda_{\text{max}} = 343 \text{ nm}$). Notably, due to a strong twist the π -conjugation between the biphenyl and the carbazole center decreased. Compound **3** pronounces a similar emission profile compared to **2**, which is however marginally blue shifted by 4 nm.

Table 4: Data of UV-vis, fluorescence, and quantum yield measurements.

compound	UV-vis ^a λ_{max} (nm)	ϵ^a ($\text{L} \cdot \text{mol}^{-1} \cdot \text{cm}^{-1}$)	UV-vis ^a λ_{onset} (nm)	E_g^b (eV)	emission ^a λ_{max} (nm)	quantum yield Φ_F (%)
CBP	242	75380	352	3.52	374	78.9
	293	45120				
	318	32700				
	340	23780				
1	242	102530	348	3.56	414	8.5
	253	98460				
	291	35920				
	326	17540				
	339	18160				
2	239	76690	347	3.57	343	36.9
	259	64920				
	293	44660			359	
	326	11430				
	340	13880				
3	240	111570	342	3.63	339	2.6
	262	107390				
	292	35300			355	
	335	12010				
4	243	170210	364	3.41	361	15.4
	294	83235				
	339	17050			378	
	355	23830				
5	239	107650	334	3.71	444	1
	265	61700				
	307	32500				
	320	27240				

^aAll data were collected in dilute dichloromethane solution at room temperature. ^b $E_g = 1240/\lambda_{\text{onset}}$.

Interestingly, the emission pattern of **4** remains similar but pronounces a fluorescence band that is strongly red shifted by 22 nm compared to **3**. This was attributed as well to the stronger conjugation of both CF₃-moieties at the 2,7-position. By analyzing the emission spectra of **5** the fluorescence band appears at $\lambda_{\text{max}} = 444$ nm. This broad bathochromically shifted band may point at excited state intramolecular charge transfer (ICT) with the carbazole unit acting as donor and the biphenyl scaffold as acceptor.^[117]

Recorded fluorescence quantum yield (Φ_F) of the carbazole series **1** – **5** are summarized in table 4. Measurements were performed in a diluted methylene chloride solution using a Hamamatsu Quantaurus-QY integrated sphere fluorimeter. In summery, one can comment a relative low quantum yield throughout the whole series compared to CBP, concluding an enhanced triplet yield in these derivatives.

Phosphorescence spectra of the series **1** – **5** were recorded in aerated and frozen 2-methyltetrahydrofuran solutions at 77 K with a concentration of 10⁻⁵ M using gated steady state conditions. The corresponding spectra of CBP and **1** – **5** are displayed in figure 14. In respect to potential matrix material in blue emitting phOLEDs triplet energies were determined according to $E_T = 1240/\lambda_{\text{phos}}$ from the highest energy peak of the phosphorescence spectra and are summarized in table 5.

Table 5: E_T values obtained from gated steady state phosphorescence measurements.

compound	phosphorescence ^a λ_{phos} (nm)	E_T ^b (eV)
CBP	459	2.7
1	451	2.75
2	432	2.87
3	444	2.79
4	420	2.95
5	431	2.88

^aTriplet energies of **1** – **5** were measured in 2-MeTHF glass matrix at 77 K. ^b $E_T = 1240/\lambda_{\text{phos}}$.

To our delight for all investigated CBP derivatives **1** – **5** triplet state energies were observed. Furthermore, E_T values ranging from 2.75 eV to 2.95 eV are all higher comparing with parent compound CBP (2.7 eV). Since the values do not differ tremendously two conclusions are stated.

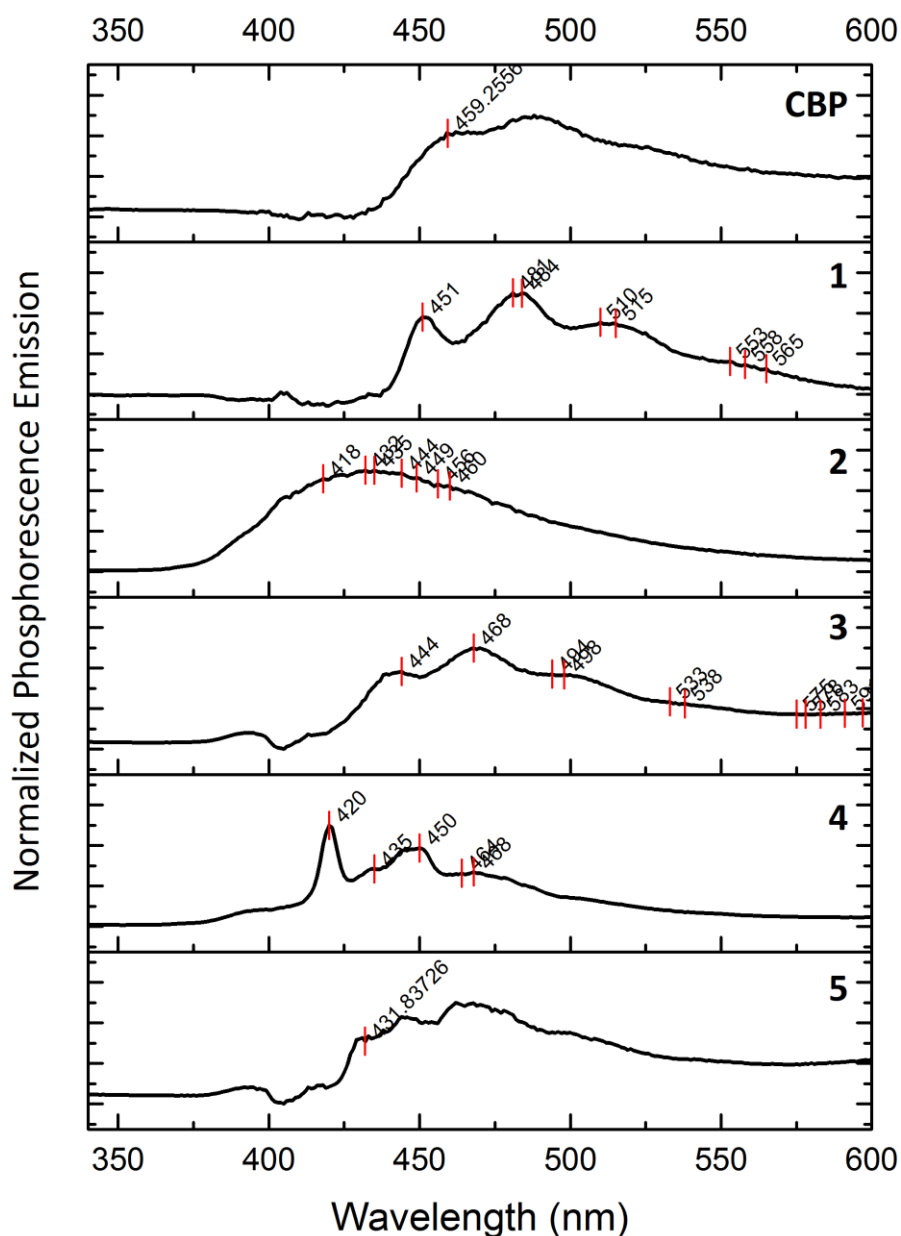


Figure 14: Gated phosphorescence spectra of the carbazole derivatives **1** – **5** in 2-MeTHF glass matrix at 77 K.

As expected the carbazole and biphenyl subunit are efficiently decoupled, leading to higher triplet state energies. Secondly, the hypothesis that the triplet state will mainly be located on the fragment with the lowest triplet energy can be confirmed, since E_T values are not affected by varying the substitution pattern on the carbazole and is in well agreement with the literature reported values of 3.1 eV for N-ethylcarbazole^[118] and 2.9 eV for biphenyl.^[119] This blue shift of the phosphorescence makes these CBP derivatives **1 – 5** with interlocked carbazole-biphenyl junctions interesting host materials for blue phosphorescent emitters.

Electrochemical Properties

In order to obtain the HOMO and LUMO levels, electrochemical properties of the series **1 – 5** were of particular interest. Therefore, *in vacuo* calculations of **2** using Spartan10 using a density function method and a B3LYP 6-31G* basis set were performed (Figure 15). The results revealed that the HOMO is mainly located on the carbazole moiety, whereas the LUMO is almost exclusively localized on the biphenyl backbone. This clear localization of the frontier orbitals raised the hope that their energy levels might be tuned independently.

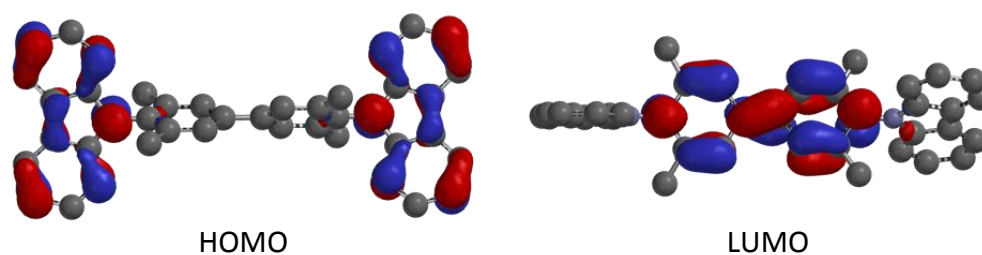


Figure 15: Calculated HOMO and LUMO of **2** using a density function method using a B3LYP 6-31G* basis set.

To characterize the electrochemical properties of the CBP derivative series **1 – 5**, cyclic voltammograms (CV) were performed with an AutoLab PGSTAT302 potentiostat-galvanostat controlled by resident NOVA 9.1 software using a conventional single-compartment three-electrode cell. A Pt disk (diameter of 2 mm) served as working electrode, a Pt wire was used as auxiliary electrode, and the reference electrode was a saturated potassium chloride

calomel electrode (SCE). The supporting electrolyte was 0.15 N Bu₄NPF₆ in methylene chloride. All potentials are quoted relative to SCE with ferrocene–ferrocenium at +450 mV as internal standard. In all the experiments the scan rate was 100 mV/s for cyclic voltammetry and the pulse frequency was 15 Hz for differential pulse voltammetry (DPV). Solutions were purged with argon to remove the oxygen and argon was passed over the solution during the experiment. The oxidation potentials for the series **1–5** were determined by DPV measurements (Figure 16). The obtained energy levels of the frontier orbitals are summarized in table 6. Notably, for none of the compounds reduction potentials were observed within the detectable window (recorded to –2.0 V/SCE). After the correction of the vacuum energy level (5.1 eV)^[120] the HOMO energy levels of the compounds were estimated by their oxidation potentials. Thus, the LUMO energy levels were obtained by adding the optical energy band gap (E_g) to the HOMO level ($E_{\text{LUMO}} = E_{\text{HOMO}} + E_g$).

Table 6: Energy levels of HOMO and LUMO.

compound	E_{ox} vs. Fc ⁺ /Fc (V)	$E_{\text{HOMO}}^{\text{a}}$ (eV)	$E_{\text{LUMO}}^{\text{b}}$ (eV)
CBP	0.87	–5.97	–2.45
1	0.8	–5.90	–2.34
2	0.92	–6.02	–2.45
3	1.37	–6.47	–2.85
4	1.36	–6.46	–3.05
5	0.56	–5.66	–1.95

^aPeak position of the first oxidation peaks and HOMO energy levels were calculated by their oxidation potentials after correction of the vacuum energy level (5.1 eV)^[120]. ^bLUMO energy levels were obtained by adding the optical energy gap ($E_{\text{LUMO}} = E_{\text{HOMO}} + E_g$).

Analyzing the frontier orbitals of **1**, the four methyl substituents mounting on both carbazoles at the positions 1 and 8 induce a slight lifting of the HOMO level due to the inductive electron donation (+I effect) compared to parent structure CBP. Interestingly the LUMO level is lifted by the same value in spite of the successful decoupling of carbazole-

biphenyl junction. As expected, when the methyl groups are attached at the biphenyl **2**, the energy levels for both the HOMO and the LUMO, are very comparable to the ones of CBP. Exchanging the methyl groups with electron withdrawing CF₃-substituents (-I effect) in **3** and **4** the oxidation potentials are increased by 450 mV and 440 mV, respectively, compared to **2** and lower the energy level of the HOMO considerably. These results are somehow invalidating the hypothesis of individually addressable energy levels of the frontier orbitals, as the LUMO levels for both compound **3** and **4** are shifted towards lower energy. Increase of the HOMO energy level was observed for the methoxy-substituted compound **5**, due to stronger +I effect lowering the oxidation potential by 360 mV compared to **2**. Also here, the other frontier orbital did not remain unaffected, according to the concomitant lifting of the LUMO level.

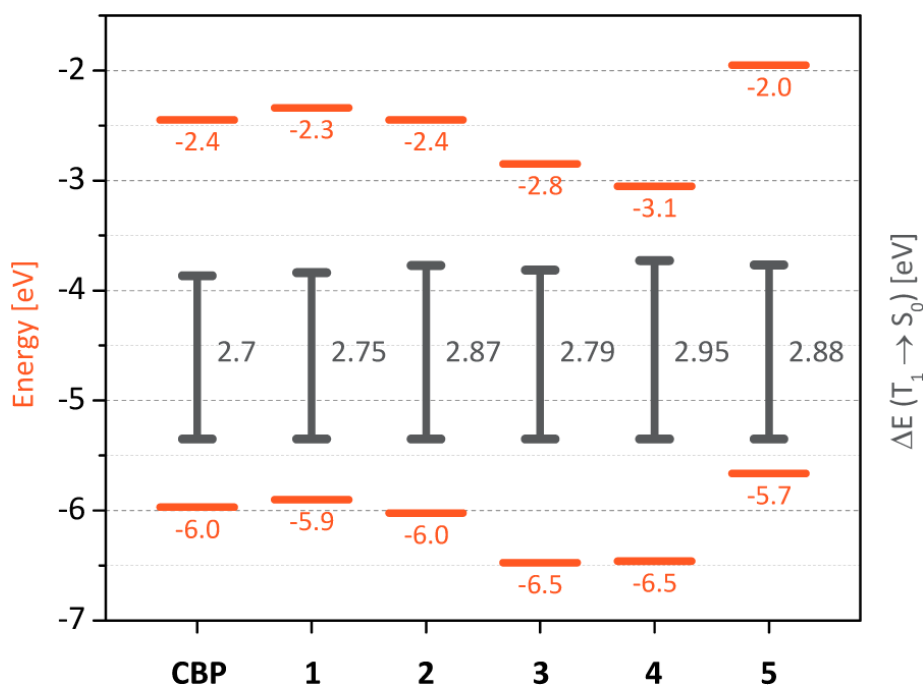


Figure 16: Energy diagram showing the position of the frontier orbital of the CBP derivatives (orange). The dark grey line displays the position of the triplet energies.

As the positions 3 and 6 of the carbazole subunit are not substituted, the CBP derivatives **1**, **2**, **4**, and **5** displayed an irreversible oxidation behavior in CVs. This observation is exemplified for **2** in figure 17 (left). The observation of an oxidation peak at about 1.5 V/SCE is assigned to the oxidation of the carbazole units. Lowering the potential in this cyclic measurement revealed the expected reduction peaks between 1.2 – 1.3 V, as well as an

additional well defined peak in the range between 0.9 – 1.0 V. This peak can be assigned to the generated radical cation localized at the 3,6-position of the carbazole after the oxidation. The proximity of radical cations at the electrode surface conducts an intermolecular coupling between the carbazole subunits resulting in an electrochemically irreversible oxidation. Repeating the oxidation cycle, the oxidation scan displays a new oxidation peak in the region between 1.05 V and 1.15 V/SCE according to the oxidation of the dimerization product accumulated at the Pt electrode. As expected, blocking of the reactive 3,6-position of the carbazole units, revealed a fully reversible oxidation behavior of compound **3** (Figure 17, right). This dimerization reaction has been reported for structurally related CBP derivatives^[82] and *N*-aryl carbazoles.^[121]

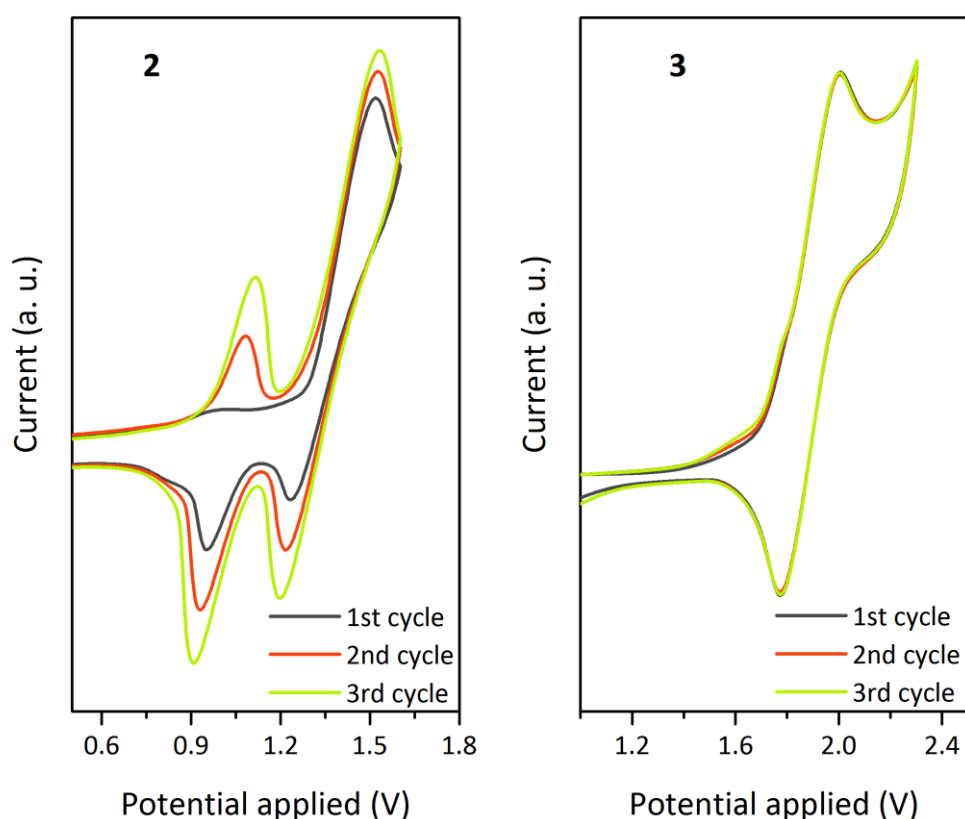


Figure 17: CV (three cycles, scan rate 100 mV/s, 10^{-3} M in methylene chloride) of **2** (left) and **3** (right) recorded against SCE.

The electrochemical studies led to the conclusion that the energy levels of these CBP derivatives can be tuned to some extent by varying the substituents. Nevertheless, the

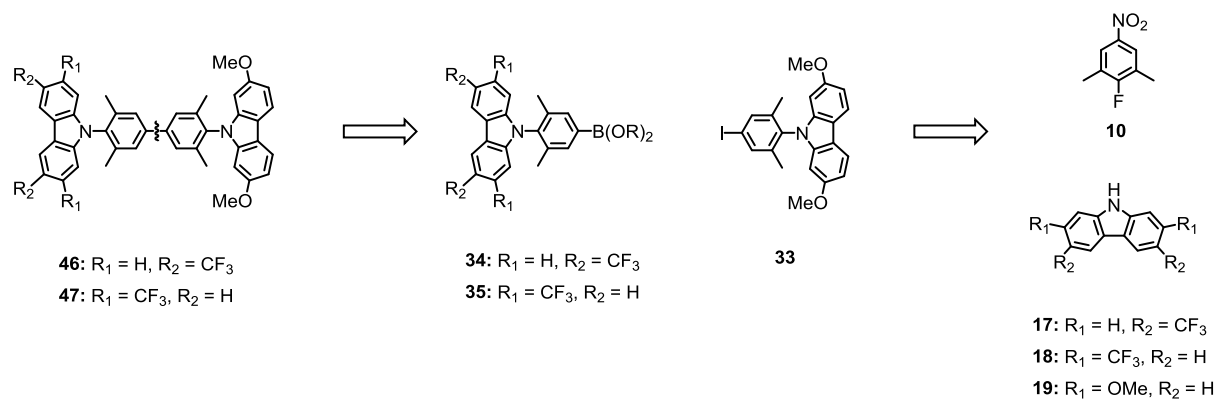
substitution pattern seems to affect the HOMO and LUMO levels not considerably. This capability of shifting the values of the frontier orbitals is particularly appealing involving them in multilayer OLED architectures. As radical ions are involved in charge transport pathways within the device, the functionalization of the carbazole subunit at the 3,6-position would include certain advantages due to its stability against electrochemical oxidation forming reactive radical anions.

Conclusion and Future Perspectives

The successful synthesis of CBP derivatives **1** – **5** with a twisted carbazole-biphenyl junction was achieved. Attachment of bulky substituents on the carbazole subunit or at the biphenyl backbone decreased π -conjugation throughout the rod. All compounds synthesized within this project are fully characterized. The assembled carbazoles, which have been synthesized in this course, were connected with the corresponding fluoro nitro compounds, affording N-*para*-nitrophenyl-carbazole precursors. The nitro moiety was transformed into the N-*para*-iodophenyl derivatives and subsequently dimerized either by Turbo Grignard reaction or by Suzuki–Miyaura type couplings, requiring in addition the corresponding boronic ester derivatives. The assembling of the N-*para*-nitrophenyl-carbazole precursors has been spotted as the key step in this synthetic strategy using S_NAr reaction conditions. The perfectly activated *para*-nitrofluorobenzenes allowed overcoming issues in coupling spatial demanding building blocks, providing a nitro moiety at the desired position readily available for further transformations. Noteworthy is also the synthesis of the CF_3 -substituted carbazole building blocks assembled by C–H activation using Pd-catalyzed environment. This work enables the synthesis of any possible substitution pattern of carbazoles bearing electronic withdrawing or donating substituents starting from the corresponding precursors. The almost perpendicular inter-plane twist angle, revealed by solid-state structures of the derivatives **2**, **3**, and **4** was corroborated by DFT calculations for **2** and **5**. To our delight all new CBP derivatives **1** – **5** displayed stability towards thermal degradation. Moreover, the long lasting amorphous state emphasizes the application potential of these CBP derivatives as matrix material in blue emitting OLEDs. This was attributed to the twisted angle between the carbazole and biphenyl subunit decreasing the capability of π – π interactions between these subunits. Additionally, the different substituents attached to the carbazole moiety seem to further enhance the amorphous steady state due to spatial demanding orientation. Derivatized CBPs with four methyl groups at the 3,3',5,5'-positions of the biphenyl backbone were pushed in the spotlight regarding the photophysical properties. Satisfyingly, the electron withdrawing CF_3 -substituents occupying the positions 3 and 6 (**3**) or positions 2 and 7 (**4**) of the carbazole unit, displayed a shift towards lower energy of the HOMO and LUMO level, whereas the electron donating methoxy-substituents stabilized the frontier orbital on an increased energy level. These findings are strongly supporting the hypothesis of the

capability of fine-tune the energy levels of the frontier orbitals by inductive effects. The remaining requirement of a matrix material in blue emitting OLEDs, the high triplet state energy, was fulfilled throughout the hole series showing all enhanced E_T values compared to parent compound CBP.

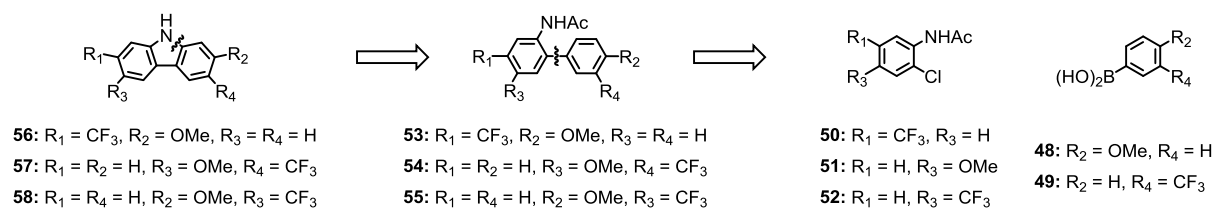
Having these *N-para*-iodophenyl **33** and *N-para*-boronic esters **34** and **35** derivatives in hand it would be very interesting to synthesize the corresponding asymmetric CBP derivatives **46** and **47** bearing on one side carbazoles, functionalized with electron-donating groups on one side, and on the other side electron-withdrawing groups, regarding photophysical properties. These bipolar host materials would express intra- or intermolecular charge transport properties in the excited state may affecting electronically properties in fluorescence and phosphorescence experiments (Scheme 11).



Scheme 11: Assembling strategy of asymmetric CBP derivatives **46** and **47**. Therefore the previously synthesized *para*-iodo precursor will be coupled in Suzuki–Miyaura protocol with the corresponding boronic esters **34** and **35**, which leads to the donor–acceptor CBP derivatives **46** and **47**, respectively.

Furthermore, having enabled the synthesis of substitute carbazole building blocks, the same synthetic strategy could be considered for the synthesis of a carbazole subunit bearing alternated substitution pattern (Scheme 12). For the syntheses of the carbazoles **56** – **58** the coupling between commercial available boronic acids **48** and **49** and the corresponding readily available chlorines **50** – **52** via a Suzuki–Miyaura protocol is envisaged. The C–H activation C–C bond formation using Pd-catalyzed reaction conditions leads to the acetyl-protected carbazoles, which could be deprotected in acidic environment yielding the carbazoles **56** – **58** substituted with an alternated pattern. Following the same assembling

strategy as developed for **3**, a new series of CBP derivatives could be synthesized may display interesting photophysical properties with high triplet state energies.



Scheme 12: Synthetic strategy of the carbazole building blocks **56** – **58** bearing alternating substitution pattern. The carbazole synthon will be synthesized in a Pd-catalyzed C–H activation C–N bond formation reaction. For the diaryl compounds **53** – **55** Suzuki–Miyaura reaction between the corresponding chlorines **50** – **52** and the commercially available boronic acids is considered.

Experimental Section

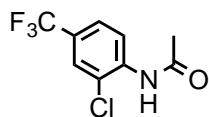
General Remarks

All commercially available compounds were purchased and used as received unless explicitly stated otherwise. CDCl_3 was purchased from Cambridge Isotope Laboratories, Inc. ^1H NMR was recorded on a Bruker DPX-NMR spectrometer operating at 400 MHz. ^{13}C NMR were recorded on a Bruker DPX-NMR spectrometer operating at 101 MHz. The chemical shifts are reported in parts per million (ppm) relative to tetramethylsilane or a residual solvent peak, and the J values are given in Hz. GC-MS was performed on a Shimadzu GCMS-2020 SE equipped with a Zebron 5 MS Inferno column which allowed to achieve temperatures up to 350 °C. High-resolution mass spectra (HRMS) were measured as HR-ESI-ToF-MS with a Maxis 4G instrument from Bruker with the addition of NaOAc. MALDI-TOF analyses were performed on a Bruker microflex system. For column chromatography, usually silica gel Siliaflash® p60 (40 – 63 μm) from Silicycle was used, and TLC was performed on silica gel 60 F254 glass plates with a thickness of 0.25 mm purchased from Merck.

UV-visible absorption spectra in DCM were recorded at room temperature on a Shimadzu UV-1800 spectrometer. Emission spectra were recorded on a Horiba Jobin-Yvon FluoroMax 4 fluorimeter. Gated emission spectra were recorded in frozen 2-MeTHF solution at 77 K, with a flash delay of 0.05 ms, a sample window of 60 ms and a time per flash of 70 ms. The flash count was set to 20 to increase S/N. The electrochemical measurements were performed with an AutoLab PGSTAT302 potentiostat-galvanostat controlled by resident NOVA 9.1 software using a conventional single-compartment three-electrode cell. A Pt disk of 2 mm \varnothing served as working electrode, as auxiliary a Pt wire was used and the reference electrode was a saturated potassium chloride calomel electrode (SCE). The supporting electrolyte was 0.15 N Bu_4NPF_6 in DCM. All potentials are quoted relative to SCE with ferrocene/ferrocenium at +450 mV as internal standard. In all the experiments the scan rate was 100 mV/s for cyclic voltammetry and the pulse frequency was 15 Hz for differential pulse voltammetry (DPV).

Synthetic Procedures

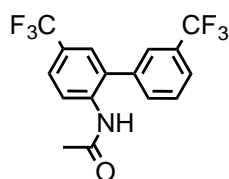
***N*-(2-chloro-4-(trifluoromethyl)phenyl)acetamide (20):** 4-Amino-3-chlorobenzotrifluoride



(1.00 g, 5.11 mmol, 1.0 eq.) was dissolved in 40 mL DCM (crown cap) in an oven dried argon flushed schlenk flask. Triethylamine (0.8 mL, 5.6 mmol, 1.1 eq.) was added at room temperature followed by dropwise addition of

AcCl (0.41 mL, 5.6 mmol, 1.1 eq.). The yellow solution was stirred for 2 hours at room temperature. Adding water (100 mL) and DCM (100 mL) quenched the reaction. Product was extracted with DCM (3 x 100 mL) and the combined organic layers were washed with brine. Organic phase was dried over MgSO₄ and solvent was removed. Product was further purified by CC (SiO₂; c-hexane : ethyl acetate, 5:1 – 2:1 gradient) yielding **20** (1.13 g, 4.76 mmol, 93%) as white solid. ¹H – NMR (400 MHz, CDCl₃, 25 °C): δ = 8.57 (d, *J* = 8.7 Hz, 1H), 7.74 (br s, 1H), 7.64 (d, *J* = 1.7 Hz, 1H), 7.54 – 7.51 (m, 1H), 2.28 (s, 3H) ppm. ¹³C – NMR (101 MHz, CDCl₃, 25 °C): δ = 168.5, 137.8, 126.5 (q, *J* = 33.5 Hz, 1C), 126.3 (q, *J* = 4.1 Hz, 1C), 125.1 (q, *J* = 3.7 Hz, 1C), 123.4 (q, *J* = 272.0 Hz, 1C), 122.3, 121.2, 25.0 ppm. ¹⁹F – NMR (377 MHz, CDCl₃): δ = –62.4 ppm. MS (EI, 70 eV): *m/z* (%) = 237 (10), 202 (27), 197 (33), 195 (100), 176 (19), 145 (24). HRMS (ESI): *m/z* calcd. for [C₉H₇ClF₃NO+H]⁺ 238.0241; found: 238.0238.

***N*-(3',5-bis(trifluoromethyl)-[1,1'-biphenyl]-2-yl)acetamide (21):** 3-(Trifluoromethyl)-

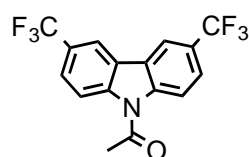


phenylboronic acid (4.00 g, 21.0 mmol, 2.0 eq.) was added to a solution of *N*-(2-chloro-4-(trifluoromethyl)phenyl)acetamide (2.50 g, 10.5 mmol, 1.0 eq.) in a mixture of 20 mL THF and water (20 : 1). To the clear solution K₃PO₄ (4.84 g, 21.0 mmol, 2.0 eq.) was added and degassed for

15 minutes. SPhos Pd G2 (151 mg, 0.21 mmol, 2 mol%) was added and the resulting green suspension was stirred at 80 °C for 12 hours. Reaction was cooled to rt, *t*BME (50 mL) was added and reaction mixture was filtered over a Celite pad. Product was extracted with ethyl acetate (3 x 100 mL), washed with water (1 x 100 mL) and brine (1 x 100 mL). Organic layer was dried over MgSO₄ and solvent was removed under reduced pressure. Product was further purified by column chromatography (SiO₂; Ethyl acetate: c-hexane, 1 : 2 – 2 : 1 gradient) providing **21** (3.3 g, 9.5 mmol, 91%) as white solid. ¹H – NMR (400 MHz, CDCl₃, 25 °C): δ = 8.45 (d, *J* = 8.6 Hz, 1H), 7.76 – 7.74 (m, 1H), 7.68 – 7.65 (m, 3H), 7.61 – 7.58 (m, 1H),

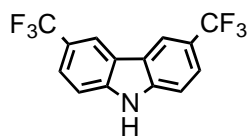
7.50 – 7.49 (m, 1H), 7.06 (br s, 1H), 2.06 (s, 3H) ppm. ^{13}C – NMR (101 MHz, CDCl_3 , 25 °C): δ = 168.5, 137.9, 137.8, 132.7, 132.1 (q, J = 32.8 Hz, 1C), 130.8, 130.2, 137.76, 127.2 (q, J = 3.8 Hz, 1C), 126.7 (q, J = 32.2 Hz, 1C), 126.4 (q, J = 3.7 Hz, 1C), 126.2 (q, J = 3.6 Hz, 1C), 125.7 (q, J = 3.8 Hz, 1C), 124.0 (q, J = 271.7 Hz, 1C), 123.8 (q, J = 272.7 Hz, 1C), 122.1, 24.7 ppm. ^{19}F – NMR (377 MHz, CDCl_3): δ = –62.2, –62.7 ppm. MS (EI, 70 eV): m/z (%) = 347 (26), 306 (16), 305 (100), 284 (39), 235 (32), 216 (21). HRMS (ESI): m/z calcd. for $[\text{C}_{16}\text{H}_{11}\text{F}_6\text{NO}+\text{H}]^+$ 348.0818; found: 348.0817.

3,6-bis(trifluoromethyl)-9-acetylcarbazol (22): *N*-(3',5-bis(trifluoromethyl)-[1,1'-biphenyl]-2-



yl)-acetamide (1.00 g, 2.88 mmol, 1.0 eq.) was added to an oven dried schlenk flask, followed by finely powdered activated molecular sieve (3Å) and $\text{Pd}(\text{OAc})_2$ (12.9 mg, 2 mol%). Flask was evacuated and dry $\text{Cu}(\text{OAc})_2$ (106 mg, 20 mol%) was added and mixture was suspended in toluene (20 mL). Argon atmosphere was changed into oxygen by applying vacuum and flashing by oxygen using an oxygen filled balloon. This sequence was repeated three times and reaction mixture was lowered in a oil bath and stirred at 120 °C. Every 6 hours $\text{Pd}(\text{OAc})_2$ (12.9 mg, 2 mol%) was added until full conversion was observed by TLC. Afterwards reaction was cooled to room temperature and filtered over a Celite pad and diluted with water (100 mL) and ethyl acetate (100 mL). Product was extracted using ethyl acetate (2 x 100 mL), washed with brine (1 x 100 mL) and combined organic layers were dried over MgSO_4 . Solvent was removed and column chromatography (SiO_2 ; *c*-hexane : ethyl acetate, 5 : 1) afforded **22** (975 mg, 2.82 mmol, 98%) as white solid. ^1H – NMR (400 MHz, CDCl_3 , 25 °C): δ = 8.36 (d, J = 8.9 Hz, 2H), 8.24 (d, J = 1.5 Hz, 2H), 7.81 (dd, J = 8.9, 1.5 Hz, 2H), 2.96 (s, 3H) ppm. ^{13}C – NMR (101 MHz, CDCl_3 , 25 °C): δ = 169.9, 140.9, 126.5 (q, J = 33.0 Hz, 2C), 125.4, 125.07 (q, J = 3.6 Hz, 2C), 124.2 (q, J = 272.0 Hz, 2C), 117.6 (q, J = 3.9 Hz, 2C), 116.7, 27.9 ppm. ^{19}F – NMR (377 MHz, CDCl_3): δ = –61.45 ppm. MS (EI, 70 eV): m/z (%) = 345 (18), 304 (15), 303 (100), 284 (17). EA: calcd. for $\text{C}_{16}\text{H}_9\text{F}_6\text{NO}$: C 55.66, H 2.63, N 4.06; found: C 55.64, H 2.95, N 4.42.

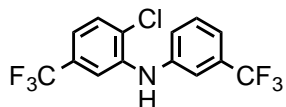
3,6-bis(trifluoromethyl)-9H-carbazole (17): A stock solution was prepared by adding 5 mL



methanol dropwise to a cooled solution of 1 mL concentrated sulfuric acid. 3,6-bis(trifluoromethyl)-9-acetylcabazol (50 mg, 0.145 mmol, 1.0 eq.) was suspended in 3 mL stock solution in a one necked round

bottom flask. Resulting suspension was stirred under air at 60 °C for one hour. Sat. aq. Na₂CO₃ (20 mL) solution was added carefully and product was extracted with methylene chloride (2 x 20 mL). Combined organic layers were washed with brine (1 x 10 mL), dried over MgSO₄ and solvent was removed at reduced pressure. Further purification by column chromatography (SiO₂; c-hexane : ethyl acetate, 1 : 5) yielded **17** (43 mg, 0.14 mmol, 98%) as white crystalline solid. ¹H – NMR (400 MHz, CDCl₃, 25 °C): δ = 8.42 (br s, 1H), 8.37 (d, *J* = 1.9 Hz, 2H), 7.72 (dd, *J* = 8.5, 1.9 Hz, 2H), 7.53 (d, *J* = 8.5 Hz, 2H) ppm. ¹³C – NMR (101 MHz, CDCl₃, 25 °C): δ = 141.5, 125.07 (q, *J* = 271.4 Hz, 2C), 123.8 (q, *J* = 3.5 Hz, 2C), 122.9 (q, *J* = 32.5 Hz, 2C), 122.7, 118.4 (q, *J* = 4.2 Hz, 2C) ppm. ¹⁹F – NMR (377 MHz, CDCl₃): δ = –60.5 ppm. MS (EI, 70 eV): *m/z* (%) = 304 (16), 303 (100), 302 (11), 284 (33), 253 (20), 234 (13). HRMS (ESI): *m/z* calcd. for [C₁₄H₇F₆N-H]⁺ 302.0410; found: 302.0412.

2-chloro-5-(trifluoromethyl)-N-(3-(trifluoromethyl)phenyl)aniline (24): Pd₂(dba)₃ · CHCl₃

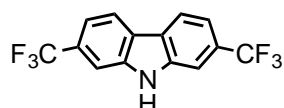


(0.23 g, 1 mol%) and BINAP (0.42 g, 3 mol%), were placed in a oven dried argon flushed schlenk flask. Degassed toluene was added under counter flow of argon and resulting solution was stirred for 15

minutes. 3-Bromobenzotrifluoride (3.1 mL, 22 mmol, 1.0 eq.), followed by NaOtBu (3.1 g, 31 mmol, 1.4 eq.) were added and stirring at room temperature was continued for 30 min. Afterwards, 2-chloro-5-(trifluoromethyl)aniline (3.7 mL, 26 mmol, 1.2 eq.) was added drop wise and schlenk flask was heated in a oil bath at 90 °C for 12 hours. Reaction was cooled to room temperature, diluted with *t*BME (100 mL) and filtered over a Celite pad. *t*BME was removed and crude product was taken up in petroleum ether (75 mL), dried over MgSO₄ and filtered over a silica pad affording **24** (6.9 g, 20.3 mmol, 92%) as yellow oil. ¹H – NMR (400 MHz, CDCl₃, 25 °C): δ = 7.51 – 7.45 (m, 3H), 7.40 – 7.39 (m, 1H), 7.37 – 7.34 (m, 2H), 7.12 – 7.39 (m, 1H), 6.31 (br s, 1H) ppm. ¹³C – NMR (101 MHz, CDCl₃, 25 °C): δ = 141.3, 140.2, 132.5 (q, *J* = 32.5 Hz, 1C), 130.6, 130.4, 130.4 (q, *J* = 34.7 Hz, 1C), 125.2 (q, *J* = 1.6 Hz, 1C), 123.9 (q, *J* = 272.5 Hz, 1C), 123.8 (q, *J* = 272.4 Hz, 1C), 123.3 (q, *J* = 1.5 Hz, 1C), 120.2 (q, *J* = 3.8 Hz, 1C),

117.7 (q, $J = 3.9$ Hz, 1C), 117.3 (q, $J = 3.8$ Hz, 1C), 112.1 (q, $J = 3.9$ Hz, 1C) ppm. ^{19}F – NMR (377 MHz, CDCl_3): $\delta = -62.9, -63.0$ ppm. MS (EI, 70 eV): m/z (%) = 341 (33), 340 (17), 339 (100), 320 (14), 304 (16), 303 (10), 285 (13), 284 (78), 236 (10), 235 (72), 75 (12), 69 (15). HRMS (ESI): m/z calcd. for $[\text{C}_{14}\text{H}_7\text{F}_6\text{N}-\text{H}]^-$ 338.0177; found: 338.0177.

2,7-bis(trifluoromethyl)-9H-carbazole (18): 5-(trifluoromethyl)-*N*-(3-(trifluoromethyl)-



phenyl)aniline (1.0 g, 2.9 mmol, 1.0 eq.), $\text{Pd}(\text{OAc})_2$ (66 mg, 10 mol%), $(t\text{Bu})_3\text{PH} \cdot \text{BF}_4$ (70 mg, 8 mol%) and NaOtBu (0.73 g, 7.4 mmol, 2.5 eq.) were placed in a oven dried argon flushed micro wave vial. Three

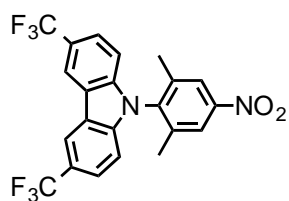
vacuum/argon cycles were performed before the compounds were suspended in degassed toluene (20 mL). Microwave vial was sealed and heated in the microwave for 3 hours at 160 °C. After vial was cooled to room temperature hydrochloric acid (1 M, 20 mL) was added and product was extracted with ethyl acetate (2 x 50 mL). Organic layer was dried over MgSO_4 and after the solvent was removed, crude product was purified by column chromatography (SiO_2 ; c-Hexane : toluene, 2 : 1) providing **18** (0.72 mg, 2.4 mmol, 81%) as white crystalline solid. ^1H – NMR (400 MHz, CDCl_3 , 25 °C): $\delta = 8.38$ (br s, 1H), 8.20 – 8.18 (m, 2H), 7.76 – 7.75 (m, 2H), 7.55 – 7.53 (m, 2H) ppm. ^{13}C – NMR (101 MHz, CDCl_3 , 25 °C): $\delta = 139.5, 129.2$ (q, $J = 32.2$ Hz, 2C), 125.1, 124.7 (q, $J = 272.1$ Hz, 2C), 121.5, 117.1 (q, $J = 3.7$ Hz, 2C), 108.5 (q, $J = 4.3$ Hz, 2C). ^{19}F – NMR (377 MHz, CDCl_3): $\delta = -61.3$ ppm. MS (EI, 70 eV): m/z (%) = 304 (17), 303 (100), 284 (21), 234 (12). HRMS (ESI): m/z calcd. for $[\text{C}_{14}\text{H}_7\text{F}_6\text{N} - \text{H}]^-$ 302.0410; found: 302.0412.

Representative procedure of aromatic nucleophilic substitution (**11** and **12**, **25 – 27**):

1,8-dimethyl-9-(4-nitrophenyl)carbazole (11): Under argon atmosphere 1,8-dimethylcarbazole (400 mg, 2.05 mmol, 1.0 eq.) was added to a two necked round bottom flask equipped with a reflux condenser. Addition of cesium carbonate (3.36 g, 10.3 mmol, 5.0 eq.) followed by DMF (21 mL) resulted in a suspension, which was stirred for 30 minutes at room temperature. Afterwards, 2-fluoro-1,3-dimethyl-5-nitrobenzene (694 mg, 4.09 mmol, 2.0 eq) was poured in all in once and reaction mixture was stirred at 155 °C for 12 hours. The black mixture was diluted with water and crude product was extracted with ethyl acetate (3 x 50 mL). Organic phases were dried over MgSO₄ and solvent was removed. **11** (557 mg, 1.76 mmol, 86%) was isolated as yellow solid after purification by column chromatography (SiO₂; c-hexane : ethyl acetate, 10 : 1). ¹H – NMR (400 MHz, CDCl₃, 25 °C): δ = 8.33 (d, *J* = 8.8 Hz, 2H), 7.99 (d, *J* = 7.6 Hz, 2H), 7.66 (d, *J* = 8.8 Hz, 2H), 7.19 (dd, *J* = 7.5 Hz, 7.5 Hz, 2H), 7.11 (d, *J* = 7.2 Hz, 2H), 1.89 (s, 6H). ¹³C – NMR (101 MHz, CDCl₃, 25 °C): δ = 148.6, 147.8, 140.6, 132.3, 129.3, 124.5, 123.6, 121.2, 120.7, 118.3 ppm. MS (EI, 70 eV): *m/z* (%) = 316 (100), 270 (30). EA: calcd. for C₂₀H₁₆N₂O₂: C 75.93, H 5.10, N 8.86; found: C 76.42, H 5.39, N 9.30.

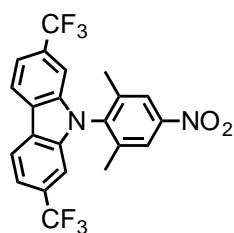
9-(2,6-dimethyl-4-nitrophenyl)carbazole (12): Carbazole (138 mg, 0.79 mmol, 1.0 eq.) yielded **12** (217 mg, 0.69 mmol, 87%) after column chromatography (SiO₂; cyclohexane : ethyl acetate, 10 : 1). ¹H – NMR (400 MHz, CDCl₃, 25 °C): δ = 8.19 (d, *J* = 7.7 Hz, 2H), 8.17 (s, 2H), 7.41 (dd, *J* = 7.7 Hz, 7.7 Hz, 2H), 7.32 (dd, *J* = 7.8 Hz, 7.8 Hz, 2H), 6.89 (d, *J* = 8.1 Hz, 2H), 1.99 (s, 6H). ¹³C – NMR (101 MHz, CDCl₃, 25 °C): δ = 147.6, 140.8, 140.4, 139.5, 126.4, 123.6, 123.3, 120.7, 120.2, 109.1 ppm. MS (EI, 70 eV): *m/z* (%) = 316 (100), 255 (38). EA: calcd. for C₂₀H₁₆N₂O₂: C 75.93, H 5.10, N 8.86; found: C 75.82, H 5.28, N 9.23.

3,6-bis(trifluoromethyl)-9-(2,6-dimethyl-4-nitrophenyl)carbazole (25): 3,6-bis(trifluoro-



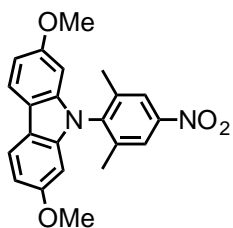
methyl)-9*H*-carbazole (418 mg, 1.4 mmol, 1.0 eq.) yielded product after purification by column chromatography (SiO₂; *c*-hexane : ethyl acetate, 10 : 1) **25** (512 mg, 1.13 mmol, 82%) as yellow solid. ¹H – NMR (400 MHz, CDCl₃, 25 °C): δ = 8.52 (dt, *J* = 1.7, 0.8 Hz, 2H), 8.21 (t, *J* = 0.7 Hz, 2H), 7.72 (ddd, *J* = 8.6, 1.7, 0.7 Hz, 2H), 7.12 – 6.75 (dt, *J* = 8.6, 0.7 Hz, 2H), 1.98 (s, 6H) ppm. ¹³C – NMR (101 MHz, CDCl₃, 25 °C): δ = 148.3, 141.8, 140.3, 139.2, 124.8 (q, *J* = 271.8 Hz, 2C), 124.5 (q, *J* = 3.5 Hz, 2C), 124.1, 123.8 (q, *J* = 32.3 Hz, 2C), 122.7, 119.0 (q, *J* = 4.0 Hz, 2C), 109.9, 18.0 ppm. ¹⁹F – NMR (377 MHz, CDCl₃): δ = –60.5 ppm. MS (EI, 70 eV): *m/z* (%) = 453 (24), 452 (100), 391 (25), 390 (16), 337 (22), 336 (25). EA: calcd. for C₂₂H₁₄F₆N₂O₂: C 58.41, H 3.12, N 6.19; found: C 58.08, H 3.74, N 6.64.

2,7-bis(trifluoromethyl)-9-(2,6-dimethyl-4-nitrophenyl)carbazole (26): 2,7-bis(trifluoro-



methyl)-9*H*-carbazole (418 mg, 1.4 mmol, 1.0 eq.) yielded 2,7-bis(trifluoromethyl)-9-(2,6-dimethyl-4-nitrophenyl)carbazole (488 mg, 1.08 mmol, 78%) as light yellow solid after column chromatography (SiO₂; *c*-hexane : toluene, 1 : 1). ¹H – NMR (400 MHz, CDCl₃, 25 °C): δ = 8.36 – 8.34 (m, 2H), 8.25 – 8.24 (m, 2H), 7.66 – 7.63 (m, 2H), 7.21 – 7.20 (m, 2H), 2.00 (s, 6H) ppm. ¹³C – NMR (101 MHz, CDCl₃, 25 °C): δ = 148.4, 140.3, 140.0, 139.0, 129.9 (q, *J* = 32.4 Hz, 2C), 125.0, 124.5 (q, *J* = 272.5 Hz, 2C), 124.3, 122.1, 117.9 (q, *J* = 3.6 Hz, 2C), 106.8 (q, *J* = 4.3 Hz, 2C), 18.0 ppm. ¹⁹F – NMR (377 MHz, CDCl₃): δ = –61.2 ppm. MS (EI, 70 eV): *m/z* (%) = 453 (25), 452 (100), 391 (19), 390 (19), 337 (23), 336 (21). EA: calcd. for C₂₂H₁₄F₆N₂O₂: C 58.41, H 3.12, N 6.19; found: C 58.04, H 3.67, N 6.41.

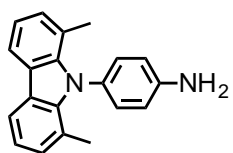
2,7-dimethoxy-9-(2,6-dimethyl-4-nitrophenyl)carbazole (27): 2,7-dimethoxy-9*H*-carbazole



(537 mg, 2.4 mmol, 1.0 eq.), yielding **27** (761 mg, 2.0 mmol, 86%) as yellow solid after purification by column chromatography (SiO₂; *c*-hexane : ethyl acetate, 10 : 1). ¹H – NMR (400 MHz, CDCl₃, 25 °C): δ = 8.19 – 8.16 (m, 2H), 7.93 (d, *J* = 8.5 Hz, 2H), 6.89 (dd, *J* = 8.5, 2.3 Hz, 2H), 6.28 (d, *J* = 2.2 Hz, 2H), 3.79 (s, 6H), 2.02 (s, 6H) ppm. ¹³C – NMR (101 MHz, CDCl₃, 25 °C): δ = 158.9, 147.8, 141.1, 140.8, 140.5, 123.9, 120.7, 117.5, 108.4, 93.7, 77.2, 55.9, 18.1 ppm. MS (EI, 70 eV): *m/z* (%) = 377 (24), 376 (100), 361 (39), 315 (10), 121 (11). HRMS (ESI): *m/z* calcd. for [C₂₂H₂₀N₂O₄+H]⁺ 377.1496; found: 377.1490.

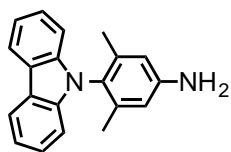
Representative procedure of reduction (**13** and **14**, **28** – **30**):

4-(1,8-dimethylcarbazol)aniline (13): 1,8-dimethyl-9-(4-nitrophenyl)carbazole (0.6 g, 2.0



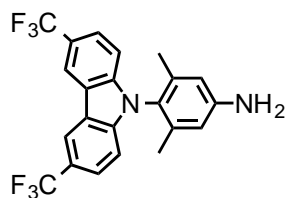
mmol, 1.0 eq.) and SnCl₂ · 2H₂O (1.7 g, 7.5 mmol, 3.8 eq.) were suspended in ethanol (10 mL) under argon atmosphere. The suspension was stirred at 80 °C for 4 hours. Ethanol was removed under reduced pressure. Crude product was taken up in toluene (50 mL) and basified with aq. sodium hydroxide (5 M, 30 mL) solution. Organic phase was dried over MgSO₄ and filtrate was concentrated and purified by column chromatography (SiO₂; *c*-hexane : toluene, 1 : 1) affording **13** (0.52 g, 1.8 mmol, 91%) as slightly orange crystals. ¹H – NMR (400 MHz, CDCl₃, 25 °C): δ = 7.98 (d, *J* = 7.4 Hz, 2H), 7.24 (d, *J* = 8.6 Hz, 2H), 7.13 (dd, *J* = 7.3 Hz, 7.3 Hz, 2H), 7.08 (d, *J* = 7.3 Hz, 2H), 6.72 (d, *J* = 8.6 Hz, 2H), 3.88 (s, 2H), 1.99 (s, 6H) ppm. ¹³C – NMR (101 MHz, CDCl₃, 25 °C): δ = 146.9, 140.7, 132.3, 132.0, 128.8, 123.7, 121.8, 119.5, 118.0, 114.3, 19.6 ppm. MS (EI, 70 eV): *m/z* (%) = 286.1 (100), 287.0 (22.2). HRMS (ESI): *m/z* calcd. for [C₂₀H₁₉N₂+H]⁺ 287.1543; found: 287.1541.

4-carbazole-3,5-dimethylaniline (14): 9-(2,6-dimethyl-4-nitrophenyl)carbazole (0.26 g, 0.82 mmol, 1.0 eq.) yielded **14** as slightly orange crystals (0.22 g, 0.8 mmol,



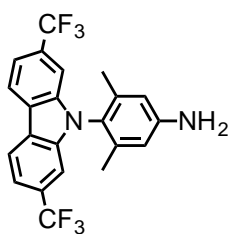
94%), after work up and was used without further purification. ^1H – NMR (400 MHz, CDCl_3 , 25 °C): δ = 8.16 (d, J = 7.9 Hz, 2H), 7.38 (dd, J = 7.7 Hz, 7.7 Hz 2H), 7.26 (dd, 7.6 Hz, 7.6 Hz, 2H), 6.99 (d, J = 8.0 Hz, 2H), 6.57 (s, 2H), 3.75 (s, 2H), 1.75 (s, 6H) ppm. ^{13}C – NMR (101 MHz, CDCl_3 , 25 °C): δ = 146.6, 141.0, 139.2, 126.0, 125.5, 122.9, 120.4, 119.3, 114.9, 109.7, 17.7 ppm. MS (EI, 70 eV): m/z (%) = 286.1 (100), 287.1 (21.2). HRMS (ESI): m/z calcd. for $[\text{C}_{20}\text{H}_{19}\text{N}_2+\text{H}]^+$ 287.1543; found: 287.1543.

3,6-bis(trifluoromethyl)-9-(3,5-dimethylaniline)carbazol (28): 3,6-bis(trifluoromethyl)-9-



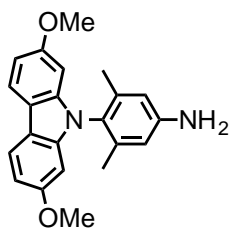
(2,6-dimethyl-4-nitrophenyl)carbazole (530 mg, 1.17, 1.0 eq.) yielded after purification by column chromatography (SiO_2 ; c-hexane : toluene, 1 : 1 + 5% TEA) **28** (454 mg, 1.07 mmol, 92%) as light brownish solid. ^1H – NMR (400 MHz, CDCl_3 , 25 °C): δ = 8.48 – 8.47 (m, 2H), 7.69 – 7.66 (m, 2H), 7.13 – 7.10 (m, 2H), 6.59 (s, 2H), 3.86 (br s, 2H), 1.73 (s, 6H) ppm. ^{13}C – NMR (101 MHz, CDCl_3 , 25 °C): δ = 147.4, 143.2, 138.7, 125.2 (q, J = 272.5 Hz, 2C), 123.9, 123.9 (q, J = 3.8 Hz, 2C), 122.7 (q, J = 32.2 Hz, 2C), 122.2, 118.5 (q, J = 4.2 Hz, 2C), 115.0, 110.3, 17.6 ppm. ^{19}F – NMR (377 MHz, CDCl_3): δ = –60.3 ppm. MS (EI, 70 eV): m/z (%) = 422 (100), 423 (23), 421 (11). HRMS (ESI): m/z calcd. for $[\text{C}_{22}\text{H}_{16}\text{F}_6\text{N}_2+\text{H}]^+$ 423.1290; found: 423.1294.

2,7-bis(trifluoromethyl)-9-(3,5-dimethylaniline)carbazole (29): 2,7-bis(trifluoromethyl)-9-



(2,6-dimethyl-4-nitrophenyl)carbazole (230 mg, 0.51 mmol, 1.0 eq.) afforded **29** (199 mg, 0.47 mmol, 93%) after purification by column chromatography (SiO_2 ; c-hexane : toluene, 1 : 1) as light brownish oil, which solidified upon standing. ^1H – NMR (400 MHz, CDCl_3 , 25 °C): δ = 8.29 – 8.27 (m, 2H), 7.57 – 7.55 (m, 2H), 7.30 – 7.29 (m, 2H), 6.61 – 6.60 (m, 2H), 3.85 (br s, 2H), 1.74 (s, 6H) ppm. ^{13}C – NMR (101 MHz, CDCl_3 , 25 °C): δ = 147.4, 141.3, 138.8, 129.3 (q, J = 32.1 Hz, 2C), 124.8 (q, J = 272.3 Hz, 2C), 124.5, 123.6, 121.6, 116.8 (q, J = 3.6 Hz, 2C), 115.1, 107.3 (q, J = 4.3 Hz, 2C), 17.6 ppm. ^{19}F – NMR (377 MHz, CDCl_3): δ = –61.0 ppm. MS (EI, 70 eV): m/z (%) = 423 (32), 422 (100), 421 (12), 353 (17), 211 (13), 120 (17). HRMS (ESI): m/z calcd. for $[\text{C}_{22}\text{H}_{16}\text{F}_6\text{N}_2+\text{H}]^+$ 423.1490; found: 423.1293.

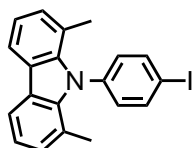
2,7-dimethoxy-9-(3,5-dimethylaniline)carbazol (30): 2,7-dimethoxy-9-(2,6-dimethyl-4-



nitrophenyl)carbazole (482 mg, 1.28, 1.0 eq.) afforded **30** (429 mg, 1.24 mmol, 97%) as light brownish solid after purification by column chromatography (SiO₂; c-hexane : toluene, 1 : 1 + 5% TEA). ¹H – NMR (400 MHz, CDCl₃, 25 °C): δ = 7.90 (d, *J* = 8.5 Hz, 1H), 6.83 (dd, *J* = 8.5, 2.3 Hz, 1H), 6.57 (s, 1H), 6.40 (d, *J* = 2.3 Hz, 1H), 3.79 (s, 6H), 3.76 (br s, 2H), 1.78 (s, 6H) ppm. ¹³C – NMR (101 MHz, CDCl₃, 25 °C): δ = 158.6, 146.6, 142.5, 139.1, 125.3, 120.2, 117.0, 115.0, 107.8, 93.8, 77.2, 55.8, 17.8 ppm. MS (EI, 70 eV): *m/z* (%) = 347 (24), 346 (100), 332 (11), 331 (49), 173 (17). HRMS (ESI): *m/z* calcd. for [C₂₂H₂₂N₂O₂+H]⁺ 347.1754; found: 347.1755.

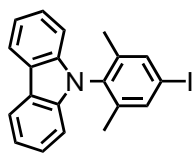
Sandmeyer reaction for **15** and **16** (Method A):

9-(4-iodophenyl)-1,8-dimethylcarbazole (15): Boron trifluoride etherate (0.93 mL, 7.33 mmol, 4.2 eq.) was placed into an argon flushed oven dried two-necked



round bottom flask at –30 °C. A solution of 4-(1,8-dimethylcarbazol)aniline (500 mg, 1.75 mmol, 1.0 eq.) in THF (5 mL) was added drop wise and stirred for 20 minutes. Subsequently, a solution of *tert*-butyl nitrite (736 mg, 6.43 mmol, 3.7 eq.) in THF (5 mL) was added drop wise and the resulting mixture was allowed to warm to 0 °C. At –5 °C diethyl ether (10 mL) was added, whereas the diazonium salt participated out, filtered off and washed with cold diethyl ether. In a second flask, KI (412 mg, 2.48 mmol, 1.4 eq.) and iodine (311 mg, 1.22 mmol, 0.7 eq.) were dissolved in acetonitrile (7.5 mL). The diazonium salt was added in one portion at 0 °C, the reaction mixture was warmed to room temperature and stirred for 30 minutes. Afterwards, the black reaction mixture was quenched with sat. aq. Na₂S₂O₃ solution. The product was extracted with ethyl acetate, dried over MgSO₄, and concentrated under reduced pressure. After purification by column chromatography (SiO₂; c-hexane : DCM, 4 : 1) **15** was obtained as white solid (521 mg, 1.31 mmol, 75%). ¹H – NMR (400 MHz, CDCl₃, 25 °C): δ = 7.98 (d, *J* = 7.3 Hz, 2H), 7.79 (d, *J* = 8.4 Hz, 2H), 7.24 (dd, *J* = 7.4 Hz, 7.4 Hz, 2H), 7.09 (d, *J* = 7.5 Hz, 2H), 1.93 (s, 6H) ppm. ¹³C – NMR (101 MHz, CDCl₃, 25 °C): δ = 141.9, 140.4, 137.5, 133.2, 129.0, 124.1, 121.4, 120.1, 118.1, 94.2, 19.8 ppm. MS (EI, 70 eV): *m/z* (%) = 397 (100), 398 (22), 254 (17). EA: calcd. for C₂₀H₁₆I₁N: C 60.47, H 4.06, N 3.53; found: C 60.56, H 4.26, N 3.86

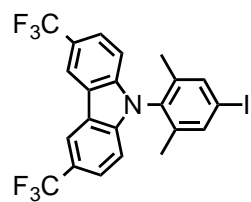
9-(4-iodo-2,6-dimethylphenyl)carbazole (16): 4-carbazole-3,5-dimethylaniline (200 mg, 0.70



mmol, 1.0 eq.) yielded 9-(4-iodo-2,6-dimethylphenyl)carbazole (219 mg, 0.55 mmol, 79 %) as white solid after purification by column chromatography (SiO₂; cyclohexane : DCM, 4 : 1). ¹H – NMR (400 MHz, CDCl₃, 25 °C): δ = 8.16 (d, *J* = 7.8 Hz, 2H), 7.64 (s, 2H), 7.39 (dd, *J* = 8.3 Hz, 7.2 Hz, 2H), 7.28 (dd, *J* = 8.1 Hz, 7.3 Hz, 2H), 6.93 (d, *J* = 8.1 Hz, 2H), 1.81 (s, 6H) ppm. ¹³C – NMR (101 MHz, CDCl₃, 25 °C): δ = 140.5, 140.0, 137.7, 134.6, 126.1, 123.0, 120.5, 119.7, 109.3, 94.7, 17.2 ppm. MS (EI, 70 eV): *m/z* (%) = 397 (100), 268 (34), 255 (68), 254 (60), 127(24). EA: calcd. for C₂₀H₁₆I₁N: C 60.47, H 4.06, N 3.53; found: C 61.01, H 4.31, N 3.78.

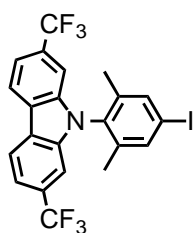
Sandmeyer reaction for 31 and 32 (Method A):

3,6-bis(trifluoromethyl)-9-(4-iodo-2,6-dimethylphenyl)carbazole (31): BF₃ diethyletherate



(76.0 μ l, 0.62 mmol, 2.0 eq.) was placed into an argon flushed oven dried two-necked round bottom flask at –10 °C. 3,6-bis(trifluoromethyl)-9-(3,5-dimethylaniline)carbazole (130 mg, 0.31 mmol, 1.0 eq.) was dissolved in dichloromethane (5 mL) and added drop wise to the cooled flask. Subsequently, *tert*-butyl nitrite (61.6 μ l, 0.462 mmol, 1.5 eq.) dissolved in 1 mL dichloromethane was added carefully via syringe to the beige suspension. Resulting mixture was stirred at 0 °C for 1 hour, followed by the addition of potassium iodide (72.3 mg, 0.431 mmol, 1.4 eq.) and iodine (54.8 mg, 0.216 mmol, 0.7 eq.) in one portion. Reaction was warmed to room temperature over 4 hours and was diluted with water (20 mL) and dichloromethane (30 mL). Extraction with dichloromethane (2 x 30 mL), drying over MgSO₄ and concentration afforded brown product. Further purification by column chromatography (SiO₂; c-hexane : DCM, 10 : 1) yielded **31** (148 mg, 0.278 mmol, 90%) as white solid. ¹H – NMR (400 MHz, CDCl₃, 25 °C): δ = 8.51 – 8.49 (m, 2H), 7.72 – 7.70 (m, 4H), 7.08 – 7.06 (m, 2H) 1.82 (s, 6H) ppm. ¹³C – NMR (101 MHz, CDCl₃, 25 °C): δ = 142.3, 140.1, 138.2, 133.3, 125.1 (q, *J* = 271.5 Hz), 124.2 (q, *J* = 3.6 Hz), 123.1 (q, *J* = 32.4 Hz) 122.4, 118.7 (q, *J* = 4.1 Hz), 110.1, 95.9, 17.2 ppm. ¹⁹F – NMR (377 MHz, CDCl₃): δ = –60.4 ppm. MS (EI, 70 eV): *m/z* (%) = 534 (21), 533 (100), 391 (12), 337 (15) 336 (18). EA: calcd. for C₂₂H₁₄F₆I₁N: C 49.55, H 2.65, N 2.63; found: C 49.92, H 3.01, N 2.94.

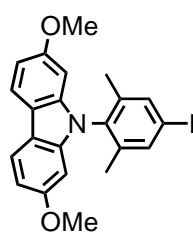
2,7-bis(trifluoromethyl)-9-(4-iodo-2,6-dimethylphenyl)carbazole (32):



2,7-bis(trifluoromethyl)-9-(3,5-dimethylaniline)carbazol (223 mg, 0.53 mmol, 1.0 eq.) afforded after purification by column chromatography (SiO₂, c-hexane : DCM, 10 : 1) **32** (230 mg, 0.431 mmol, 82%) as white solid. ¹H – NMR (400 MHz, CDCl₃, 25 °C): δ = 8.31 – 8.29 (m, 2H), 8.71 (m, 2H), 7.61 – 7.59 (m, 2H), 7.23 – 7.22 (m, 2H), 1.81 (s, 6H) ppm. ¹³C – NMR (101 MHz, CDCl₃, 25 °C): δ = 140.4, 140.1, 138.4, 133.1, 129.6 (q, *J* = 32.2 Hz, 2C), 124.7, 124.6 (q, *J* = 272.4 Hz, 2C), 121.8, 117.4 (q, *J* = 3.8 Hz, 2C), 107.0 (q, *J* = 4.3 Hz, 2C), 96.0, 17.2 ppm. ¹⁹F – NMR (377 MHz, CDCl₃): δ = –61.1 ppm. MS (EI, 70 eV): *m/z* (%) = 534 (23), 533 (100), 391 (13), 390 (17), 337 (26), 336 (27), 77 (11). EA: calcd. for C₂₂H₁₄F₆N: C 49.55, H 2.65, N 2.63; found: C 49.83, H 3.20, N 3.12.

Sandmeyer reaction for 33 (Method C):

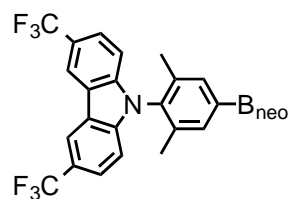
2,7-dimethoxy-9-(4-iodo-2,6-dimethylphenyl)carbazole (33):



2,7-dimethoxy-9-(3,5-dimethyl-aniline)carbazol (214 mg, 0.62 mmol, 1.0 eq.) was added to a solution of *p*-TsOH · H₂O (356 mg, 1.85 mmol, 3.0 eq.) in MeCN (2.5 mL). The resulting suspension was kept at 10 °C, while a solution of NaNO₂ (87.0 mg, 1.85 mmol, 2.0 eq.) and potassium iodide (259 mg, 1.54 mmol, 2.5 eq.) in water (0.5 mL) was added drop wise. The reaction mixture was stirred for 10 minutes at this temperature and the allowed to warm up and stirred for another 2 hours. Reaction was diluted with water (10 mL), aq. NaHCO₃ (1 M, until pH = 10) and extracted with ethyl acetate (3 x 20 mL). Combined organic layers were washed extensively with aq. sat. Na₂S₂O₃ solution dried over MgSO₄ and removed at reduced pressure. Crude product was purified by column chromatography (SiO₂; c-hexane : toluene, 2 : 1) yielding **33** (234 mg, 512 mmol, 83%) as white solid. ¹H – NMR (400 MHz, CDCl₃, 25 °C): δ = 7.91 (d, *J* = 8.5 Hz, 2H), 7.64 (s, 2H), 6.86 (dd, *J* = 8.5, 2.3 Hz, 2H), 6.33 (d, *J* = 2.3 Hz, 2H), 3.80 (s, 6H), 1.85 (s, 6H) ppm. ¹³C – NMR (101 MHz, CDCl₃, 25 °C): δ = 158.7, 141.6, 140.7, 137.9, 134.6, 120.5, 117.2, 108.2, 94.9, 93.7, 55.9, 17.4 ppm. MS (EI, 70 eV): *m/z* (%) = 458 (25), 457 (100), 442 (36), 330 (13), 272 (10), 228 (11), 121 (11). HRMS (ESI): *m/z* calcd. for [C₂₂H₂₀INO₂+H]⁺ 458.0611; found: 458.0602.

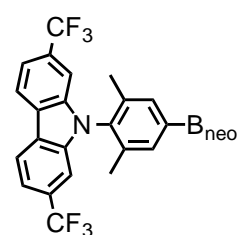
Borylation reaction for 34 – 36:

3,6-bis(trifluoromethyl)-9-(4-(5,5-dimethyl-1,3,2-dioxaborinan-2-yl)-2,6-dimethylphenyl)-



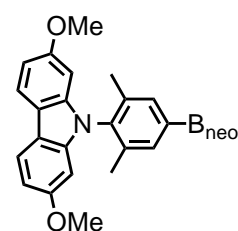
carbazole (34): 3,6-bis(trifluoromethyl)-9-(4-iodo-2,6-dimethylphenyl)carbazole (50.0 mg, 93.4 μmol , 1.0 eq.) was placed in a oven dried argon flushed schlenk flask and dissolved in THF (1 mL) and cooled to $-10\text{ }^\circ\text{C}$. Turbo Grignard (78.7 μl , 0.102 mmol, 1.1 eq.) was added drop wise and conversion was followed by GC/MS. After full conversion, the addition of triisopropyl borate (25.8 μl , 0.11 mmol, 1.2 eq.) yielded in a milky solution, which was stirred for 2 hours at room temperature. Neopentyl glycol (12.7 mg, 0.12 mmol, 1.3 eq.) was added in one shot, solution turned slowly clear and was stirred for 12 hours at room temperature. Reaction was quenched with aq. sat. NH_4Cl (5 mL), diluted with water (5 mL), and extracted with ethyl acetate. Combined organic layers were dried over MgSO_4 , filtered over a small silica pad and concentrated, yielding crude **34**, which was used for the following coupling without further purification. ^1H – NMR (400 MHz, CDCl_3 , $25\text{ }^\circ\text{C}$): δ = 8.49 – 8.48 (m, 2H), 7.74 – 7.73 (m, 2H), 7.69 – 7.66 (m, 2H), 7.05 – 7.03 (m, 2H), 3.84 (s, 4H), 1.84 (s, 6H), 1.09 (s, 6H) ppm.

2,7-bis(trifluoromethyl)-9-(4-(5,5-dimethyl-1,3,2-dioxaborinan-2-yl)-2,6-dimethylphenyl)-



carbazole (35): 3,6-bis(trifluoromethyl)-9-(4-iodo-2,6-dimethylphenyl)carbazole (87.0 mg, 0.163 mmol, 1.0 eq.) yielded crude **35**. ^1H – NMR (400 MHz, CDCl_3 , $25\text{ }^\circ\text{C}$): δ = 8.31 – 8.29 (m, 2H), 7.76 (m, 2H), 7.58 – 7.56 (m, 2H), 7.22 – 7.21 (m, 2H), 3.85 (s, 4H), 1.84 (s, 6H), 1.09 (s, 6H) ppm.

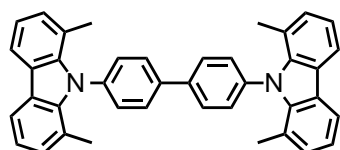
2,7-dimethoxy-9-(4-(5,5-dimethyl-1,3,2-dioxaborinan-2-yl)-2,6-dimethylphenyl)carbazole



(36): 2,7-dimethoxy-9-(4-iodo-2,6-dimethylphenyl)carbazole (75.0 mg, 164 μmol , 1.0 eq.) yielded crude **36**. ^1H – NMR (400 MHz, CDCl_3 , $25\text{ }^\circ\text{C}$): δ = 7.91 (d, J = 8.5 Hz, 2H), 7.70 (s, 2H), 6.84 (dd, J = 8.5, 2.3 Hz, 2H), 6.32 (d, J = 2.3 Hz, 2H), 3.84 (s, 4H), 3.76 (s, 6H), 1.89 (s, 6H), 1.08 (s, 6H) ppm.

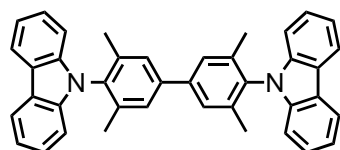
Homo-coupling reaction for 1 and 2:

4,4'-di(1,8-dimethylcarbazole)1,1'-biphenyl (1): 9-(4-iodophenyl)-1,8-dimethylcarbazole



(155 mg, 0.39 mmol, 1.0 eq.) and THF (3 mL) was added into a dry schlenk flask under argon atmosphere. The solution was cooled to $-10\text{ }^{\circ}\text{C}$ and Turbo Grignard (0.33 mL (1.3 M), 0.47 mmol, 1.1 eq.) was added. After 1 hour, the ice bath was removed and TEMPO (124 mg, 0.78 mmol, 2.0 eq.) was added. The mixture was stirred 1 hour at room temperature while a white solid participated. The reaction was quenched with sat. aq. NH_4Cl solution. THF was distilled under reduced pressure and the residue was extracted with dichloromethane. The combined organic phases were dried over MgSO_4 , filtered and concentrated under reduced pressure. The crude product was purified by column chromatography (SiO_2 ; c-hexane : DCM, 5 : 1) providing **1** as a white solid (101 mg, 0.187 mmol, 96%). ^1H – NMR (400 MHz, CDCl_3 , $25\text{ }^{\circ}\text{C}$): δ = 8.05 (d, J = 7.7 Hz, 4H), 7.85 (d, J = 8.3 Hz, 4H), 7.67 (d, J = 8.3 Hz, 4H), 7.21 (dd, J = 7.4 Hz, 7.4 Hz, 4H), 7.16 (d, J = 6.7 Hz, 4H), 2.04 (s, 12H) ppm. ^{13}C – NMR (101 MHz, CDCl_3 , $25\text{ }^{\circ}\text{C}$): δ = 141.7, 140.6, 140.4, 131.9, 128.9, 126.8, 124.0, 121.6, 119.9, 118.1, 19.8. MS (Maldi-TOF): m/z (%) = 540.4 (100), 331.3(8), 310.3 (17). EA: calcd. for $\text{C}_{40}\text{H}_{32}\text{N}_2$: C 88.85, H 5.97, N 5.18; found: C 88.54, H 6.23, N 5.51.

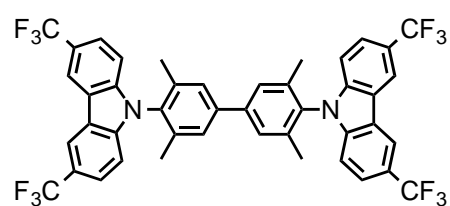
4,4'-dicarbazole-3,3'-5,5'-tetramethyl-biphenyl (2): 9-(4-iodo-2,6-dimethylphenyl)carbazole



(151 mg, 0.38 mmol, 1.0 eq.) afforded **2** (100 mg, 0.18 mmol, 96%) as a white solid after purification by column chromatography (SiO_2 ; c-hexane : DCM, 5 : 1). ^1H – NMR (400 MHz, CDCl_3 , $25\text{ }^{\circ}\text{C}$): δ = 8.24 (d, J = 7.9 Hz, 4H), 7.62 (s, 4H), 7.46 (dd, J = 8.2 Hz, 7.1 Hz, 4H), 7.34 (dd, J = 8.0 Hz, 7.1 Hz, 4H), 7.07 (d, J = 8.1 Hz, 4H), 2.00 (s, 12H) ppm. ^{13}C – NMR (101 MHz, CDCl_3 , $25\text{ }^{\circ}\text{C}$): δ = 140.9, 140.3, 138.6, 134.1, 127.5, 126.0, 123.0, 120.5, 119.5, 109.5, 17.8 ppm. MS (Maldi-TOF): m/z (%) = 540 (100), 310 (7), 268 (20). EA: calcd. for $\text{C}_{40}\text{H}_{32}\text{N}_2$: C 88.85, H 5.97, N 5.18; found: C 88.49, H 6.28, N 5.32.

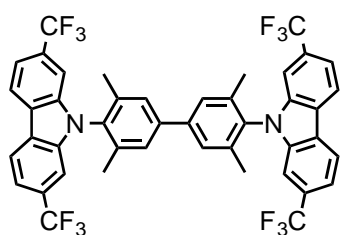
Suzuki–Miyaura reaction for **3** – **5**:

bis(3,6-bis(trifluoromethyl)-9,9'-(3,3',5,5'-tetramethyl-[1,1'-biphenyl]-4,4'-diyl)-carbazole)



(3): 3,6-bis(trifluoromethyl)-9-(4-iodo-2,6-dimethylphenyl)carbazole (45 mg, 84 μmol , 0.9 eq.), potassium phosphate (40 mg, 0.2 mmol, 2.0 eq.) and 3,6-bis(trifluoromethyl)-9-(4-(5,5-dimethyl-1,3,2-dioxaborinan-2-yl)-2,6-dimethylphenyl)-carbazole (approximately 48 mg, 93 μmol , 1.0 eq) were suspended in 1 mL (THF : water; 20 : 1) and the suspension was degassed for 20 minutes. Subsequently, SPhos Pd G2 (1.4 mg, 2 mol%) was added and reaction mixture was stirred at 70 °C for 12 hours. After cooling, reaction was diluted with water (5 mL) and ethyl acetate (5 mL). Crude product was extracted with ethyl acetate (2 x 5 mL), combined organic layer were washed with brine and dried over MgSO_4 . After solvent was evaporated, crude product was purified by column chromatography (SiO_2 ; c-hexane : DCM, 10 : 1) affording **3** (70 mg, 86.1 μmol , 93% over two steps) as white solid. ^1H – NMR (400 MHz, CDCl_3 , 25 °C): δ = 8.54 – 8.53 (m, 4H), 7.75 – 7.72 (m, 4H), 7.62 (s, 4H), 7.17 – 7.15 (m, 4H), 1.97 (s, 12H) ppm. ^{13}C – NMR (101 MHz, CDCl_3 , 25 °C): δ = 142.6, 141.7, 138.5, 133.1, 128.1, 125.1 (q, J = 271.5 Hz), 124.1 (q, J = 3.3 Hz), 123.1 (q, J = 32.3 Hz), 122.5, 118.7 (q, J = 3.9 Hz), 110.3, 17.8 ppm. ^{19}F – NMR (377 MHz, CDCl_3): δ = –60.3 ppm. MS (Maldi-TOF): m/z (%) = 813 (30), 445 (100). EA: calcd. for $\text{C}_{44}\text{H}_{28}\text{F}_{12}\text{N}_2$: C 65.03, H 3.47, N 3.45; found: C 64.46, H 3.93, N 3.73.

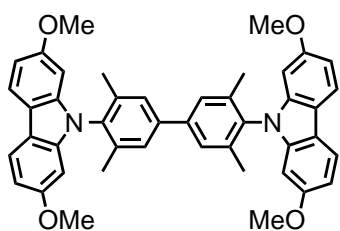
bis(2,7-bis(trifluoromethyl)-9,9'-(3,3',5,5'-tetramethyl-[1,1'-biphenyl]-4,4'-diyl)carbazole



(4): 2,7-bis(trifluoromethyl)-9-(4-iodo-2,6-dimethylphenyl)-carbazole (78 mg, 0.15 mmol, 0.9 eq) afforded **4** (130 mg, 0.15 mmol, 95% over two steps) as white solid after column chromatography (SiO₂; c-hexane : DCM, 10 : 1). ¹H – NMR (400 MHz, CDCl₃, 25 °C): δ = 8.35 (d, *J* = 8.2 Hz, 4H), 7.67 (s, 4H), 7.62

(dd, *J* = 8.2, 1.6 Hz, 4H), 7.34 (d, *J* = 1.6 Hz, 4H), 1.98 (s, 12H) ppm. ¹³C – NMR (101 MHz, CDCl₃, 25 °C): δ = 141.8, 140.7, 138.4, 132.8, 129.6 (q, *J* = 32.3 Hz), 128.4, 124.8, 124.7 (q, *J* = 272.3 Hz), 121.8, 117.2 (q, *J* = 3.5 Hz), 107.3 (q, *J* = 4.4 Hz), 17.9 ppm. ¹⁹F – NMR (377 MHz, CDCl₃): δ = -61.1 ppm. MS (Maldi-TOF): *m/z* (%) = 812 (24), 444 (100). EA: calcd. for C₄₄H₂₈F₁₂N₂: C 65.03, H 3.47, N 3.45; found: C 63.23, H 3.81, N 3.54.

bis(2,7-dimethoxy-9,9'-(3,3',5,5'-tetramethyl-[1,1'-biphenyl]-4,4'-diyl)carbazole) (5): 2,7-

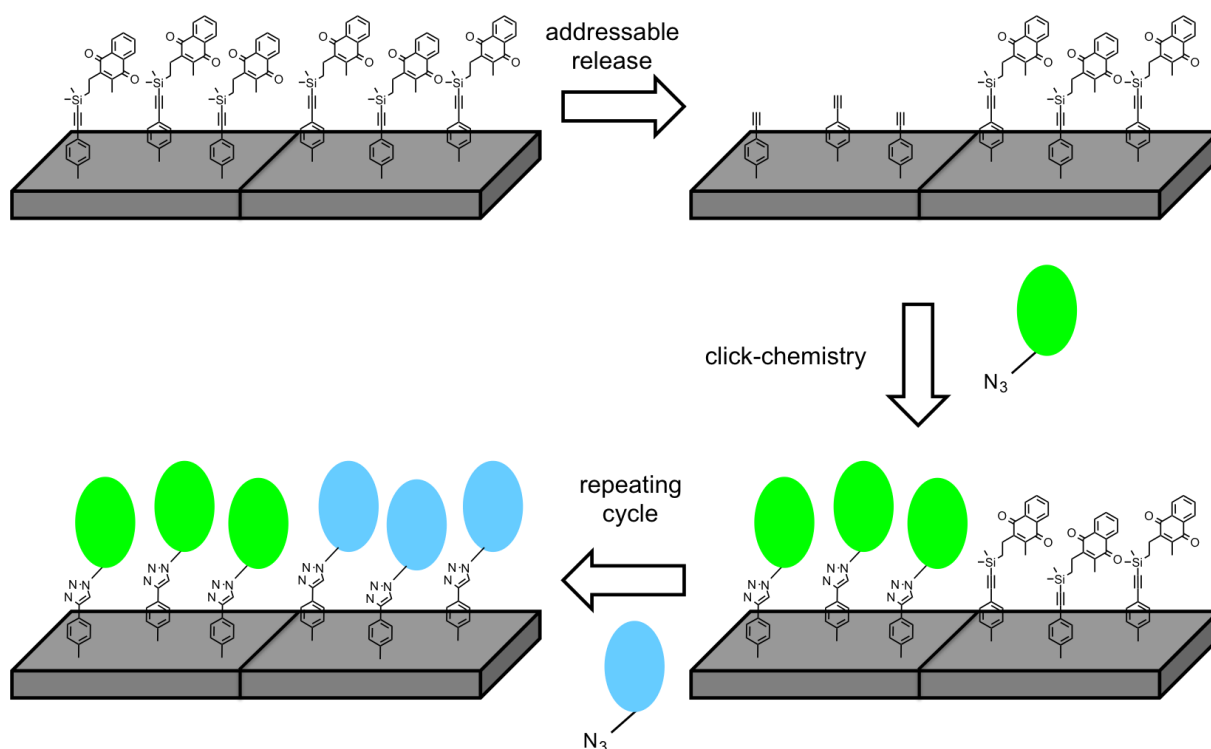


dimethoxy-9-(4-iodo-2,6-dimethylphenyl)carbazole (66 mg, 0.14 mmol, 0.9 eq) yielded **5** (0.1 g, 0.2 mmol, 97% over two steps) as white solid after purification by column chromatography (SiO₂; c-hexane : ethyl acetate, 1 : 10). ¹H – NMR (400 MHz, CDCl₃, 25 °C): δ = 7.95 (d, *J* = 8.5 Hz, 1H), 7.61 (s, 1H), 6.89 (dd, *J* = 8.5, 2.3

Hz, 1H), 6.44 (d, *J* = 2.3 Hz, 1H), 3.82 (s, 6H), 2.01 (6H) ppm. ¹³C – NMR (101 MHz, CDCl₃, 25 °C): δ = 58.7, 141.9, 141.0, 138.7, 134.1, 127.7, 120.5, 117.3, 107.9, 94.0, 77.2, 55.9, 18.0 ppm. HRMS (ESI): *m/z* calcd. for [C₄₄H₄₀N₂O₄+H]⁺ 661.3061; found: 661.3055.

Chapter 2

Development of Novel Ethynyl Protecting Group for SAM Formation



Introduction

Self-Assembled Monolayer

The most common technique to prevent corrosion is covering a metal substrate with polymeric films. For example home appliances are made of steel covered by a polymeric layer. This self-assembled monolayer (SAM) has witnessed tremendous growth in various fields of research. The origin of SAMs is given by interactions between monomers, constructing systems without any guidance from external sources except the environment. In proteins self-assembly results in supramolecular organizations of multiple components conducting very complex structures. The formation of an monolayer of surfactant molecules on a solid surface is just one example of the general phenomena of self-assembly.^[122] The surfactant molecules typically consist of a head and a tail group. Owing to intermolecular interactions of the head group with the surface, two-dimensional molecular structures—usually with a thickness of 1 – 3 nm—are arranged on the surface in a well-defined manner (Figure 18). These well defined and organized SAMs are formed within seconds to hours by the immersion of a substrate in a dilute solution (ca. 1 mM) of the surfactant.^[123]

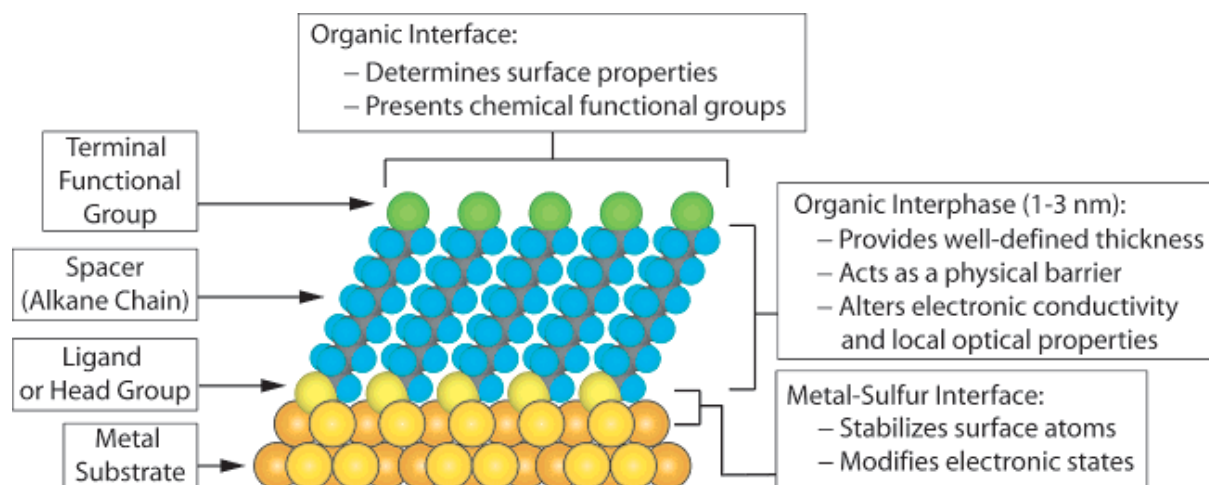


Figure 18: Anatomy and characteristics of an alkanthiolate SAM formed on a gold substrate. SAMs are formed within seconds to hours by dipping a substrate into a diluted solution of the surfactant. Reprinted from Whitesides and co-workers.^[124]

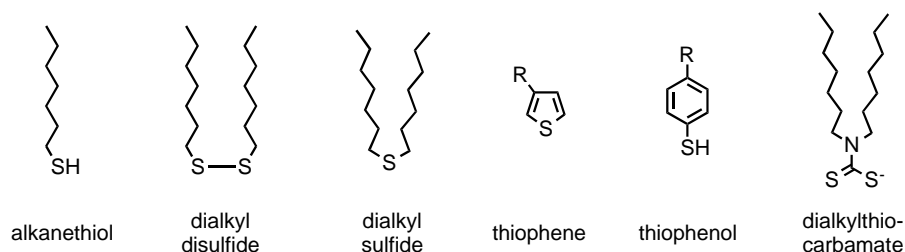
Due to formation of ultrathin films with controlled thicknesses,^[125,126] this elegant, efficient, and low cost tool of SAM formation allows the study of fundamental phenomena such as

distance dependent electron transfer^[127] and mechanism of single electron transistor.^[128] The density of packing and stability of SAMs are tuned by the length of the hydrocarbon unit that influences van der Waals (VdW) and $\pi-\pi$ interactions. This dense monolayer enables applications including chemical sensing,^[129,130] control of surface properties such as wettability and friction,^[131] and corrosion protection.^[132] Since chemistry has been moving away from traditional disciplines into interdisciplinary areas, the demand for miniaturized biosensors—particularly for diagnostic applications—research activity in SAMs is rapidly growing.^[133] The simple experimental handling of SAM formation enables immobilization of highly selective biomolecules (e.g., antibodies, enzymes, nucleic acids) or biological systems (e.g., receptors, cells) on an electrochemical, optical, or piezoelectric transducer.^[134] The quality of SAMs can be evaluated by electrochemical techniques, such as cyclic voltammetry (CV)^[135–137] and impedance measurements^[138] or non-electrochemical techniques, such as ellipsometry,^[139] X-ray photoelectron spectroscopy (XPS),^[140,141] infrared spectroscopy (IR),^[142] scanning tunneling spectroscopy (STM),^[143] atomic force microscopy (AFM),^[144] fluorescence spectroscopy, and surface plasmon resonance.

Besides the successful formation of monolayers using organosilicon derivatives, other substrates including silicon oxide,^[145–149] aluminum oxide,^[150,151] quartz,^[152,153] and glass^[154] have been used. However its quality of SAMs often suffers from handling difficulties while production. More commonly, thiol molecules (R–SH) are used in SAM formation on gold surfaces creating complex structures by the so-called bottom-up approach.

Thiolate SAMs on Gold Surface

The most studied and most understood SAMs are alkanthiolates on a Au(111) surface, because thin films as well as colloids made of gold are easy to produce. Furthermore, gold does not have a stable surface oxide, which makes it possible to handle and manipulate gold surfaces under atmospheric conditions rather than under ultra-high vacuum environment. Due to the high affinity of thiols to gold, they can readily displace adventitious materials from the surface. The alkanthiol surfactant has three parts: (i) the sulfur headgroup that forms a strong covalent bond with the substrate, (ii) the hydrocarbon chain (of variable length) that stabilizes the SAM through VdW interactions with neighboring chains, and (iii) the terminal group that can have different functionalities.



Scheme 13: Surfactants based on sulfur compounds possibly forming SAMs on gold substrates.

Molecular structures of investigated thiols, including alkanthiols,^[139,155–160] di-*n*-alkyl sulfides,^[130,161,162] di-*n*-alkyl disulfides,^[163] thiophenols,^[164,165] thiophenes,^[166] and thiocarbamate^[167] are shown in scheme 13. Different studies showed that the different individual steps involved in the formation of the monolayer vary tremendously between short and long alkylthiolates. Whereas 2 to 12 hours are sufficient to form a well-ordered SAM in the case of long chain alkanthiols, at least 24 hours are required for short-chain alkanthiols or alkanthiols bearing other tail groups than methyl to form well-ordered SAMs.^[168] Using the dithiol version even shorter deposition times were observed in solution.^[169]

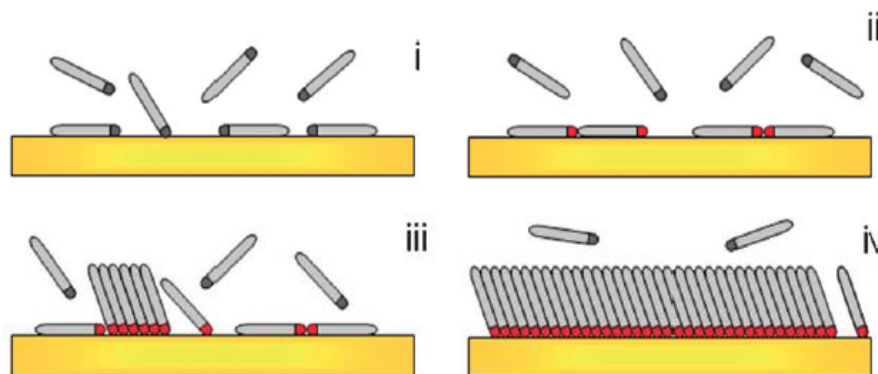


Figure 19: Illustration of the different steps forming a densely packed, crystalline 2D monolayer on a gold substrate; (i) physisorption, (ii) lying down phase formation, (iii) standing up phase and (iv) completed SAM formation. Reprinted from Salvarezza and co-workers.^[168]

The most simple description of SAM growth relies on an initial physisorption step, on which duration strongly depends on the surfactant's concentration,^[170] followed by subsequent chemisorption of the molecule, and finally formation of ordered domains with crystals in a closed-packed configuration (Figure 19).^[155,171–173] The physisorption process was followed at 5 K for methanethiol and dialkyl dimethyl molecules by using STM techniques.^[174] The most accepted hypothesis for the chemisorption of free thiols is that hydrogen atoms at the thiol

moiety are released as H₂ molecule.^[175–177] In strong contrast to long-chain alkyl-thiols, methyl thiolate SAMs are only formed using methyl disulfide, because direct reaction of methanethiol only leads to physisorption, since the S–H bond can not be cleaved.^[178] This discrepancy may be explained by the energy gain of the covalent RS–Au bond formation. The strong affinity of sulfur to gold (with bond strength of approximately 40 kcal · mol⁻¹)^[125] leads to an energy gain of ca. –5 kcal · mol⁻¹ for the covalent RS–Au bond.^[179] In contrast, the adsorption energy for alkyldithiol is ca. –12 kcal · mol⁻¹, which is twice as high and therefore more favorable. This measurement is supporting the faster replacement rate for alkanethiols compared to dialkyl disulfides.^[180] The possible mechanism of the SAM formation from dithiol is an oxidative addition of the dithiol.^[122] Formation process of the closed-packed layer is considerably slower affording a maximum density of molecules and minimum defects of the SAM. This is strongly dependent on experimental factors including solvent, temperature, concentration of surfactant, purity of surfactant, concentration of oxygen in solution, cleanliness of the substrate,^[124] but also structural effects of the compound itself, e.g., gauche defects, chain–chain interaction (VdW, dipole–dipole),^[170] or surface mobility of the chains.^[122] Chain–chain interactions contribute to the stability of the SAM, as well as the distance between the alkane chains. The reduced distance between the chains results in a tilted angle of 26° – 37° in order to optimize VdW forces.^[181–183] Since the CH₂ stretching vibrations are sensitive to packing density and the presence of gauche defects, IR-spectroscopy is the choice of analyzing technique.^[183] The surface mobility of the molecules allows self healing processes.^[184] However, issues containing thermal instability,^[185,186] limited electrochemical potential window,^[187] and oxidation of metal sulfate bonds^[184] are making this approach questionable for sensing applications.

SAMs on Carbon-Based Surfaces

The unique properties of graphene such as large surface area,^[188,189] excellent thermal conductivity,^[190] electric conductivity,^[189,191,192] and strong mechanical strength^[193] attracted the scientific field in recent years. Furthermore, graphene can be produced in large quantities from chemical^[194–197] or thermal^[198] reduction of graphene oxide. This is of important relevance since carbon is one of the most widely used material in electroanalysis and shows excellent performance in biosensors.^[199–204] These superior properties allowed

the production of thin film layers on flexible surfaces for lightweight conductive and transparent devices.^[205] Most of carbon based surfaces have been functionalized through oxidation^[206,207] leading to superficial carboxylic, quinoic, ketonic, or hydroxylic groups, which were then further reacted the appropriate surfactant. This approach of functionalization is difficult to control and often leads to undesirable corrosion of the carbon surface.^[208,209] Another surface modification was successfully implemented by electrochemical reduction of diazonium salts. This technique is superior among others including clean and nondestructive chemical functionalization of different substrate materials like carbon,^[210] metal,^[211] and semiconductors,^[212] as well as selective electrochemical modification of individual objects.^[213]

Electrografting of Aryl Diazonium Salts

Diazonium functionalities are typically prepared in a one-step reaction from aromatic amines, which are readily available. Tetrafluoroborates are particularly useful as counter ions as they are stable in aprotic and acidic environment (even stable in air for hours), but not stable in aqueous solutions above $\text{pH} \approx 2 - 3$.

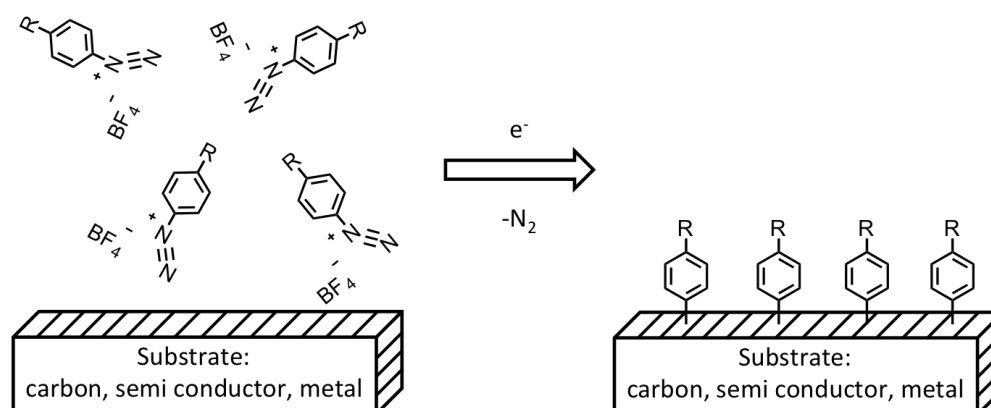


Figure 20: Functionalization of different surfaces, including carbon, semiconductor, and metal by diazonium salt. The aryl unit can be functionalized by a suitable group (R).

As various groups can be attached to the aryl unit, it is possible to obtain surfaces bearing a broad range of functionalization, e.g., alkyl, halogen alkyl, carboxylic, ester, cyanide, halides,

nitro, alcohols, thiols, and triple bonds (Figure 20). This modularity is very attractive for practical applications in biosensing. The method used for the electrografting process is rather simple, using typical electrochemical reaction conditions. The diazonium salt is dissolved in an aprotic media ($c = 1 - 10 \text{ mM}$) with a supporting electrolyte (0.1 M tetrabutylammonium tetrafluoroborate in acetonitrile) and subsequently reduced using the surface to be modified as a cathode. The potential is set by a potentiostat at the potential of the voltammetric peak of the diazonium for a variable period of time (seconds to minutes). This simple method enables the functionalization of a large amount of substrates, including carbon (glassy carbon and carbon fibers, pyrolyzed photoresist, pyrolyzed Teflon, carbon nanotubes),^[205,210,213–219] semiconductors (Si, GaAs),^[212,220,221] and noble metals (Au, Pt).^[222] Since this method is based on reductive reaction conditions, it enables the modification of easily oxidizable industrial materials such as Fe,^[211] Zn, Ni, Co^[222], Cu,^[222,223] and Pd.^[220] The low reduction potential, not rigorous exclusion of dioxygen, functional group tolerance, and different substrate capability make this method extremely appealing for research and industrial applications.

Mechanism of Grafting

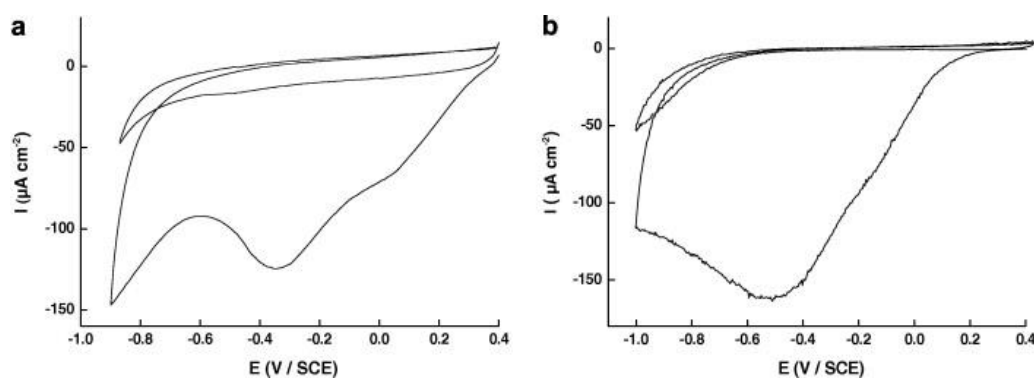
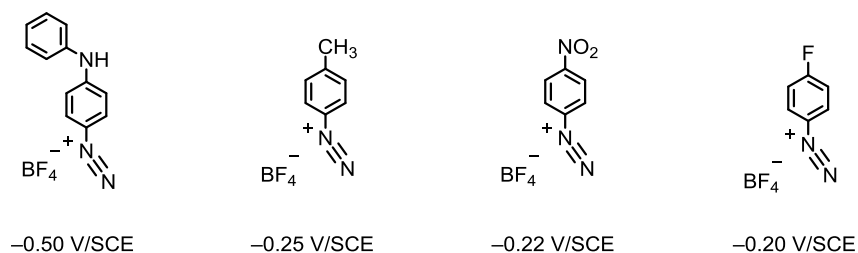


Figure 21: Cyclic voltammograms (first and fifth cycles) in 2 mM solution of AEBD diazonium salt in acetonitrile (+0.1 M NBu_4BF_4) using (a) gold electrode and (b) glassy carbon electrode. Reprinted from Chaussé and co-workers.^[224]

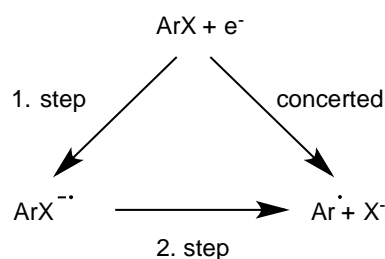
Cyclic voltammetry of (4-aminoethyl)benzenediazonium (AEBD) was performed using gold and glassy carbon electrodes (Figure 21).

In case of both electrodes the voltammogram exhibits a broad irreversible wave in the first cycle at $E_p = -0.35$ V/SCE and -0.51 V/SCE with gold and glassy carbon, respectively.^[224] The fact that the voltammetric wave is irreversible indicates that the diazonium gets reduced to dinitrogen via electron transfer. As the dinitrogen is in the gaseous state at room temperature, it leaves the system and the reduction is therefore irreversible. During the fifth scan the wave completely disappears, which is indicative of covering the surface by the organic compound. The relatively low reduction potential (ca. -0.5 V/SCE) is consistent with the characteristics of diazonium salts.^[210] However, this reduction potential can be modified depending on the functionality attached at the *p*-position on the aryl unit, ranging from -0.5 V/SCE (electron-donating substituents) to -0.2 V/SCE (electron-withdrawing substituents).^[213]



Scheme 14: Study of the electronic effects of the substituents at the *p*-position ranging from electron-donating (left, -0.5 V/SCE) to electron-withdrawing (right, -0.2 V/SCE) groups. Data obtained from Pilan and co-workers.^[213]

Because the mechanism of grafting by diazonium salts bases on an electron uptake, a comparison with the well-known aryl halogen reduction mechanism is reliable. Depending on the stability of the radical formed from aryl halides, the radical is formed closer (shorter lifetime) or farther (longer lifetime) away from the electrode due to diffusion processes after radical anion formation at the electrode. Therefore, if the radical is formed in a stepwise fashion (Scheme 15), it will react faster with a proton, abstracted from the solvent, or recombine with other radicals, because it is far away from the electrode. This stepwise radical formation, including cleavage of the intermediate radical anion (Scheme 15, 2. step), is more commonly observed in electrochemical cleavage experiments.^[225]



Scheme 15: Possible pathways of the aryl radical formation. In the stepwise pathway the aryl halogen gets first reduced and forms in a second step the reactive aryl radical. If the radical is formed following a concerted pathway, the radical is formed on the surface of the electrode.

However, if the electron transfer is concerted (radical is formed in one step) with the cleavage of the halogen, the radical will be formed on the surface of the electrode (Scheme 15, concerted).^[226] Nevertheless, the radical anion is a lot faster reduced than the parent aryl halide, leading to subsequent reduction into the aryl anion rather than allow the covalent binding with the surface.^[227] Since the diazonium salt is cleaved under milder reduction conditions (-0.16 V/SCE for benzene-diazonium),^[228] this functionality allows the grafting process with various substrates.^[210,229–231] This unique behavior of electrode grafting can be attributed to two specific features. (i) The very strong electron-withdrawing character of the positively charged diazonium group. (ii) The generation of the aryl radical is a concerted process that involves the electron transfer and the cleavage of dinitrogen before the formation of the covalent bond.^[225] The radical formation after dinitrogen cleavage is most likely contributing to the surface modification, since no grafting was observed for aryl halogens^[225] and anthracene,^[232] which preferably form radical anions and anionic species, respectively.

Characterization of the Grafted Organic Layer

The organic groups bonded to the surface can be characterized by electro-chemistry as long as they are electroactive. Therefore, nitro groups are often used, since they are reversibly reduced in aprotic medium by one electron to its stable radical anion ($E_p = -1.20$ V/SCE) (Figure 22a).^[211] A perfect example represents the electrografting of 4-nitrobenzene diazonium tetrafluoroborate salt (PNBD), which provides a surface modified with 4-nitrophenyl groups. Thereafter the electrode is thoroughly rinsed with acetone in an

ultrasonic bath for 5 min in the absence of oxygen and transferred to a new solution containing only the solvent and the supporting electrolyte (acetonitrile and 0.1 M tetrabutylammonium tetrafluoroborate). Under these conditions, a very broad reversible wave was observed around $E_p = -1.17$ V/SCE (Figure 22b).^[211] This observation reveals not only the presence of the reducible nitro groups showing a potential close to that of nitrobenzene itself, but also that their bonding to the surface is strong enough to resist rinsing in ultrasonic bath. Since the cathodic and anodic peaks are not shifting, the redox active species are bonded to the surface rather than diffuse away or towards the electrode. The same observation was reported for carbon-based substrates using almost identical experimental conditions.^[210]

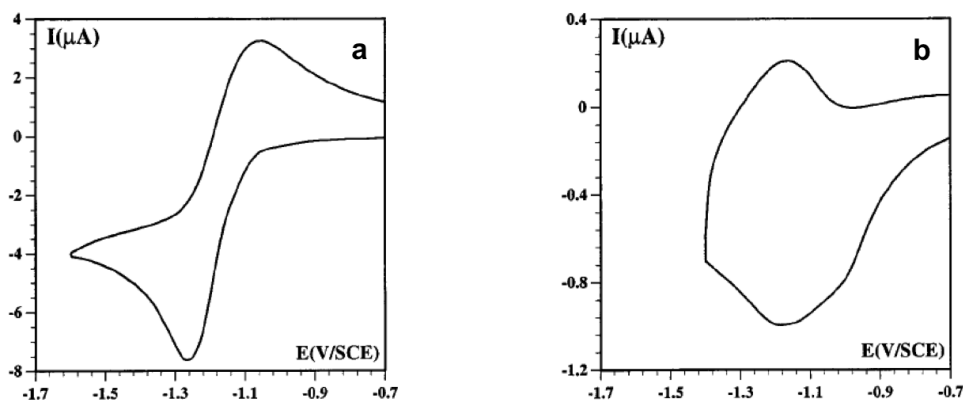


Figure 22: Cyclic voltammetry of nitrobenzene in acetonitrile ($c = 2$ mM) and 0.1 M tetrabutylammonium tetrafluoroborate using (a) an iron electrode and (b) an iron electrode electrografted with 4-nitrophenyl groups. Reprinted from Podvorica and co-workers.^[211]

The irreversible reduction process into the corresponding hydroxylamine or amine group has revealed the fact that these nitro groups remain intact in acidic aqueous media. This reduction was completed, indicated by the missing electrochemical signal of the nitro-phenyl group.^[215,233]

Another valuable technique to characterize the grafted electrode is the Fourier transform infra red (FTIR) spectroscopy. This analyzing technique takes advantage of the specific symmetric (1542 cm^{-1}) and asymmetric (1358 cm^{-1}) stretching bands of nitro moiety in PNBD. Both stretching vibrations were clearly observed by analyzing the grafted surface.^[222] Furthermore, the difference ($\nu_{\text{asymmetric}} - \nu_{\text{symmetric}} = 173 - 174\text{ cm}^{-1}$) for the modified

surface was equal to what could be expected for a solid ($159 - 177 \text{ cm}^{-1}$).^[234] FTIR is a suitable method since it reveals also information about the orientation of the grafted molecules. The in-plane CH-vibration of the aromatic ring (ca. 1044 cm^{-1})^[235] appears as strong band in the spectra of PNBD. However, this band appears much weaker in the surface modified by PNBD, supporting the fact that the phenyl unit is oriented perpendicular to the surface. The missing stretching band of the diazonium in the region between $2300 - 2130 \text{ cm}^{-1}$, indicates that PNBD is not merely absorbed on the surface,^[216,222] rather the radical cleavage of the diazonium salt on the electrode took place.

X-ray photoelectron spectroscopy (XPS) is a common technique to characterize a modified surface, and is therefore also a valuable method to investigate the grafted electrodes. Again, the PNBD is a widely used compound for grafting due to its characteristic binding energies of the electrons in the corresponding orbitals of C (1s), O (1s), and N (1s) appearing at ca. 285 eV, 530 eV, and 400 eV, respectively (Figure 23).^[207,210,236] In the case of metals and semiconductors, the attenuation of the signal is related to the atoms of the surface, which allows an estimation of the thickness of the organic layer.

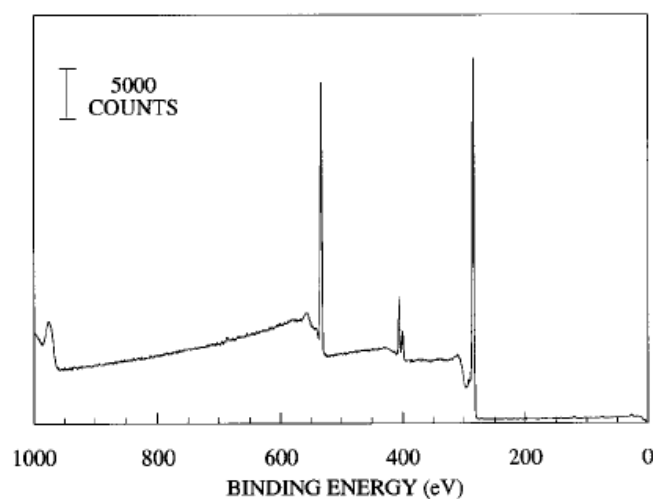


Figure 23: X-ray photoelectron survey spectrum for a 4-nitrophenyl modified glassy carbon electrode measured from grafting in a solution of PNBD (5 mM) in acetonitrile using tetrabutylammonium tetrafluoroborate (0.1 M) as supporting electrolyte. Reprinted from Bélanger and co-workers.^[236]

Atomic force microscopy (AFM)^[137,218,233] and scanning tunneling microscopy (STM)^[221] allow the observation of the modified surface by the "naked eye". The formation of a layer of variable height was observed by estimating the thickness of the organic layers following a

AFM scratch procedure.^[218] The term AFM scratching is used when the tip is scanned under strong loading forces to remove the organic layer on a relatively hard substrate. Using this technique the organic material is removed from the surface in a well-defined manner, leaving deep trenches with the characteristic shape of the used tip (Figure 24a). In the presented example for AFM imaging, a pyrolyzed photoresist film (PPF) was used, due to its relatively similar behavior towards electro-reduction of the diazonium ion compared to glassy carbon electrodes and their surface flatness (PPF roughness was estimated to be around 0.7 nm by AFM experiments). After grafting of triisopropylsilyl-protected *p*-ethynylbenzene diazonium and subsequent deprotection of triisopropylsilyl (TIPS) using tetrabutylammonium fluoride (TBAF) a very thin layer thickness (ca. 0.65 nm) was measured using AFM scratching method (Figure 24b). This measured height corresponds to the length of the ethynylbenzene molecule, supporting the fact of the formation of a single monolayer (Figure 24c). The TIPS protecting group for the *p*-ethynylbenzene diazonium moiety enabled the control of the deposition process by self-inhibition.^[137]

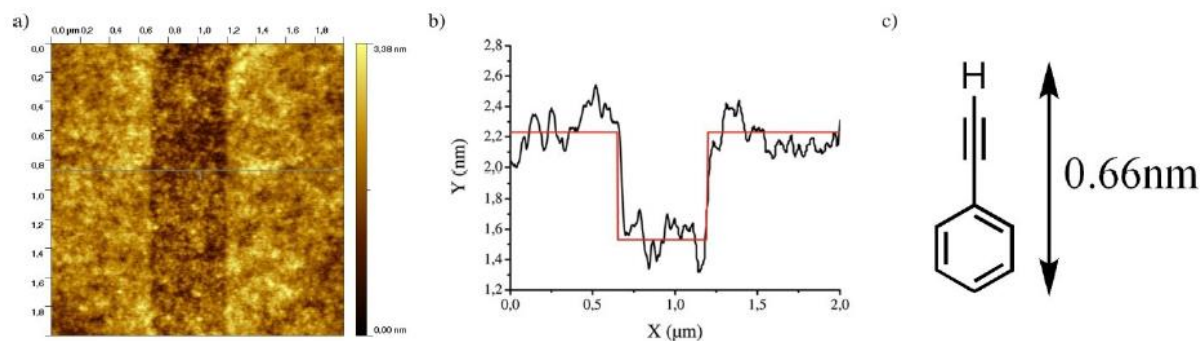


Figure 24: 2 x 2 μm topographic picture of PPF substrate modified with *p*-ethynylbenzene diazonium, showing a 0.4 x 2 μm scratch. b) Line profile (black) and adjustment curve (red) of the AFM picture presented in a). c) ethynylbenzene and its average length calculated with Chem 3D. Reprinted from Leroux and co-workers.^[137]

Having an ethynyl moiety SAM on a surface is very appealing for post functionalization by click chemistry.^[237] Due to its very mild reaction conditions and high selectivity it enables the attachment of any azide-derivatized electrochemical active biosensor.

Stability of Organic Layer

The bond strength between the surface and the organic layer was demonstrated by different experiments. First indication of a strong binding is represented in the resist of ultrasonic cleaning in a variety of solvents, including acetonitrile, *N,N'*-dimethylformamide, dimethyl sulfoxide, benzene benzonitrile, acetone, methanol, ethanol, methylene chloride, and chloroform^[207,211,238] representing almost all commonly organic solvents used in electrochemical experiments.

To examine long term stability of a glassy carbon electrode, PNBD electrografted electrode remained intact after six months when left on a laboratory bench.^[207]

Stability towards acidic or basic environment was demonstrated by 4-bromophenyl layers grafted on silica electrode, which resisted strong acidic conditions like 40% HF for 2 minutes and NH₄F (10 M) for one minute.^[212,221] When the same organic compound was grafted on a GaAs electrode, resistance towards concentrated hydrochloric acid and ammonium hydroxide for 5 minutes was observed.^[238]

Thermal stability was investigated using a 4-nitrophenyl modified carbon samples, which revealed excellent thermal stability when heated up to 700 K in ultra high vacuum.^[210]

Depending on the substituent at the aryl unit, a broad electrochemical resistance window was detected ranging from 2.6 to 5.6 V/SCE for 4-diethylamino- and 4-bromobenzene, respectively.^[239]

As mentioned above the organic layer can only be removed by AFM scratching methods. The resistance towards aggressive reagents, organic solvents, and high temperatures clearly excludes the involvement of non-covalent bonds, such as dipole–dipole, hydrogen bonding, or VdW interactions.

Sensing Based on Diazonium Grafting

A sensing device can be divided into two parts: (i) the active surface layer and (ii) the connection between the recognition-transduction component (transducer) and the surface. The ability of the active surface to specifically and selectively recognize the target species defines the performance of the sensor device. Other important features, such as long-term stability and reusability, require covalent attachment of the transducer. As mentioned above

diazonium salts represent an attractive covalent surface modification since they tolerate a broad range of functional groups. The preparation of an active surface can be conducted via two main approaches: (i) direct functionalization of the surface using diazonium salt reduction followed by immobilization of the desired bio-macromolecule and (ii) derivatization of the biomolecule by a diazonium functionality and subsequent grafting of the modified biomolecule to the surface.

Following the first approach, a gold electrode was electrochemically modified by 4-carboxyphenyl diazonium. Post-modification of the electrode with Gly-Gly-His using standard peptide-coupling conditions, a sensor for the selective detection of Cu^{2+} , Pb^{2+} and Cd^{2+} was prepared.^[240]

A grafted monolayer of histidine-tagged proteins showed a controlled molecular orientation. It was shown that the bioactivity remained intact after the covalently binding of metal complexes. This versatile, fast, and simple method enabled the electrocatalytic detection of a neutravidin–horseradish peroxidase conjugate.^[241,242]

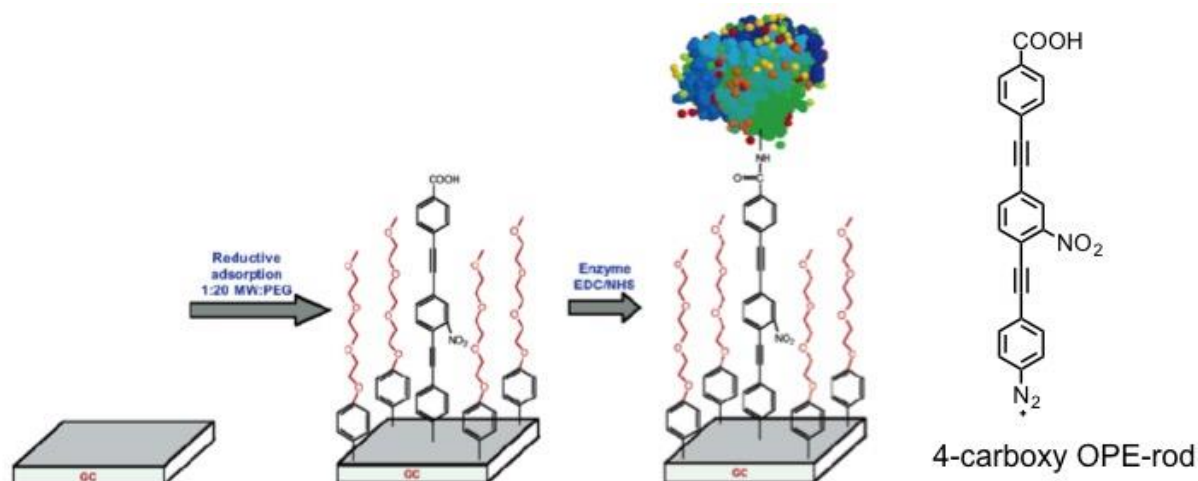
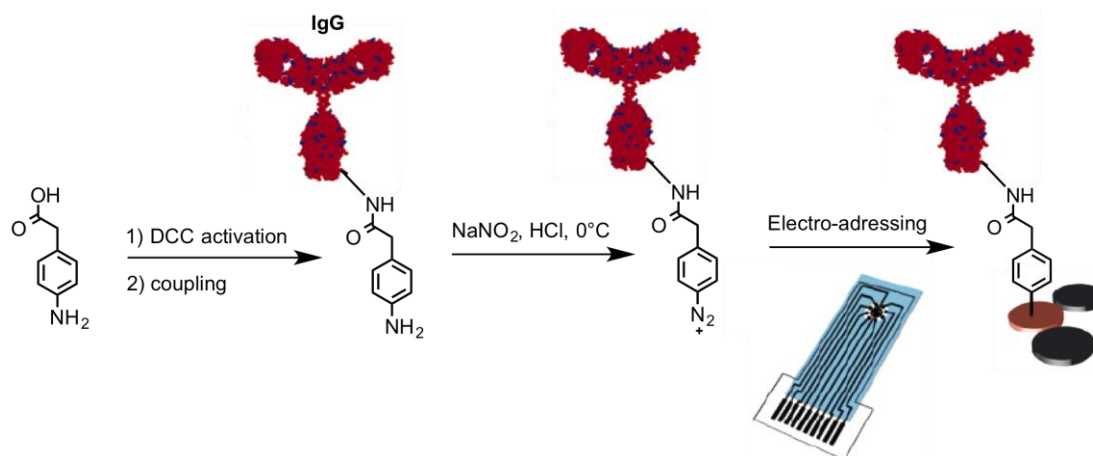


Figure 25: Illustration of a glassy carbon electrode grafted with a mixed monolayer of 4-carboxy OPE-rod and a PEG-functionalized benzene component. Reprinted from Gooding and co-workers.^[243]

A very elegant design for the attachment of glucose oxidase, was the modification of a carbon electrode by a mixed monolayer of a 4-carboxy OPE-rod and a PEG-functionalized benzene molecule, assembled from the respective aryl diazonium salts. The PEG facilitate efficient electron transfer from the grafted protein to the underlying electrode, since the

PEG moiety could penetrate into the redox active centers being buried deep within the glycoprotein and therefore reduce the tunneling distance (Figure 25).^[243]



Scheme 16: Modification of an electrode array by diazonium-functionalized antibody. Reprinted from Blum and co-workers.^[244]

Following the second approach 4-carboxymethylaniline was attached to IgG antibodies and subsequent diazotization afforded to the respective diazonium salt at the modified antibody. The drawback of this strategy relies on the reaction conditions used for the diazotization step. The conversion of the attached aryl amine into a diazonium requires 20 mM HCl and 20 mM NaNO₂. These rather harsh reaction conditions may not be compatible with other proteins. The modified antibodies were attached to different elements of a screen-printed graphite electrode micro-array simply by control of the potentials on each electrode in the array (Scheme 16). The antibody arrays were then used for detecting rheumatoid factor and other IgG antibodies via chemical luminescence with detection limits down to 50 fM.^[244,245] Another interesting example of environmental relevance was shown by grafting poly(acrylic acid) (PAA) on a surface. This active layer was successfully investigated for a switchable functionality used for the uptake and electro induced removal of copper ions. This simple strategy provides an efficient absorption of copper ions, which could be completely removed by acidification of the polymer film leading to a proton copper exchange. This approach was extended to capture and electrochemically release metal ions in real industrial waste solutions.^[246]

Electrochemically Sensitive Protecting Groups

Electrochemically removable protecting groups have attracted the scientific field for decades due to mild reaction conditions under which the deprotection occurs.^[247] Nowadays, functional groups like alcohols,^[248,249] ketones,^[250] aldehydes,^[251] carboxylic acids,^[252] amines,^[253,254] and phosphoric acids^[255] can be revealed by electrochemical deprotection. This leads to a tremendous variety of surface immobilization^[207] and functionalization.^[256] The work published by Kim and co-workers is particularly interesting.^[252] They were able to immobilize dithiol **A** on a gold surface forming a SAM. Furthermore, they showed the release of a free carboxylic acid by electrochemical deprotection. The carboxylic acids pointing away from the surface where then covalently bound to amino-derivatized oligodeoxynucleotides (Figure 26).

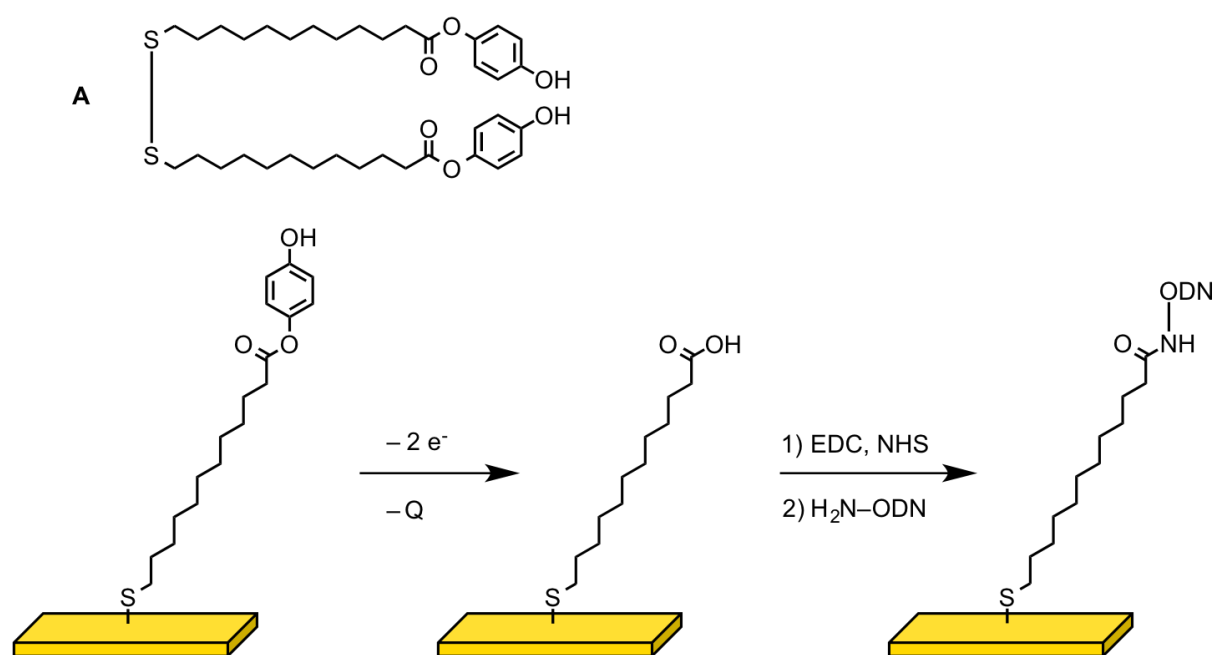


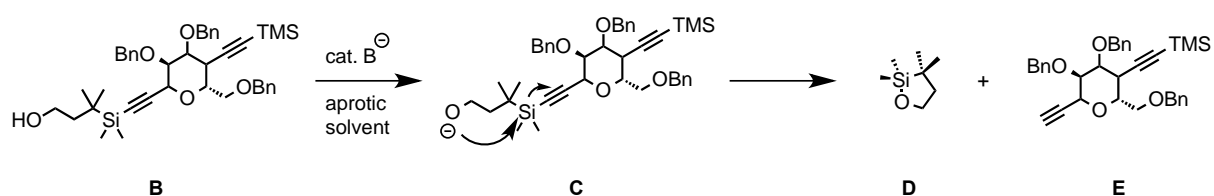
Figure 26: SAM formation of dithiol **A** on gold surface followed by oxidative cleavage of the carboxylic protecting group triggered by an electrochemical potential. Free carboxylic functionalities were post-functionalized with amino-derivatized oligodeoxynucleotides by peptide chemistry using 1-ethyl-3-[3-(dimethylamino)-propyl]carbodiimide hydrochloride (EDC) and N-hydroxysuccinimide (NHS).^[252]

Because of the above mentioned disadvantages of a SAM formed on a gold surface, a stronger bond between the surface and the surfactant is required. As click chemistry allow very mild reactions, which allow further surface modification, the functional group of choice would be an ethynyl group. It was shown that the ethynyl group remains intact after surface

modification using diazonium electrografting methods as well as post-functionalization by click chemistry.^[137,242,257,258] In order to minimize the number of chemical steps in the formation of the surface-active layer it is important to find a strategy that releases the ethynyl moiety by using exclusively electrochemical reaction conditions. Since the controlled attachment of a monolayer requires an ethynyl protecting group^[137] this electrochemically cleavable group needs to be developed. As the ethynyl moiety is also used as a building block in various fields in organic chemistry, a tremendous amount of protecting groups have been developed so far.^[259] This fact makes the development of a reductive method for ethynyl release even more attractive, due to its orthogonality to other deprotecting reagents and very mild reaction conditions, such as low temperature and non-basic or acidic environment.

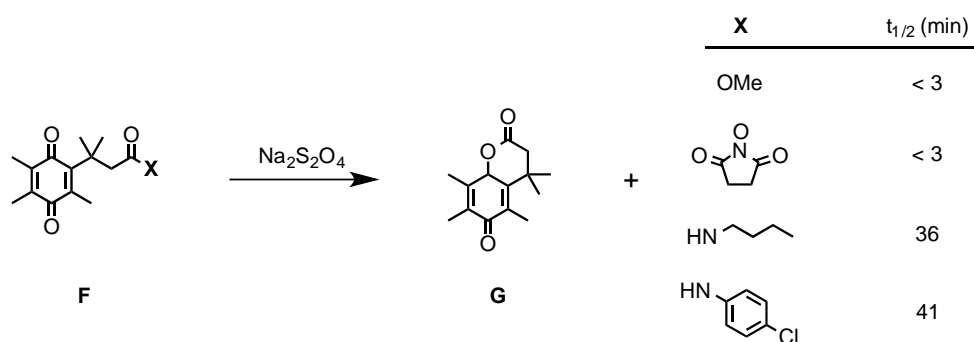
Aim of the Work

The use of benzene-diazonium salts for SAM formation enables the covalent attachment of various functional moieties on different substrate materials including, carbon, metals, and semi-conductors. Corgier and co-workers modified a carbon-based surface by using an antibody bearing the diazonium functionality. The drawback of this biosensing approach is that the protein has to survive the conditions of the diazonium formation.^[244] To overcome this issue, Leroux and co-workers developed another method, where the post-modification was successfully carried out under mild click-chemistry conditions. Nevertheless, the release of the acetylene moiety required treatment with tetrabutylammonium fluoride in order to cleave the TIPS protecting group.^[137] Therefore a protecting group that can be cleaved by applying a reductive potential could save one step, since any surface can be grafted by applying a small negative potential using diazonium salts. Vasella and co-workers reported an inspiring approach for a new acetylene protecting group. They were able to release the free acetylene by deprotonating the alcohol **B** followed by a nucleophilic attack on the silyl moiety **C**, forming a 5-membered oxo-silyl ring **D**, and final release of the free acetylene **E** (Scheme 17).^[260]



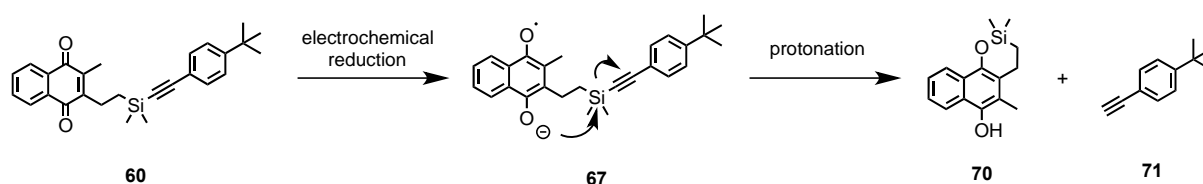
Scheme 17: Proposed mechanism of releasing the free acetylene **E**, upon the formation a 5-membered oxo-silyl ring **D**.^[260]

Another interesting work was reported by Carpino and co-workers.^[261] They were able to reduce different quinones **F** under mild reaction conditions using sodium dithionite ($\text{Na}_2\text{S}_2\text{O}_4$) as a reducing reagent. The reduced quinone moiety underwent spontaneous cyclisation to the corresponding lactones **G** releasing leaving group (**X**) (Scheme 18).



Scheme 18: Lactone formation **G** after reduction of **F** with sodium dithionite releasing the leaving group (**X**) within minutes.^[261]

The aim of this work was to develop a novel acetylene protecting group that can be cleaved under reductive reaction conditions using either sodium dithionite or electro-chemistry. By combining the strategies of Vasella and Carpino the synthesis of a new acetylene protecting group that is attached to an ethynyl benzene moiety (**60**) was envisaged. This new protecting group comprises a quinone as an electrochemically reducible subunit attached to the silyl-acetylene moiety. By applying electrochemical reduction conditions the quinone should form the radical anion **67**, which may undergo a nucleophilic attack on the silyl moiety forming a 6-membered oxo-silyl ring **70** releasing the free acetylene **71** (Scheme 19). These reaction conditions are not only mild, but also orthogonal to the alkyne deprotection procedures known in literature.^[262–267]



Scheme 19: Possible mechanism of new electrochemically cleavable acetylene protecting group. The reduced radical anion **67** performs a nucleophilic attack on the silane center, releasing the acetylene **71** upon formation of the 6-membered oxo-silyl ring **70**. As this mechanism includes a bond-forming as well as a bond-breaking process, the cleavage of the acetylene **71** becomes irreversible.

The future objective of this project will be the formation of SAM on various surfaces (e.g., carbon, ITO). In order to enable the SAM formation of ethynylbenzene, the electrochemically cleavable protecting group is attached acetylene moiety. Moreover, functionalization of the benzene group in *para*-position with a surface-binding group will

lead to a strong bond between the protected ethynylbenzene compound and the surface (Figure 27, left). The diazonium salt derivatized compound **73a** is perfectly suited for electrografting approaches as it possesses all of the required features of a free acetylene SAM formation using exclusively electrochemistry. By using a negative potential (ca. $E^{\circ} = -0.4$ V/SCE) the protected acetylene moiety will be grafted on a surface forming a SAM. Subsequently, the acetylene protecting group will be cleaved at a more negative potential (Figure 27) following the proposed mechanism in scheme 19. For the post-functionalization of this free acetylene SAM click chemistry is considered. This approach would represent the first grafting of free acetylene fully provided by electrochemistry. A similar approach will be followed for the ethylenediaminetetraacetic acid (EDTA) derivatized compound **73b** by dipping an ITO substrate into a solution of this compound, which leads as well to a SAM. Subsequently electrochemically cleavage of the protecting group will lead to a SAM of ethynylbenzene on an ITO substrate.

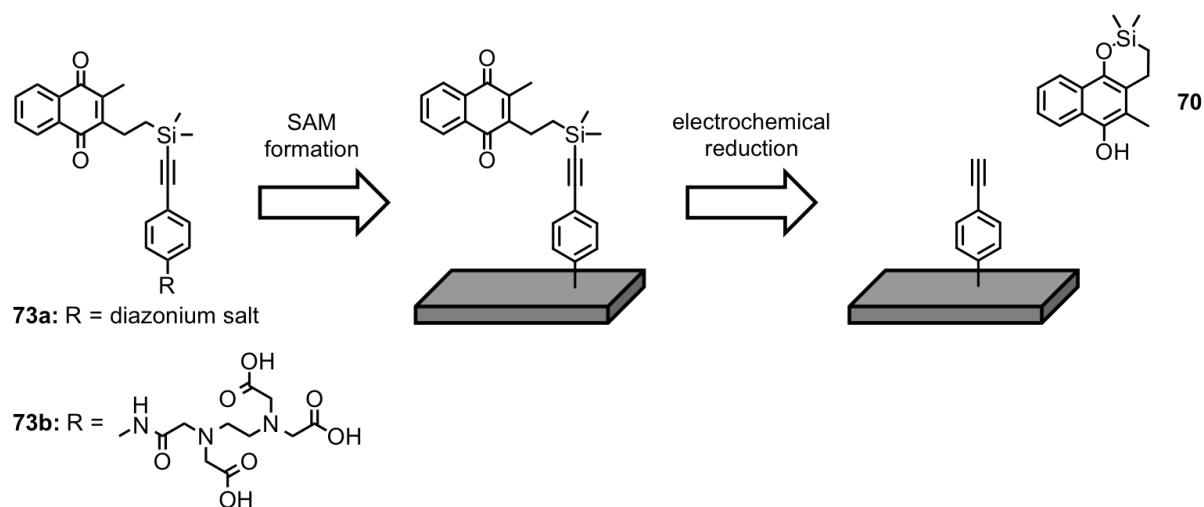


Figure 27: Future objective of this project: SAM formation of protected ethynylbenzene on a surface (carbon or ITO). Upon applying a negative potential, the quinone will get reduced and release the free acetylene, which can be post-modified by click chemistry.

Molecular Design

The approach towards a reductively cleavable acetylene protecting group was to spatially separate the actual connection to the acetylene from the redox active moiety. This leads to increased stability of the acetylene, while allowing a synthetic fine-tuning of the redox potential such that an efficient and mild cleavage can be realized. The release of the acetylene is therefore a two-step process: (i) the redox sensitive moiety is activated and (ii) interacts with the center next to the alkyne, which causes the liberation of the acetylene. If the alkyne is liberated not only by a bond-breaking, but also bond-forming step, it becomes irreversible. The quinone was quickly identified as an ideally suited redox moiety (Figure 28). Quinones are not readily modified and possess well-documented electrochemical properties^[268] but also form—upon reduction—the radical anion that is predominately located on the two oxygen atoms.

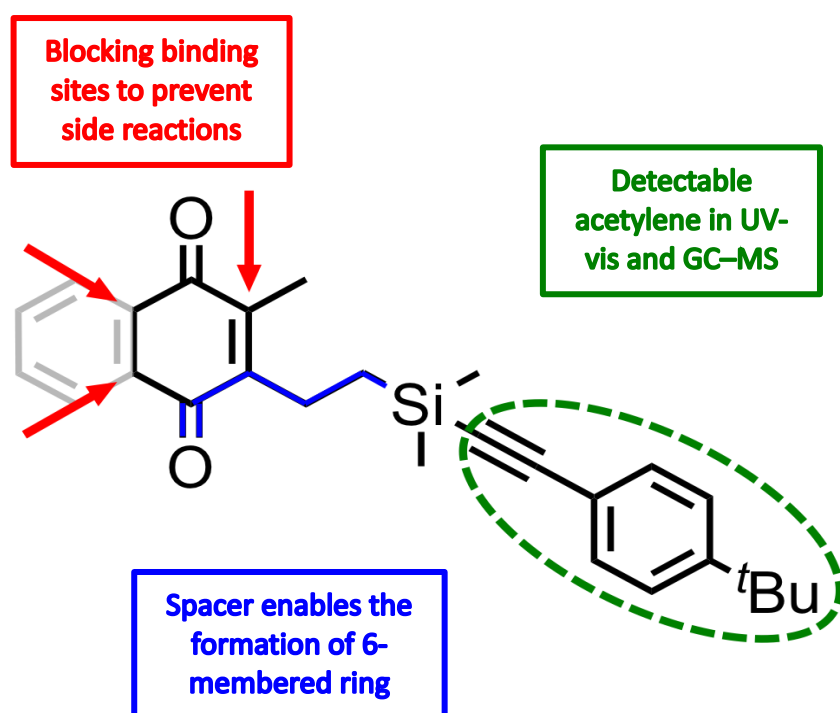


Figure 28: Molecular design of a novel acetylene protecting group, which can be cleaved electrochemically. The red arrows are indicating the binding sites blocked by a phenyl unit or a methyl moiety. The blue line is pointing out the 6-membered oxo-silyl ring, which will be formed. The green dotted line is showing the acetylene of choice due to its well distinguishable optical properties, compared to the quinone subunit.

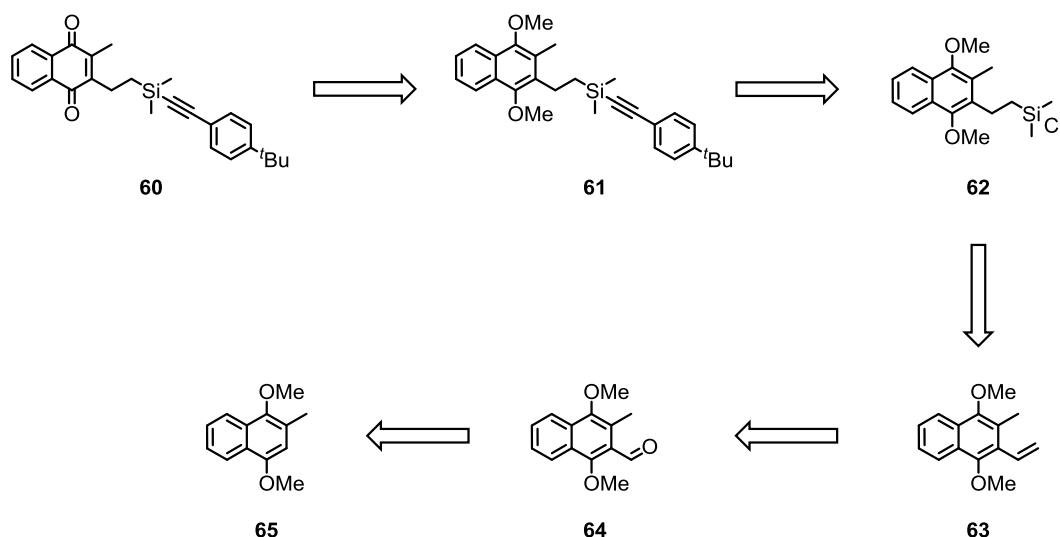
When considering suitable quinone moieties one quickly realizes that while the low redox potential of *p*-benzoquinone ($E^{\circ} = -0.45$ V/SCE in acetonitrile)^[269] was in an ideal range, it also enables spontaneous dimerization, Diels–Alder cyclization,^[270] and Michael addition.^[271] It was therefore crucial to modify the quinone such that side reactions can be prevented while retaining the low redox potential. Figure 28 (red arrows) indicates the required changes to the quinone backbone. It was found that the commercially available menadione was an excellent candidate. Not only are all three reaction sites blocked except where the installation of the alkyl spacer was envisaged, the additional aromatic ring possibly lowers the required potential to form the radical anion ($E^{\circ} = -0.71$ V/SCE in acetonitrile for menadione).^[269]

In order to enable the efficient attack of the silyl moiety by the formed anion, it was important to separate the two mentioned reactive centers in an appropriate distance from each other. The insertion of an alkyl spacer (Figure 28, blue) that will be attached to the remaining free center of the quinone, completely breaks the electrical communication between the acetylene and the quinone backbone. Its length was chosen such that the resulting attack leads to the spontaneous formation of an energetically favored six-membered ring.^[261]

To complete the test system, the commercially available 4-*tert*-butylphenylacetylene (Figure 28, green) was chosen since the optical properties ($\lambda_{\text{max}} = 245$ nm in 1,2 dichloroethane)^[272] are readily distinguishable from the quinone π - π^* transition of menadione ($\lambda_{\text{max}} = 263$ nm).^[273] The liberated acetylene can, due to its molecular weight (158.24 g · mol⁻¹) also be detected by gas chromatography–mass spectrometry (GC–MS) giving a second indicator for the success of the reaction.

Synthetic Strategy

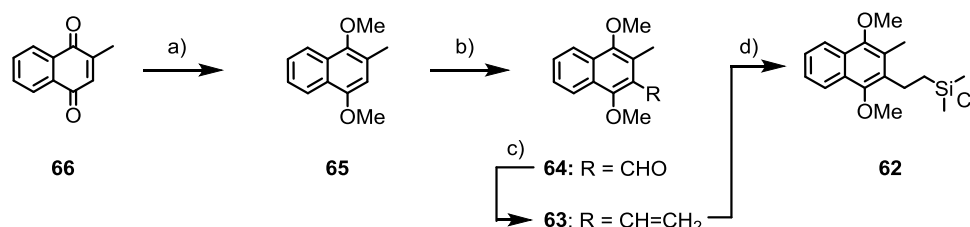
To realize the synthesis of a novel acetylene protecting group, which can be cleaved upon reductive reaction conditions, the following synthetic strategy was envisaged (Scheme 20). As the quinone moiety represents an instable and readily reactive functionality, this subunit will be installed at the very last step of the synthetic pathway to prevent undesired side reactions during the synthesis. In order to attach the desired acetylene moiety, silyl-chloride will be readily exchanged by commercially available 4-*tert*-butylphenylacetylene using S_N2 -reaction conditions. The probably most challenging step within this strategy will be the synthesis of silane chloride **62**. For the installation of the silane moiety, hydrosilylation of Wittig product **63** is considered. As the silane chloride is sensitive to air and moisture a very clean and efficient reaction is required in order to facilitate purification. Furthermore, purification methods other than column chromatography have to be considered for the isolation of silane chloride **62** in large quantities under exclusion of moisture and air. The synthesis of the desired aldehyde **64** required for the Wittig olefination reaction is already reported in literature starting from the commercially available menadione (**66**).^[274]



Scheme 20: Synthetic strategy of target compound **60**. As the quinone moiety is prone for degradation, this functionality will be installed in the very latest reaction step via oxidation of the dimethoxy precursor **61**. For the synthesis of **61**, the commercially available 4-*tert*-butylphenylacetylene (**71**) is attached using S_N2 -reaction conditions. The key step of this strategy is the synthesis of silyl-chloride **62** via hydrosilylation. Wittig-olefination of aldehyde **64** leads to the precursor **63**. For the synthesis of **64** Rieche-formylation of the dimethoxy-protected menadione **65** is considered.

Results and Discussion

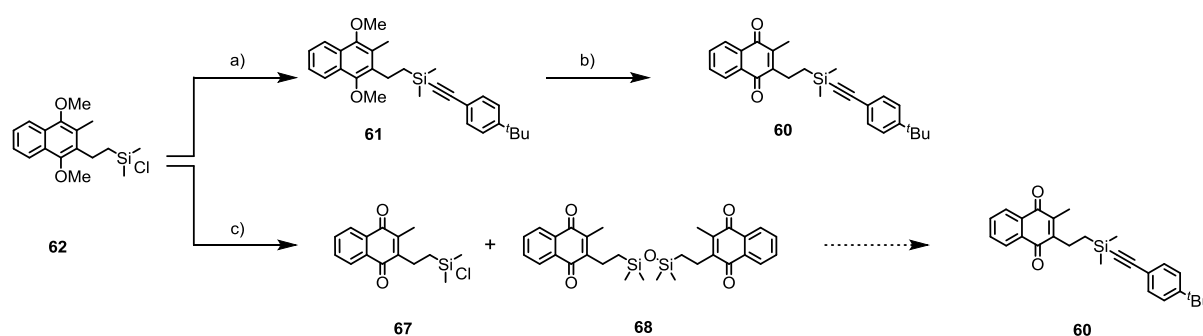
Synthesis



Scheme 21: Reagent and reaction conditions: a) SnCl₂, HCl, MeOH, 1 h, rt; then K₂CO₃, Me₂SO₄, acetone, 4 h, reflux, 68% over two steps; b) TiCl₄, dichloro(methoxy)methane, CH₂Cl₂, 3 h, 0 °C, 90%; c) MeP(Ph₃)Br, *n*-BuLi, THF, 0 °C to rt, 3h, 90%; d) Karstedt's catalyst, dimethylchlorosilane, 34 °C, 3 h, 75%.

The straightforward synthesis of the quinone **60** started from the commercially available menadione (**66**), which was in a first step reduced by tin chloride under acidic conditions in methanol. The crude dihydroxy product was directly methylated using dimethyl sulfate in acetone at reflux temperature providing the dimethoxy product **65** in good yield of 68% over two steps.^[275] Subsequently, the dimethoxy **65** was transformed in 90% into the aldehyde **64** using classical Rieche-formylation reaction conditions.^[274] Formylated product **64** was subjected to a Wittig olefination reaction with methyltriphenylphosphonium bromide as olefination reagent affording **63** in 90%. The key step of this synthetic strategy was conducted via hydrosilylation reaction conditions, providing silyl-chloride **62** in 75% using Karstedt's catalyst as Pt(0) source. Since the silyl-chloride **62** is sensitive to air and moisture the crude reaction mixture was subjected to Kugelrohr distillation after completed conversion. This purification technique allowed not only the isolation of the product **62** in large quantities but also working constantly under an inert atmosphere. Direct oxidation of the silyl-chloride **62** is very challenging as most oxidizing reagent require water as solvent due to the diminished solubility of the oxidant in organic solvents (e.g. Fremy's salt, FeCl₃).^[276,277] Moreover, water often provides the oxygen moiety (e.g., (diacetoxyiodo)-benzene, cer(IV)-ammoniumnitrat (CAN), AgO, CoF₃)^[278-281] and throughout the whole oxidizing pathway nor negatively charged oxygen or a free alcohol (e.g., BBr₃, *N*-bromosuccinimide)^[282,283] are allowed due to the fast formation of the 6-membered oxo-silyl ring. To overcome the solubility issue of the oxidant, the oxidizing reagent was immobilized

on silica. Therefore, CAN was dissolved in water, added to silica and stirred for a few minutes. The silyl-chloride **62** was dissolved in methylene chloride and added to the immobilized CAN.^[284] Analysis of the ¹H NMR indicated the presence quinone, but the GC-MS trace showed a mass way too high for the desired product (**67**) but fitting perfectly with the oxo-bridged dimer **68**. This observation was attributed to chloro-oxygen exchange, which originates from the remaining water encapsulated in the silica. Delightfully, a fast and simple two-step method including the attachment of 4-*tert*-butylphenylacetylene provided **61**, followed by subsequent oxidation, using CAN as oxidizing agent in a mixture of water and acetonitrile (1 : 2) yielded the bench stable quinone **60** in 77% over two steps (Scheme 22).



Scheme 22: Reagent and reaction conditions: a) 4-*tert*-Butylphenylacetylene, *n*-BuLi, THF, $-78\text{ }^{\circ}\text{C}$, 1 h; b) CAN, MeCN : water (2 : 1), rt, 1 h, 77% over two steps; c) CAN (immobilized on silica), DCM, rt, 1 h, 72% (**68**).

Chemical Reduction

Having the quinone **60** in hand, the deprotection step was investigated first by pure chemical reduction using sodium dithionite (redox potential ranging from $E^{\circ} = -0.65$ to -0.75 V/NHE).^[285] Therefore, screenings of different organic aprotic solvents that are prone for $S_{\text{N}}2$ -reaction and well mixable with water were investigated. The use of water is essential, because it enables the dissociation of $\text{Na}_2\text{S}_2\text{O}_4$ into the reactive species $2\text{Na}^+\text{(SO}_4^{\text{-}})$. The organic solvents of choice were acetone, *N,N*-dimethylformamide (DMF), and dimethyl sulfoxide (DMSO). In the experiment the quinone **60** was dissolved in a mixture of organic solvent and water (20 : 1). The resulting yellow mixture was degassed for 10 minutes followed by the addition of 20 equivalents of the reduction reagent. Instant

decolourization was observed, indicating the end of the reaction. A small reaction sample was taken out and injected into the GC–MS (Figure 29). To our delight, the GC–MS trace showed no starting material present after one minute for all investigated solvents. Moreover, the two expected products were observed (Figure 29, red line). Even more delightfully, not only the mass of the free acetylene **71** but also the mass of the 6-membered oxo-sily ring **70** was detected. Isolation of the formed products provided the free acetylene **71** in quantitative yield. Unfortunately, the isolation the 6-membered oxo-silyl product **70** has not been achieved yet.

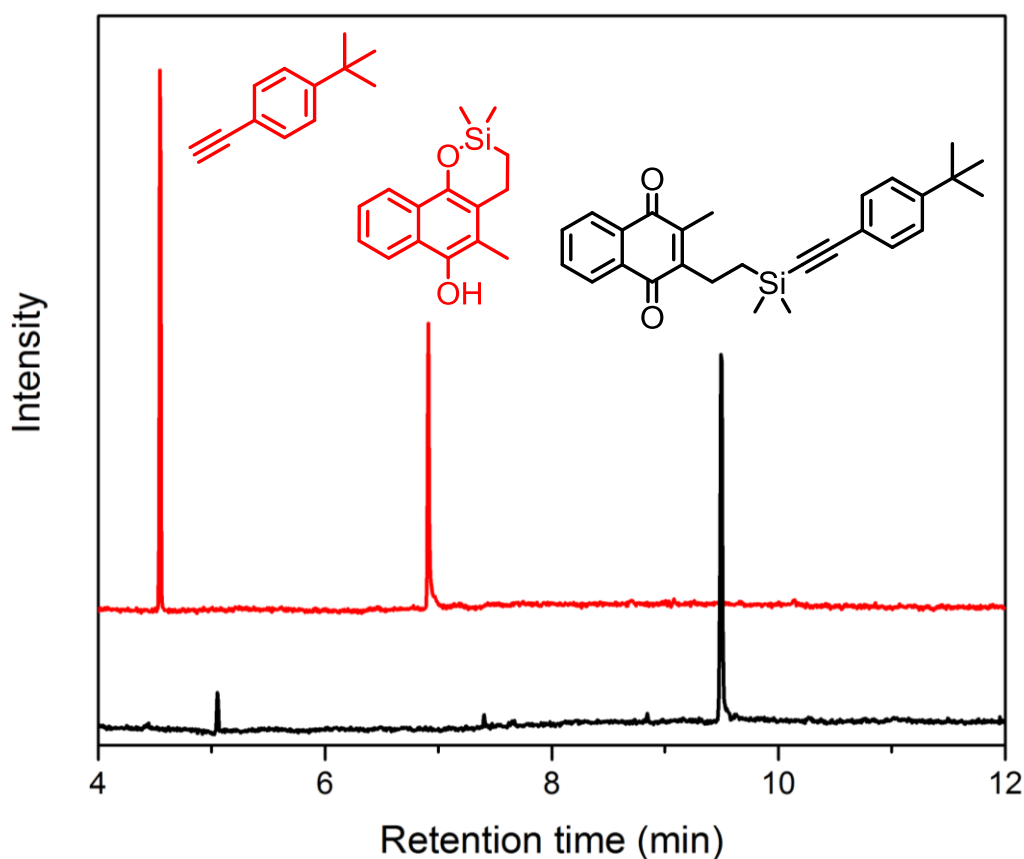


Figure 29: Stacked GC–MS trace of quinone **60** exemplified for reaction performed in DMSO (black line) and of the reaction mixture 1 min after the addition of Na₂S₂O₄ (red line). The mass peaks of the red line matched perfectly to the corresponding free acetylene **71** and the 6-membered oxo-sily ring **70**, respectively.

Electrochemical Reduction

Next, the electrochemical cleavage of the acetylene protecting group was investigated by spectroelectrochemistry techniques. To observe the acetylene release in a spectroelectrochemical cell, absorption spectra of the acetylene **71** (red) and quinone **60** (black) in acetonitrile using a concentration of 10^{-5} M was recorded first. The recorded spectra are shown in figure 30 and the absorption bands are listed in table 7.

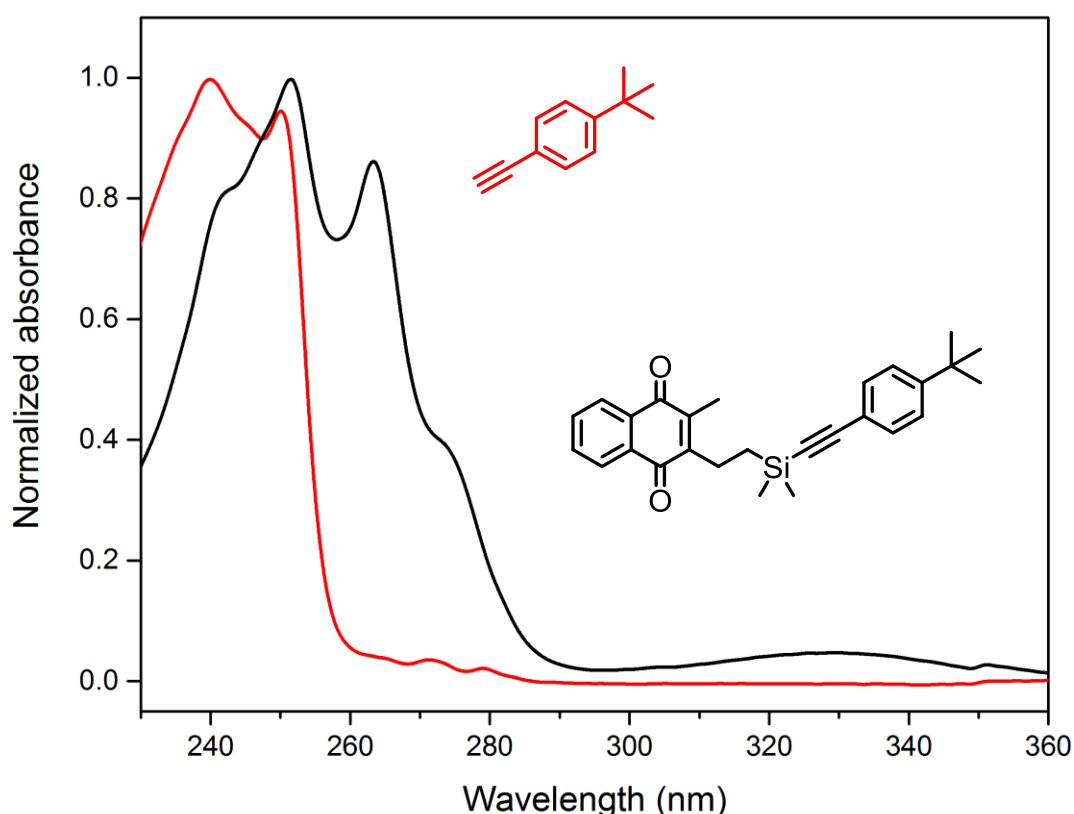


Figure 30: Normalized absorption spectra of acetylene **71** (red) and quinone **60** (black) in acetonitrile (10^{-5} M).

The acetylene **71** (red) displays two absorption bands at $\lambda_{\text{max}} = 240$ nm and at $\lambda_{\text{max}} = 250$ nm, which were assigned to the π - π^* transition bands.^[272,286] Based on the structural design it was anticipated that the quinone subunit would not interact electronically with the phenylacetylene unit, due to the insulating alkyl spacer. The intense band at $\lambda_{\text{max}} = 252$ nm was thus assigned to the benzene-type π - π^* transition band, whereas the other intense peak at $\lambda_{\text{max}} = 263$ nm was attributed to the quinone type transition band. The absorption band of

relatively low intensity at $\lambda_{\text{max}} = 333$ nm was also assigned to the benzene-type excitation.^[273]

To characterize the electrochemical properties, CV of the quinone **60** were recorded with an AutoLab PGSTAT302 potentiostat-galvanostat controlled by resident NOVA 9.1 software using a conventional single-compartment three-electrode cell. A glassy carbon disk (diameter of 2 mm) served as the working electrode, and a Pt wire was used as auxiliary electrode. The reference electrode was a saturated potassium chloride calomel electrode (SCE). The supporting electrolyte was 0.1 M Et₄NBF₄ in acetonitrile. All potentials are quoted relative to SCE using a scan rate of 100 mV/s for cyclic voltammetry. Solutions were purged with argon to remove the oxygen and argon was passed over the solution during the experiment. The concentration of the quinone **60** was 1 mM. The recorded values of reduction potentials are summarized in table 7.

Table 7: Measured UV-vis data of acetylene **71** and quinone **60**.

Compound	UV-vis ^a λ_{max} (nm)	ϵ^a (L · mol ⁻¹ · cm ⁻¹)	E _{red1} vs. SCE [Ⓜ] (V)	E _{red2} vs. SCE ^b (V)
71	240	75380	–	–
	250	73120		
60	252 (P-Band)	102530	–0.84	–1.17
	263 (Q-Band)	98460		
	333 (N-Band)	3590		

^aUV-vis spectra were measured in acetonitrile at a concentration of 10⁻⁵ M. ^bRecorded reduction values measured in acetonitrile with a concentration of 1 mM with a supporting electrolyte tetraethylammonium tetrafluoroborate in a concentration of 0.1 M.

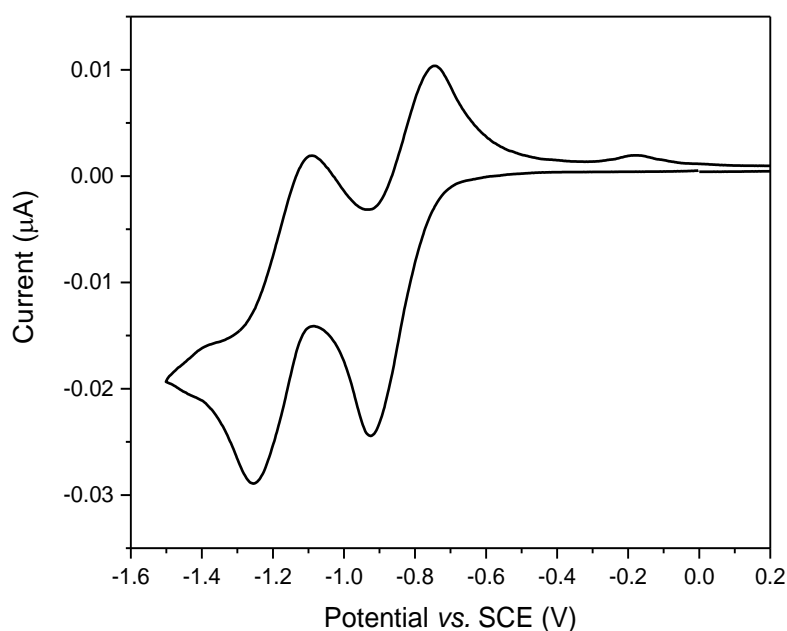


Figure 31: CV spectra of quinone **60** in acetonitrile with a concentration of 1 mM using tetraethylammonium tetrafluoroborate as supporting electrolyte in a concentration of 0.1 M.

Quinone **60** showed two one-electron reduction peaks in acetonitrile corresponding to one two-electron reduction process for a quinone. The first reduction peak at $E^{\circ} = -0.84$ V/SCE arises from the radical anion, and notably the second one at $E^{\circ} = -1.17$ V/SCE from the dianion species (Figure 31). The two redox potentials are in well agreement with reported values for different quinone derivatives.^[287]

The spectroelectrochemical experiments were all recorded with a sample concentration of 10^{-5} M, using a conventional single-compartment three-electrode cell. A Pt mesh with a size of 0.25 cm² served as working electrode, and a Pt wire was used as auxiliary electrode. The reference electrode was a saturated potassium chloride calomel electrode (SCE). The UV-vis spectra were recorded on a Cary 5000 UV/Vis/NIR spectrometer from Varian.

To determine the stability of the free acetylene towards degradation at the applied potential, spectroelectrochemical investigation of acetylene **71** was performed first. Observed UV-vis absorption spectra of acetylene **71** were recorded at potential of $E^{\circ} = 0$ V/SCE as shown in figure 32 (black line). Subsequently, UV-vis spectra were recorded repetitively when the negative potential was applied and held just below the value needed for the first reduction step ($E^{\circ} = -0.9$ V/SCE) (Figure 32, blue to red lines).

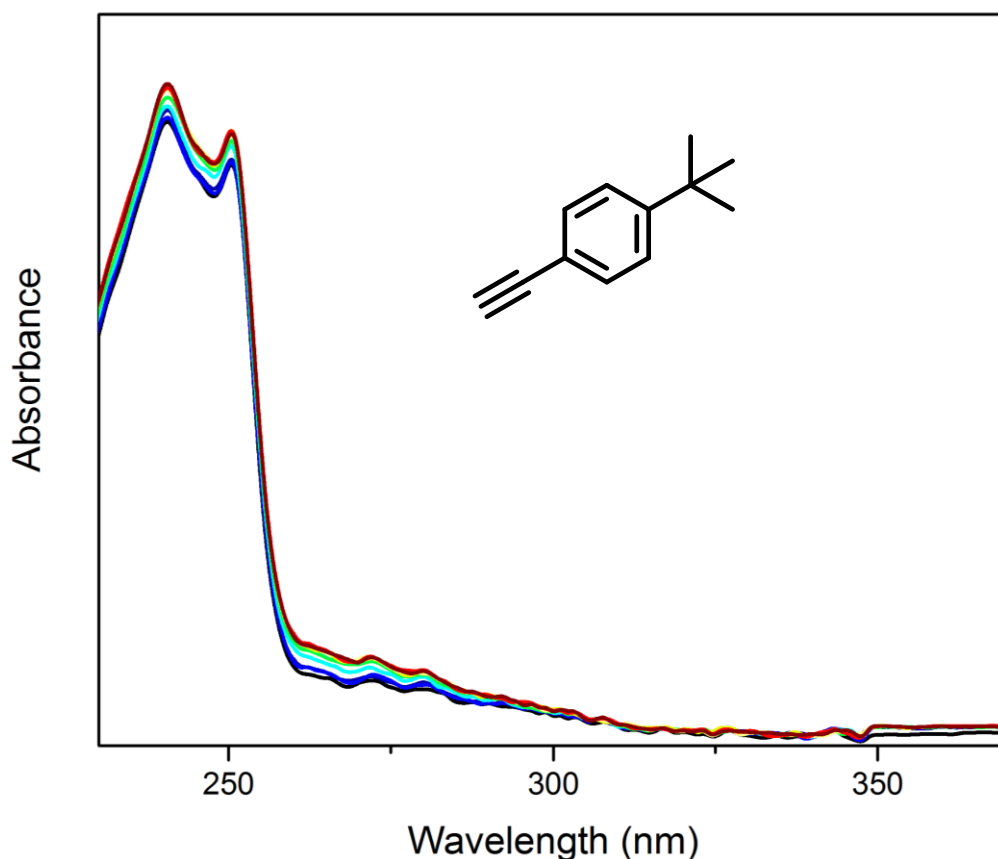


Figure 32: Absorption spectra of acetylene **71** dissolved in acetonitrile with a concentration of 10^{-5} M in a spectroelectrochemical cell containing 0.1 M tetraethylammonium tetrafluoroborate as electrolyte. After a potential of $E^o = -0.9$ V/SCE was applied, absorption spectra were performed continuously going from the blue to the red line.

UV-vis absorption spectra of acetylene **71** remains constant after applying a constant potential of $E^o = -0.9$ V/SCE confirming the stability of **71** at this potential. This experiment is crucial, since the absorption band at $\lambda_{\text{max}} = 240$ nm can be assigned exclusively to the release of the free acetylene **71**. Furthermore, no dimerization of the acetylene was observed in the course of the measurement, due to no new intense absorption bands arising in the range of 300 – 330 nm.^[272] In the spectroelectrochemical analysis of the quinone **60**, the focus was set on the absorption bands at $\lambda_{\text{max}} = 240$ nm exclusively attributed to the free acetylene and at $\lambda_{\text{max}} = 263$ nm exhibiting purely by the quinone subunit.^[273]

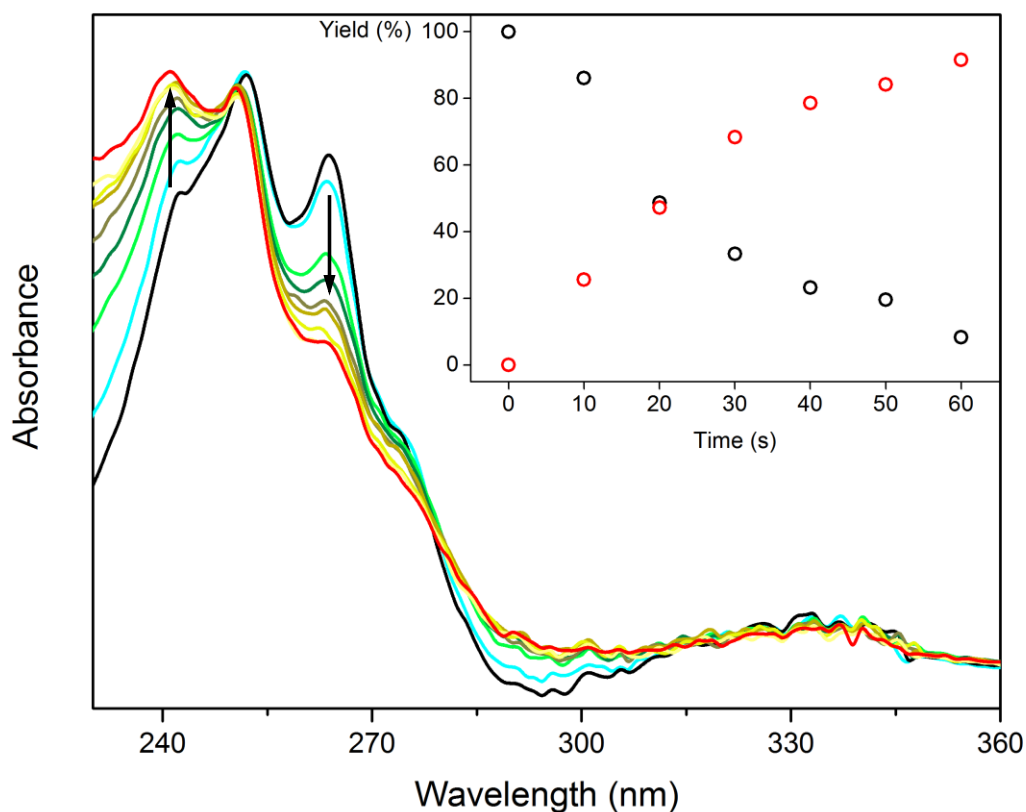
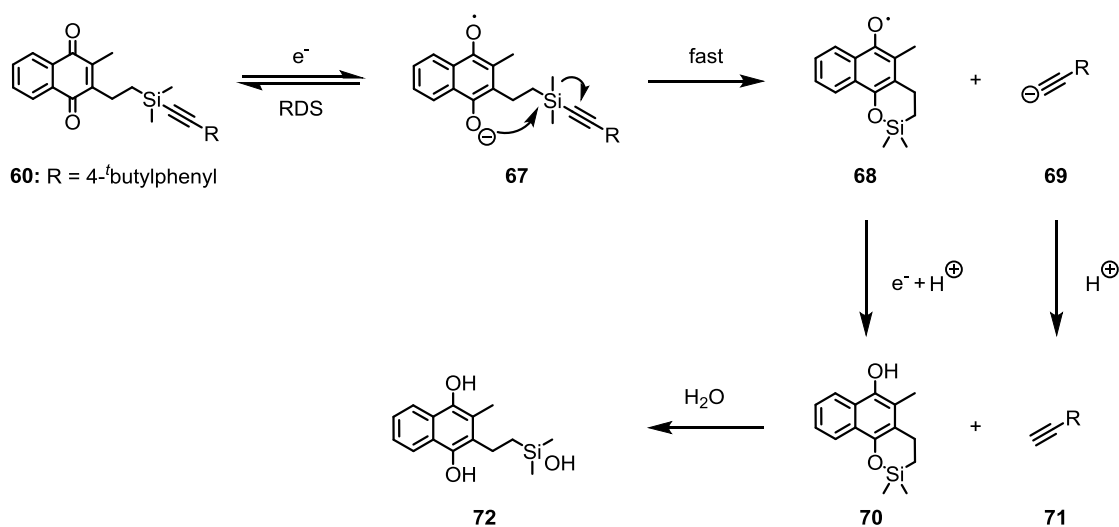


Figure 33: Absorption spectra of quinone **60** dissolved in acetonitrile with a concentration of 10^{-5} M in a spectroelectrochemical cell containing 0.1 M tetraethylammonium tetrafluoroborate as electrolyte. After a potential of $E^o = -0.9\text{V/SCE}$ was applied, absorption spectra were performed continuously going from the black to the red line. Trends of the corresponding absorption bands are indicated by black arrow. The inset displays the progression of the reaction every 10 seconds. The yield corresponds to relative intensities at peak maxima $\lambda_{\text{max}} = 263$ nm (quinone, black circles) and $\lambda_{\text{max}} = 240$ nm (acetylene, red circles).

As expected the absorption band at $\lambda_{\text{max}} = 263$ nm decreases continuously and remains constant, after completed one electron reduction of the quinone **60**. At the same time the absorption band at $\lambda_{\text{max}} = 240$ nm starts to increase until all quinone **60** was reduced. No new band above 300 nm was observed which allowed ruling out dimerization of the liberated alkyne (Figure 33). Pleasingly the reaction runs to completion within 60 seconds as shown in figure 33 (inset). Generally, the absorption spectrum is dominated by the free acetylene moiety after 60 seconds and the crossing event of the reaction progress after 20 seconds, both observations are strongly hinting at a very efficient nucleophilic attack ones reduction of the quinone occurs.



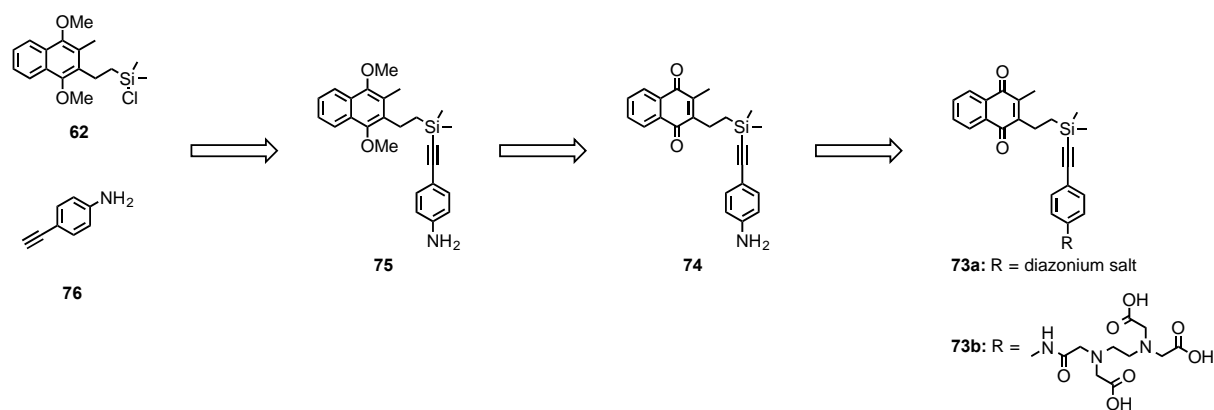
Scheme 23: Proposed mechanism of reductive cleavage of the acetylene protecting group. One electron reduction (RDS), followed by fast intramolecular 6-membered oxo-silyl ring formation **68**, and final release of the free acetylene **69**. Hydrolysis of **70** leads to the dihydroxy compound **72**.

Because no hydroquinone with the acetylene still attached (**67**) was measured by GC–MS and the crossing event observed by spectroelectrochemical investigations, the reduction of quinone **60** forming **67** was quoted as the rate-determining step (RDS) of the cleavage mechanism. Upon the nucleophilic attack of the oxygen on the silyl moiety, the intermediate **68** is formed resulting in a release of the acetylene **69**. Subsequent protonation of the released acetylene **69** leads to **71**, which was isolated in quantitative yield using chemical reductive conditions. Electron uptake followed by *in situ* protonation yields the oxo-silyl **70**. As the isolation of the 6-membered oxo-silyl ring **70** has not yet been achieved, hydrolysis during aqueous work up or column chromatography is most likely. This fact is supported due to the successful isolation of compound **72**.

Conclusion and Future Perspectives

The successful synthesis of the model compound **60** bearing a chemically and electrochemically reducible protecting group was achieved. By spatially separating the redox active center with an insulating alkyl spacer from the acetylene and substituting the quinone moiety accordingly achieved a fine-tuned redox potential and structural integrity. Following the synthetic strategy, aldehyde **64** was synthesized in analogy to a literature known procedure, starting from the commercially available meandione (**66**). Subsequent Wittig-olefination provided compound **63** in high yield and gram quantities. The introduction of the silyl-chloride moiety was provided by hydrosilylation reaction conditions afforded **62** in 75%. The oxidation of the silyl-chloride **62** has not yet been successful, yielding exclusively the oxo-bridged dimer **68**. To overcome this issue, absolute water-free oxidation reaction conditions have to be envisaged. This is still a very challenging issue, since most of the oxidation agents are only soluble in water, or water is released at some point in the course of the reaction. Delightfully, the synthesis of the target compound **60** was achieved in 77% over two steps after insertion of the acetylene moiety, followed by oxidation using CAN. By applying chemical reaction conditions using sodium dithionite as a reducing reagent, the quantitative and exclusive formation of two products, the free acetylene **71** and the 6-membered oxo-silyl **70**, was observed by GC-MS analysis. Furthermore, the electrochemically-triggered release of acetylene using spectroelectrochemical techniques was investigated. The quinone **60** was reduced electrochemically, as shown by the decrease of the absorption band at $\lambda_{\text{max}} = 263$ nm while the acetylene **71** is released as indicated by an increase of the absorption band at $\lambda_{\text{max}} = 240$ nm, after applying a constant potential at $E^{\circ} = -0.9$ V/SCE. These results are strongly supporting the proposed mechanism of the reduction-release process. This work shows the first example of releasing the acetylene induced by an electrochemical potential.

As the future goal of this project is the electrografting of a protected ethynylbenzene the synthetic strategy of compound **73** is envisaged (Scheme 24). The advantage of this compound upon other free acetylene grafted molecules would be that the immobilization of **73** on a surface and subsequent release of the acetylene protecting group is provided exclusively by applying a negative electrochemical potential.



Scheme 24: To enable the synthesis of the compounds **73a** and **73b**, the amine **74** is required. In analogy to the previously developed synthetic strategy of quinone **60**, the oxidation of the dimethoxy **18**, leads to the quinone **74**. For the synthesis of dimethoxy **75**, a S_N2 -reaction between the acetylene **76** and the previously synthesized silyl-chloride **62** are considered.

In this synthetic strategy for both, the diazotized compound **73a** as well as the EDTA derivatized compound **73b** the quinone **74** is required. In analogy to the previously developed synthetic strategy of quinone **60** a late step oxidation of dimethoxy **75** is envisaged. The synthesis of the dimethoxy **75** is considered in a S_N2 -reaction between the acetylene building block^[288] and the previously synthesized silyl-chloride **62**. Another advantage of this synthetic strategy is the attachment of a variable surface linker (e.g., EDTA derivatives) as the synthesis of the active aryl-amine **74** is envisaged.

A low negative electrochemical potential (ca. $E^0 = -0.4$ V/SCE) will lead to grafting of the molecule **73a** on the surface of the electrode (Figure 34, A). In the case of the EDTA derivatized compound **73b**, the ITO substrate will be dipped into a solution of the compound **73b**, which will lead to a SAM on the ITO. By applying a negative potential (ca. $E^0 = -0.9$ V/SCE), the quinone-derived SAM will be reduced and releases the free acetylene, which could be post-functionalized by click-chemistry with any azide-derivatized compound (e.g., DNA, antibody, dye, etc.). As the cleavage of the acetylene protecting group relies on a

negative electrochemical potential, specific areas of a grafted SAM could be addressed individually (Figure 34, B). The now free acetylenes are prone for post-functionalization by click-chemistry forming a functionalized surface (Figure 34, C). Is this process repeated a multifunctional surface could be achieved (Figure 34, D).

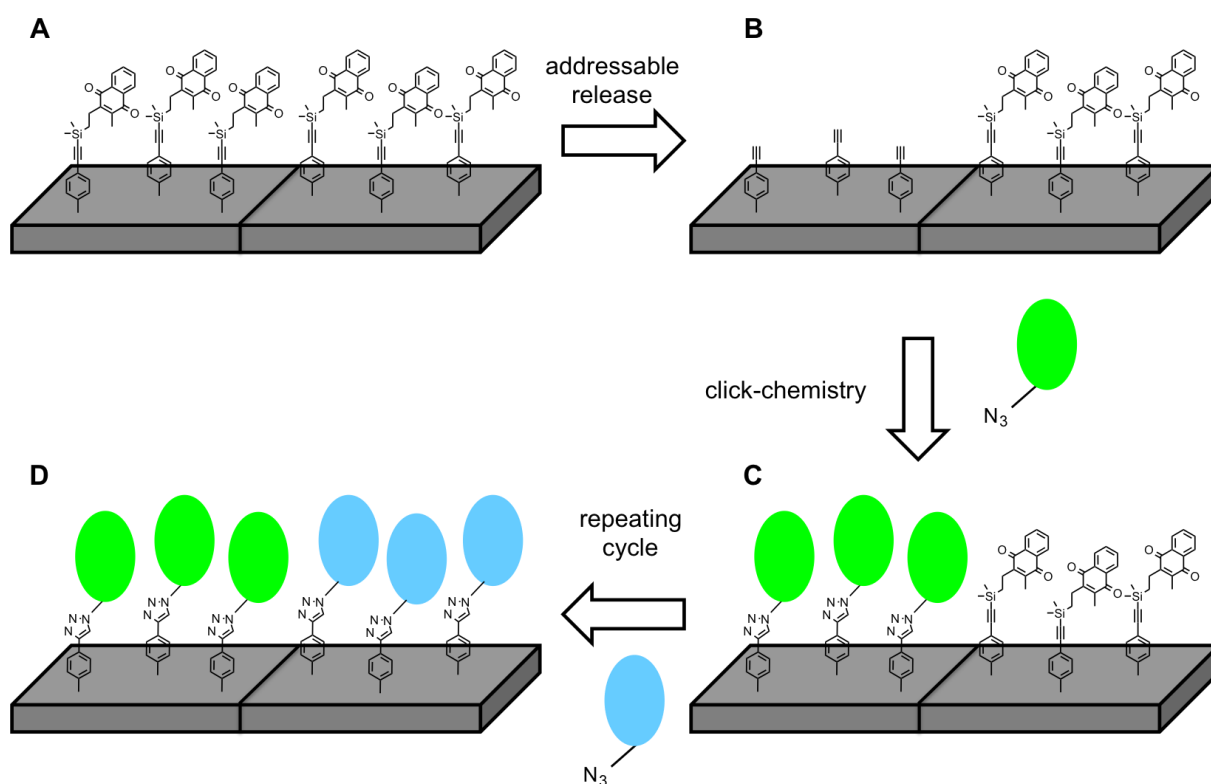


Figure 34: Concept of multi-functionalized SAMs. In the first step the diazotized compound **73** will be grafted on surface forming a SAM. As the cleaving of the protecting group occurs when a negative potential is applied, this SAM formation of *p*-ethynylbenzene could be achieved exclusively by electrochemistry at individual addressable areas. The now accessible free acetylene could be involved in a click-chemistry reaction forming a functionalized surface. When this process is repeated a multifunctional surface could be realized

Experimental Section

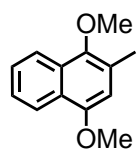
General Remarks

All commercially available compounds were purchased and used as received unless explicitly stated otherwise. CDCl_3 was purchased from Cambridge Isotope Laboratories, Inc. ^1H NMR was recorded on a Bruker DPX-NMR spectrometer operating at 400 MHz. ^{13}C NMR were recorded on a Bruker DPX-NMR spectrometer operating at 101 MHz. The chemical shifts are reported in parts per million (ppm) relative to tetramethylsilane or a residual solvent peak, and the J values are given in Hz. GC-MS was performed on a Shimadzu GCMS-2020 SE equipped with a Zebron 5 MS Inferno column which allowed to achieve temperatures up to 350 °C. High-resolution mass spectra (HRMS) were measured as HR-ESI-ToF-MS with a Maxis 4G instrument from Bruker with the addition of NaOAc. MALDI-TOF analyses were performed on a Bruker microflex system. For column chromatography, usually silica gel Siliaflash® p60 (40–63 μm) from Silicycle was used, and TLC was performed on silica gel 60 F254 glass plates with a thickness of 0.25 mm purchased from Merck.

UV-Visible absorption spectra in acetylene were recorded at room temperature on a Shimadzu UV-1800 spectrometer. The electrochemical measurements were performed with an AutoLab PGSTAT302 potentiostat-galvanostat controlled by resident NOVA 9.1 software using a conventional single-compartment three-electrode cell. A glassy carbon disk of 2 mm \varnothing served as working electrode, as auxiliary a Pt wire was used and the reference electrode was a saturated potassium chloride calomel electrode (SCE). The supporting electrolyte was 0.1 N tetraethylammonium tetrafluoroborate in acetonitrile. Solutions were purged with argon to remove the oxygen and argon was passed over the solution during the experiment. All potentials are quoted relative to SCE with ferrocene/ferrocenium at +450 mV as internal standard. In all the experiments the scan rate was 100 mV/s for cyclic voltammetry. All spectroelectrochemical experiments were recorded with a sample concentration of 10^{-5}M , using a conventional single-compartment three-electrode cell. A Pt mesh 1 cm^2 served as working electrode, as auxiliary a Pt wire was used and the reference electrode was a saturated potassium chloride calomel electrode (SCE). The UV-Vis spectra were recorded on a Cary 5000 UV/Vis/NIR spectrometer from Varian.

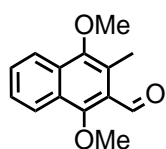
Synthetic Procedures

1,4-Dimethoxy-2-methylnaphthalene (65): Menadione (4.99 g, 29.0 mmol, 1.0 eq.) was



suspended in methanol (80 mL) in a 50 mL round bottom flask. A solution of tin(II) chloride (22.0 g, 116 mmol, 4.0 eq.) in conc. HCl (19 mL) was added drop wise over 30 min. The reaction mixture was stirred at room temperature for 30 minutes. Before the methanol was evaporated under reduced pressure and the residue was poured into water (33 mL). The precipitation was filtered and diluted in acetone (66 mL), and dried over MgSO₄. K₂CO₃ (30.1 g, 218 mmol, 7.5 eq.) and dimethyl sulfate (20.3 g, 160 mmol, 5.5 eq.) was added to the solution and suspension was refluxed for 4 hours. The unsolved components were filtered and the filtrate was concentrated under reduced pressure. The residue was diluted in diethyl ether (20 mL) and aq. NaOH (20 %, 20 mL). The organic layer was washed with brine, dried over MgSO₄, filtered, and concentrated under reduced pressure. The crude product was purified by column chromatography (SiO₂, toluene). 1,4-Dimethoxy-2-methylnaphthalene (3.97 g, 19.6 mmol, 68 %) was obtained as white crystals. ¹H – NMR (400 MHz, CDCl₃, 25 °C): δ = 8.19 (d, *J* = 8.4 Hz, 1H), 8.03 (d, *J* = 8.4 Hz, 1H), 7.51 (dd, *J* = 8.4, 6.8 Hz, 1H), 7.42 (dd, *J* = 8.4, 6.8 Hz, 1H), 6.61 (s, 1H), 3.97 (s, 3H), 3.87 (s, 3H), 2.45 (s, 3H). ppm. ¹³C – NMR (101 MHz, CDCl₃, 25 °C): δ = 151.5, 147.0, 128.6, 126.5, 125.6, 125.2, 124.6, 122.2, 121.5, 106.8, 61.2, 55.6, 16.3 ppm. MS (EI, 70 eV): *m/z* (%) = 202.0 (57), 188.0 (13), 187.0 (100), 159.1 (31), 144.1 (16), 128.0 (13), 116.1 (12), 115.1 (22). HRMS (ESI): *m/z* calcd. for [C₁₃H₁₄O₂+H]⁺ 203.1067; found: 203.1067.

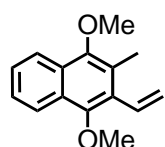
1,4-Dimethoxy-3-methyl-2-naphthaldehyde (64): 1,4-Dimethoxy-2-methyl-naphthalene



(3.90 g, 13.3 mmol, 1eq.) was dissolved in dry dichloromethane (28 mL) under argon atmosphere. A solution of TiCl₄ (1 M in DCM, 21.6 mL, 21.6 mmol, 1.1 eq.) was added dropwise at 0 °C followed by 1,1-dichloroethyl methyl ether (1.93 mL, 21.6 mmol, 1.1 eq.). The reaction mixture was stirred for 3 hours at 0 °C, poured into ice and extracted with ethyl acetate. The combined organic layers were washed with brine, dried over MgSO₄, filtered and concentrated under reduced pressure. The crude product was purified by column chromatography (SiO₂, ethyl acetate : cyclohexane 1 : 10). 1,4-Dimethoxy-3-methyl-2-naphthaldehyde (4.01 g, 17.43 mmol, 90%) was obtained as

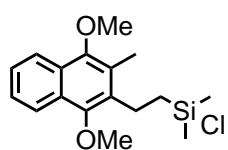
white crystals. ^1H – NMR (400 MHz, CDCl_3 , 25 °C): δ = 10.73 (s, 1H), 8.20 (d, J = 8.4 Hz, 0H), 8.11 (d, J = 8.4 Hz, 1H), 7.66 (dd, J = 8.4, 6.8 Hz, 1H), 7.55 (dd, J = 8.4, 6.8 Hz, 1H), 4.07 (s, 3H), 3.87 (s, 3H), 2.65 (s, 3H) ppm. ^{13}C – NMR (101 MHz, CDCl_3 , 25 °C): δ = 192.4, 160.2, 150.6, 131.9, 129.4, 127.0, 126.3, 126.1, 125.0, 123.2, 122.6, 65.5, 61.4, 13.0 ppm. MS (EI, 70 eV): m/z (%) = 231.1 (15), 230.1 (100), 216.0 (12), 215.0 (83), 200.0 (48), 187.0 (15), 172.0 (33), 144.1 (25), 129.1 (14), 128.1 (26), 127.1 (22), 116.1 (23), 115.1 (51), 77.1 (12), 76.0 (10). HRMS (ESI): m/z calcd. for $[\text{C}_{14}\text{H}_{14}\text{O}_3+\text{H}]^+$ 231.1016; found: 231.1016.

1,4-dimethoxy-2-methyl-3-vinylnaphthalene (63): Methyltriphenylphosphonium bromide



(698 mg, 1.91 mmol, 1.1 eq.) was suspended in dry THF (8 mL) under argon atmosphere. The suspension was cooled to 0 °C and *n*-BuLi (1.2 mL, 1.6 M in hexane, 1.91 mmol, 1.1 eq.) was added dropwise. The solution was stirred for 1 h at 0 °C. A solution of 1,4-dimethoxy-3-methyl-2-naphthaldehyde (401 mg, 1.74 mmol, 1.0 eq.) in dry THF (4 mL) was added and the cooling bath was removed. After stirring 3 h at room temperature, adding of 2 M aq. HCl solution quenched the reaction and the reaction mixture was extracted with ethyl acetate. The combined organic layers were dried over MgSO_4 , filtered and concentrated under reduced pressure. The crude product was purified by column chromatography (SiO_2 , Toluene). 1,4-Dimethoxy-2-methyl-3-vinylnaphthalene (359 mg, 1.57 mmol, 90 %) was obtained as white solid. ^1H – NMR (400 MHz, CDCl_3 , 25 °C): δ = 8.13 – 8.02 (m, 2H), 7.52 – 7.44 (m, 2H), 6.88 (dd, J = 17.9, 11.7 Hz, 1H), 5.79 (dd, J = 17.9, 2.1 Hz, 1H), 5.65 (dd, J = 11.7, 2.1 Hz, 1H), 3.87 (s, 2H), 3.84 (s, 3H), 2.44 (s, 3H), 1.56 (s, 1H) ppm. ^{13}C – NMR (101 MHz, CDCl_3 , 25 °C): δ = 150.2, 150.0, 131.4, 128.1, 128.0, 127.5, 126.1, 125.7, 125.5, 122.6, 122.0, 120.5, 61.3, 60.9, 13.6 ppm. MS (EI, 70 eV): m/z (%) = 229.1 (16), 228.1 (100), 214.1 (11), 213.1 (68), 198.0 (51), 185.1 (18), 183.1 (16), 182.1 (33), 181.0 (29), 155.1 (13), 153.1 (17), 152.1 (18), 142.1 (13), 141.1 (29), 115.1 (26), 77.1 (11), 76.0 (19). HRMS (ESI): m/z calcd. for $[\text{C}_{15}\text{H}_{16}\text{O}_2+\text{H}]^+$ 229.1223; found: 229.1223.

Chloro(2-(1,4-dimethoxy-3-methylnaphthalen-2-yl)ethyl)dimethylsilane (62): 1,4-

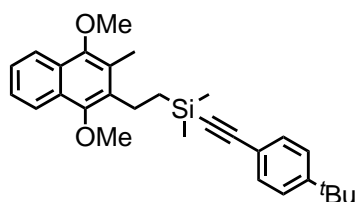


Dimethoxy-2-methyl-3-vinylnaphthalene (890 mg, 3.90 mmol, 1.0 eq.)

was placed in a 5 mL flask under argon atmosphere. Chlorodimethylsilane (651 μ L, 5.85 mmol, 1.5 eq.) was added followed by the carefully addition

of the Karstedt's catalyst (780 μ L, 0.1 mol/L in xylene, 78.0 μ mol, 0.02 eq.). The reaction mixture was stirred at 34 °C for 3 hours. After cooling to room temperature, the mixture was dissolved in dry DCM and filtered directly over a Celite® plug into a bulb to bulb distillation flask under argon atmosphere. DCM and xylene was distilled off. The crude product was purified by bulb to bulb distillation at 190 °C ($5 \cdot 10^{-2}$ mbar). Chloro(2-(1,4-dimethoxy-3-methylnaphthalen-2-yl)ethyl)dimethylsilane (943 mg, 2.92 mmol, 75%) was obtained as a colorless oil. ^1H – NMR (400 MHz, CDCl_3 , 25 °C): δ = 8.10 – 7.98 (m, 2H), 7.52 – 7.42 (m, 2H), 3.92 (s, 3H), 3.87 (s, 3H), 2.95 – 2.87 (m, 2H), 2.42 (s, 3H), 1.18 – 1.08 (m, 2H), 0.51 (s, 6H) ppm. ^{13}C – NMR (101 MHz, CDCl_3 , 25 °C): δ = 150.4, 149.5, 133.3, 127.6, 127.4, 126.1, 125.6, 125.5, 122.3, 120.5, 62.4, 61.5, 20.7, 20.1, 12.3, 1.4 ppm. MS (EI, 70 eV): m/z (%) = 324.0 (38), 323.0 (24), 322.0 (100), 309.0 (25), 308.0 (15), 307.0 (65), 294.0 (20), 293.0 (12), 292.0 (52), 277.0 (15), 276.0 (11), 257.0 (25), 256.0 (10), 241.0 (11), 215.0 (11), 184.0 (10), 183.0 (19), 165.0 (12), 155.1 (31), 153.1 (12), 141.1 (14), 128.0 (19), 115.0 (16), 95.0 (23), 93.0 (64). Due to the sensitive nature of silane-chlorides towards air and moisture, the expected mass of the hydrolyzed product was detected by ESI. HRMS (ESI): m/z calcd. for $[\text{C}_{17}\text{H}_{24}\text{ClO}_3\text{Si}+\text{Na}]^+$ 327.1387; found: 327.1393.

((4-(tert-butyl)phenyl)ethynyl)(2-(1,4-dimethoxy-3-methylnaphthalen-2-yl)ethyl)di-



methylsilane (61): 4-tert-Butylphenylacetylene (0.57 mL, 3.05

mmol, 1.05 eq.) was dissolved in THF (9 mL), cooled to –78 °C

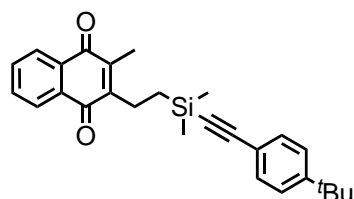
and *n*-BuLi (2.08 mL, 1.6 M in hexane, 3.33 mmol, 1.15 eq.) was

added dropwise. After stirring for 1 hour at –78 °C the reaction

solution was added drop wise to a solution of chloro(2-(1,4-dimethoxy-3-methylnaphthalen-2-yl)ethyl)di-methylsilane (936 mg, 2.90 mmol, 1.0 eq.) in THF (14 mL) at room temperature and stirred for 30 minutes. The reaction was quenched with sat. aq. NH_4Cl solution and extracted with *t*BME. The combined organic layers were dried over MgSO_4 , filtered and concentrated under reduced pressure. The crude product was purified by column

chromatography (SiO₂, c-hexane : ethyl acetate, 20 : 1). ((4-(tert-butyl)phenyl)ethynyl)(2-(1,4-dimethoxy-3-methylnaphthalen-2-yl)ethyl)dimethyl-silane (1.10 g, 2.90 mmol, 86%) was obtained as a colorless oil. ¹H – NMR (400 MHz, CDCl₃, 25 °C): δ = 8.07 – 7.02 (m, 2H), 7.47 – 7.42 (m, 4H), 7.35 – 7.33 (m, 2H), 3.94 (s, 3H), 3.88 (s, 3H), 2.98 – 2.94 (m, 2H), 2.46 (s, 3H), 1.32 (s, 9H), 1.02 – 0.97 (m, 2H), 0.34 (s, 6H) ppm. ¹³C – NMR (101 MHz, CDCl₃, 25 °C): δ = 152.0, 150.3, 149.4, 134.4, 131.9, 127.5, 127.4, 126.3, 125.4, 125.3, 122.4, 122.3, 120.2, 106.4, 91.2, 62.4, 61.4, 35.0, 31.3, 21.6, 17.6, 12.3, 1.7 ppm. MS (EI, 70 eV): m/z (%) = 445.1 (25), 444.1 (57), 414.0 (12), 399.0 (12), 272.1 (29), 271.1 (100), 257.0 (13), 256.0 (14), 215.0 (27), 207.0 (11), 200.1 (17), 199.0 (10), 185.1 (19), 89.1 (18), 57.1 (34). HRMS (ESI): m/z calcd. for [C₂₉H₃₆O₂Si+K]⁺ 483.2116; found: 483.2116.

2-(2-(((4-(tert-butyl)phenyl)ethynyl)dimethylsilyl)ethyl)-3-methylnaphthalene-1,4-dione

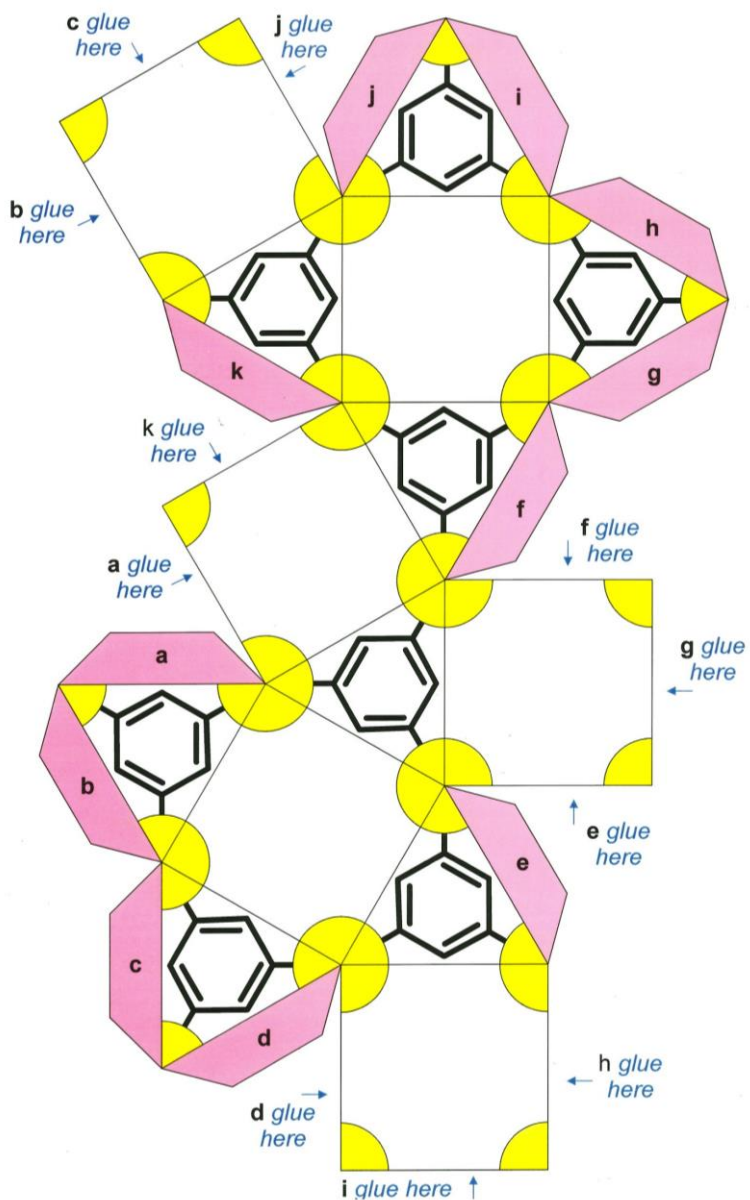


(60): ((4-(tert-butyl)phenyl)ethynyl)(2-(1,4-dimethoxy-3-methylnaphthalen-2-yl)ethyl)dimethylsilane (80.5 mg, 0.181 mmol, 1.0 eq.) was dissolved in acetonitrile (3 mL) and water (1.5 mL). To the solution ammonium cerium(IV) nitrate (257

mg, 0.46 mmol, 2.55 eq.) was added. The mixture was stirred for 1 h at room temperature followed by the extraction with DCM. The combined organic layers were washed with brine, dried over MgSO₄, filtered and concentrated under reduced pressure. The crude product was purified by column chromatography (SiO₂ c-hexane : ethyl acetate, 20 : 1). 2-(2-(((4-(tert-butyl)phenyl)ethynyl)dimethylsilyl)ethyl)-3-methylnaphthalene-1,4-dione (67.3 mg, 0.181 mmol, 90%) was obtained as a slightly yellow oil. ¹H – NMR (400 MHz, CDCl₃, 25 °C): δ = 8.10 – 8.03 (m, 2H), 7.70 – 7.64 (m, 2H), 7.37 (d, *J* = 8.3 Hz, 2H), 7.31 (d, *J* = 8.3 Hz, 2H), 2.82 – 2.70 (m, 2H), 2.23 (s, 3H), 1.30 (s, 9H), 0.92 – 0.82 (m, 2H), 0.31 (s, 5H). ppm. ¹³C – NMR (101 MHz, CDCl₃, 25 °C): δ = 185.5, 184.6, 151.9, 149.5, 142.1, 133.3, 133.2, 132.2, 131.7, 126.2, 126.1, 125.2, 119.9, 106.5, 91.6, 34.8, 31.1, 21.3, 15.8, 12.4, -1.9 ppm. MS (EI, 70 eV): m/z (%) = 414.1 (12), 400.1 (31), 399.1 (100), 387.2 (22), 386.1 (66), 385.2 (21), 371.1 (23), 299.1 (11), 257.1 (11), 256.1 (37), 255.0 (14), 241.0 (30), 215.1 (30), 213.0 (10), 200.0 (19), 199.1 (16), 185.1 (20), 158.1 (10), 143.1 (36), 128.1 (14), 115.1 (18), 57.1 (21). HRMS (ESI): m/z calcd. for [C₂₇H₃₀O₂Si+Na]⁺ 437.1907; found: 437.1910.

Chapter 3

Progress Towards the Synthesis of Thiospherophane



Introduction

Fullerene

Molecules with highly symmetric shapes like cycles,^[289] cubes,^[290,291] or balls^[292] have attracted the attention of scientists for a long time. Within the family of poly-aromatic hydrocarbons, a very prominent group of such symmetric structures is the allotrope family of fullerenes. Especially the first description of the structural nature and chemical reactivity of C_{60} opened up a new area of chemistry which is still ongoing today.^[292] After the first synthetic preparation in macroscopic quantities^[293] the carbon allotrope C_{60} received more attention than hardly any other of the family.^[294,295] The buckminsterfullerene C_{60} —named after the American architect Buckminster Fuller—is composed of 32 faces, of which 12 are pentagons and 20 are hexagons (Figure 35).^[296] The pentagons are the structural reason for the football-shaped fullerene. The 60 equivalent carbon atoms lie on the surface of a sphere distributed with the symmetry of a truncated icosahedron.^[297] This highly symmetric allotrope exhibits enhanced stability as it can accept up to 6 additional electrons without degradation at surprisingly low redox potentials.^[298]

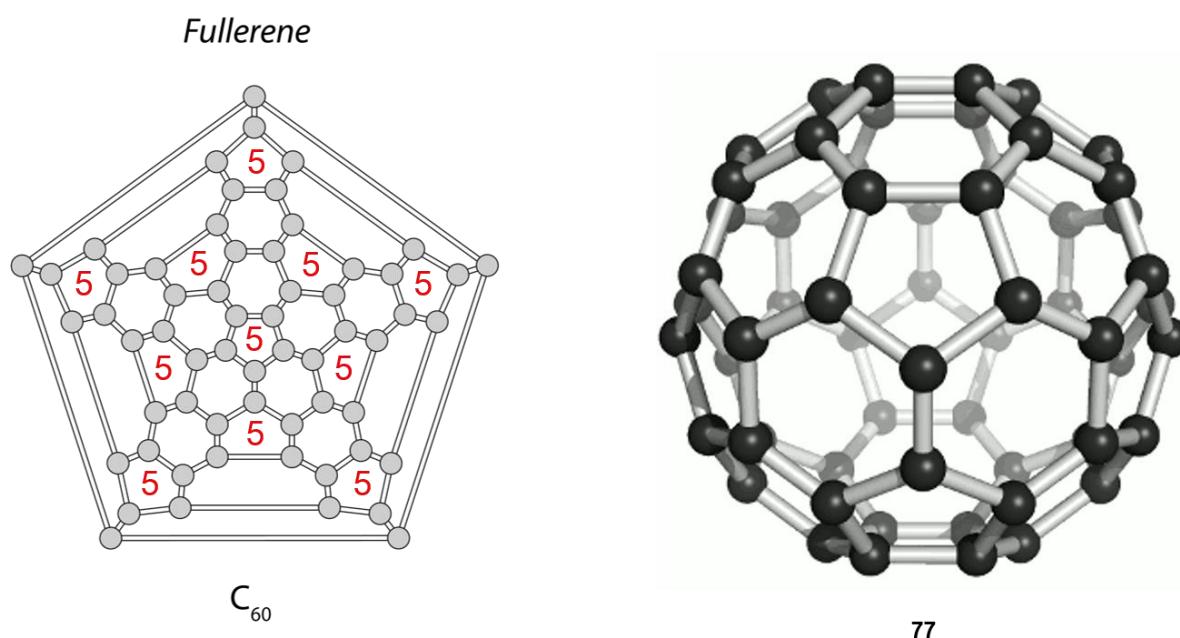


Figure 35: Different drawings of the fullerene-molecule (77).

Fullerenes are not only interesting because of their electronic properties. The 30 π -bonds react in pericyclic-type reactions more likely as electron-deficient arenes or alkenes, which makes them an interesting platform for Diels–Alder cycloaddition reactions for preparing functionalized fullerenes.^[296,299] Functionalized fullerene species are found in various application fields, such as drug delivery, reactive oxygen species quenching, dye-sensitized solar cells, and SAM formation.^[300–303]

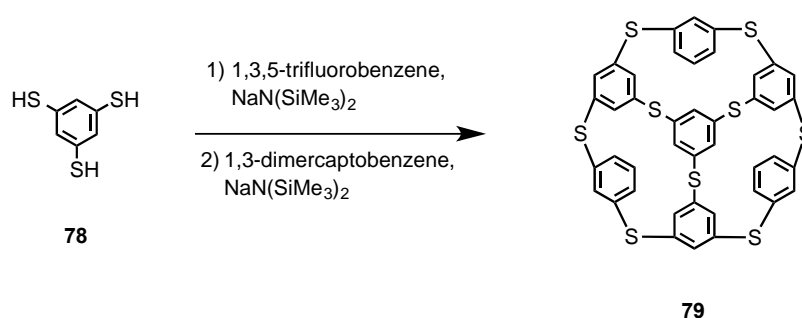
Heterofullerenes

Compounds where one or more carbon atoms of the hollow fullerene is replaced by heteroatoms, such as nitrogen (N), boron (B), or sulfur (S) are very interesting compounds as their chemical reactivity, photophysical properties, and solid-state characteristics can be enhanced compared to the parent fullerene. Most theoretical and experimental work has been devoted for N- and B-doped heterofullerenes.^[304–308] Quickly after the first bulk synthesis of C₆₀-fullerene a synthesis in bulk materials of aza[60]fullerene (C₅₉N) and its dimer ([C₅₉N]₂) was accomplished.^[309,310] This development quickly made azafullerenes the most studied heterofullerenes by far.

The charge transfer between the N and carbon (C) atom results in an unbalanced charge distribution making the N–C [6,6]-bond preferential for electrophilic and nucleophilic attacks.^[311] This peripheral attachments leads to an exceptional ensemble of functionalized azafullerenes, which show enhanced chemical properties, exhibit variable electronic properties and represent potential low cost candidates in hydrogen fuel cells.^[308,311–314] In strong contrast to that, studies of sulfur-containing heterofullerenes are very rare for theoretical as well as experimental work.^[297,315–317] Theoretical calculations predict that the spherical structure of C₆₀ can be distorted by doping the fullerene with sulfur atoms, although the electronegativity of C and S are similar. This will ultimately lead to different electronic properties of C₅₉S compared to those of C₅₉N.^[297] Unfortunately, no syntheses confirming this structural behavior has been reported so far. Arc discharge-vaporization of graphite in the presence of a sulfur source was investigated for the syntheses of S-doped fullerenes. However, only a mixture of compounds with substantial sulfur enrichment was isolated by column chromatography. Evidences for the existence of molecular structures such as C₅₈S, C₅₆S₂, C₅₂S₄, C₅₀S₅, and C₃₆S₁₂ were detected by mass spectroscopy.^[297] These

results as well as theoretical observations revealed that the doping of fullerene with a single sulfur atom is the most unstable sulfur doped fullerene.^[297,315] Interestingly, the more reactive C₇₀ fullerene was successfully doped by one sulfur atom by chemical synthesis forming an open-cage C₆₉S thiafullerene.^[316]

A very promising strategy for the synthesis of a sulfur doped fullerene-type structure was presented by West and co-workers.^[318] The molecular bowl structure consists of benzene subunits, which are connected via sulfur atoms, was achieved in two steps using exclusively nucleophilic aromatic substitution (S_NAr) reactions (Scheme 25). Analysis of solid-state structure revealed a conformation of a large molecular bowl **79**.



Scheme 25: Synthesis and X-ray structure of a molecular bowl structure (**79**), presenting a promising candidate for host–guest interactions.^[318]

These observations inspired the synthesis of a highly symmetric heterospherophane structure based on benzene subunits, which are connected via heteroatoms (e.g., oxygen, nitrogen, or sulfur). However, the synthesis of an open-shell structure comprising a sulfur-doped fullerene was not realized so far by controlled chemical syntheses or laser-ablation techniques.

Aim of the Work

The development of fullerene C_{60} in bulk material allowed the preparation of functionalized fullerenes, which are established nowadays in various fields (e.g., solar cells, SAM formation). Doping of the fullerene with heteroatoms such as nitrogen, boron, or oxygen showed enhanced chemical and physical properties. However, doping fullerene with sulfur was only discussed in theory so far. Synthetic approaches of doping were only successful for the more reactive C_{70} fullerene.

The aim of this work was to design and synthesize a symmetric, ball-shaped structure containing 48 carbon atoms and 12 sulfur atoms ($C_{48}S_{12}$); the thiospherophane **80** (Figure 36, left). This ball shaped molecule consists of eight identical subunits. The benzene subunits are interconnected via sulfur atoms. The insertion of these sulfur heteroatoms would transform the fullerene closed-shell structure into a hollow open-shell structure, allowing host-guest interaction. This can be shown by comparison the 2D-molecular structures of thiospherophane **80** and fullerene **77** (Figure 36, middle and right). The thiospherophane **80** clearly exhibits less atom-atom connections compared to fullerene, strongly hinting on an open-shell structure. Furthermore, it would be very interesting to investigate its stability towards electrochemical degradation as well as photo-physical properties. Although this hollow molecular cage has never been synthesized in a controlled fashion or using laser-ablation techniques Ross and co-workers have investigated this structure in a theoretical work.^[319] Moreover, this supramolecular host structure was classified as cuboctahedron according to the topology of the shell.^[320]

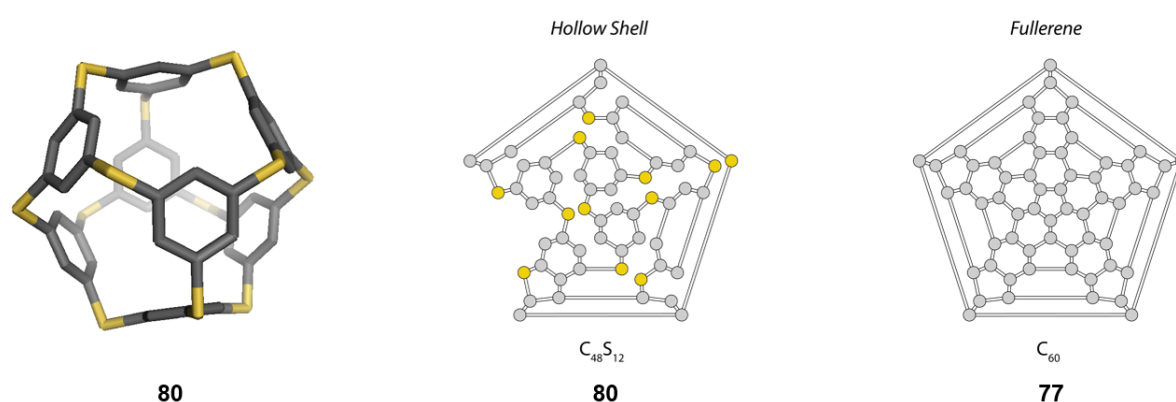


Figure 36: Thiospherophane **80** presented as 3D (left) and 2D structure (middle). To compare the structural relation between target structure **80** and fullerene **77**, 2D structure of fullerene is shown as well (right).

Synthetic Strategies

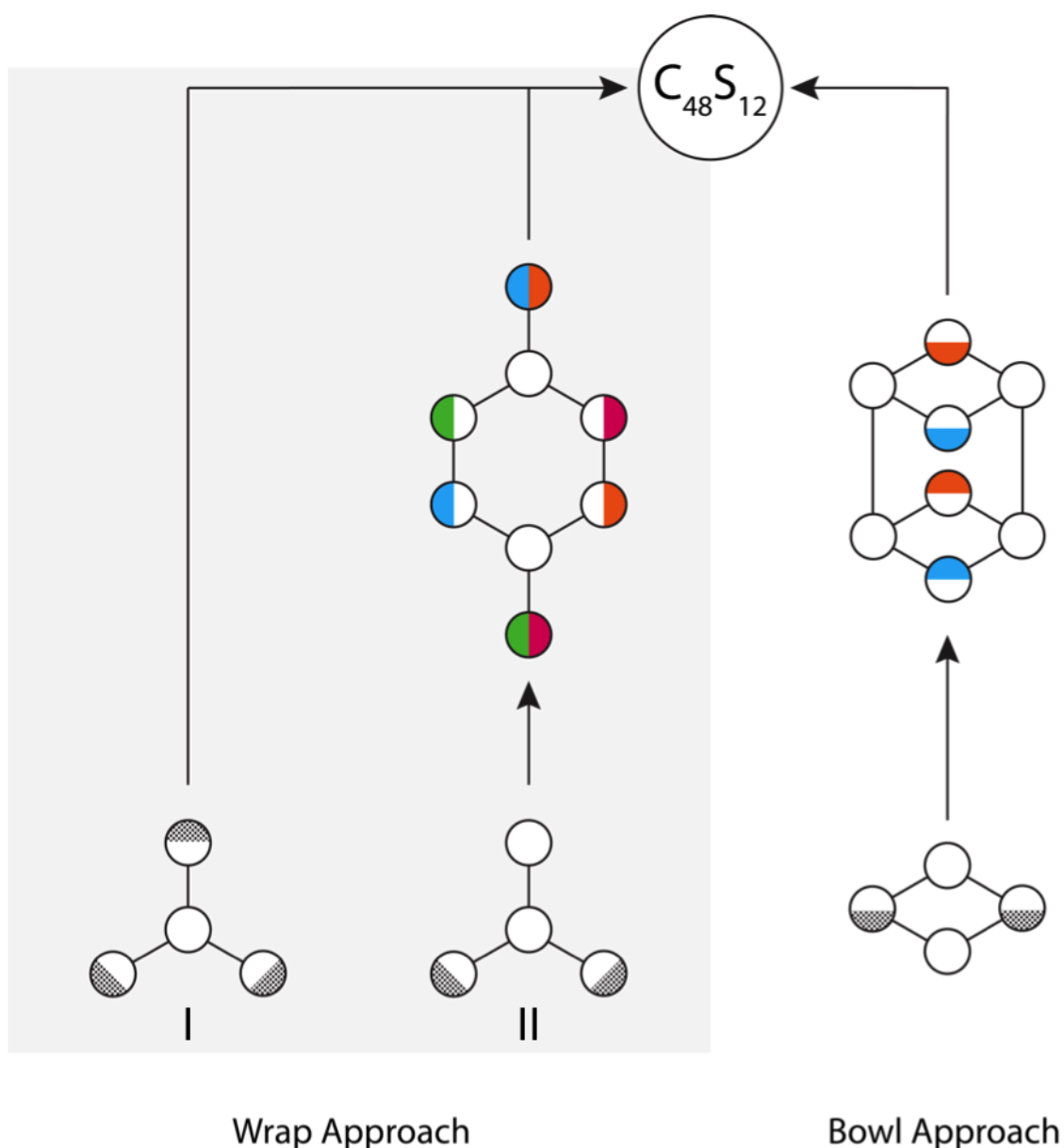


Figure 37: Three different synthetic assembly strategies of **80** ($C_{48}S_{12}$) were followed simultaneously. In the wrap approach I, two symmetric half-sphere monomer will be connected forming **80**. In the wrap approach II, the two asymmetric monomers will be connected first in a synthetically controlled fashion followed by the assembling of **80**. Following the bowl approach, two half-spheres will be connected and subsequently assembled to **80**.

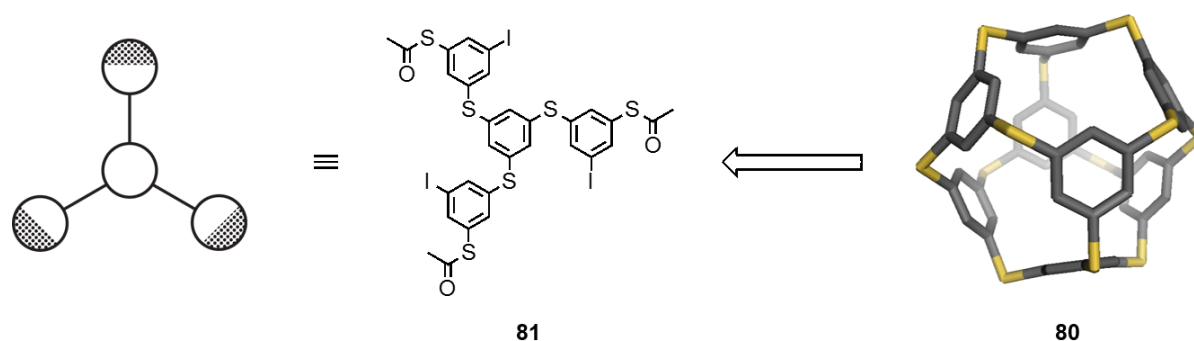
The synthetic strategy of the highly symmetric thiospherophane **80** is separated into two main approaches; the wrap approach and the bowl approach. The wrap approaches are further divided into wrap approach I (Figure 37, left) and wrap approach II (Figure 37, middle). Bond forming connections, which have to be made, are indicated by the dotted or colored area within the circles.

Following wrap approach I six bonds have to be formed in the last step. The advantage of this approach will be the synthesis of the required symmetric monomer in large quantities, which can be achieved within three steps. However, as the monomer is bearing six reaction sides, undesired reaction outcome—like higher oligomer formation—would be difficult to control.

In wrap approach II the asymmetric monomer allows dimer formation in a controlled fashion as it bears only two active reaction sites. To assemble target structure **80** only four bonds have to be formed. For a visual guideline of the connections that are required for the assembly of **80**, the areas of the circle are indicated in the corresponding colors. The biggest drawback of this approach would be that the assembly of **80** requires thirteen steps, not including the syntheses of the four different building blocks.

Following the strategy of the bowl approach, thiospherophane **80** would be synthesized within five steps. The biggest advantage of this strategy will be the pre-organized structure of the dimer. Both required connections for the last step are already perfectly oriented towards each other, minimizing undesired side reactions. Similarly to the wrap approach II, the dimer formation in a controlled manner from the asymmetric monomer is considered.

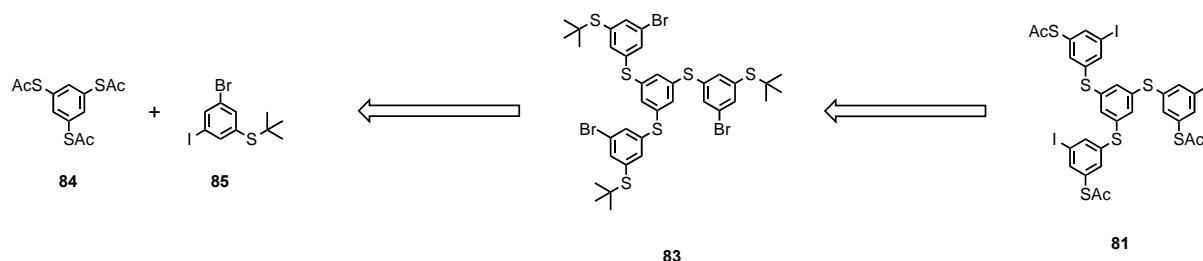
Wrap Approach I



Scheme 26: In the synthetic strategy of the wrap approach I six bonds have to be formed in the last step for the assembly of **80**.

As the molecule of interest is symmetric, the assembly strategy is based on the symmetric monomers **81** (Scheme 26). In the wrap approach I six bonds have to be made in the last step. As earlier studies revealed difficulties in the assembly of **80** using nucleophilic aromatic substitution (S_NAr) reaction conditions, palladium catalyzed reaction conditions are now envisaged. The advantages of this reaction would be lower reaction temperature less

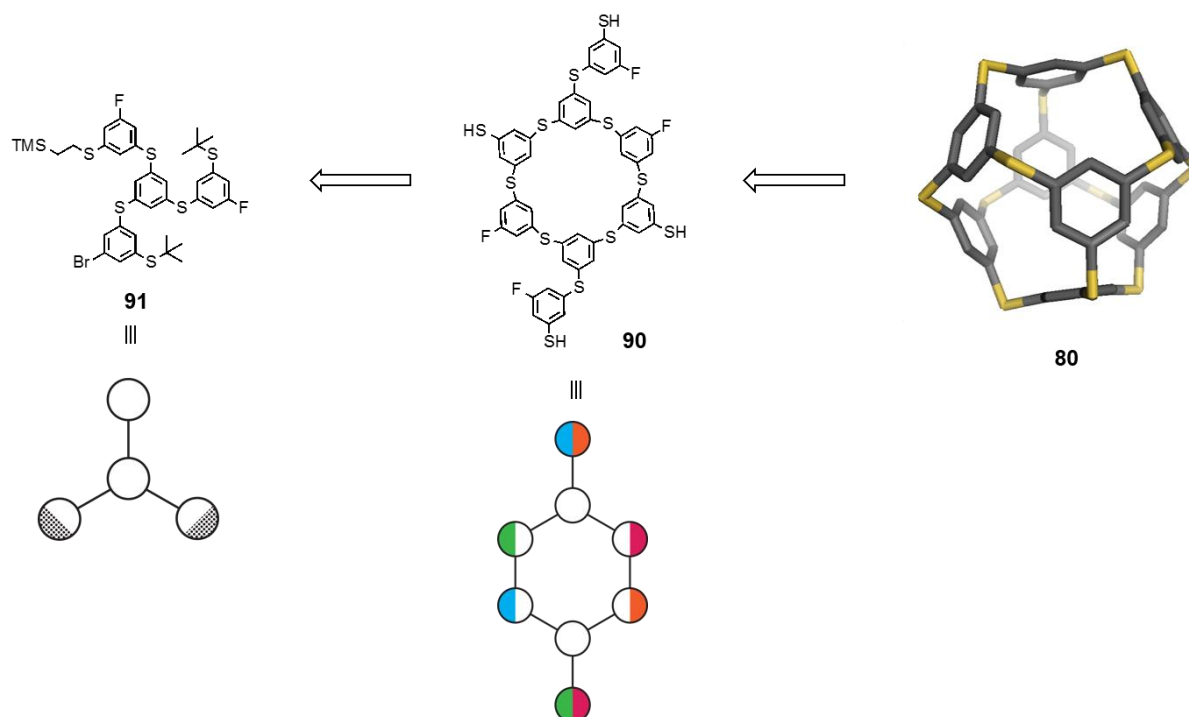
sensitivity towards moisture and therefore better control of side reactions. To avoid the formation of oligomers high dilution conditions are considered. Furthermore it is expected that after formation of the first connection the intramolecular reaction is faster than the intermolecular reaction.



Scheme 27: Synthetic strategy of monomer **81**. The building block **85** will be attached three times on the core building block **84** using Pd-catalyzed C–S bond forming reaction conditions. Subsequently, halogen exchange of bromide **83** into the iodine followed by transprotection of the *tert*-butyl protecting group into the acetyl-protected sulfur will lead to the symmetric monomer **81**.

The required acetyl-protected thiol **81** could be provided by transprotection of the corresponding *tert*-butyl protecting group.^[321,322] In order to reduce the reaction temperature the bromine precursor **83** will be transformed into the more reactive iodine. Profiting of the symmetrical structure of monomer **81** only two building blocks are required. The *tert*-butylsulfanyl group should be a feasible protecting group to assemble building block **83**, accessible through a palladium catalyzed reaction of 1,3,5 (tri-S-acetyl)-benzene (**84**) and (3-bromo-5-iodophenyl)(*tert*-butyl)sulfane (**85**) (Scheme 27).

Wrap Approach II



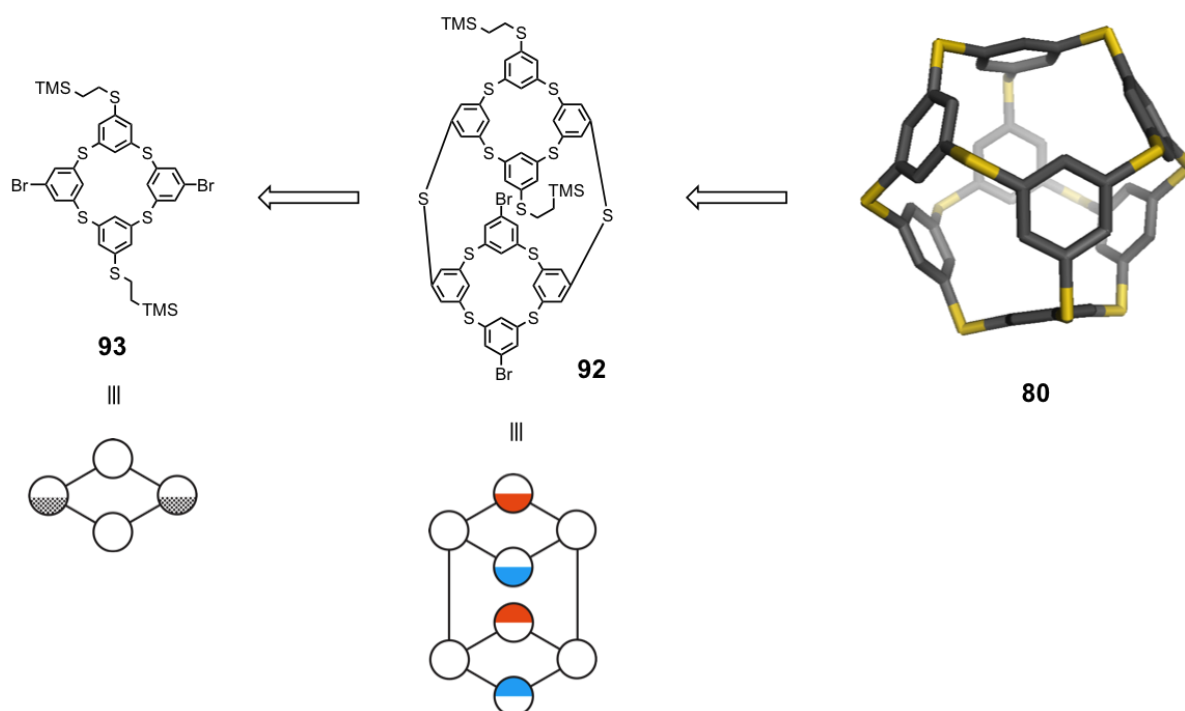
Scheme 28: In the assembly strategy of the wrap approach II the asymmetric monomer **91** will form a dimer in a stepwise fashion as it bears two individual addressable reaction sites. After cleaving the *tert*-butyl moieties, the dimer **90** will provide the precursor of the final assembly step. In this last reaction step, four bonds have to be connected in the correct manner using S_NAr reaction conditions in order to form the target structure **80**.

The assembly strategy of wrap approach II would profit from two advantages: (i) the last step includes the formation of only four bonds via S_NAr reaction conditions and (ii) since the bond formation of the intramolecular reaction will be faster compared to intermolecular reaction, the probability of oligomer formation could be further reduced. Therefore the synthesis of the precursor **90** is envisaged, bearing already all the atoms required for the target structure **80**. As the free thiols are hard to handle this dimer will be assembled with protected sulfur moieties, which can be cleaved in quantitative yield. Following this strategy the asymmetric monomer **91** bearing individually addressable reaction sites enables the connection of two monomers in a stepwise fashion according to the full control of the reactions sides. The efficient and clean transformation of the bromide moiety of the monomer **91** into the corresponding iodine is imperative as the separation of these compounds would be rather difficult in this case. Additionally, the two sulfur-protecting groups of choice have to survive these halogen exchange reaction conditions. As cleavage of

these sulfur-protecting groups must occur in a selective manner, the individual addressable release is imperative for this stepwise assembling. As the ethyl-trimethylsilyl (ethyl-TMS) protecting group is sensitive to F^- -sources, whereas the *tert*-butyl protecting group remains unaffected under such conditions, these will be the two orthogonal protecting groups of choice (Scheme 28).

Bowl Approach

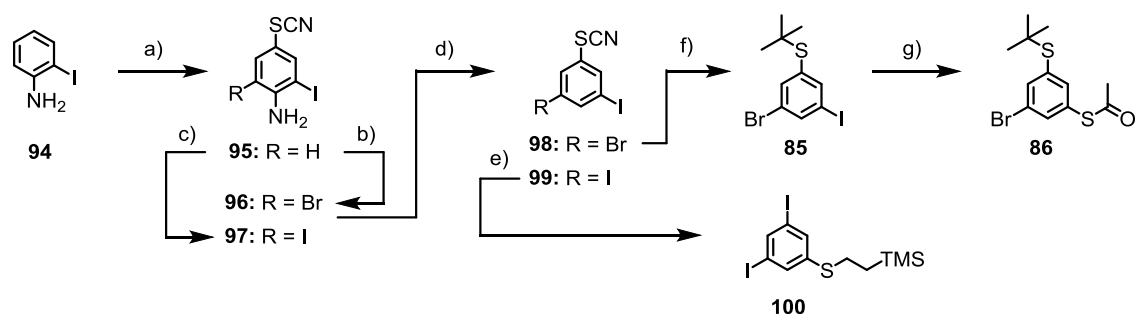
Following the strategy of the bowl approach, only two bonds have to be made in the last reaction step. This would significantly reduce undesired side reactions, such as higher oligomer formation, in a very effective manner since the Pd-catalyzed S–C bond formation reaction could be performed in very high dilution. Moreover, the pre-organized structure of the dimer **92** preferably leads to the target structure **80**. For the stepwise dimerization reaction of **93** Pd-catalyzed thioether formation reaction conditions are considered.



Scheme 29: In the bowl approach the dimer **92** will be formed in analogy to **90** starting from the monomer **93**. As this dimer **92** already exhibits a pre-organized structure, Pd-catalyzed C–S bond forming reaction conditions may lead to the desired thiospherophane **92**.

Results and Discussion

Bowl Approach

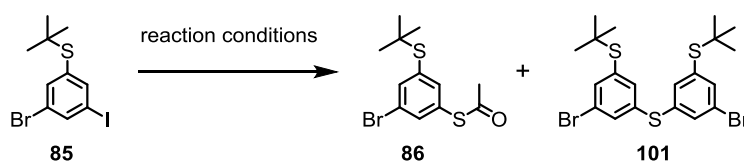


Scheme 30: Synthesis of building blocks **86** and **100**. Reaction conditions: a) NH_4SCN , Oxone[®], MeOH, rt, 3 h, 90%; b) NBS, CHCl_3 , 0 °C, 4 h, 87%; c) Ag_2SO_4 , I_2 , EtOH, rt, 12 h, 91%; d) $\text{BF}_3 \cdot \text{Et}_2\text{O}$, *tert*-butylONO, THF, -10 °C, 1 h, $\text{FeSO}_4 \cdot 7\text{H}_2\text{O}$, DMF, rt, 0.5 h, **98** (97%), **99** (92%); e) LAH, THF, rt, 2 h, vinyl-TMS, AIBN, di-*tert*-butylperoxide, 105 °C, 12 h, 92%; f) LAH, THF, rt, 2 h, 2-chloro-2-methylpropane, AlCl_3 , rt, 0.5 h, 93%; g) $\text{Pd}(\text{dba})_2$, dppf, KSAc, K_3PO_4 , MePh, 75 °C, 12 h, 92%.

Syntheses of both building blocks **86** and **100** started from commercially available 2-iodoaniline (**94**). The thiocyanide moiety was installed using oxidative conditions providing **95** in good yield. Since the amine group is a strong directing group, bromination of **95** with *N*-bromosuccinimide (NBS) in chloroform occurred exclusively in *ortho*-position affording aniline **96** in 87% yield.^[323] Deamination was originally performed in a mixture of boiling toluene and ethanol using sodium nitrite in a diazotization reaction.^[323] However, this reaction procedure requires large quantities of solvent, and resulted in a mixture of products, which were difficult to separate. A much more convenient method was the diazotization using *tert*-butylnitrite and BF_3 -etherate. The diazonium salt was cleaved using iron sulfate as single electron transfer (SET) source followed by the proton abstraction from *N,N'*-dimethylformamide (DMF) providing iodine **98** in excellent yield.^[324] Subsequently, thiocyanide was reduced by lithium aluminum hydride (LAH).^[325] The crude free thiol product was subjected to a reaction mixture using 2-chloro-2-methylpropane as solvent and a catalytic amount of Lewis acid aluminum trichloride affording precursor **85** in 93% over two steps.^[321] The S-acetyl moiety was installed via Pd-catalyzed reaction conditions using potassium thioacetate as sulfur source, affording the first building block **86** in excellent yield after screening of reaction conditions (Table 8). It was crucial to degas and distill the solvent prior to use. Since tripotassium phosphate (K_3PO_4) is a highly hygroscopic base, sufficient

quantities were dried at 200 °C in a Kugelrohr apparatus. The first entry represents the reaction conditions developed by Park and co-worker yielding a 1 : 1 mixture of thioether **101** and desired product **86**.^[326] The thioether formation occurs between the already formed compound **86**, which starts to react with the remaining starting material **85** before reaction runs to completion. Therefore an excess of potassium thioacetate was used in the second entry to prevent undesired thioether formation (entry 2). However, only slight improve was confirmed by GC–MS analysis. Increasing the temperature inverted the ratio probably due to the faster thioether formation compared to the attachment of the acetylated sulfur moiety (entry 3). Unfortunately, a higher catalyst loading did not improve the outcome of the reaction (entry 4). However, using pure toluene (MePh) as solvent prevented thioether formation very efficiently affording exclusively desired compound **86** (entry 5). Only using toluene allows lowering the amount of potassium thioacetate (KSAC) to 1.1 equivalents (entry 6).

Table 8: Optimization of C–S bond forming reaction conditions between potassium thioacetate and aryl iodide **85** providing **86**.

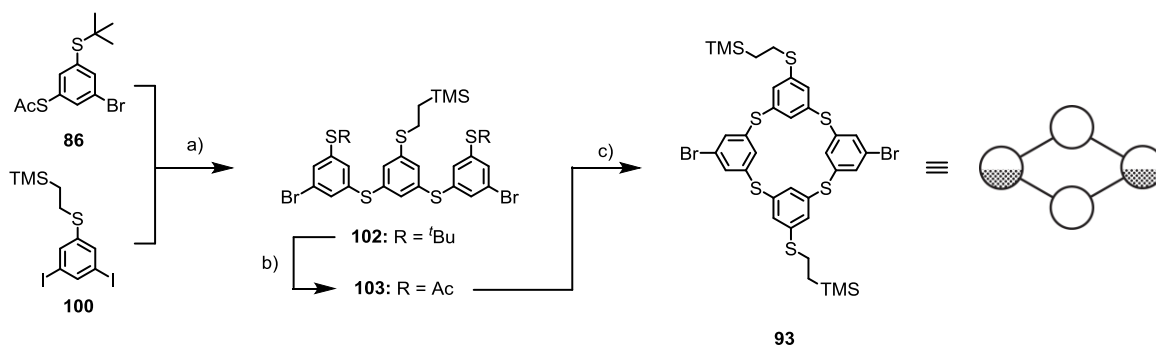


entry	Pd(dba) ₂ (mol %)	dppf (mol %)	KSAC (eq.)	MePh : acetone (mL)	temperature (°C)	86 : 101 (%) ^a
1	5	7	1	7 : 3	75	50 : 50
2	5	7	5	7 : 3	75	65 : 35
3	5	7	5	7 : 3	90	30 : 70
4	10	14	5	7 : 3	75	40 : 60
5	5	7	5	10 : 0	75	100 : 0
6	5	7	1.1	10 : 0	75	100 : 0

^aA small reaction sample was injected into GC/MS after 5 hours. Yields were determined by GC/MS analysis.

The synthesis of building block **100** started from the previously synthesized iodine **95**, which was iodinated with high regioselectivity using a mixture of iodine and silver sulfate in

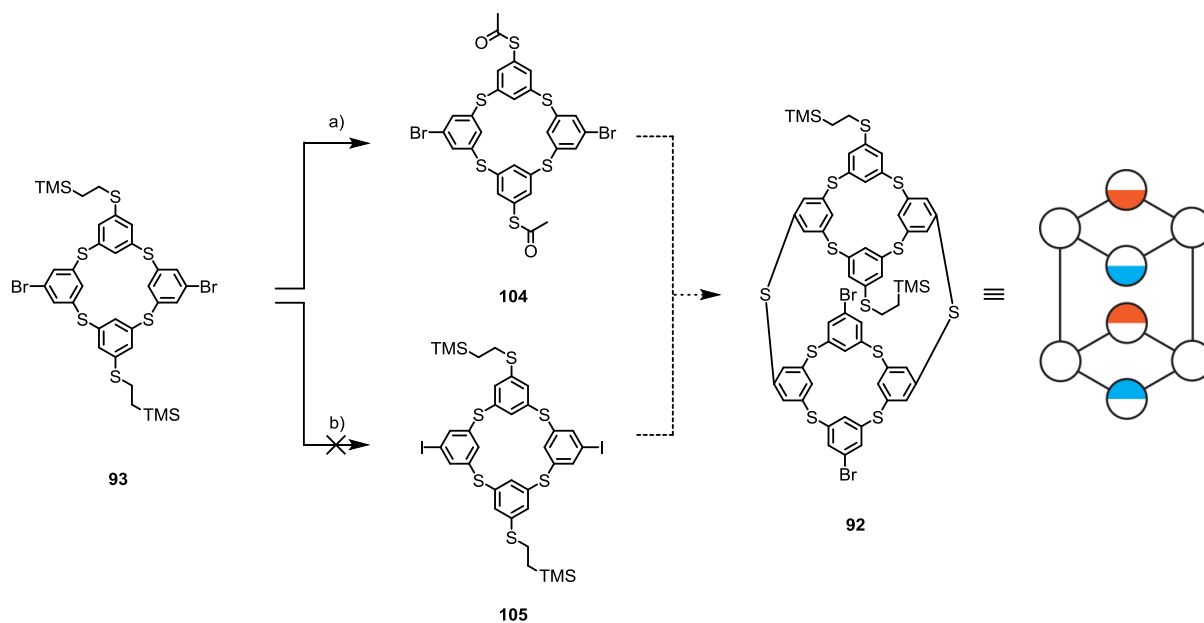
ethanolic solution providing diiodo compound **97** in 93%. Following a synthetic procedure in analogy to **98**, compound **99** was isolated in excellent yield. Subsequently, ethyl-TMS sulfur protecting group was installed after reduction of the thiocyanide group by LAH via radical reaction of free thiol and vinyl-TMS affording building block **100** in 92%.



Scheme 31: Synthesis of molecular bowl structure **93**. Reaction conditions: a) Pd(*dba*)₂, dppf, K₃PO₄, MePh : acetone (7 : 3), 75 °C, 12 h, 84%; b) BBr₃, AcCl, DCM, 0 °C – rt, 0.5 h, 72%; c) Pd(*dba*)₂, dppf, **100**, K₃PO₄, MePh : acetone (7 : 3), 75 °C, 12 h, 58%.

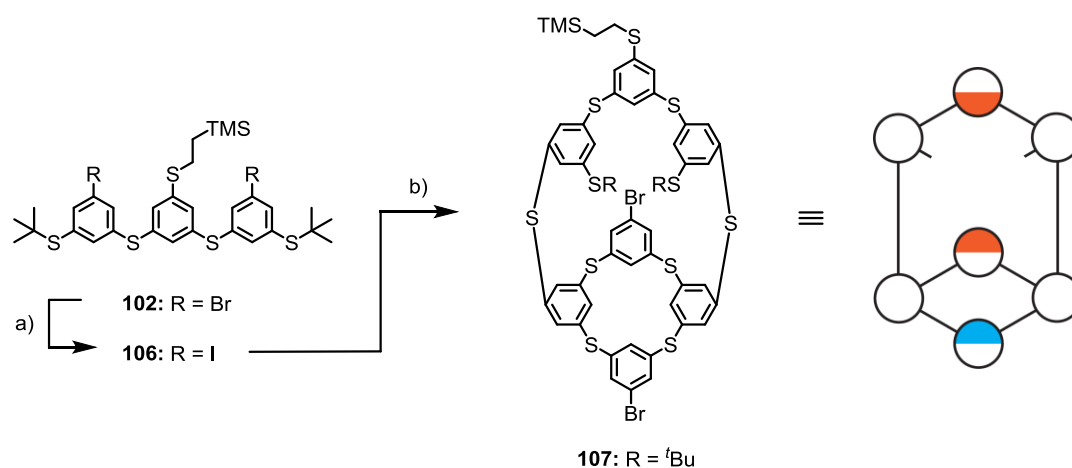
The two building blocks **86** and **100** were connected via Pd-catalyzed S–C bond forming reaction conditions, providing trimer **102** in 84%. Delightfully, the successful transprotection of the *tert*-butyl protecting groups into the corresponding acetylated sulfur moieties was achieved in 72%, while retaining the ethyl-TMS protecting group. Therefore the starting material **102** was dissolved in a degassed mixture of acetyl chloride and methylene chloride. Subsequently, equimolar amounts of BBr₃ were added dropwise at 0 °C. As every acetyl group attachment is accompanied with increased polarity, the progression of the reaction is followed by thin layer chromatography (TLC). On average, the reaction was stopped after 30 minutes to prevent over transprotection since mono acetylate sulfur can be efficiently separated from the desired product **103** by column chromatography. The key step of this synthetic strategy is the formation of the molecular bowl **93**. The major challenge was to prevent undesired oligomer formation as both building blocks exhibit two active reaction sites. In order to favor intramolecular bond formation after the first C–S connection pseudo high-diluted reaction condition were applied. Therefore, both starting materials **100** and **103** were dissolved in a mixture of toluene and acetone (7 : 3). This solution was added over 4 hours using a syringe pump into a reaction flask containing bis(dibenzylideneacetone)-

palladium(0) [Pd(dba)₂], 1,1'-bis(diphenylphosphino)ferrocene (dppf), and K₃PO₄ suspended in a mixture of toluene and acetone (7 : 3) pre-heated at 75 °C. Delightfully, the monomer **93** was isolated in excellent 58% via Pd-catalyzed reaction conditions. This yield is remarkable since both precursors **100** and **103** provide a flat, flexible structure bearing two active reaction sites, whereas the desired product **93** comprises high molecular strain forming a bowl-shaped structure.



Scheme 32: To enable the stepwise assembly of dimerization in the bowl approach the sulfur protecting group was transformed into the corresponding acetylated protecting group providing **104** in 74%. However, the halogen exchange from the bromine into the corresponding iodine **105** using aromatic Finkelstein reaction conditions has not yet been successful even after screening of various reaction conditions.

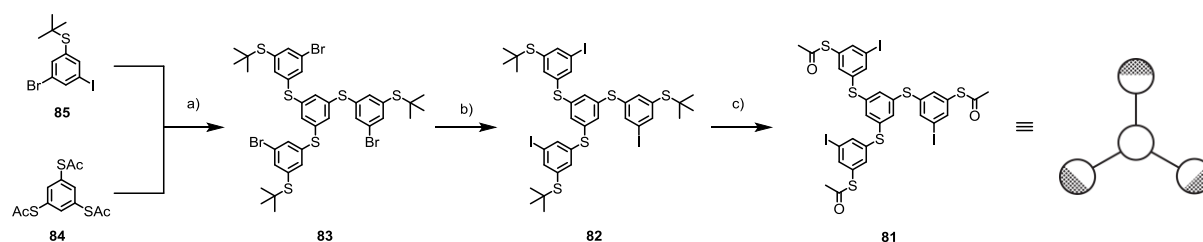
The assembly strategy of **92** required the two building blocks **104** and **105**. Transprotection from ethyl-TMS protected sulfur **93** into the corresponding acetylated sulfur **104** was conducted by deprotection with tetrabutylammonium fluoride (TBAF) followed by reprotection with acetyl chloride.^[327] However, the aromatic Finkelstein reaction was not successful in this case.^[328] None of the variation of the reaction conditions such as addition of equimolar amounts of copper(I) iodide (CuI), large excess of sodium iodide (NaI), longer reaction time, or higher temperatures did lead to the desired transformation. Interestingly, the molecular backbone remains intact as mainly dehalogenated as well as mono iodinated products were observed. Apparently, the low reactivity towards halogen exchange originates from the molecular strain making the halogens not accessible for the copper ligand system.



Scheme 33: Synthesis of dimer **107**. Reaction conditions: a) CuI, NaI, *N,N'*-dimethylethylene-diamine, dioxane, 110 °C, 24 h, 91%; b) Pd(dba)₂, dppf, K₃PO₄, MePh : acetone (7 : 3), 75 °C, 12 h, 12%.

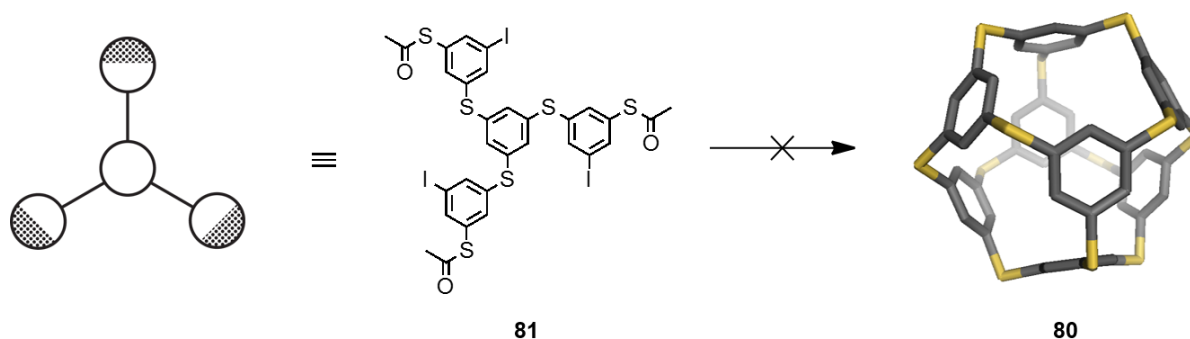
To prove the capability of this approach in an indirect fashion, the dibromide **102** was converted into the corresponding diiodine **106** in 91%. This observation strongly supports the hypothesis that this Finkelstein reaction proceeds smoothly if the flexibility of the investigated compound remains intact. Furthermore, coupling the precursor **106** with the previously synthesized monomer **104** afforded **107** in 12% by applying similar reaction condition employed for **93**. Certainly, this reaction requires further investigations for improvement. However, this observation allows two conclusions. (i) Even though the possible reaction sites were reduced to a number as low as two, the formation of the macromolecule **80** is very challenging. (ii) The Pd-catalyzed C–S bond formation reaction is powerful enough to form such macromolecular structures.

Wrap Approach I



Scheme 34: Synthesis of symmetric monomer **81**. Reaction conditions: a) Pd(dba)₂, dppf, K₃PO₄, MePh : acetone (7 : 3), 75 °C, 3 d, 92%; b) CuI, NaI, *N,N'*-dimethylethylenediamine, dioxane, 110 °C, 24 h, 98%; c) BBr₃, AcCl, DCM, rt, 1 h, 81%.

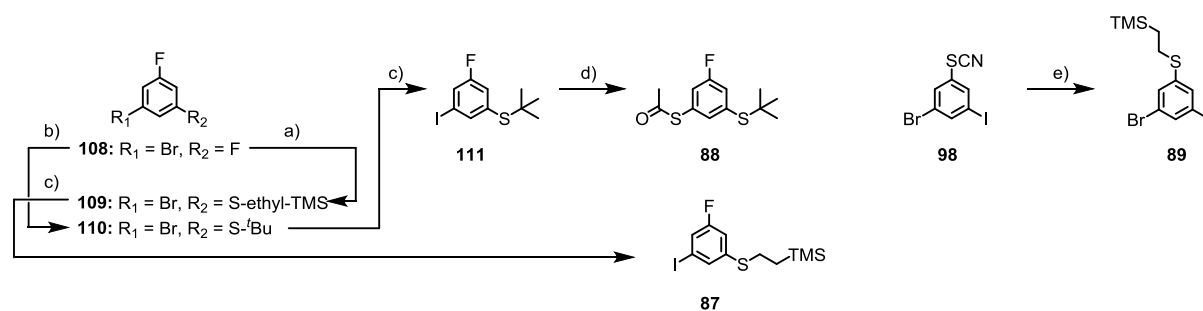
Acetyl protected 1,3,5-trimercaptobenzene (**84**) was coupled with the previously synthesized precursor **85** in a Pd-catalyzed reaction providing monomer **83** in excellent yield of 92% (three bonds).^[326] Performing this reaction at temperatures not higher than 75 °C allowed to prevent side reactions with the bromine. Therefore, both building blocks **84** and **85** were dissolved in a mixture of toluene and acetone (7 : 3), followed by the addition of the base and the catalytic system. Subsequently, an aromatic Finkelstein reaction quantitatively exchanged the bromides into the corresponding iodides **82**.^[328] Reaction is utilizing a catalyst system comprising CuI and a 1,2-diamine ligand using sodium iodide as iodine source. For the assembly of thiospherophane **80**, acetyl protected thiol monomer **81** was required. The synthesis of monomer **81** was successfully achieved in 81% by using the well known transprotection reaction conditions including Lewis acid BBr₃ cleaving the *tert*-butyl moiety, and acetyl chloride as free thiol scavenger.^[321]



Scheme 35: Attempted six C–S bond formation in one step using Pd-catalyzed reaction conditions has not yet been successful. In all cases of investigated reaction conditions, insoluble solids were obtained. It is most likely that the symmetric monomer **81** underwent oligomer formation.

Having monomer **81** in hand, several reaction conditions have been investigated for the assembly of thiospherophane **80**. However none of them led to the formation of target structure **80**, as none of the analysis techniques (e.g., ^1H NMR, direct analysis in real time (DART) mass spectrometry, matrix-assisted laser desorption/ionization time-of-flight (MALDI-TOF) mass spectrometry, TLC) allowed the observation of the desired product **80** even in traces. This screening of reaction conditions included the slow addition of the starting material over 12 hours into the catalytic reaction mixture using a syringe pump, high dilution (10^{-5} M), and addition of equimolar amounts of the catalyst and ligand. In all cases insoluble solids were obtained that did not show any specific mass signal or UV-vis activities. It is most likely that the monomer **81**, bearing six active reaction sites, underwent higher oligomer formation. Since the Pd-catalyzed thioether formation seems to be a very powerful assembly method, the further optimized wrap approach II was investigated.

Wrap Approach II

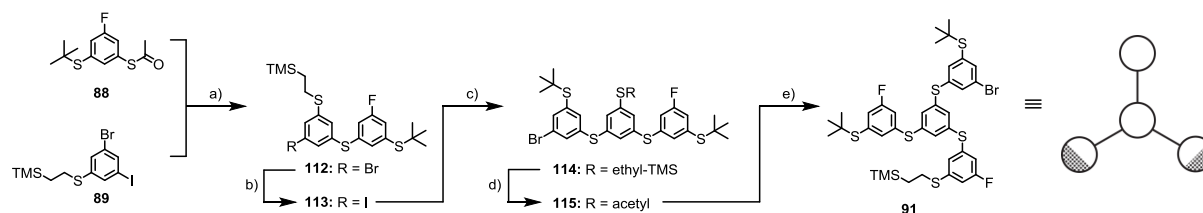


Scheme 36: Synthesis of building blocks **87**, **88**, and **89**. Reaction conditions: a) NaH, 2-(trimethylsilyl)ethane-1-thiol, DMF, 0 °C, 12 h, 81%; b) NaH, *tert*-butylSH, DMF, 0 °C, 5 h, 83%; c) CuI, NaI, *N,N'*-dimethylethylenediamine, dioxane, 110 °C, 24 h, **87** (97%), **111** (98%); d) Pd(dba)₂, dppf, KSAC, K₃PO₄, MePh, 75 °C, 12 h, 92%; e) LAH, THF, rt, 2 h, vinyl-TMS, AIBN, di-*tert*-butyl-peroxide, 105 °C, 12 h, 93%.

To apply the assembly strategy of the wrap approach II three additional building blocks **87** – **89** are required. Syntheses of both building blocks **87** and **88** started from the commercially available 1-bromo-3,5-difluorobenzene (**108**). The ethyl-TMS protected thiol moiety was introduced via $\text{S}_{\text{N}}\text{Ar}$ reaction using sodium hydride as a base and the freshly distilled 2-(trimethylsilyl)ethane-1-thiol dissolved in DMF. The reaction was performed at 0 °C affording **109** in 81%. In a similar reaction using 2-methyl-2-propanethiol, the

corresponding precursor **110** was isolated in 83%. Aromatic Finkelstein reaction provided the first building block **87** as well as the iodoaryl **111** in high yield of 97% and 98%, respectively. The S-acetyl moiety was successfully installed using already developed Pd-catalyzed reaction conditions, providing second building block **88** in 92%. The third building block **89** was synthesized in analogy to **100** from the previously synthesized iodobenzene **98**. Also in this case, the free thiol was protected with ethyl-TMS via radical conditions providing **89** in 96%.^[329]

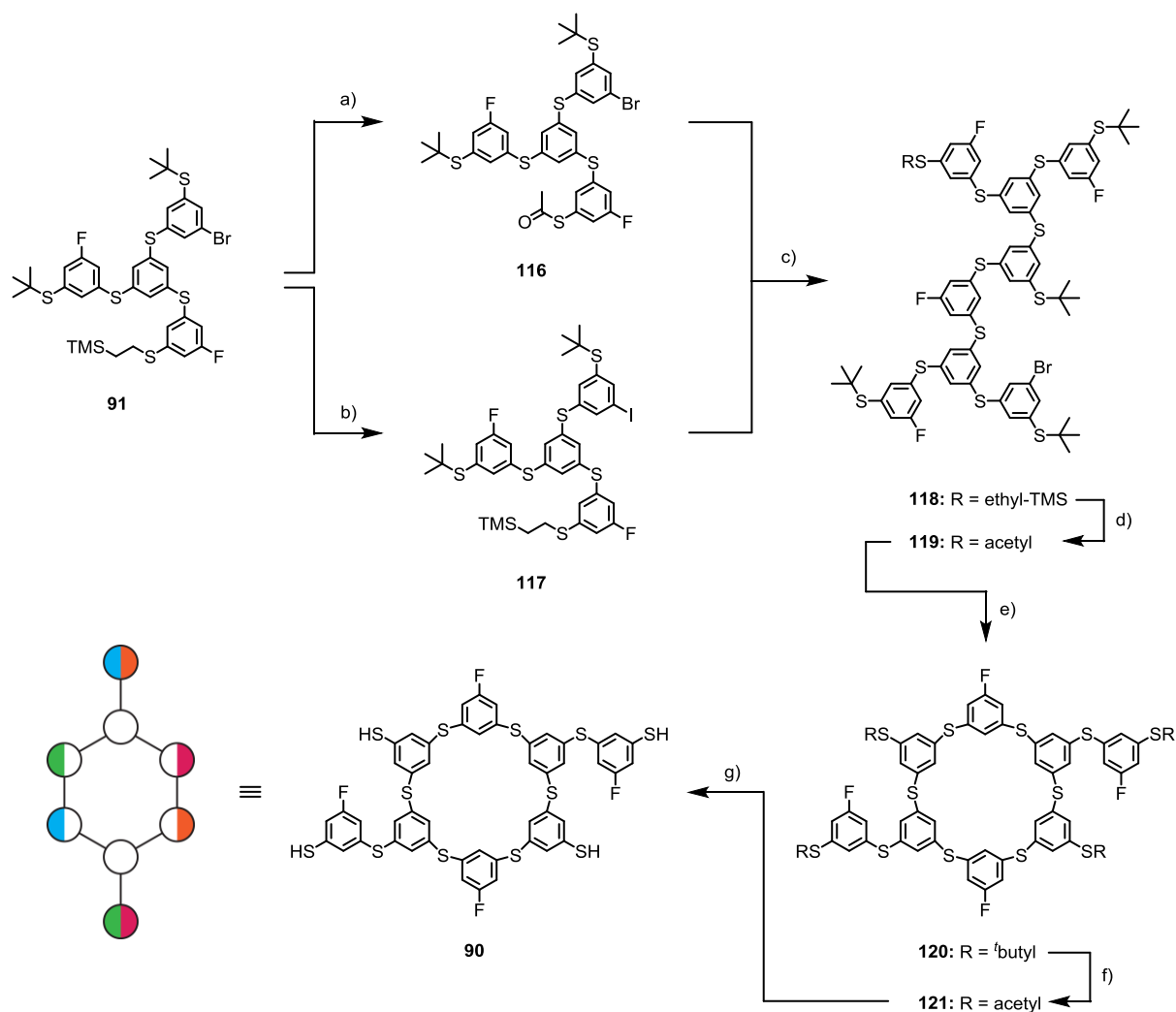
Having all four building blocks **86** – **89** in hand the synthetic strategy of monomer **91** was followed (Scheme 37). Formation of thioether **112** was achieved in excellent yield as **88** reacts exclusively with the iodine moiety of **89**.^[326] Aromatic Finkelstein reaction provided **113** in quantitative yield.^[328] Building block **86** was then attached to iodo-aryl **113** via Pd-catalyzed reaction affording **114** in 91%. Subsequently, transprotection from the ethyl-TMS protected into the corresponding acetyl-protected thiol **115** was conducted with TBAF in ice cold THF leaving the *tert*-butyl moieties unaffected. The free thiol was in situ re-protected with a large excess of acetyl chloride providing **115** in good yield.^[327] In order to prevent dithiol formation it was crucial to degas the solvent using a constant argon stream prior to use.



Scheme 37: Synthesis of asymmetric monomer **91**. Reaction conditions: a) Pd(dba)₂, dppf, K₃PO₄, MePh : acetone (7 : 3), 75 °C, 12 h, 94%; b) CuI, NaI, *N,N'*-dimethylethylene-diamine, dioxane, 110 °C, 24 h, 100%; c) Pd(dba)₂, dppf, **88**, K₃PO₄, MePh : acetone (7 : 3), 75 °C, 12 h, 91%; d) TBAF, AcCl, THF, 0 °C – rt, 3 h, 81%; e) Pd(dba)₂, dppf, **87**, K₃PO₄, MePh : acetone (7 : 3), 75 °C, 12 h, 93%.

Occasionally formed dithiol could readily be transformed into **115** using reductive conditions such as zinc and acetyl chloride with a catalytic amount of AlCl₃ suspended in acetonitrile at 40 °C.^[330] The remaining building block **87** was attached via Pd-catalyzed reaction as above mentioned in 93%. Monomer **91**, bearing two individual addressable moieties, namely the bromide and the S-ethyl-TMS, allows the stepwise dimerization of the corresponding

monomers **116** and **117**, respectively (Scheme 38). Using reaction conditions in analogy to **115**, S-acetyl protected monomer **116** was isolated in good yield. The aromatic Finkelstein reaction provided the other required monomer **117** in 94%. The two monomers **116** and **117** were connected via Pd-catalyzed C–S bond formation affording exclusively the desired dimer **118** in 89%. Profiting from the fact that the iodine moiety of monomer **117** is enabled to react with the S-acetyl protected group of monomer **116** at temperature lower than 80 °C, prevent undesired side reactions with the bromide. Reducing the reaction sites to a number as low as one of each monomer, higher oligomer formation can be excluded. This observation was strongly supported by mass analysis using DART as well as by NMR techniques strongly pointing at the exclusive formation of dimer **118**.



Scheme 38: Synthesis of precursor **90**. Reaction conditions: a) TBAF, AcCl, THF, 0 °C – rt, 3 h, 73%; b) CuI, NaI, *N,N'*-dimethylethylene-diamine, dioxane, 110 °C, 24 h, 94%; c) Pd(dba)₂, dppf, K₃PO₄, MePh : acetone (7 : 3), 75 °C, 12 h, 89%; d) TBAF, AcCl, THF, 0 °C – rt, 3 h, 71%; e) Pd(dba)₂, dppf, K₃PO₄, MePh : acetone (7 : 3), 110 °C, 12 h, 82%; f) BBr₃, AcCl, DCM, rt, 1 h, 67%; g) aq. NH₄OH (25%), THF, rt, 0.5 h, then HCl (3 M), quant.

Transprotection of the remaining ethyl-TMS moiety provided corresponding S-acetyl protected dimer **119** in good yield. The second bond formation was conducted via Pd-catalyzed reaction conditions affording symmetric dimer **120** in 82%. Also in this case the formation of higher oligomer was prevented as the reaction was performed in high dilution (10^{-5} M). In contrast to previously mentioned thioether formation higher temperature of 110 °C were required, as the bromide was involved in this case. The symmetric structure of **120** is strongly supported by the observation using ^1H NMR analysis (Figure 38). Compound **90** comprising for free thiol moieties is very challenging to purify by column chromatography. Therefore a clean and efficient deprotection is required without the need for column chromatography. Pleasingly, the acetyl protecting group is cleanly cleaved under basic conditions (ammonium hydroxide) and was ideally suited.^[331]

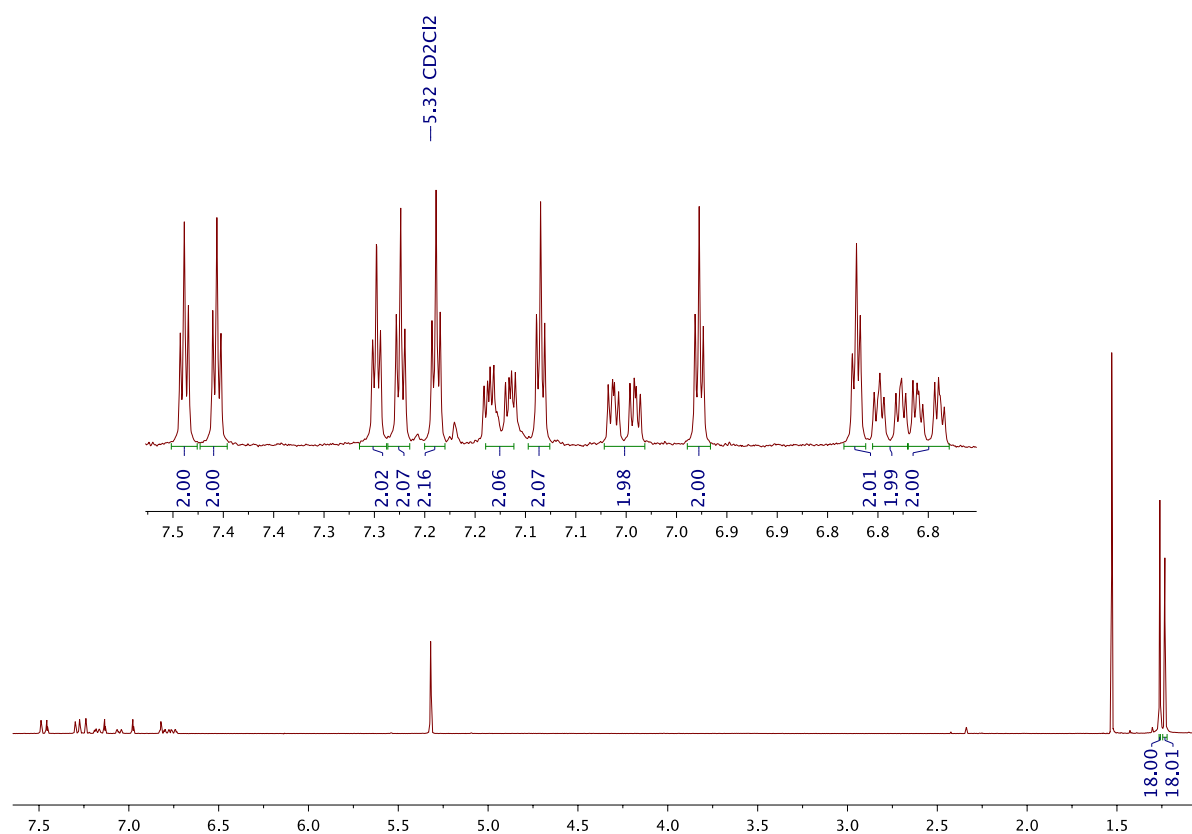
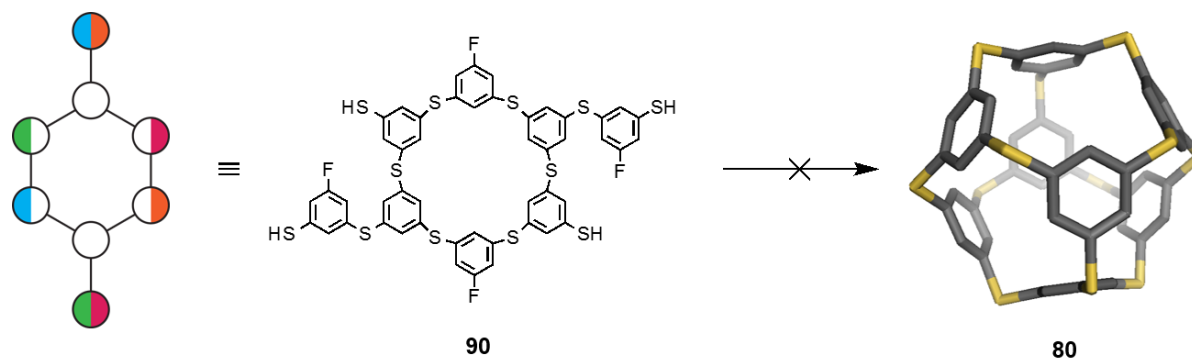


Figure 38: ^1H NMR of symmetric compound **120** measured in deuterated methylene chloride.

Hence the *tert*-butyl protected dimer **120** needs to be transprotected into the acetyl-protected precursor **121**. Dimer **120** was therefore dissolved in a thoroughly degassed mixture of dichloromethane and a large excess of acetyl chloride. To this solution an equimolar amount of BBr₃ is added dropwise at 0 °C. The cooling bath was removed and reaction conversion was followed by thin layer chromatography, affording acetyl protected compound **121** in acceptable yield (67%). The acetylated precursor **121** was successfully converted into the free thiol **90**. Reaction was conducted in a mixture of tetrahydrofuran (THF) and a ten-fold excess of aq. NH₄OH. After stirring this reaction mixture for 0.5 hours at room temperature, thiolate was protonated by dropwise addition of aq. HCl (3 M). The product **90** was extracted with methylene chloride and isolated after evaporation of solvent in quantitative yield.



Scheme 39: In the strategy of the wrap approach II four connections are required for the assembly of target molecule **80**. This was investigated using various nucleophilic aromatic substitution reaction conditions. Unfortunately, none of the investigated reactions has yet been successful.

Despite great effort the assembly of the thiospherophane **80** from its precursor **90** using nucleophilic aromatic substitution reaction conditions has not yet been successful (Scheme 39). The reaction conditions, which were investigated, are summarized in table 9.

Table 9: Investigated reaction conditions for the assembly of thiospherophene **80**.

entry	base	solvent	temperature (°C)	product (%) ^a
1	NaN(SiMe ₃) ₂	DMA	90	–
2	NaN(SiMe ₃) ₂	DMI	90	–
3	K ₂ CO ₃	DMSO	90	–
4	NaH	DMI	90	–

^aReaction was stopped after three days. Investigated analyzing methods (TLC, ¹H NMR, DART) showed no evidence for the formation of thiospherophane **80**.

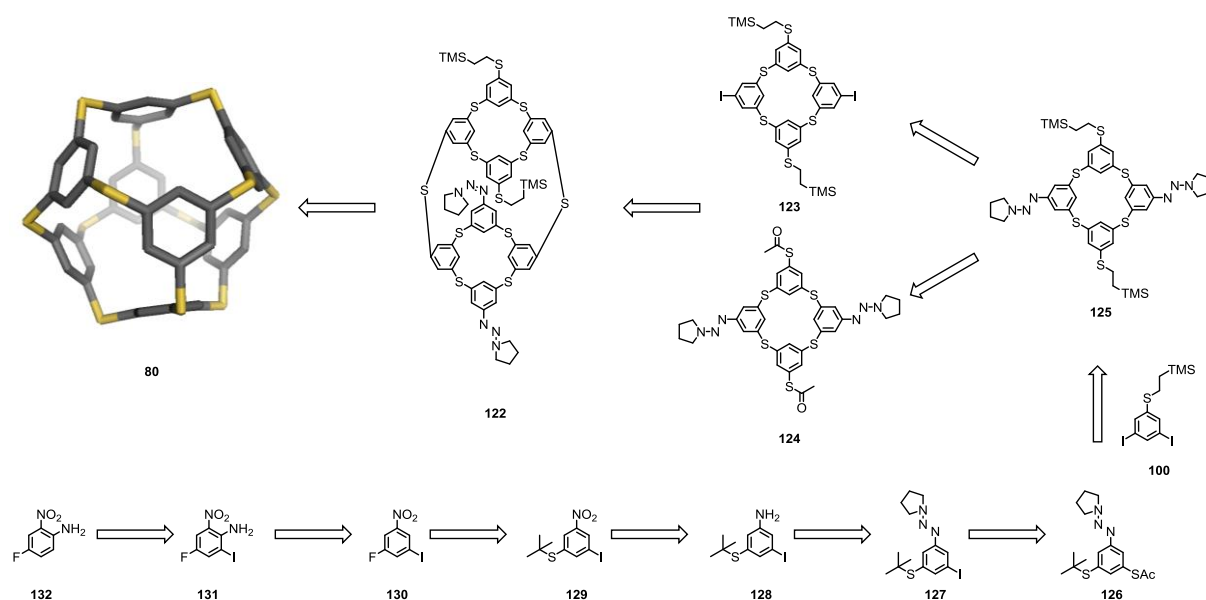
In a first attempt reaction conditions were applied in analogy to the reported synthesis of a sulfur containing molecular bowl structure.^[318] Therefore, precursor **90** was dissolved in freshly distilled demthylacetamide (DMA) under very high dilution (10⁻⁵ M). A slight excess of the base sodium bis(trimethylsilyl)amide (NaN(SiMe₃)₂) was dissolved in DMA (2 M) and was added dropwise over 6 hours at 90 °C. No product formation has been observed by DART or MALDI-TOF mass spectroscopy after stirring the reaction mixture for 3 days. Switching the solvent to 1,3-dimethyl-2-imidazolidinone (DMI), which is prone to conduct nucleophilic aromatic substitution reactions, was also not successful by following the same reaction procedure (entry 2). Using either a mixture of potassium carbonate and dimethylsulfoxide (DMSO) or sodium hydride and DMI (entries 3 and 4) did not lead to any formation of target structure **80**. However, this is the first synthesis of a precursor bearing all the required atoms for the formation of thiospherophane **80**.

Conclusion and Future Perspectives

The advantages of the bowl approach are the reduced number of C–S bond formations in each step, as well as using very powerful Pd-catalyzed reaction conditions. In this approach the formation of the molecular bowl **92** is very challenging as its synthesis starts from building blocks that are flat and very flexible. As the desired product comprises strong molecular strain forming a molecular bowl, oligomer formation would be very reliable. To prevent oligomer formation in this key step, pseudo high diluted Pd-catalyzed reaction conditions were applied. The assembly of the dimer **92** follows a stepwise dimerization strategy. In order to realize this stepwise assembly, monomer **93** was transformed into the corresponding building blocks **104** and **105**, respectively. When monomer **93** was exposed to TBAF, which cleaved the ethyl-TMS protecting group, was successfully reprotected with acetyl chloride providing acetylated building block **104** in good yield. Unfortunately, the aromatic Finkelstein reaction did not lead to the second building block **105** even after intensive screening of reaction conditions. This issue was attributed to the structural conformation of the monomer **93**, probably shielding the bromine moiety from the catalytic copper–ligand system. To overcome this issue other approaches, such as masking of the halide should be considered. A possible strategy would be the dialkyltriazine, which can be converted into the corresponding aryl iodide using methyl iodide as iodine source.

In the following assembly strategy, all the gathered knowledge is combined. Similarly to the proposed synthesis of the dimer **92**, the dimer formation of **122** is considered in a stepwise fashion using Pd-catalyzed reaction conditions connecting the monomer **123** with **124**. As the aromatic Finkelstein reaction turned out to be the challenging step, the iodine moiety will be introduced masked as a dialkylated triazine. This functional group can be converted into the corresponding iodine **124** by methyl iodide. However, to realize the synthesis of the monomer **125** an additional building block **126** is required, whereas the diiodo building block **100** is already available from previously developed approaches. Since this dialkylated triazine moiety is synthesized from the free amine, the synthetic strategy starts from the commercial available 4-fluoro-2-nitroaniline (**132**). The amine group acts in this case as directing group, ensuring the regioselectivity of the iodination, which leads to precursor **131**. Subsequent deamination may provide **130** and installation of the *tert*-butyl protected sulfur moiety leads to intermediate **129**. Reduction of the nitro-group by tin chloride is expected to form the

desired free amine **128**. By quenching the formed diazonium salt with the appropriate dialkyl amine under basic conditions leads to **127**. As described above, the acetylated sulfur functionality will be introduced via Pd-catalyzed reaction using potassium thioacetate as the protected sulfur source. With the building blocks **100** and **126** the synthetic strategy of the monomer **126** follows the approach to the molecular bowl structure **93** as close as possible. This approach is possibly superior as it allows the assembly of thiospherophane **80** in a stepwise fashion using powerful Pd-catalyzed reaction conditions. As the number of reactive sites is reduced to two, the probability of side reaction is significantly minimized. Furthermore, the pre-organized structural conformation is expected to facilitate the synthesis of thiospherophane **80**.



Scheme 40: Assembly strategy of thiospherophane **80** including an iodine-masked monomer to enable a stepwise dimerization. Additionally a synthetic strategy of the iodine-masked building block is presented.

In the wrap approach I the synthesis of thiospherophane **80** was investigated from the symmetric monomer **81**. The synthesis of the symmetric monomer was achieved in high yields and large quantities starting from the readily available building blocks **84** and **85**. However, the synthesis of target structure **80** was not successful yet were six bonds have to be made in one step using Pd-catalyzed reaction conditions.

In the wrap approach II the synthesis of the asymmetric monomer **91** was achieved in excellent yield. Subsequently, the ethyl-TMS sulfur protecting group was transferred into the corresponding acetylated sulfur compound **116**. Using aromatic Finkelstein conditions the bromide was exchanged with an iodine providing **117**. The connection of the two monomers was provided by the Pd-catalyzed reaction as each monomer bears only one reactive side. Transprotection and second C–S bond formation allowed the isolation of the symmetric dimer **120**. To enable the nucleophilic aromatic substitution reaction the *tert*-butyl moieties were removed in a two step reaction affording the free thiols in quantitative yield. Even though the number of C–S-bonds which have to be formed is reduced to four, the assembly of thiospherophane **80** was not successful using various S_NAr reaction conditions. On a positive note, this approach represents the first synthesis of a molecular structure comprising all atoms required for the target structure **80**.

Experimental Section

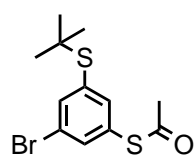
General Remarks

All commercially available compounds were purchased and used as received unless explicitly stated otherwise. CDCl_3 and CD_2Cl_2 was purchased from Cambridge Isotope Laboratories, Inc. ^1H NMR was recorded on a Bruker DPX-NMR spectrometer operating at 400 MHz. ^{13}C NMR were recorded on a Bruker DPX-NMR spectrometer operating at 101 MHz. The chemical shifts are reported in parts per million (ppm) relative to tetramethylsilane or a residual solvent peak, and the J values are given in Hz. GC-MS was performed on a Shimadzu GCMS-2020 SE equipped with a Zebron 5 MS Inferno column which allowed to achieve temperatures up to 350 °C. DART analyses were performed on a Shimadzu LC-MS 2020 system. For column chromatography, usually silica gel Siliaflash® p60 (40–63 μm) from Silicycle was used, and TLC was performed on silica gel 60 F254 glass plates with a thickness of 0.25 mm purchased from Merck.

Synthetic Procedures

2-(trimethylsilyl)ethane-1-thiol:^[332] Vinyltrimethylsilane (29.1 mL, 194 mmol, 1.0 eq.) was added to an argon flushed oven dried one-necked round bottom flask equipped with a reflux condenser. Using an argon counter flow, freshly distilled thiolacetic acid (12.7 mL, 175 mmol, 0.9 eq.) and AIBN (325 mg, 1.94 mmol, 1 mol%) was added and flask was lowered into a preheated oil bath and reaction mixture was stirred at 60 °C for 3.5 hours. Reaction conversion was followed by GC/MS. After full conversion, reaction was cooled to room temperature and reflux condenser was replaced with a short distillation bridge. S-(2-(trimethylsilyl)ethyl) ethanethioate (24.2 g, 137 mmol, 84%) was obtained after distillation (82 °C, 20 mbar) as transparent liquid and transferred to a 1L 2-necked round bottom flask charged with K₂CO₃ (21.4 g, 153 mmol, 1.1 eq.) dissolved in MeOH (150 mL) and water (75 mL). Suspension was degassed for 30 minutes followed by the addition of Et₂O (75 mL). Reaction was stirred for 4 hours under argon atmosphere and was carefully quenched by the addition of citric acid (29.8 g, 153 mmol, 1.1 eq.) in small portions. Et₂O (200 mL) was added and reaction mixture transferred to a separating funnel. Separated organic layer was washed with aq. 1% citric acid solution (2 x 100 mL). Organic layer was dried over MgSO₄ and filtered in a one necked round bottom flask and distilled off. 2-(trimethylsilyl)ethane-1-thiol (17.4 g, 129 mmol, 94%) was obtained after fractional distillation (55 °C, 33 mbar) as transparent liquid. ¹H – NMR (400 MHz, CDCl₃, 25 °C): δ = 2.65 – 2.55 (m, 2H), 1.50 (t, *J* = 6.7 Hz, 1H), 0.99 – 0.92 (m, 2H), 0.02 (s, 9H) ppm.

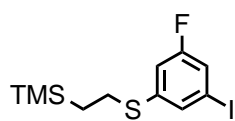
3-bromo-5-(*tert*-butylthio)-acetylthio-phenyl (86): Pd(dba)₂ (627 mg, 1.1 mmol, 5 mol%),



dppf (838 mg, 1.5 mmol, 7 mol%) were placed in a oven dried argon flushed 100 mL schlenk flask equipped with a rubber septum. To remove remaining oxygen three vacuum/argon flush cycles were performed. Afterwards, K₃PO₄ (5.6 g, 25.9 mmol, 1.2 eq.) and potassium thioacetate (2.7 g, 23.8 mmol, 1.1 eq.) were added with an argon counter flow. K₃PO₄ was dried for 4 hours in a Kugelrohr apparatus at 200°C before use. Previously degassed toluene (50 mL) and 3-bromo-5-iodophenyl-(*tert*-butyl)sulfane (8.0 g, 21.6 mmol, 1.0 eq.) were added and the resulting reaction mixture was degassed for another 30 minutes. Subsequently, schlenk flask was lowered in an oil bath preheated at 75 °C and reaction was stirred for 12 hours at this

temperature. After completed conversion, cooled reaction mixture was filtered over a short Celite plug to remove the palladium residues. Crude product was extracted with ethyl acetate (1 x 100 mL) and washed with aq. sat. NH_4Cl (2 x 50 mL). Organic layer was washed with brine (1 x 50 mL), dried over MgSO_4 and removed at reduced pressure. Crude product was further purified by column chromatography (SiO_2 ; c-hexane : MePh, 5 : 1 – 1 : 1) providing 3-bromo-5-(*tert*-butylthio)-acetylthio-phenyl (6.6 g, 20.7 mmol, 96%) as yellowish solid. ^1H – NMR (400 MHz, CDCl_3 , 25 °C): δ = 7.71 (t, J = 1.6 Hz, 1H), 7.56 (t, J = 1.6 Hz, 1H), 7.51 (t, J = 1.6 Hz, 1H), 2.44 (s, 3H), 1.31 (s, 9H) ppm. ^{13}C – NMR (101 MHz, CDCl_3 , 25 °C): δ = 192.6, 141.6, 140.6, 137.0, 135.9, 129.8, 122.1, 47.2, 31.1, 30.5 ppm. MS (EI, 70 eV): m/z (%) = 320.1 (9), 318.0 (9), 264.0 (56), 262.0 (54), 221.9 (53), 220.0 (52), 141.0 (11), 140.0 (18), 139.0 (10), 96.0 (10), 95.0 (21), 63.1 (13), 58.0 (72), 57.1 (100), 55.1 (10). EA: calcd. for $\text{C}_{12}\text{H}_{15}\text{BrOS}_2$: C 45.14, H 4.74, N 0.00; found: C 45.98, H 4.12, N 0.00.

3-fluoro-5-iodophenyl-thio-ethyltrimethylsilane (87): 3-bromo-5-fluorophenyl-thio-

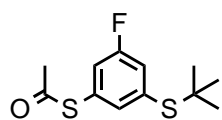


ethyltrimethylsilane (5.0 g, 16.3 mmol, 1.0 eq.), CuI (156 mg, 0.8 mmol, 5 mol%) and NaI (4.9 g, 32.6 mmol, 2.0 eq.) were placed in an oven dried argon flushed micro wave vial equipped with a rubber septum.

Afterwards, vacuum was applied for 30 minutes followed by the addition of dioxane (7 mL) and *N-N'*-dimethylethylenediamine (0.2 mL, 1.6 mmol, 0.1 eq.). The resulting blue suspension was stirred at 110 °C for 12 hours. Subsequently, the cooled reaction was poured into aq. sat. NH_4Cl (100 mL) and product was extracted with methylene chloride (100 mL). The separated organic layer was washed with brine (100 mL), dried over MgSO_4 and removed at reduced pressure. Crude product was further purified by Kugelrohr distillation ($1.5 \cdot 10^{-1}$ mbar, 155 °C) affording 3-fluoro-5-iodophenyl-thio-ethyltrimethylsilane (5.6 g, 15.8 mmol, 97%) as transparent oil. ^1H – NMR (400 MHz, CDCl_3 , 25 °C): δ = 7.35 (m, 1H), 7.21 – 7.18 (m, 1H), 6.93 – 6.90 (m, 1H), 2.96 – 2.92 (m, 2H), 0.95 – 0.91 (m, 2H), 0.07 (s, 9H) ppm. ^{13}C – NMR (101 MHz, CDCl_3 , 25 °C): δ = 162.3 (d, J = 253.2 Hz, 1C), 142.3 (d, J = 8.0 Hz, 1C), 132.0 (d, J = 3.0 Hz, 1C), 121.7 (d, J = 23.9 Hz, 1C), 114.2 (d, J = 23.1 Hz, 1C), 93.7 (d, J = 8.8 Hz, 1C), 29.1, 16.5, –1.6 ppm. ^{19}F – NMR (377 MHz, CDCl_3): δ = –110.6 ppm. MS (EI, 70 eV): m/z (%) = 354.1 (2), 326.1 (5), 311.1 (3), 184.1 (6), 169.1 (4), 127.1 (3), 126.1 (13), 109.1 (3), 107.1 (2), 102.2 (5), 101.2 (47), 94.1 (4), 83.1 (2), 82.1 (3), 81.1 (3), 77.1 (4), 75.1 (16),

74.0 (62), 73.1 (100), 72.1 (4), 69.0 (5), 63.1 (5), 59.1 (11), 58.1 (15), 57.1 (4), 55.1 (3). EA: calcd. for C₁₁H₁₆FISSi: C 37.29, H 4.55, N 0.00; found: C 37.35, H 4.53, N 0.00.

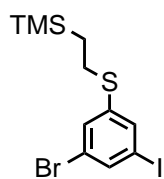
3-(*tert*-butylthio)-5-fluoro-acetylthio-phenyl (88): Pd(dba)₂ (935 mg, 1.6 mmol, 5 mol%),



dppf (1.3 g, 2.3 mmol, 7 mol%) were placed in an oven-dried argon-flushed 200 mL Schlenk flask equipped with a rubber septum. To remove remaining oxygen, three vacuum/argon flush cycles were performed.

Afterwards, K₃PO₄ (8.4 g, 38.6 mmol, 1.2 eq.) and potassium thioacetate (4.1 g, 35.4 mmol, 1.1 eq.) were added with an argon counter flow. K₃PO₄ was dried for 4 hours in a Kugelrohr apparatus at 200 °C before use. Previously degassed toluene (50 mL) and 3-iodo-5-fluorophenyl-(*tert*-butyl)sulfane (10.0 g, 32.2 mmol, 1.0 eq.) was added and the resulting reaction mixture was degassed for another 30 minutes. Subsequently, the Schlenk flask was lowered in an oil bath preheated at 75 °C and the reaction was stirred for 12 hours at this temperature. After completed conversion, the cooled reaction mixture was filtered over a short Celite plug to remove the palladium residues. Crude product was extracted with ethyl acetate (1 x 100 mL) and washed with aq. sat. NH₄Cl (2 x 50 mL). Organic layer was washed with brine (1 x 50 mL), dried over MgSO₄ and removed at reduced pressure. Crude product was further purified by column chromatography (SiO₂; *n*-hexane : MePh, 5 : 1 – 1 : 1) providing 3-(*tert*-butylthio)-5-fluoro-acetylthio-phenyl (7.7 g, 29.8 mmol, 92%) as transparent oil. ¹H – NMR (400 MHz, CDCl₃, 25 °C): δ = 7.37 (m, 1H), 7.31 – 7.27 (m, 1H), 7.19 – 7.15 (m, 1H), 2.44 (s, 3H), 1.32 (s, 9H) ppm. ¹³C – NMR (101 MHz, CDCl₃, 25 °C): δ = 192.6, 161.9 (d, *J* = 251.9 Hz, 1C), 138.6 (d, *J* = 3.1 Hz, 1C), 135.8 (d, *J* = 7.6 Hz, 1C), 129.6 (d, *J* = 9.0 Hz, 1C), 125.0 (d, *J* = 20.7 Hz, 1C), 121.6 (d, *J* = 22.6 Hz, 1C), 47.1, 31.1, 30.4 ppm. ¹⁹F – NMR (377 MHz, CDCl₃): δ = –111.8 ppm. MS (EI, 70 eV): *m/z* (%) = 258.2 (21), 204.1 (11), 203.1 (13), 202.1 (100), 160.1 (98), 126.1 (13), 115.1 (11), 114.1 (16), 58.0 (85), 57.1 (97), 55.1 (12). EA: calcd. for C₁₂H₁₅FOS₂: C 55.79, H 5.85, N 0.00; found: C 55.41, H 5.93, N 0.00.

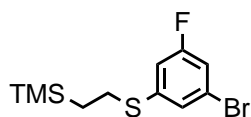
3-bromo-5-iodophenyl-thio-ethyltrimethylsilane (89): 1-bromo-3-iodo-5-



thiocyanato- benzene (10.0 g, 29.4 mmol, 1.0 eq.) was placed in a oven dried argon flushed 500 mL round bottom flask and dissolved in dry THF (230 mL). To the clear solution LAH (1 M in THF, 30.9 mL, 30.9 mmol, 1.1 eq.) was added dropwise.

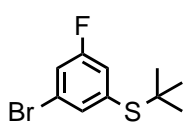
After 2 hours stirring at RT to the solution was added carefully a mixture of ice and THF followed by pure water. The product was extracted with methylene chloride (100 mL) and washed with aq. HCl (1 M, 50 mL). Organic layer was dried over MgSO₄ and solvent was removed at vacuum. The crude thiol was placed in a oven dried argon flushed micro wave vial equipped with a septum. Subsequently, vinyl-TMS (17.6 mL, 118 mmol, 4.0 eq.), AIBN (49.3 mg, 0.3 mmol, 1 mol%) and di-*t*-butyl-peroxide (0.5 mL, 2.9 mmol, 0.1 eq.) were added with a argon counter flow. Afterwards, MW-vial was sealed and reaction mixture was stirred at 105 °C over night. The cooled reaction mixture was directly purified by column chromatography (SiO₂; c-hexane : MePh, 10 : 1) providing 3-bromo-5-iodophenyl-thio-ethyltrimethylsilane (11.4 g, 27.5 mmol, 93%) as a slightly yellow oil, which solidified upon standing. ¹H – NMR (400 MHz, CDCl₃, 25 °C): δ = 7.61 (t, *J* = 1.6 Hz, 1H), 7.49 (t, *J* = 1.6 Hz, 1H), 7.33 (t, *J* = 1.6 Hz, 1H), 2.97 – 2.90 (m, 2H), 0.95 – 0.89 (m, 2H), 0.07 (s, 9H) ppm. ¹³C – NMR (101 MHz, CDCl₃, 25 °C): δ = 142.2, 136.4, 134.9, 129.8, 123.1, 94.6, 29.2, 16.6, -1.6 ppm. MS (EI, 70 eV): *m/z* (%) = 416.1 (0.1), 414.1 (0.1), 388.1 (0.4), 386.1 (0.3), 373.0 (0.2), 371.0 (0.1), 281.2 (0.1), 246.1 (0.2), 244.1 (0.2), 209.2 (0.1), 208.2 (0.2), 207.1 (1.0), 188.0 (0.2), 186.1 (0.2), 139.0 (0.1), 137.1 (0.2), 135.2 (0.2), 134.1 (0.2), 133.1 (0.2), 127.0 (0.2), 121.1 (0.1), 115.0 (0.1), 109.0 (0.2), 108.1 (0.3), 107.1 (1.6), 106.1 (0.2), 105.1 (0.1), 103.2 (0.3), 102.2 (0.6), 101.2 (5.5), 96.1 (0.3), 91.1 (0.3), 90.1 (0.4), 89.1 (0.3), 86.1 (0.2), 85.1 (0.2), 83.0 (0.2), 82.0 (0.4), 81.1 (0.3), 78.1 (0.1), 77.1 (0.3), 76.1 (0.5), 75.1 (6.3), 74.1 (9.2), 73.1 (100.0), 72.1 (1.2), 71.1 (0.5), 70.1 (0.4), 69.1 (0.7), 67.1 (0.1), 65.1 (0.1), 64.1 (0.4), 63.1 (7.3), 62.1 (1.2), 61.1 (0.6), 60.1 (0.6), 59.1 (4.4), 58.1 (5.6), 57.1 (1.2), 56.1 (0.2), 55.1 (1.2), 54.1 (0.1), 53.1 (0.5), 51.1 (0.2), 50.1 (0.4). EA: calcd. for C₁₁H₁₆BrISSi: C 31.82, H 3.88, N 0.00; found: C 30.02, H 3.39, N 0.00.

3-bromo-5-fluorophenyl-thio-ethyltrimethylsilane (109): NaH (2.1 g, 51.8 mmol, 2.0 eq.)



was added to a 250 mL 3-necked round bottom flask and suspended in dry DMF (50 mL). TMS-ethanthiol (3.9 mL, 24.6 mmol, 0.9 eq.) was carefully added at 0 °C to this suspension and resulting reaction mixture was stirred for 1 hour at this temperature. Subsequently, 1-bromo-3,5-difluorobenzene (5.0 g, 25.9 mmol, 1.0 eq.) was added and reaction mixture was stirred for 12 hours at 0 °C. Water was added to quench the reaction and product was extracted with Et₂O (3 x 100mL). Combined organic layers were washed with brine (2 x 100mL), dried over MgSO₄ and removed at reduced pressure. Purification by Kugelrohr distillation (7.4 · 10⁻² mbar, 96 °C) provided 3-bromo-5-fluorophenyl-thio-ethyltrimethylsilane (6.1 g, 19.8 mmol, 81%) as transparent oil. ¹H – NMR (400 MHz, CDCl₃, 25 °C): δ = 7.16 – 7.15 (m, 1H), 7.03 – 7.00 (m, 1H), 6.91 – 6.87 (m, 1H), 2.97 – 2.93 (m, 2H), 0.95 – 0.91 (m, 2H), 0.07 (s, 9H) ppm. ¹³C – NMR (101 MHz, CDCl₃, 25 °C): δ = 162.7 (d, J = 252.0 Hz, 1C), 142.3 (d, J = 8.5 Hz, 1C), 126.0 (d, J = 3.1 Hz, 1C), 122.8 (d, J = 10.4 Hz, 1C), 116.0 (d, J = 24.7 Hz, 1C), 113.4 (d, J = 23.2 Hz, 1C), 29.0, 16.5, -1.62 ppm. ¹⁹F – NMR (377 MHz, CDCl₃): δ = -110.6 ppm. MS (EI, 70 eV): m/z (%) = 308.1 (1), 306.1 (1), 280.1 (1), 278.1 (1), 265.0 (2), 263.0 (2), 184.1 (2), 183.1 (1), 169.1 (1), 139.1 (1), 137.1 (1), 132.6 (1), 127.1 (1), 126.1 (5), 109.1 (1), 107.1 (1), 103.2 (1), 102.2 (1), 101.2 (13), 94.1 (1), 83.0 (1), 82.0 (1), 81.1 (1), 77.1 (2), 75.1 (5), 74.1 (9), 73.1 (100), 72.1 (1), 69.0 (1), 63.1 (1), 59.1 (4), 58.1 (4). EA: calcd. for C₁₁H₁₆BrFSSi: C 42.99, H 5.25, N 0.00; found: C 43.16, H 5.14, N 0.00.

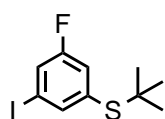
3-bromo-5-fluorophenyl-(tert-butyl)sulfane (110): 1-bromo-3,5-difluorobenzene (8.0 g, 41.5



mmol, 1.0 eq.) was dissolved in 90 mL DMF (crown cap) in a oven dried argon flushed 250 mL 3-necked round bottom flask. The clear solution was cooled to 0 °C and sodium 2-methyl-2-methyl-2-propanethiol (4.9 g, 39.4 mmol, 0.9 eq.) was added. The transparent mixture was stirred for 5 hours at 0 °C. The reaction was quenched with water (50 mL) and extracted with tBME (100 mL). The organic layer was washed with HCl (1 M, 50 mL) and water (2 x 50 mL). The organic layer was dried over MgSO₄ and solvent was removed at reduced pressure. Crude product was purified by column chromatography (SiO₂; c-hexane : MePh, 10 : 1) providing 3-bromo-5-fluorophenyl-(tert-butyl)sulfane (8.2 g, 31.2 mmol, 83%) as transparent oil. ¹H – NMR (400 MHz, CDCl₃, 25

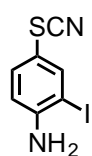
$^{\circ}\text{C}$): $\delta = 7.48 - 7.47$ (m, 1H), $7.27 - 7.24$ (m, 1H), $7.21 - 7.18$ (m, 1H), 1.31 (s, 9H) ppm. ^{13}C – NMR (101 MHz, CDCl_3 , $25\text{ }^{\circ}\text{C}$): $\delta = 162.0$ (d, $J = 253.3$ Hz, 1C), 136.7 (d, $J = 8.0$ Hz, 1C), 135.7 (d, $J = 3.3$ Hz, 1C), 122.9 (d, $J = 20.6$ Hz, 1C), 122.0 (d, $J = 10.0$ Hz, 1C), 119.6 (d, $J = 24.3$ Hz, 1C), 47.2 , 31.1 ppm. ^{19}F – NMR (377 MHz, CDCl_3): $\delta = -110.8$ ppm. MS (EI, 70 eV): m/z (%) = 264.1 (1), 262.2 (1), 208.1 (4), 207.1 (1), 206.1 (3), 205.1 (1), 128.1 (1), 127.1 (4), 126.1 (10), 106.1 (1), 100.1 (1), 94.1 (1), 93.1 (1), 87.1 (1), 83.1 (2), 82.1 (2), 81.1 (3), 74.1 (1), 73.1 (1), 69.1 (4), 68.1 (1), 63.1 (3), 62.1 (1), 61.1 (1), 59.1 (2), 58.2 (5), 57.2 (100), 56.2 (3), 55.1 (4), 53.1 (1), 51.1 (1), 50.1 (2). EA: calcd. for $\text{C}_{10}\text{H}_{12}\text{BrFS}$: C 45.64, H 4.60, N 0.00; found: C 45.65, H 4.63, N 0.00.

3-iodo-5-fluorophenyl-(tert-butyl)sulfane (111): 3-bromo-5-fluorophenyl-(tert-butyl)sulfane



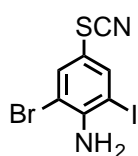
(5.7 g, 21.7 mmol, 1.0 eq.), CuI (209 mg, 1.1 mmol, 5 mol%) and NaI (6.5 g, 43.4 mmol, 2.0 eq.) were placed in a oven dried argon flushed micro wave vial equipped with a rubber septum. Afterwards, vacuum was applied for 30 minutes followed by the addition of dioxane (9 mL) and $N\text{-}N'$ -dimethylethylenediamine (0.3 mL, 2.2 mmol, 0.1 eq.). The resulting blue suspension was stirred at $110\text{ }^{\circ}\text{C}$ for 12 hours. Subsequently, the cooled reaction was poured into aq. sat. NH_4Cl (100 mL) and product was extracted with methylene chloride (100 mL). The separated organic layer was washed with brine (100 mL), dried over MgSO_4 and removed at reduced pressure. Crude product was further purified by column chromatography (SiO_2 ; c-hexane : MePh , 10 : 1) providing 3-iodo-5-fluorophenyl-(tert-butyl)sulfane (6.6 g, 21.3 mmol, 98%) as transparent oil. ^1H – NMR (400 MHz, CDCl_3 , $25\text{ }^{\circ}\text{C}$): $\delta = 7.69 - 7.68$ (m, 1H), $7.46 - 7.43$ (m, 1H), $7.24 - 7.21$ (m, 1H), 1.31 (s, 9H) ppm. ^{13}C – NMR (101 MHz, CDCl_3 , $25\text{ }^{\circ}\text{C}$): $\delta = 161.6$ (d, $J = 254.4$ Hz, 1C), 141.5 (d, $J = 3.2$ Hz, 1C), 136.8 (d, $J = 7.6$ Hz, 1C), 125.3 (d, $J = 23.5$ Hz, 1C), 123.6 (d, $J = 20.6$ Hz, 1C), 92.9 (d, $J = 8.5$ Hz, 1C), 47.1 , 31.1 ppm. ^{19}F – NMR (377 MHz, CDCl_3): $\delta = -110.9$ ppm. MS (EI, 70 eV): m/z (%) = 309.9 (22), 253.8 (90), 127.0 (24), 126.0 (35), 83.0 (10), 58.0 (16), 57.1 (100). EA: calcd. for $\text{C}_{10}\text{H}_{12}\text{FIS}$: C 38.72, H 3.90, N 0.00; found: C 38.69, H 3.99, N 0.00.

2-iodo-4-thiocyanatoaniline (95): 2-Iodoaniline (20.0 g, 89.5 mmol, 1.0 eq.) was suspended



in methanol (750 mL, Baker quality) in a 2 L round bottom flask. Subsequently, ammonium thiocyanate (10.2 g, 134 mmol, 1.5 eq.) and Oxone® monopersulfate (41.2 g, 134 mmol, 1.5 eq.) were added and the resulting suspension was stirred for 3 hours at room temperature. To quench the completed reaction water (400 mL) and methylene chloride (500 mL) were added. The organic phase was separated and dried over MgSO₄ and solvent was removed under reduced pressure. Crude product was recrystallized from methanol providing 2-iodo-4-thiocyanatoaniline (22.3 g, 80.7 mmol, 90%) as white solid. ¹H – NMR (400 MHz, CDCl₃, 25 °C): δ = 7.85 (d, *J* = 2.2 Hz, 1H), 7.36 (dd, *J* = 8.5, 2.2 Hz, 1H), 6.73 (d, *J* = 8.5 Hz, 1H), 4.43 (br s, 2H). ppm. ¹³C – NMR (101 MHz, CDCl₃, 25 °C): δ = 149.2, 143.2, 134.3, 115.1, 111.9, 110.7, 83.6 ppm. MS (EI, 70 eV): *m/z* (%) = 276.0 (51), 150.2 (11), 149.2 (99), 127.0 (45), 123.1 (19), 122.1 (49), 121.1 (12), 105.2 (83), 96.0 (28), 95.1 (24), 91.1 (32), 90.1 (12), 78.1 (20), 74.2 (11), 70.1 (18), 69.0 (53), 65.1 (18), 64.1 (34), 63.1 (81), 62.1 (33), 61.1 (22), 58.0 (22), 53.1 (19), 52.1 (100), 51.1 (17), 50.1 (14). EA: calcd. for C₇H₅I₁N₂S: C 30.45, H 1.83, N 10.15; found: C 30.50, H 1.83, N 9.96.

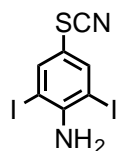
2-bromo-6-iodo-4-thiocyanatoaniline (96): 2-iodo-4-thiocyanatoaniline (13.2 g, 47.8 mmol,



1.0 eq.) was dissolved in chloroform (135 mL, Baker quality) in a 500 mL round bottom flask and was cooled to 0 °C. To this solution NBS (9.0 g, 50 mmol, 1.1 eq.) was added in portions. Reaction conversion was followed by GC/MS revealing completion after 4 hours. Water (100 mL) was added to quench the reaction and product was extracted with methylene chloride (2 x 100 mL). The combined organic layers were washed with aq. sat. Na₂S₂O₃ and were dried over MgSO₄. Organic layer was filtered over a small silica plug and solvent was removed. Crude product was recrystallized by petroleum ether affording 2-bromo-6-iodo-4-thiocyanatoaniline (14.7 g, 41.4 mmol, 87%) as beige solid. ¹H – NMR (400 MHz, CDCl₃, 25 °C): δ = 7.82 (d, *J* = 2.1 Hz, 1H), 7.66 (d, *J* = 2.1 Hz, 1H), 4.95 (br s, 2H) ppm. ¹³C – NMR (101 MHz, CDCl₃, 25 °C): δ = 146.5, 142.2, 136.9, 111.4, 111.2, 107.0, 82.4 ppm. MS (EI, 70 eV): *m/z* (%) = 356.0 (25), 354.0 (25), 275.1 (24), 229.1 (19), 227.1 (18), 148.2 (46), 147.2 (11), 127.0 (58), 122.2 (18), 121.1 (22), 120.1 (20), 95.1 (20), 94.1 (17), 93.1 (25), 90.1 (32), 89.1 (24), 88.1 (14), 78.1 (28), 76.1 (13), 74.1 (14), 73.1 (12), 70.1 (19), 69.0 (54), 67.9 (10), 65.1 (13), 64.1 (12), 63.1 (56), 62.1 (61), 61.1 (43), 60.1

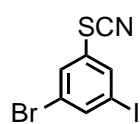
(12), 59.0 (11), 58.1 (26), 53.1 (18), 52.1 (100), 51.1 (27), 50.1 (16). EA: calcd. for $C_7H_4BrIN_2S$: C 23.68, H 1.14, N 7.89; found: C 24.05, H 1.21, N 7.43.

2,6-diiodo-4-thiocyanatoaniline (97): Ag_2SO_4 (4.7 g, 14.8 mmol, 1.0 eq.) and iodine (3.9 g,



15.5 mmol, 1.1 eq.) were placed in a oven dried argon flushed 250 mL 2-necked round bottom flask. Reactants were dissolved in 65 mL ethanol, followed by the addition of 2-iodo-4-thiocyanatoaniline (4.1 g, 14.8 mmol, 1.0 eq.). Resulting reaction mixture was stirred for 12 hours at room temperature. Afterwards, reaction mixture was filtered over Celite to remove precipitated AgI. Water (100 mL) was added to the filtrate and crude product was extracted with ethyl acetate (2 x 100 mL). Combined organic layers were washed with aq. sat. $Na_2S_2O_3$ solution (100 mL) and brine (100 mL), dried over $MgSO_4$ filtrated and concentrated. Crude product was further purified by column chromatography (SiO_2 ; c-hexane : ethyl acetate, 5 : 1) providing 2,6-diiodo-4-thiocyanatoaniline (5.4 g, 13.4 mmol, 91%) as beige solid. 1H – NMR (400 MHz, $CDCl_3$, 25 °C): δ = 7.85 (s, 2H), 4.98 (br s, 2H) ppm. ^{13}C – NMR (101 MHz, $CDCl_3$, 25 °C): δ = 148.5, 143.3, 111.9, 111.2, 80.7 ppm. MS (EI, 70 eV): m/z (%) = 401.8 (100), 275.9 (11), 274.9 (83), 231.0 (11), 149.0 (12), 148.0 (66), 122.0 (14), 121.0 (33), 120.0 (12), 95.0 (12), 94.0 (12), 93.0 (11), 90.0 (24), 89.1 (19), 78.1 (12), 74.1 (14), 69.0 (16), 63.0 (30), 62.0 (26), 61.0 (17), 52.1 (24). EA: calcd. for $C_7H_4I_2N_2S$: C 20.92, H 1.00, N 6.97; found: C 21.14, H 0.95, N 6.93.

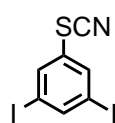
1-bromo-3-iodo-5-thiocyanatobenzene (98): $BF_3 \cdot Et_2O$ (13.9 mL, 110 mmol, 1.5 eq.) was



added to 3-necked oven dried argon flushed round bottom flask equipped with a thermometer at -10 °C. To this solution 2-bromo-6-iodo-4-thiocyanatoaniline (26.0 g, 73.2 mmol, 1.0 eq.) dissolved in THF (50 mL) was added dropwise keeping the temperature below 0 °C. Subsequently, *tert*-butyl nitrite (11.7 mL, 87.8 mmol, 1.2 eq.) was dissolved in THF (50 mL) and added dropwise to the mixture of 2-bromo-6-iodo-4-thiocyanatoaniline in $BF_3 \cdot Et_2O$. The resulting suspension was stirred at -10 °C for 1 hour. For further precipitation pentane (40 mL) was added and solid BF_4 - diazonium salt was filtered off. Meanwhile, $FeSO_4 \cdot 7H_2O$ (12.3 g, 80.5 mmol, 1.1 eq.) was dissolved in DMF (200 mL, Baker quality). The diazonium salt was added in small portions (N_2 evolution!) to this

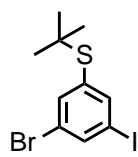
black reaction mixture. After completed addition the black reaction was poured into ice water. Crude product was extracted with methylene chloride (2 x 100 mL) and combined organic layers were washed with aq. HCl (1 M, 2 x 100 mL). Organic layer was dried over MgSO₄ and solvent was removed under reduced pressure affording 1-bromo-3-iodo-5-thiocyanatobenzene (24.1 g, 70.9 mmol, 97%) as white solid after recrystallization from petroleum ether. ¹H – NMR (400 MHz, CDCl₃, 25 °C): δ = 7.90 (t, *J* = 1.6 Hz, 1H), 7.78 (t, *J* = 1.6 Hz, 1H), 7.64 (t, *J* = 1.6 Hz, 1H) ppm. ¹³C – NMR (101 MHz, CDCl₃, 25 °C): δ = 150.0, 136.3, 131.4, 127.9, 124.3, 108.9, 95.3 ppm. MS (EI, 70 eV): *m/z* (%) = 341.0 (30), 339.0 (32), 214.0 (31), 212.0 (30), 133.1 (100), 127.0 (17), 107.0 (20), 106.0 (15), 75.1 (74), 74.1 (64), 73.1 (12), 69.0 (19), 63.1 (52), 62.1 (22), 61.0 (12). EA: calcd. for C₇H₃BrINS: C 24.73, H 0.89, N 4.12; found: C 24.85, H 1.02, N 4.09.

1,3-diiodo-5-thiocyanatobenzene (99): BF₃ · Et₂O (2.4 mL, 18.6 mmol, 1.5 eq.) was added to



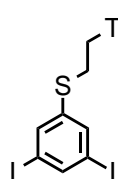
3-necked oven dried argon flushed round bottom flask equipped with a thermometer at –10 °C. To this solution 2,6-iodo-4-thiocyanatoaniline (5.0 g, 12.4 mmol, 1.0 eq.) dissolved in THF (10 mL) was added dropwise keeping the temperature below 0 °C. Subsequently, *tert*-butyl nitrite (2.0 mL, 14.9 mmol, 1.2 eq.) was dissolved in THF (10 mL) and added dropwise to the mixture of 2,6-iodo-4-thiocyanatoaniline in BF₃ · Et₂O. The resulting suspension was stirred at –10 °C for 1 hour. For further precipitation pentane (10 mL) was added and solid BF₄-diazonium salt was filtered off. Meanwhile, FeSO₄ · 7H₂O (2.1 g, 13.6 mmol, 1.1 eq.) was dissolved in DMF (40 mL, Baker quality). The diazonium salt was added in small portions (N₂ evolution!) to this black reaction mixture. After completed addition the black reaction was poured into ice water. Crude product was extracted with methylene chloride (2 x 100 mL) and combined organic layers were washed with aq. HCl (1 M, 2 x 100 mL). Organic layer was dried over MgSO₄ and solvent was removed under reduced pressure affording 1,3-diiodo-5-thiocyanatobenzene (4.4 g, 11.4 mmol, 92%) as white solid after recrystallization from petroleum ether. ¹H – NMR (400 MHz, CDCl₃, 25 °C): δ = 8.08 (t, *J* = 1.4 Hz, 1H), 7.80 (d, *J* = 1.4 Hz, 2H) ppm. ¹³C – NMR (101 MHz, CDCl₃, 25 °C): δ = 146.3, 136.9, 127.7, 108.9, 95.6 ppm. MS (EI, 70 eV): *m/z* (%) = 386.7 (100), 259.8 (54), 133.0 (72), 75.0 (39), 74.0 (30), 63.0 (23). EA: calcd. for C₇H₄I₂N₂S: C 21.73, H 0.78, N 3.62; found: C 21.69, H 0.72, N 3.65.

3-bromo-5-iodophenyl-(*tert*-butyl)sulfane (85): 1-bromo-3-iodo-5-thiocyanatobenzene



(10.0 g, 29.4 mmol, 1.0 eq.) was placed in a oven dried argon flushed 500 mL round bottom flask and dissolved in dry THF (230 mL). To the clear solution LAH (1 M in THF, 30.9 mL, 30.9 mmol, 1.05 eq.) was added dropwise. After 2 hours stirring at RT to the solution was added carefully a mixture of ice and THF followed by pure water. The product was extracted with methylene chloride (100 mL) and washed with aq. HCl (1 M, 50 mL). Organic layer was dried over MgSO₄ and solvent was removed at vacuum. The crude thiol was placed in a 2-necked oven dried argon flushed 100 mL round bottom flask equipped with a washing flask containing aq. sat NaOH solution. 2-Chloro-2-methylpropane (25.2 mL, 229 mmol, 7.8 eq.) was added followed by AlCl₃ (198 mg, 1.47 mmol, 5 mol%). After gas evolution has stopped methylene chloride (100 mL) was added and reaction mixture was quenched with aq. sat NaHCO₃ (50 mL). Crude product was extracted with methylene chloride (2 x 100 mL) and washed with brine (1 x 100 mL). Combined organic layers were dried over MgSO₄ and solvent was removed at reduced pressure. Residue was purified by column chromatography (SiO₂, c-hexane : MePh, 10 : 1) yielding 3-bromo-5-iodophenyl-(*tert*-butyl)sulfane (10.1 g, 27.2 mmol, 93%) as beige solid. ¹H – NMR (400 MHz, CDCl₃, 25 °C): δ = 7.85 (t, *J* = 1.6 Hz, 1H), 7.82 (t, *J* = 1.6 Hz, 1H), 7.64 (t, *J* = 1.6 Hz, 1H), 1.30 (s, 9H) ppm. ¹³C – NMR (101 MHz, CDCl₃, 25 °C): δ = 144.2, 139.9, 139.1, 136.9, 122.5, 93.9, 47.2, 31.1 ppm. MS (EI, 70 eV): *m/z* (%) = 371.9 (41), 369.9 (39), 316.8 (12), 315.9 (100), 314.9 (16), 313.9 (100), 188.9 (18), 187.9 (25), 186.9 (18), 185.9 (23), 108.0 (42), 107.0 (52), 75.0 (15), 74.0 (12), 69.0 (12), 63.0 (85), 62.0 (18), 57.9 (100), 57.0 (100), 55.1 (15). EA: calcd. for C₁₀H₁₂BrIS: C 32.37, H 3.26, N 0.00; found: C 31.45, H 3.19, N 0.00.

(2-((3,5-diiodophenyl)thio)ethyl)trimethylsilane (100): 3-diiodo-5-thiocyanatobenzene



(2.0 g, 5.1 mmol, 1.0 eq.) was placed in a oven dried argon flushed 100 mL round bottom flask and dissolved in dry THF (50 mL). To the clear solution LAH (1 M in THF, 5.4 mL, 5.4 mmol, 1.05 eq.) was added dropwise. After 2 hours stirring at room temperature to the solution was added carefully a mixture of ice and THF followed by pure water. The product was extracted with methylene chloride (100 mL) and washed with aq. HCl (1 M, 50 mL). Organic layer was dried over MgSO₄ and solvent was removed at vacuum. The crude thiol was placed in a oven dried argon flushed micro wave vial equipped with a septum. Subsequently, vinyl-TMS (3.1 mL, 20.7 mmol, 4.0 eq.), AIBN (8.5 mg, 0.1 mmol, 1 mol%) and di-*tert*-butyl-peroxide (0.1 mL, 0.8 mmol, 0.1 eq.) were added with an argon counter flow. Afterwards, MW-vial was sealed and reaction mixture was stirred at 105 °C over night. The cooled reaction mixture was directly purified by column chromatography (SiO₂; c-hexane : MePh, 10 : 1) providing 3-bromo-5-iodophenylthio-ethyltrimethylsilane (2.2 g, 4.76 mmol, 92%) as a slightly yellow oil. ¹H – NMR (400 MHz, CDCl₃, 25 °C): δ = 7.80 (t, *J* = 1.5 Hz, 1H), 7.52 (d, *J* = 1.5 Hz, 2H), 2.94 – 2.90 (m, 2H), 0.94 – 0.89 (m, 2H), 0.07 (s, 9H) ppm. ¹³C – NMR (101 MHz, CDCl₃, 25 °C): δ = 142.2, 141.9, 135.6, 95.0, 29.2, 16.6, –1.6 ppm. MS (EI, 70 eV): *m/z* (%) = 461.7 (2.57), 433.8 (10.21), 418.7 (3.5), 291.9 (5.67), 107.0 (4.12), 101.1 (19.96), 75.0 (6.59), 74.1 (10.13), 73.1 (100), 63.0 (5.67), 58.9 (2.72), 58.0 (3.15). EA: calcd. for C₁₁H₁₆I₂SSi: C 28.59, H 3.49, N 0.00; found: C 27.69, H 3.01, N 0.00.

Bibliography

- [1] M. Gantenbein, M. Hellstern, L. Le Pleux, M. Neuburger, M. Mayor, *Chem. Mater.* **2015**, DOI 10.1021/cm5045754.
- [2] P. Visser, *Opt. Photonik* **2008**, *3*, 27–29.
- [3] P. Cinzano, F. Falchi, C. D. Elvidge, *Mon. Not. R. Astron. Soc.* **2001**, *328*, 689–707.
- [4] R. Chepesiuk, *Environ. Health Perspect.* **2009**, *117*, A20–A27.
- [5] S. Matta, S. M. Mahmud, in *IECON 2010 - 36th Annu. Conf. IEEE Ind. Electron. Soc.*, **2010**, pp. 3316–3321.
- [6] F. Wieland, H. Gueldner, O. R. Hild, in *2012 Int. Conf. Renew. Energy Res. Appl. ICRERA*, **2012**, pp. 1–5.
- [7] N. Thejokalyani, S. J. Dhoble, *Renew. Sustain. Energy Rev.* **2014**, *32*, 448–467.
- [8] S. R. Forrest, *Org. Electron.* **2003**, *4*, 45–48.
- [9] J. Kido, M. Kimura, K. Nagai, *Science* **1995**, *267*, 1332–1334.
- [10] Y.-S. Tyan, *J. Photonics Energy* **2011**, *1*, 011009–011009–15.
- [11] C. Sekine, Y. Tsubata, T. Yamada, M. Kitano, S. Doi, *Sci. Technol. Adv. Mater.* **2014**, *15*, 034203.
- [12] W. Brütting, J. Frischeisen, T. D. Schmidt, B. J. Scholz, C. Mayr, *Phys. Status Solidi A* **2013**, *210*, 44–65.
- [13] C. W. Tang, S. A. VanSlyke, *Appl. Phys. Lett.* **1987**, *51*, 913–915.
- [14] J. H. Burroughes, D. D. C. Bradley, A. R. Brown, R. N. Marks, K. Mackay, R. H. Friend, P. L. Burns, A. B. Holmes, *Nature* **1990**, *347*, 539–541.
- [15] G. Gu, G. Parthasarathy, P. E. Burrows, P. Tian, I. G. Hill, A. Kahn, S. R. Forrest, *J. Appl. Phys.* **1999**, *86*, 4067–4075.
- [16] Y. Tao, C. Yang, J. Qin, *Chem. Soc. Rev.* **2011**, *40*, 2943–2970.
- [17] Y. Shirota, H. Kageyama, *Chem. Rev.* **2007**, *107*, 953–1010.
- [18] P. Strohriegel, J. v. Grazulevicius, *Adv. Mater.* **2002**, *14*, 1439–1452.
- [19] K. Goushi, R. Kwong, J. J. Brown, H. Sasabe, C. Adachi, *J. Appl. Phys.* **2004**, *95*, 7798–7802.
- [20] D.-H. Lee, Y.-P. Liu, K.-H. Lee, H. Chae, S. M. Cho, *Org. Electron.* **2010**, *11*, 427–433.
- [21] S.-J. Su, E. Gonmori, H. Sasabe, J. Kido, *Adv. Mater.* **2008**, *20*, 4189–4194.

- [22] S. H. Kim, J. Jang, K. S. Yook, J. Y. Lee, M.-S. Gong, S. Ryu, G. Chang, H. J. Chang, *J. Appl. Phys.* **2008**, *103*, 054502.
- [23] J. Lee, J.-I. Lee, J.-W. Lee, H. Y. Chu, *Org. Electron.* **2010**, *11*, 1159–1164.
- [24] H. Sasabe, E. Gonmori, T. Chiba, Y.-J. Li, D. Tanaka, S.-J. Su, T. Takeda, Y.-J. Pu, K. Nakayama, J. Kido, *Chem. Mater.* **2008**, *20*, 5951–5953.
- [25] J. Lee, N. Chopra, S.-H. Eom, Y. Zheng, J. Xue, F. So, J. Shi, *Appl. Phys. Lett.* **2008**, *93*, 123306.
- [26] M. A. Baldo, S. R. Forrest, *Phys. Rev. B* **2000**, *62*, 10958–10966.
- [27] H. Ishii, K. Sugiyama, E. Ito, K. Seki, *Adv. Mater.* **1999**, *11*, 605–625.
- [28] K. A. Higginson, X.-M. Zhang, F. Papadimitrakopoulos, *Chem. Mater.* **1998**, *10*, 1017–1020.
- [29] Y. q. Li, M. k. Fung, Z. Xie, S.-T. Lee, L.-S. Hung, J. Shi, *Adv. Mater.* **2002**, *14*, 1317–1321.
- [30] V. I. Adamovich, S. R. Cordero, P. I. Djurovich, A. Tamayo, M. E. Thompson, B. W. D’Andrade, S. R. Forrest, *Org. Electron.* **2003**, *4*, 77–87.
- [31] M. E. Kondakova, T. D. Pawlik, R. H. Young, D. J. Giesen, D. Y. Kondakov, C. T. Brown, J. C. Deaton, J. R. Lenhard, K. P. Klubek, *J. Appl. Phys.* **2008**, *104*, 094501.
- [32] H. Kim, Y. Byun, R. R. Das, B.-K. Choi, P.-S. Ahn, *Appl. Phys. Lett.* **2007**, *91*, 093512.
- [33] Q. Wang, J. Ding, D. Ma, Y. Cheng, L. Wang, X. Jing, F. Wang, *Adv. Funct. Mater.* **2009**, *19*, 84–95.
- [34] C.-C. Wu, C.-W. Chen, T.-Y. Cho, *Appl. Phys. Lett.* **2003**, *83*, 611–613.
- [35] X. Cai, A. B. Padmaperuma, L. S. Sapochak, P. A. Vecchi, P. E. Burrows, *Appl. Phys. Lett.* **2008**, *92*, 083308.
- [36] T. Tsutsui, H. Tokuhisa, M. Era, **1998**, pp. 230–239.
- [37] M. A. Baldo, D. F. O’Brien, Y. You, A. Shoustikov, S. Sibley, M. E. Thompson, S. R. Forrest, *Nature* **1998**, *395*, 151–154.
- [38] M. A. Baldo, D. F. O’Brien, M. E. Thompson, S. R. Forrest, *Phys. Rev. B* **1999**, *60*, 14422–14428.
- [39] C. W. Tang, S. A. VanSlyke, *Appl. Phys. Lett.* **1987**, *51*, 913–915.
- [40] M.-T. Lee, C.-H. Liao, C.-H. Tsai, C. H. Chen, *Adv. Mater.* **2005**, *17*, 2493–2497.
- [41] C. Adachi, M. A. Baldo, S. R. Forrest, M. E. Thompson, *Appl. Phys. Lett.* **2000**, *77*, 904–906.

- [42] M. A. Baldo, S. Lamansky, P. E. Burrows, M. E. Thompson, S. R. Forrest, *Appl. Phys. Lett.* **1999**, *75*, 4–6.
- [43] S. Lamansky, P. Djurovich, D. Murphy, F. Abdel-Razzaq, H.-E. Lee, C. Adachi, P. E. Burrows, S. R. Forrest, M. E. Thompson, *J. Am. Chem. Soc.* **2001**, *123*, 4304–4312.
- [44] Y. Sun, N. C. Giebink, H. Kanno, B. Ma, M. E. Thompson, S. R. Forrest, *Nature* **2006**, *440*, 908–912.
- [45] S. Reineke, F. Lindner, G. Schwartz, N. Seidler, K. Walzer, B. Lüssem, K. Leo, *Nature* **2009**, *459*, 234–238.
- [46] H. Yersin, in *Transit. Met. Rare Earth Compd.*, Springer Berlin Heidelberg, **2004**, pp. 1–26.
- [47] S.-J. Yeh, M.-F. Wu, C.-T. Chen, Y.-H. Song, Y. Chi, M.-H. Ho, S.-F. Hsu, C. H. Chen, *Adv. Mater.* **2005**, *17*, 285–289.
- [48] M.-H. Tsai, H.-W. Lin, H.-C. Su, T.-H. Ke, C. -c. Wu, F.-C. Fang, Y.-L. Liao, K.-T. Wong, C.-I. Wu, *Adv. Mater.* **2006**, *18*, 1216–1220.
- [49] C.-L. Li, Y.-J. Su, Y.-T. Tao, P.-T. Chou, C.-H. Chien, C.-C. Cheng, R.-S. Liu, *Adv. Funct. Mater.* **2005**, *15*, 387–395.
- [50] R. J. Holmes, S. R. Forrest, Y.-J. Tung, R. C. Kwong, J. J. Brown, S. Garon, M. E. Thompson, *Appl. Phys. Lett.* **2003**, *82*, 2422–2424.
- [51] S. Lamansky, P. Djurovich, D. Murphy, F. Abdel-Razzaq, R. Kwong, I. Tsyba, M. Bortz, B. Mui, R. Bau, M. E. Thompson, *Inorg. Chem.* **2001**, *40*, 1704–1711.
- [52] K. H. Kim, J. Y. Lee, T. J. Park, W. S. Jeon, G. P. Kennedy, J. H. Kwon, *Synth. Met.* **2010**, *160*, 631–635.
- [53] B. Geffroy, P. le Roy, C. Prat, *Polym. Int.* **2006**, *55*, 572–582.
- [54] J.-H. Jou, S.-H. Peng, C.-I. Chiang, Y.-L. Chen, Y.-X. Lin, Y.-C. Jou, C.-H. Chen, C.-J. Li, W.-B. Wang, S.-M. Shen, et al., *J. Mater. Chem. C* **2013**, *1*, 1680–1686.
- [55] S. Tokito, T. Iijima, Y. Suzuri, H. Kita, T. Tsuzuki, F. Sato, *Appl. Phys. Lett.* **2003**, *83*, 569–571.
- [56] P. Wang, Z. Xie, S. Tong, O. Wong, C.-S. Lee, N. Wong, L. Hung, S. Lee, *Chem. Mater.* **2003**, *15*, 1913–1917.
- [57] J. Li, D. Liu, Z. Hong, S. Tong, P. Wang, C. Ma, O. Lengyel, C.-S. Lee, H.-L. Kwong, S. Lee, *Chem. Mater.* **2003**, *15*, 1486–1490.
- [58] M. Ikai, S. Tokito, Y. Sakamoto, T. Suzuki, Y. Taga, *Appl. Phys. Lett.* **2001**, *79*, 156–158.

- [59] C. Adachi, M. A. Baldo, M. E. Thompson, S. R. Forrest, *J. Appl. Phys.* **2001**, *90*, 5048–5051.
- [60] A. B. Padmaperuma, L. S. Sapochak, P. E. Burrows, *Chem. Mater.* **2006**, *18*, 2389–2396.
- [61] M.-H. Tsai, T.-H. Ke, H.-W. Lin, C.-C. Wu, S.-F. Chiu, F.-C. Fang, Y.-L. Liao, K.-T. Wong, Y.-H. Chen, C.-I. Wu, *ACS Appl. Mater. Interfaces* **2009**, *1*, 567–574.
- [62] T. Tsuzuki, S. Tokito, *Adv. Mater.* **2007**, *19*, 276–280.
- [63] Z. Q. Gao, M. Luo, X. H. Sun, H. L. Tam, M. S. Wong, B. X. Mi, P. F. Xia, K. W. Cheah, C. H. Chen, *Adv. Mater.* **2009**, *21*, 688–692.
- [64] T. Förster, *Discuss. Faraday Soc.* **1959**, *27*, 7–17.
- [65] D. L. Dexter, *J. Chem. Phys.* **1953**, *21*, 836–850.
- [66] X. Gong, J. c. Ostrowski, D. Moses, G. c. Bazan, A. j. Heeger, *Adv. Funct. Mater.* **2003**, *13*, 439–444.
- [67] H. Yersin, W. J. Finkenzeller, in *Highly Effic. OLEDs Phosphorescent Mater.* (Ed.: H. Yersin), Wiley-VCH Verlag GmbH & Co. KGaA, **2007**, pp. 1–97.
- [68] Y.-L. Liao, C.-Y. Lin, K.-T. Wong, T.-H. Hou, W.-Y. Hung, *Org. Lett.* **2007**, *9*, 4511–4514.
- [69] S. Takizawa, V. A. Montes, P. Anzenbacher, *Chem. Mater.* **2009**, *21*, 2452–2458.
- [70] Y. Tao, Q. Wang, C. Yang, Q. Wang, Z. Zhang, T. Zou, J. Qin, D. Ma, *Angew. Chem.* **2008**, *120*, 8224–8227.
- [71] Z. Ge, T. Hayakawa, S. Ando, M. Ueda, T. Akiike, H. Miyamoto, T. Kajita, M. Kakimoto, *Adv. Funct. Mater.* **2008**, *18*, 584–590.
- [72] M.-Y. Lai, C.-H. Chen, W.-S. Huang, J. T. Lin, T.-H. Ke, L.-Y. Chen, M.-H. Tsai, C.-C. Wu, *Angew. Chem.* **2008**, *120*, 591–595.
- [73] J. H. Kim, D. Y. Yoon, J. W. Kim, J.-J. Kim, *Synth. Met.* **2007**, *157*, 743–750.
- [74] S.-J. Su, H. Sasabe, T. Takeda, J. Kido, *Chem. Mater.* **2008**, *20*, 1691–1693.
- [75] M. M. Rothmann, S. Haneder, E. Da Como, C. Lennartz, C. Schildknecht, P. Strohriegel, *Chem. Mater.* **2010**, *22*, 2403–2410.
- [76] H.-H. Chou, C.-H. Cheng, *Adv. Mater.* **2010**, *22*, 2468–2471.
- [77] M. Leung, C.-C. Yang, J.-H. Lee, H.-H. Tsai, C.-F. Lin, C.-Y. Huang, Y. O. Su, C.-F. Chiu, *Org. Lett.* **2006**, *9*, 235–238.
- [78] H.-F. Chen, S.-J. Yang, Z.-H. Tsai, W.-Y. Hung, T.-C. Wang, K.-T. Wong, *J. Mater. Chem.* **2009**, *19*, 8112–8118.

- [79] Y. Tao, Q. Wang, C. Yang, Q. Wang, Z. Zhang, T. Zou, J. Qin, D. Ma, *Angew. Chem. Int. Ed.* **2008**, *47*, 8104–8107.
- [80] M.-H. Tsai, Y.-H. Hong, C.-H. Chang, H.-C. Su, C.-C. Wu, A. Matoliukstyte, J. Simokaitiene, S. Grigalevicius, J. V. Grazulevicius, C.-P. Hsu, *Adv. Mater.* **2007**, *19*, 862–866.
- [81] C. Adachi, R. C. Kwong, P. Djurovich, V. Adamovich, M. A. Baldo, M. E. Thompson, S. R. Forrest, *Appl. Phys. Lett.* **2001**, *79*, 2082–2084.
- [82] P. Schrögel, A. Tomkevičienė, P. Strohrriegl, S. T. Hoffmann, A. Köhler, C. Lennartz, *J. Mater. Chem.* **2011**, *21*, 2266.
- [83] J. He, H. Liu, Y. Dai, X. Ou, J. Wang, S. Tao, X. Zhang, P. Wang, D. Ma, *J. Phys. Chem. C* **2009**, *113*, 6761–6767.
- [84] K. Brunner, A. van Dijken, H. Börner, J. J. A. M. Bastiaansen, N. M. M. Kiggen, B. M. W. Langeveld, *J. Am. Chem. Soc.* **2004**, *126*, 6035–6042.
- [85] K.-T. Wong, Y.-M. Chen, Y.-T. Lin, H.-C. Su, C. Wu, *Org. Lett.* **2005**, *7*, 5361–5364.
- [86] P.-I. Shih, C.-L. Chiang, A. K. Dixit, C.-K. Chen, M.-C. Yuan, R.-Y. Lee, C.-T. Chen, E. W.-G. Diau, C.-F. Shu, *Org. Lett.* **2006**, *8*, 2799–2802.
- [87] Q. Wang, J. Ding, D. Ma, Y. Cheng, L. Wang, F. Wang, *Adv. Mater.* **2009**, *21*, 2397–2401.
- [88] X. Ren, J. Li, R. J. Holmes, P. I. Djurovich, S. R. Forrest, M. E. Thompson, *Chem. Mater.* **2004**, *16*, 4743–4747.
- [89] T. Tsuboi, S.-W. Liu, M.-F. Wu, C.-T. Chen, *Org. Electron.* **2009**, *10*, 1372–1377.
- [90] J. N. Moorthy, S. Saha, *Eur. J. Org. Chem.* **2009**, *2009*, 739–748.
- [91] M. C. Van Zandt, E. O. Sibley, E. E. McCann, K. J. Combs, B. Flam, D. R. Sawicki, A. Sabetta, A. Carrington, J. Sredy, E. Howard, et al., *Bioorg. Med. Chem.* **2004**, *12*, 5661–5675.
- [92] C. K. Arnatt, Y. Zhang, *Tetrahedron Lett.* **2012**, *53*, 1592–1594.
- [93] D. A. Watson, M. Su, G. Teverovskiy, Y. Zhang, J. García-Fortanet, T. Kinzel, S. L. Buchwald, *Science* **2009**, *325*, 1661–1664.
- [94] R. B. Bedford, M. Betham, *J. Org. Chem.* **2006**, *71*, 9403–9410.
- [95] Y.-C. Chen, G.-S. Huang, C.-C. Hsiao, S.-A. Chen, *J. Am. Chem. Soc.* **2006**, *128*, 8549–8558.
- [96] M. Kozaki, K. Okada, *Org. Lett.* **2004**, *6*, 485–488.

- [97] C. Sambigiato, S. P. Marsden, A. J. Blacker, P. C. McGowan, *Chem. Soc. Rev.* **2014**, *43*, 3525–3550.
- [98] G. Zyryanov, I. Kovalev, I. Egorov, V. Rusinov, O. Chupakhin, *Chem. Heterocycl. Compd.* **2011**, *47*, 571–574.
- [99] Q. Wu, L. Wang, *Synthesis* **2008**, *2008*, 2007–2012.
- [100] A. Krasovskiy, P. Knochel, *Angew. Chem. Int. Ed.* **2004**, *43*, 3333–3336.
- [101] M. Maji, A. Studer, *Synthesis* **2009**, *2009*, 2467–2470.
- [102] G. E. Carr, R. D. Chambers, T. F. Holmes, D. G. Parker, *J. Chem. Soc. [Perkin 1]* **1988**, 921–926.
- [103] M. M. Kremlev, A. I. Mushta, W. Tyrre, Y. L. Yagupolskii, D. Naumann, A. Möller, *J. Fluor. Chem.* **2012**, *133*, 67–71.
- [104] W. C. P. Tsang, R. H. Munday, G. Brasche, N. Zheng, S. L. Buchwald, *J. Org. Chem.* **2008**, *73*, 7603–7610.
- [105] B. A. Kamino, B. Mills, C. Reali, M. J. Gretton, M. A. Brook, T. P. Bender, *J. Org. Chem.* **2012**, *77*, 1663–1674.
- [106] E. Krasnokutskaya, N. Semenischeva, V. Filimonov, P. Knochel, *Synthesis* **2007**, *2007*, 81–84.
- [107] C.-Y. Liu, A. Gavryushin, P. Knochel, *Chem. – Asian J.* **2007**, *2*, 1020–1030.
- [108] P. J. Low, M. A. J. Paterson, D. S. Yufit, J. A. K. Howard, J. C. Cherryman, D. R. Tackley, R. Brook, B. Brown, *J. Mater. Chem.* **2005**, *15*, 2304–2315.
- [109] P. Schrögel, N. Langer, C. Schildknecht, G. Wagenblast, C. Lennartz, P. Strohhriegl, *Org. Electron.* **2011**, *12*, 2047–2055.
- [110] M.-H. Tsai, Y.-H. Hong, C.-H. Chang, H.-C. Su, C.-C. Wu, A. Matoliukstyte, J. Simokaitiene, S. Grigalevicius, J. V. Grazulevicius, C.-P. Hsu, *Adv. Mater.* **2007**, *19*, 862–866.
- [111] J. He, H. Liu, Y. Dai, X. Ou, J. Wang, S. Tao, X. Zhang, P. Wang, D. Ma, *J. Phys. Chem. C* **2009**, *113*, 6761–6767.
- [112] R. J. Holmes, S. R. Forrest, Y.-J. Tung, R. C. Kwong, J. J. Brown, S. Garon, M. E. Thompson, *Appl. Phys. Lett.* **2003**, *82*, 2422–2424.
- [113] S. M. Bonesi, R. Erra-Balsells, *J. Lumin.* **2001**, *93*, 51–74.
- [114] S. Gong, X. He, Y. Chen, Z. Jiang, C. Zhong, D. Ma, J. Qin, C. Yang, *J. Mater. Chem.* **2012**, *22*, 2894.

- [115] L. Deng, X. Wang, Z. Zhang, J. Li, *J. Mater. Chem.* **2012**, *22*, 19700–19708.
- [116] J.-F. Morin, M. Leclerc, *Macromolecules* **2001**, *34*, 4680–4682.
- [117] Y. Zheng, A. S. Batsanov, V. Jankus, F. B. Dias, M. R. Bryce, A. P. Monkman, *J. Org. Chem.* **2011**, *76*, 8300–8310.
- [118] G. W. Haggquist, H. Katayama, A. Tsuchida, S. Ito, M. Yamamoto, *J. Phys. Chem.* **1993**, *97*, 9270–9273.
- [119] P. J. S. Gomes, C. Serpa, L. G. Arnaut, *J. Photochem. Photobiol. Chem.* **2006**, *184*, 228–233.
- [120] C. M. Cardona, W. Li, A. E. Kaifer, D. Stockdale, G. C. Bazan, *Adv. Mater.* **2011**, *23*, 2367–2371.
- [121] J. F. Ambrose, R. F. Nelson, *J. Electrochem. Soc.* **1968**, *115*, 1159–1164.
- [122] A. Ulman, *Chem. Rev.* **1996**, *96*, 1533–1554.
- [123] N. K. Chaki, K. Vijayamohanan, *Biosens. Bioelectron.* **2002**, *17*, 1–12.
- [124] J. C. Love, L. A. Estroff, J. K. Kriebel, R. G. Nuzzo, G. M. Whitesides, *Chem. Rev.* **2005**, *105*, 1103–1170.
- [125] L. H. Dubois, R. G. Nuzzo, *Annu. Rev. Phys. Chem.* **1992**, *43*, 437–463.
- [126] C. D. Bain, G. M. Whitesides, *Angew. Chem. Int. Ed. Engl.* **1989**, *28*, 506–512.
- [127] A. M. Becka, C. J. Miller, *J. Phys. Chem.* **1993**, *97*, 6233–6239.
- [128] D. L. Feldheim, C. D. Keating, *Chem. Soc. Rev.* **1998**, *27*, 1–12.
- [129] C. Duan, M. E. Meyerhoff, *Anal. Chem.* **1994**, *66*, 1369–1377.
- [130] I. Rubinstein, S. Steinberg, Y. Tor, A. Shanzer, J. Sagiv, *Nature* **1988**, *332*, 426–429.
- [131] C. D. Bain, G. M. Whitesides, *J. Am. Chem. Soc.* **1988**, *110*, 5897–5898.
- [132] P. E. Laibinis, G. M. Whitesides, *J. Am. Chem. Soc.* **1992**, *114*, 9022–9028.
- [133] T. Wink, S. J. van Zuilen, A. Bult, W. P. van Bennekom, *Analyst* **1997**, *122*, 43R–50R.
- [134] M. P. Byfield, R. A. Abuknesha, *Biosens. Bioelectron.* **1994**, *9*, 373–399.
- [135] M. French, S. E. Creager, *Langmuir* **1998**, *14*, 2129–2133.
- [136] K. Bandyopadhyay, M. Sastry, V. Paul, K. Vijayamohanan, *Langmuir* **1997**, *13*, 866–869.
- [137] Y. R. Leroux, H. Fei, J.-M. Noël, C. Roux, P. Hapiot, *J. Am. Chem. Soc.* **2010**, *132*, 14039–14041.
- [138] K. Bandyopadhyay, K. Vijayamohanan, *Langmuir* **1998**, *14*, 625–629.

- [139] M. D. Porter, T. B. Bright, D. L. Allara, C. E. D. Chidsey, *J. Am. Chem. Soc.* **1987**, *109*, 3559–3568.
- [140] M.-C. Bourg, A. Badia, R. B. Lennox, *J. Phys. Chem. B* **2000**, *104*, 6562–6567.
- [141] D. G. Castner, K. Hinds, D. W. Grainger, *Langmuir* **1996**, *12*, 5083–5086.
- [142] R. G. Nuzzo, L. H. Dubois, D. L. Allara, *J. Am. Chem. Soc.* **1990**, *112*, 558–569.
- [143] G. E. Poirier, *Chem. Rev.* **1997**, *97*, 1117–1128.
- [144] L. C. Giancarlo and, G. W. Flynn, *Annu. Rev. Phys. Chem.* **1998**, *49*, 297–336.
- [145] J. Sagiv, *J. Am. Chem. Soc.* **1980**, *102*, 92–98.
- [146] P. Silberzan, L. Leger, D. Ausserre, J. J. Benattar, *Langmuir* **1991**, *7*, 1647–1651.
- [147] S. R. Wasserman, Y. T. Tao, G. M. Whitesides, *Langmuir* **1989**, *5*, 1074–1087.
- [148] J. D. Le Grange, J. L. Markham, C. R. Kurkjian, *Langmuir* **1993**, *9*, 1749–1753.
- [149] R. Maoz, J. Sagiv, *J. Colloid Interface Sci.* **1984**, *100*, 465–496.
- [150] J. Gun, R. Iscovici, J. Sagiv, *J. Colloid Interface Sci.* **1984**, *101*, 201–213.
- [151] N. Tillman, A. Ulman, J. S. Schildkraut, T. L. Penner, *J. Am. Chem. Soc.* **1988**, *110*, 6136–6144.
- [152] S. Brandriss, S. Margel, *Langmuir* **1993**, *9*, 1232–1240.
- [153] K. Mathauer, C. W. Frank, *Langmuir* **1993**, *9*, 3446–3451.
- [154] J. Gun, J. Sagiv, *J. Colloid Interface Sci.* **1986**, *112*, 457–472.
- [155] G. E. Poirier, E. D. Pylant, *Science* **1996**, *272*, 1145–1148.
- [156] P. Fenter, P. Eisenberger, J. Li, N. Camillone, S. Bernasek, G. Scoles, T. A. Ramanarayanan, K. S. Liang, *Langmuir* **1991**, *7*, 2013–2016.
- [157] C. D. Bain, G. M. Whitesides, *J. Am. Chem. Soc.* **1988**, *110*, 3665–3666.
- [158] J. Hautman, M. L. Klein, *J. Chem. Phys.* **1990**, *93*, 7483–7492.
- [159] M. A. Bryant, J. E. Pemberton, *J. Am. Chem. Soc.* **1991**, *113*, 8284–8293.
- [160] H. O. Finklea, M. S. Ravenscroft, D. A. Snider, *Langmuir* **1993**, *9*, 223–227.
- [161] E. B. Troughton, C. D. Bain, G. M. Whitesides, R. G. Nuzzo, D. L. Allara, M. D. Porter, *Langmuir* **1988**, *4*, 365–385.
- [162] E. Katz, N. Itzhak, I. Willner, *J. Electroanal. Chem.* **1992**, *336*, 357–362.
- [163] R. G. Nuzzo, D. L. Allara, *J. Am. Chem. Soc.* **1983**, *105*, 4481–4483.
- [164] M. A. Bryant, S. L. Joa, J. E. Pemberton, *Langmuir* **1992**, *8*, 753–756.
- [165] E. Sabatani, J. Cohen-Boulakia, M. Bruening, I. Rubinstein, *Langmuir* **1993**, *9*, 2974–2981.

- [166] T. T. T. Li, H. Y. Liu, M. J. Weaver, *J. Am. Chem. Soc.* **1984**, *106*, 1233–1239.
- [167] J. A. Mielczarski, R. H. Yoon, *Langmuir* **1991**, *7*, 101–108.
- [168] C. Vericat, M. E. Vela, G. Benitez, P. Carro, R. C. Salvarezza, *Chem. Soc. Rev.* **2010**, *39*, 1805.
- [169] M. A. D. Millone, H. Hamoudi, L. Rodríguez, A. Rubert, G. A. Benítez, M. E. Vela, R. C. Salvarezza, J. E. Gayone, E. A. Sánchez, O. Grizzi, et al., *Langmuir* **2009**, *25*, 12945–12953.
- [170] C. D. Bain, E. B. Troughton, Y. T. Tao, J. Evall, G. M. Whitesides, R. G. Nuzzo, *J. Am. Chem. Soc.* **1989**, *111*, 321–335.
- [171] R. Yamada, K. Uosaki, *Langmuir* **1998**, *14*, 855–861.
- [172] S. Xu, S. J. N. Cruchon-Dupeyrat, J. C. Garno, G.-Y. Liu, G. K. Jennings, T.-H. Yong, P. E. Laibinis, *J. Chem. Phys.* **1998**, *108*, 5002–5012.
- [173] F. Schreiber, A. Eberhardt, T. Y. B. Leung, P. Schwartz, S. M. Wetterer, D. J. Lavrich, L. Berman, P. Fenter, P. Eisenberger, G. Scoles, *Phys. Rev. B* **1998**, *57*, 12476–12481.
- [174] P. Maksymovych, D. C. Sorescu, J. T. Yates, *Phys. Rev. Lett.* **2006**, *97*, 146103.
- [175] R. C. Thomas, L. Sun, R. M. Crooks, A. J. Ricco, *Langmuir* **1991**, *7*, 620–622.
- [176] O. Chailapakul, L. Sun, C. Xu, R. M. Crooks, *J. Am. Chem. Soc.* **1993**, *115*, 12459–12467.
- [177] L. Kankate, A. Turchanin, A. Götzhäuser, *Langmuir* **2009**, *25*, 10435–10438.
- [178] P. G. Lustemberg, M. L. Martiarena, A. E. Martínez, H. F. Busnengo, *Langmuir* **2008**, *24*, 3274–3279.
- [179] J. B. Schlenoff, M. Li, H. Ly, *J. Am. Chem. Soc.* **1995**, *117*, 12528–12536.
- [180] H. A. Biebuyck, C. D. Bain, G. M. Whitesides, *Langmuir* **1994**, *10*, 1825–1831.
- [181] R. G. Nuzzo, B. R. Zegarski, L. H. Dubois, *J. Am. Chem. Soc.* **1987**, *109*, 733–740.
- [182] X. Torrelles, E. Barrena, C. Munuera, J. Rius, S. Ferrer, C. Ocal, *Langmuir* **2004**, *20*, 9396–9402.
- [183] P. E. Laibinis, G. M. Whitesides, D. L. Allara, Y. T. Tao, A. N. Parikh, R. G. Nuzzo, *J. Am. Chem. Soc.* **1991**, *113*, 7152–7167.
- [184] M. H. Schoenfish, J. E. Pemberton, *J. Am. Chem. Soc.* **1998**, *120*, 4502–4513.
- [185] A. B. Horn, D. A. Russell, L. J. Shorthouse, T. R. E. Simpson, *J. Chem. Soc. Faraday Trans.* **1996**, *92*, 4759–4762.
- [186] E. Delamarche, B. Michel, H. Kang, C. Gerber, *Langmuir* **1994**, *10*, 4103–4108.

- [187] A. Laforgue, T. Addou, D. Bélanger, *Langmuir* **2005**, *21*, 6855–6865.
- [188] S. Park, R. S. Ruoff, *Nat. Nanotechnol.* **2009**, *4*, 217–224.
- [189] A. K. Geim, K. S. Novoselov, *Nat. Mater.* **2007**, *6*, 183–191.
- [190] A. A. Balandin, S. Ghosh, W. Bao, I. Calizo, D. Teweldebrhan, F. Miao, C. N. Lau, *Nano Lett.* **2008**, *8*, 902–907.
- [191] R. F. Service, *Science* **2009**, *324*, 875–877.
- [192] J. Hass, W. A. de Heer, E. H. Conrad, *J. Phys. Condens. Matter* **2008**, *20*, 323202.
- [193] C. Lee, X. Wei, J. W. Kysar, J. Hone, *Science* **2008**, *321*, 385–388.
- [194] X. Fan, W. Peng, Y. Li, X. Li, S. Wang, G. Zhang, F. Zhang, *Adv. Mater.* **2008**, *20*, 4490–4493.
- [195] D. Li, M. B. Müller, S. Gilje, R. B. Kaner, G. G. Wallace, *Nat. Nanotechnol.* **2008**, *3*, 101–105.
- [196] S. Gilje, S. Han, M. Wang, K. L. Wang, R. B. Kaner, *Nano Lett.* **2007**, *7*, 3394–3398.
- [197] S. Stankovich, D. A. Dikin, R. D. Piner, K. A. Kohlhaas, A. Kleinhammes, Y. Jia, Y. Wu, S. T. Nguyen, R. S. Ruoff, *Carbon* **2007**, *45*, 1558–1565.
- [198] H. C. Schniepp, J.-L. Li, M. J. McAllister, H. Sai, M. Herrera-Alonso, D. H. Adamson, R. K. Prud'homme, R. Car, D. A. Saville, I. A. Aksay, *J. Phys. Chem. B* **2006**, *110*, 8535–8539.
- [199] R. L. McCreery, *Chem. Rev.* **2008**, *108*, 2646–2687.
- [200] J. Wang, *Electroanalysis* **2005**, *17*, 7–14.
- [201] S. N. Kim, J. F. Rusling, F. Papadimitrakopoulos, *Adv. Mater.* **2007**, *19*, 3214–3228.
- [202] K. Balasubramanian, M. Burghard, *Anal. Bioanal. Chem.* **2006**, *385*, 452–468.
- [203] Q. Zhao, Z. Gan, Q. Zhuang, *Electroanalysis* **2002**, *14*, 1609–1613.
- [204] J. Wang, M. Musameh, Y. Lin, *J. Am. Chem. Soc.* **2003**, *125*, 2408–2409.
- [205] F. L. Floch, G. Bidan, L. Pilan, E.-M. Ungureanu, J.-P. Simonato, *Mol. Cryst. Liq. Cryst.* **2008**, *486*, 271/[1313]–281/[1323].
- [206] J. B. Donnet, P. Ehrburger, *Carbon* **1977**, *15*, 143–152.
- [207] M. Delamar, R. Hitmi, J. Pinson, J. M. Saveant, *J. Am. Chem. Soc.* **1992**, *114*, 5883–5884.
- [208] W. P. Hoffman, W. C. Hurley, T. W. Owens, H. T. Phan, *J. Mater. Sci.* **1991**, *26*, 4545–4553.
- [209] E. Fitzer, R. Weiss, *Carbon* **1987**, *25*, 455–467.

- [210] P. Allongue, M. Delamar, B. Desbat, O. Fagebaume, R. Hitmi, J. Pinson, J.-M. Savéant, *J. Am. Chem. Soc.* **1997**, *119*, 201–207.
- [211] A. Adenier, M.-C. Bernard, M. M. Chehimi, E. Cabet-Deliry, B. Desbat, O. Fagebaume, J. Pinson, F. Podvorica, *J. Am. Chem. Soc.* **2001**, *123*, 4541–4549.
- [212] C. H. de Villeneuve, J. Pinson, M. C. Bernard, P. Allongue, *J. Phys. Chem. B* **1997**, *101*, 2415–2420.
- [213] M. Raicopol, L. Necula, M. Ionita, L. Pilan, *Surf. Interface Anal.* **2012**, *44*, 1081–1085.
- [214] C. A. Dyke, J. M. Tour, *Nano Lett.* **2003**, *3*, 1215–1218.
- [215] M. Delamar, G. Désarmot, O. Fagebaume, R. Hitmi, J. Pinson, J.-M. Savéant, *Carbon* **1997**, *35*, 801–807.
- [216] Y.-C. Liu, R. L. McCreery, *J. Am. Chem. Soc.* **1995**, *117*, 11254–11259.
- [217] J. K. Kariuki, M. T. McDermott, *Langmuir* **2001**, *17*, 5947–5951.
- [218] F. Anariba, S. H. DuVall, R. L. McCreery, *Anal. Chem.* **2003**, *75*, 3837–3844.
- [219] C. Combellas, F. Kanoufi, D. Mazouzi, A. Thiébault, P. Bertrand, N. Médard, *Polymer* **2003**, *44*, 19–24.
- [220] M. P. Stewart, F. Maya, D. V. Kosynkin, S. M. Dirk, J. J. Stapleton, C. L. McGuinness, D. L. Allara, J. M. Tour, *J. Am. Chem. Soc.* **2003**, *126*, 370–378.
- [221] P. Allongue, C. Henry de Villeneuve, G. Cherouvrier, R. Cortès, M.-C. Bernard, *J. Electroanal. Chem.* **2003**, *550–551*, 161–174.
- [222] M.-C. Bernard, A. Chaussé, E. Cabet-Deliry, M. M. Chehimi, J. Pinson, F. Podvorica, C. Vautrin-UI, *Chem. Mater.* **2003**, *15*, 3450–3462.
- [223] B. L. Hurley, R. L. McCreery, *J. Electrochem. Soc.* **2004**, *151*, B252–B259.
- [224] S. Griveau, D. Mercier, C. Vautrin-UI, A. Chaussé, *Electrochem. Commun.* **2007**, *9*, 2768–2773.
- [225] C. P. Andrieux, J. Pinson, *J. Am. Chem. Soc.* **2003**, *125*, 14801–14806.
- [226] J.-M. Savéant, in (Ed.: B.-A. in P.O. Chemistry), Academic Press, **2000**, pp. 117–192.
- [227] J. M. Savéant, A. Thiébault, *J. Electroanal. Chem. Interfacial Electrochem.* **1978**, *89*, 335–346.
- [228] R. A. Rossi, A. B. Pierini, A. B. Peñéñory, *Chem. Rev.* **2002**, *103*, 71–168.
- [229] A. Chaussé, M. M. Chehimi, N. Karsi, J. Pinson, F. Podvorica, C. Vautrin-UI, *Chem. Mater.* **2001**, *14*, 392–400.
- [230] K. Boukerma, M. M. Chehimi, J. Pinson, C. Blomfield, *Langmuir* **2003**, *19*, 6333–6335.

- [231] E. Coulon, J. Pinson, J.-D. Bourzat, A. Commerçon, J.-P. Pulicani, *J. Org. Chem.* **2002**, *67*, 8513–8518.
- [232] V. D. Parker, M. Tilset, O. Hammerich, *J. Am. Chem. Soc.* **1987**, *109*, 7905–7906.
- [233] P. A. Brooksby, A. J. Downard, *Langmuir* **2004**, *20*, 5038–5045.
- [234] R. A. Nyquist, Ed. , in *Interpret. Infrared Raman Nucl. Magn. Reson. Spectra*, Academic Press, San Diego, **2001**, pp. 173–230.
- [235] R. A. Nyquist, Ed. , in *Interpret. Infrared Raman Nucl. Magn. Reson. Spectra*, Academic Press, San Diego, **2001**, pp. 351–423.
- [236] C. Saby, B. Ortiz, G. Y. Champagne, D. Bélanger, *Langmuir* **1997**, *13*, 6805–6813.
- [237] V. V. Rostovtsev, L. G. Green, V. V. Fokin, K. B. Sharpless, *Angew. Chem. Int. Ed.* **2002**, *41*, 2596–2599.
- [238] J. Pinson, F. Podvorica, *Chem. Soc. Rev.* **2005**, *34*, 429–439.
- [239] M. D'Amour, D. Bélanger, *J. Phys. Chem. B* **2003**, *107*, 4811–4817.
- [240] G. Liu, T. Böcking, J. J. Gooding, *J. Electroanal. Chem.* **2007**, *600*, 335–344.
- [241] R. Blankespoor, B. Limoges, B. Schöllhorn, J.-L. Syssa-Magalé, D. Yazidi, *Langmuir* **2005**, *21*, 3362–3375.
- [242] D. Evrard, F. Lambert, C. Policar, V. Balland, B. Limoges, *Chem. – Eur. J.* **2008**, *14*, 9286–9291.
- [243] Liu, J. J. Gooding, *Langmuir* **2006**, *22*, 7421–7430.
- [244] B. P. Corgier, C. A. Marquette, L. J. Blum, *J. Am. Chem. Soc.* **2005**, *127*, 18328–18332.
- [245] B. P. Corgier, C. A. Marquette, L. J. Blum, *Biosens. Bioelectron.* **2007**, *22*, 1522–1526.
- [246] X. T. Le, P. Viel, P. Jégou, A. Sorin, S. Palacin, *Sep. Purif. Technol.* **2009**, *69*, 135–140.
- [247] V. G. Mairanovsky, *Angew. Chem. Int. Ed. Engl.* **1976**, *15*, 281–292.
- [248] S. M. Weinreb, G. A. Epling, R. Comi, M. Reitano, *J. Org. Chem.* **1975**, *40*, 1356–1358.
- [249] K. Lam, I. E. Markó, *Org. Lett.* **2009**, *11*, 2752–2755.
- [250] M. Platen, E. Stekhan, *Tetrahedron Lett.* **1980**, *21*, 511–514.
- [251] W. S. Yeo, M. Mrksich, *Adv. Mater.* **2004**, *16*, 1352–1356.
- [252] K. Kim, H. Yang, E. Kim, Y. B. Han, Y. T. Kim, S. H. Kang, J. Kwak, *Langmuir* **2002**, *18*, 1460–1462.
- [253] R. C. Roemmele, H. Rapoport, *J. Org. Chem.* **1988**, *53*, 2367–2371.
- [254] C. Goulaouic-Dubois, A. Guggisberg, M. Hesse, *J. Org. Chem.* **1995**, *60*, 5969–5972.
- [255] J. Engels, *Angew. Chem. Int. Ed. Engl.* **1979**, *18*, 148–149.

- [256] K. Maurer, A. McShea, M. Strathmann, K. Dill, *J. Comb. Chem.* **2005**, *7*, 637–640.
- [257] H. Li, F. Cheng, A. M. Duft, A. Adronov, *J. Am. Chem. Soc.* **2005**, *127*, 14518–14524.
- [258] S. Mahouche Chergui, A. Ledebt, F. Mammeri, F. Herbst, B. Carbonnier, H. Ben Romdhane, M. Delamar, M. M. Chehimi, *Langmuir* **2010**, *26*, 16115–16121.
- [259] N. M. Jenny, M. Mayor, T. R. Eaton, *Eur. J. Org. Chem.* **2011**, *2011*, 4965–4983.
- [260] C. Cai, A. Vasella, *Helv. Chim. Acta* **1995**, *78*, 732–757.
- [261] L. A. Carpino, S. A. Triolo, R. A. Berglund, *J. Org. Chem.* **1989**, *54*, 3303–3310.
- [262] S. Takahashi, Y. Kuroyama, K. Sonogashira, N. Hagihara, *Synthesis* **1980**, *1980*, 627–630.
- [263] R. Eastmond, D. R. M. Walton, *Tetrahedron* **1972**, *28*, 4591–4599.
- [264] W. E. Davidsohn, M. C. Henry, *Chem. Rev.* **1967**, *67*, 73–106.
- [265] F. Diederich, Y. Rubin, O. L. Chapman, N. S. Goroff, *Helv. Chim. Acta* **1994**, *77*, 1441–1457.
- [266] S. Höger, K. Bonrad, *J. Org. Chem.* **2000**, *65*, 2243–2245.
- [267] S. J. Havens, P. M. Hergenrother, *J. Org. Chem.* **1985**, *50*, 1763–1765.
- [268] P. S. Guin, S. Das, P. C. Mandal, *Int. J. Electrochem.* **2011**, *2011*, e816202.
- [269] C. Frontana, Á. Vázquez-Mayagoitia, J. Garza, R. Vargas, I. González, *J. Phys. Chem. A* **2006**, *110*, 9411–9419.
- [270] C. C. Nawrat, C. J. Moody, *Angew. Chem. Int. Ed.* **2014**, *53*, 2056–2077.
- [271] B. D. Mather, K. Viswanathan, K. M. Miller, T. E. Long, *Prog. Polym. Sci.* **2006**, *31*, 487–531.
- [272] M. H. Vilhelmsen, J. Jensen, C. G. Tortzen, M. B. Nielsen, *Eur. J. Org. Chem.* **2013**, *2013*, 701–711.
- [273] V. Prezhdo, O. Prezhdo, E. Ovsiankina, *Spectrochim. Acta. A. Mol. Biomol. Spectrosc.* **1995**, *51*, 2465–2472.
- [274] R. L. Nyland, M. Luo, M. R. Kelley, R. F. Borch, *J. Med. Chem.* **2010**, *53*, 1200–1210.
- [275] N. Van Tuyen, B. Kesteleyn, N. De Kimpe, *Tetrahedron* **2002**, *58*, 121–127.
- [276] A. P. Kozikowski, K. Sugiyama, J. P. Springer, *J. Org. Chem.* **1981**, *46*, 2426–2428.
- [277] P. Bovicelli, G. Borioni, D. Fabbrini, M. Barontini, *Synth. Commun.* **2008**, *38*, 391–400.
- [278] A. Pelter, S. Elgendy, *Tetrahedron Lett.* **1988**, *29*, 677–680.
- [279] P. Jacob, P. S. Callery, A. T. Shulgin, N. Castagnoli, *J. Org. Chem.* **1976**, *41*, 3627–3629.
- [280] A. P. Kostikov, N. Malashikhina, V. V. Popik, *J. Org. Chem.* **2009**, *74*, 1802–1804.

- [281] A. Tomatsu, S. Takemura, K. Hashimoto, M. Nakata, *Synlett* **1999**, 1999, 1474–1476.
- [282] J.-L. Shi, X. Chen, X.-K. Jiang, *J. Org. Chem.* **1996**, 61, 4698–4702.
- [283] D. W. Kim, H. Y. Choi, K.-J. Lee, D. Y. Chi, *Org. Lett.* **2001**, 3, 445–447.
- [284] M. Hashmat Ali, M. Niedbalski, G. Bohnert, D. Bryant, *Synth. Commun.* **2006**, 36, 1751–1759.
- [285] S. G. Mayhew, *Eur. J. Biochem.* **1978**, 85, 535–547.
- [286] X.-K. Jiang, G.-Z. Ji, D. Z.-R. Wang, J. R.-Y. Xie, *J. Phys. Org. Chem.* **1995**, 8, 781–790.
- [287] N. Gupta, H. Linschitz, *J. Am. Chem. Soc.* **1997**, 119, 6384–6391.
- [288] Z. Li, W. Zhao, Y. Zhang, L. Zhang, M. Yu, J. Liu, H. Zhang, *Tetrahedron* **2011**, 67, 7096–7100.
- [289] V. Prautzsch, S. Ibach, *J. Incl. Phenom. Macrocycl. Chem.* **1999**, 33, 427–458.
- [290] P. E. Eaton, T. W. Cole, *J. Am. Chem. Soc.* **1964**, 86, 962–964.
- [291] P. E. Eaton, *Angew. Chem.* **1992**, 104, 1447–1462.
- [292] H. W. Kroto, J. R. Heath, S. C. O'Brien, R. F. Curl, R. E. Smalley, *Nature* **1985**, 318, 162–163.
- [293] W. Krätschmer, L. D. Lamb, K. Fostiropoulos, D. R. Huffman, *Nature* **1990**, 347, 354–358.
- [294] H. W. Kroto, D. R. M. Walton, Eds. , *The Fullerenes: New Horizons for the Chemistry, Physics and Astrophysics of Carbon*, Cambridge University Press, Cambridge, **1993**.
- [295] rer nat A. Hirsch, Ed. , in *Chem. Fuller.*, Wiley-VCH Verlag GmbH, **1994**, pp. 1–36.
- [296] K. E. Geckeler, S. Samal, *Polym. Int.* **1999**, 48, 743–757.
- [297] S. Glenis, S. Cooke, X. Chen, M. M. Labes, *Chem. Mater.* **1996**, 8, 123–127.
- [298] Q. Xie, E. Perez-Cordero, L. Echegoyen, *J. Am. Chem. Soc.* **1992**, 114, 3978–3980.
- [299] Y. Rubin, S. Khan, D. I. Freedberg, C. Yeretian, *J. Am. Chem. Soc.* **1993**, 115, 344–345.
- [300] R. Partha, J. L. Conyers, *Int. J. Nanomedicine* **2009**, 4, 261–275.
- [301] T. Hino, Y. Ogawa, N. Kuramoto, *Carbon* **2006**, 44, 880–887.
- [302] F. Song, S. Zhang, D. Bonifazi, O. Enger, F. Diederich, L. Echegoyen, *Langmuir* **2005**, 21, 9246–9250.
- [303] Q. Liu, Q. Cui, X. J. Li, L. Jin, *Connect. Tissue Res.* **2014**, 55, 71–79.
- [304] A. Hirsch, B. Nuber, *Acc. Chem. Res.* **1999**, 32, 795–804.

- [305] J. C. Hummelen, C. Bellavia-Lund, F. Wudl, in *Fuller. Relat. Struct.* (Ed.: P.D.A. Hirsch), Springer Berlin Heidelberg, **1999**, pp. 93–134.
- [306] T. Guo, C. Jin, R. E. Smalley, *J. Phys. Chem.* **1991**, *95*, 4948–4950.
- [307] X. Xia, D. A. Jelski, J. R. Bowser, T. F. George, *J. Am. Chem. Soc.* **1992**, *114*, 6493–6496.
- [308] O. Vostrowsky, A. Hirsch, *Chem. Rev.* **2006**, *106*, 5191–5207.
- [309] J. C. Hummelen, B. Knight, J. Pavlovich, R. González, F. Wudl, *Science* **1995**, *269*, 1554–1556.
- [310] B. Nuber, A. Hirsch, *Chem. Commun.* **1996**, 1421–1422.
- [311] H. Sharma, I. Garg, K. Dharamvir, V. K. Jindal, *J. Phys. Chem. A* **2009**, *113*, 9002–9013.
- [312] R.-H. Xie, G. W. Bryant, G. Sun, T. Kar, Z. Chen, V. H. Smith, Y. Araki, N. Tagmatarchis, H. Shinohara, O. Ito, *Phys. Rev. B* **2004**, *69*, 201403.
- [313] R.-H. Xie, G. W. Bryant, J. Zhao, V. H. Smith, A. Di Carlo, A. Pecchia, *Phys. Rev. Lett.* **2003**, *90*, 206602.
- [314] F. Gao, G.-L. Zhao, S. Yang, J. J. Spivey, *J. Am. Chem. Soc.* **2013**, *135*, 3315–3318.
- [315] H. Jiao, Z. Chen, A. Hirsch, W. Thiel, *Phys. Chem. Chem. Phys.* **2002**, *4*, 4916–4920.
- [316] R. Zhang, T. Futagoishi, M. Murata, A. Wakamiya, Y. Murata, *J. Am. Chem. Soc.* **2014**, *136*, 8193–8196.
- [317] G. C. Vougioukalakis, M. M. Roubelakis, M. Orfanopoulos, *Chem Soc Rev* **2010**, *39*, 817–844.
- [318] A. P. West, D. Van Engen, R. A. Pascal, *J. Am. Chem. Soc.* **1989**, *111*, 6846–6847.
- [319] R. S. Ross, P. Pincus, F. Wudl, *J. Phys. Chem.* **1992**, *96*, 6169–6172.
- [320] L. R. MacGillivray, J. L. Atwood, *Angew. Chem. Int. Ed.* **1999**, *38*, 1018–1033.
- [321] C. Krüger, S. Agarwal, A. Greiner, *J. Am. Chem. Soc.* **2008**, *130*, 2710–2711.
- [322] A. Błaszczuk, M. Elbing, M. Mayor, *Org. Biomol. Chem.* **2004**, *2*, 2722–2724.
- [323] Y. Tobe, N. Utsumi, K. Kawabata, A. Nagano, K. Adachi, S. Araki, M. Sonoda, K. Hirose, K. Naemura, *J. Am. Chem. Soc.* **2002**, *124*, 5350–5364.
- [324] F. W. Wassmundt, W. F. Kiesman, *J. Org. Chem.* **1995**, *60*, 1713–1719.
- [325] B. Robillard, L. Hughes, M. Slaby, D. A. Lindsay, K. U. Ingold, *J. Org. Chem.* **1986**, *51*, 1700–1704.
- [326] N. Park, K. Park, M. Jang, S. Lee, *J. Org. Chem.* **2011**, *76*, 4371–4378.
- [327] Y. Shirai, L. Cheng, B. Chen, J. M. Tour, *J. Am. Chem. Soc.* **2006**, *128*, 13479–13489.
- [328] A. Klapars, S. L. Buchwald, *J. Am. Chem. Soc.* **2002**, *124*, 14844–14845.

- [329] C.-N. Hsiao, H. Shechter, *Tetrahedron Lett.* **1982**, *23*, 1963–1966.
- [330] M. M. Lakouraj, B. Movassagh, Z. Fadaei, *Monatshefte Für Chem. Chem. Mon.* **2002**, *133*, 1085–1088.
- [331] K. Rößler, T. Ruffer, B. Walfort, R. Packheiser, R. Holze, M. Zharnikov, H. Lang, *J. Organomet. Chem.* **2007**, *692*, 1530–1545.
- [332] A. L. Schwan, D. Brillon, R. Dufault, *Can. J. Chem.* **1994**, *72*, 325–333.

Appendix

Abbreviations

2D	2-Dimensional space
3D	3-Dimensional space
Å	Angstrom
A	Ampere
Ac	Acetyl
AIBN	Azobisisobutyronitrile
ALD	atomic layer deposition
Alq ₃	Tris(8-hydroxyquinolinato)aluminium
AEBD	(4-aminoethyl)benzenediazonium
AFM	Atomic force microscopy
aq.	Aqueous
BCP	2,9-Dimethyl-4,7-diphenyl-1,10-phenanthroline
br	broad (NMR)
^t Bu-TAZ	3-(Biphenyl-4-yl)-5-(4- <i>tert</i> -butylphenyl)-4-phenyl-4 <i>H</i> -1,2,4-triazole
calcd.	Calculated
°C	Celsius
CAN	Ceric ammonium nitrate
CBP	4,4'-Bis(<i>N</i> -carbazolyl)-1,1'-biphenyl
cd	Candela
CV	Cyclic voltammetry
δ	Delta; chemical shift in ppm (NMR)
d	doublet (NMR)
DCM	Dichloromethane
DART	Direct analysis in real time
DFT	Density functional theory
DMA	<i>N,N</i> -Dimethylacetamide
DMI	1,3-Dimethyl-2-imidazolidinone
DMF	<i>N,N</i> -Dimethylformamide
DMSO	Dimethyl sulfoxide
DNA	Deoxyribonucleic acid
dppf	1,1'-Bis(diphenylphosphino)ferrocene
DPV	Differential Pulse Voltammetry
DSC	Differential scanning calorimetry
ε	molar extinction coefficient
e ⁻	Electron
E _g	Optical energy band gap
E ^o	Electrochemical potential

E_T	Triplet energy
EDTA	Ethylenediaminetetraacetic acid
EML	Emission layer
ESI	Electrospray ionization
ETL	Electron transport layer
eV	Electron volts
Φ_F	Fluorescence quantum yield
F^-	Fluoride
Flrpic	Bis[2-(4,6-difluorophenyl)pyridinato- C^2,N](picolinato)iridium(III)
FRET	Förster resonance energy transfer
FTIR	Fourier transform infrared spectroscopy
GC	Gas chromatography
GPC	Gel permeation chromatography
HCl	Hydrochloric acid
HOMO	Highest occupied molecular orbital
HTL	Hole transport layer
ICT	Intramolecular charge transfer
$Ir(piq)_2(acac)$	Bis(1-phenylisoquinoline)(acetylacetonate)iridium(III)
$Ir(ppy)_3$	Tris[2-phenylpyridinato- C^2,N]iridium(III)
$Ir(ppy)_2(acac)$	Bis[2-(2-pyridinyl- N)phenyl-C](acetylacetonato)iridium(III)]
ISC	Intersystem crossing
ITO	Indium tin oxide
K	Kelvin
k_H	Proton abstraction rate
kcal	Kilocalorie
LAH	Lithium aluminium hydride
LED	Light emitting diode
LUMO	Lowest unoccupied molecular orbital
M	mol/L
m	Multiplet (NMR)
MALDI	Matrix-assisted laser desorption/ionization
mol	Mole
MS	Mass spectrometry
ν	Stretching vibrations
m/z	mass to charge ratio (MS)
$n-BuLi$	n -Buthyllithium
NHE	Standard hydrogen electrode
NMR	Nuclear magnetic resonance
NPB	N,N' -Di(1-naphthyl)- N,N' -diphenyl-(1,1'-biphenyl)-4,4'-diamine
OLED	Organic light emitting diode
PAA	poly(acryl acid)
$Pd(dba)_2$	Bis(dibenzylideneacetone)palladium(0)

phOLED	Phosphorescence organic light emitting diode
PNBD	4-nitrobenzene diazonium tetrafluoroborate salt
PO15	dibenzo[b,d]thiophene-2,8-diylbis(diphenylphosphine oxide)
POLED	Polymer organic light-emitting diode
PPF	pyrolyzed photoresist film
ppm	parts per million
RDS	Rate determining step
rt	Room temperature
S_0, S_1	ground and first singlet state
s	Singlet (NMR)
SAM	Self assembled monolayer
SCE	Saturated calomel electrode
SET	Single electron transfer
S_NAr	Nucleophilic aromatic substitution
S_N2	Bimolecular nucleophilic substitution
STM	scanning tunneling spectroscopy
^t Bu	<i>tert</i> -Butyl
TPD	<i>N,N'</i> -Bis(3-methylphenyl)- <i>N,N'</i> -diphenylbenzidine
T_1	First triplet state
T_c	Crystallization temperature
T_g	Glass transition temperature
T_m	Melting temperature
TAPC	4,4'-Cyclohexylidenebis[<i>N,N</i> -bis(4-methylphenyl)benzenamine]
TBAF	Tetrabutylammonium fluoride
TCTA	Tris(4-carbazoyl-9-ylphenyl)amine
TEA	Triethylamine
TEMPO	(2,2,6,6-Tetramethylpiperidin-1-yl)oxyl
THF	Tetrahydrofuran
TIPS	Triisopropylsilyl
TMS	Trimethylsilyl
TLC	Thin layer chromatography
TOF	Time of flight
TPBI	1,3,5-tris(<i>N</i> -phenylbenzimidazol-2-yl)benzene
UV	Ultraviolet
V	Bias voltage
VdW	Van der Waals force
Vis	Visible
WOLED	White organic light emitting diode
XPS	X-ray photoelectron spectroscopy

Curriculum Vitae

Markus Gantenbein

Frobenstrasse 75, 4053 Basel, M. +41.(0)79.751.8548, markus.gantenbein@unibas.ch

Swiss, 5th of April 1985

Education

- 2011 – 2015 PhD in Organic Chemistry, Department of Organic Chemistry,
University of Basel
Supervisor: Prof. Dr. Marcel Mayor, University of Basel
Referees: Prof. Dr. Edwin Constable, University of Basel
 Dr. Thomas Schäfer, BASF
- 2010 Master Thesis "*Terminally Diisocyano Functionalized and Rotational
Restricted Biphenyl Systems*"
Supervisor: Prof. Dr. Marcel Mayor, University of Basel
Referee: PD Dr. Michel Calame, University of Basel
- 2008 – 2010 Master of Science in Nanosciences, Department of Organic Chemistry,
University of Basel
- 2007 Bachelor Thesis "*S₀-S₁ Spektren von Deuteriertem 3-Hydroxychinolin
und 3-Hydroxychinolin·ND₃*"
Supervisor: Prof. Dr. Samuel Leutwyler
- 2004 – 2007 Bachelor of Chemistry, Department of Chemistry, University of Bern
- 1999 – 2003 High School in Typus W (Economics), Kantonsschule Sargans,
Switzerland

Oral presentations

- 2015 "*New CBP Derivatives with Locked Carbazole-Biphenyl Junctions –
High-Triplet State Energy Materials*", 1st Annual Meeting and Joint
MOLESCO-SYMONE Workshop, Engelberg, Switzerland
- 2014 "*Novel CBP Derivatives as Host Materials Targeting Blue Emitting
phOLEDs*", Status workshop "Functional Nanomaterials", Bad
Herrenalp, Germany

2014 “Sulfur doped Fullerene – $C_{48}S_{12}$ ”, PCC Research Seminar, University of Basel, Switzerland

Teaching Experience

2011 – 2014 Teaching Assistant for External Students, Department of Chemistry, University of Basel
Teaching Schweizer Jugend Forscht candidates as well as High School Students

2011 – 2014 Teaching Assistant for Practical Courses, Department of Chemistry, University of Basel
Teaching Undergraduate Students in practical skills, Supervising and Correcting Examinations

2012 – 2014 Supervision of two successfully completed Master Theses

2007 – 2011 Substitute Teacher in Chemistry, High School Solothurn, Switzerland

Leadership and Teamwork

2012 – 2015 Representative of PhD community in the Unterrichtskommission, Department of Chemistry, University of Basel

2013 – 2014 Member of the committee “Basel Chemistry Symposium”

List of Publications

Markus Gantenbein, Manuel Hellstern, Loïc Le Pleux, Markus Neuburger, Marcel Mayor; New 4,4'-Bis(9-carbazolyl)-Biphenyl Derivatives with Locked Carbazole-Biphenyl Junctions: High-Triplet State Energy Materials, *Chem. Mater.* **2015**, doi: 10.1021/cm5045754

Christophe Daepfen, Daniel Bachmann, Andrea Pannwitz, Isabel Kerschgens, Charlotte Laupheimer, Martin Rother, Lukas Jundt, Michel Rickhaus, Markus Gantenbein, and Ina Bodoky; Basel Chemistry Symposium 2014 – In Memory of Prof. T. Reichstein, *CHIMIA* **2015**, 69, 63-64.

Patrick Burch, Thomas R. Eaton, Johannes Hoecker, Markus Gantenbein, Lukas Jundt, Michel Rickhaus; Basel Chemistry Symposium 2013 – In Memory of Prof. C. F. Schönbein, *CHIMIA* **2013**, 67(10), 744-745.

Jürgen Rotzler, Heiko Gsellinger, Angela Bihlmeier, Markus Gantenbein, David Vonlanthen, Daniel Häussinger, Wim Klopper, Marcel Mayor; Atropisomerization of di-*para*-substituted propyl-bridged biphenyl cyclophanes, *Org. Biomol. Chem.* **2013**, 11, 110-118.

Laurent Marot, Roland Steiner, Markus Gantenbein, Daniel Mathys, Ernst; Co-deposition of rhodium and tungsten films for the first-mirror on ITER, *Journal of Nuclear Materials* **2011**, 415, 1203-1205.

